Water Technology and Sciences

Included in Thomson Reuters Science Citation Index® (ISI) • Expanded Thomson Reuters Research Alert® (ISI) • EBSCO • ProQuest

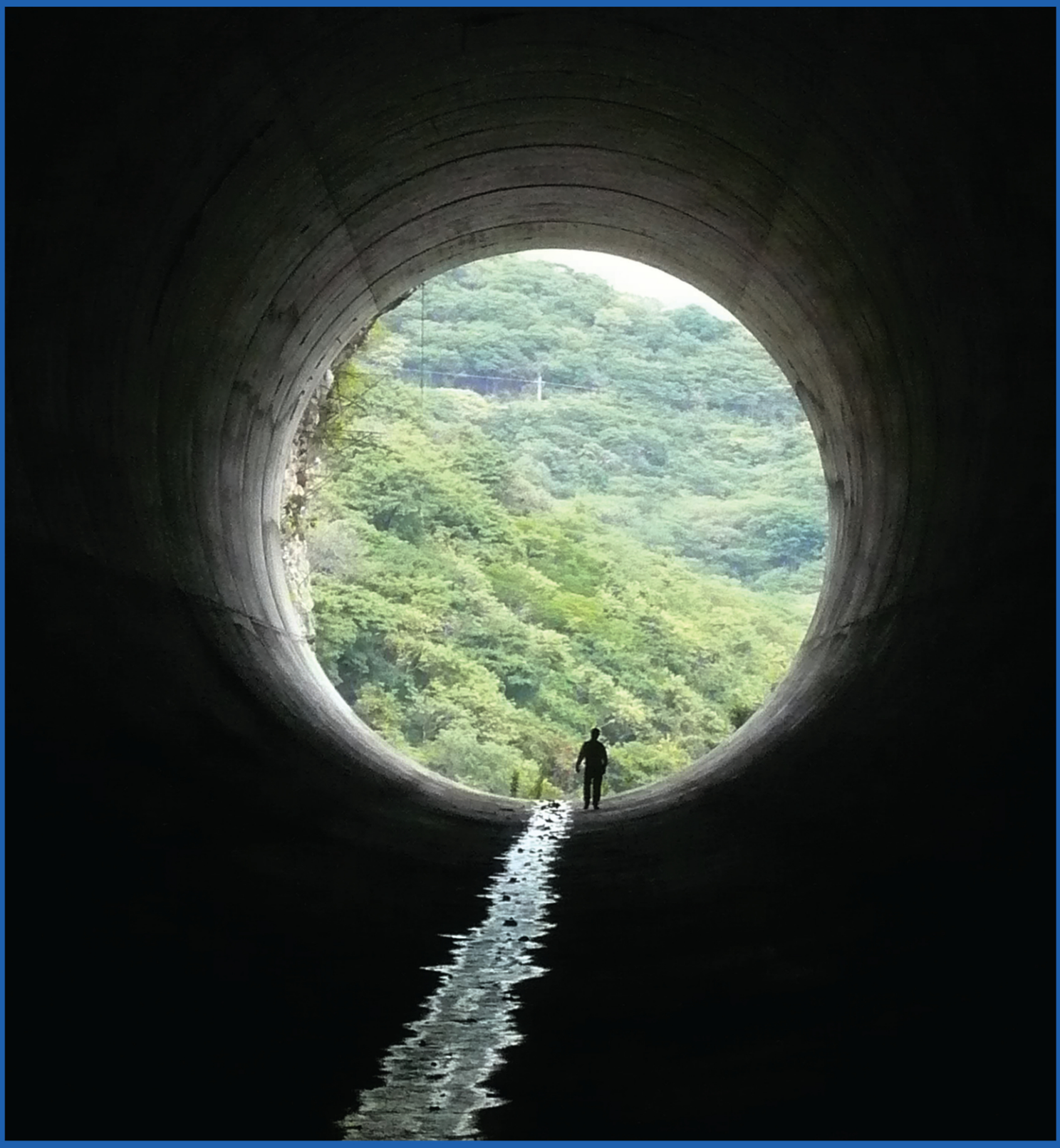

Vol. V, No. 1, January-February, 2014

Water Technology and Sciences

Editorial Committee

©***Water Technology and Sciences.*** Vol. V, No. 1, January-February, 2014, s a bimonthly publication edited by the Instituto Mexicano de Tecnología del Agua, Paseo Cuauhnáhuac 8532, Colonia Progreso, Jiutepec, Morelos, C.P. 62550, telephone +52 (777) 3 29 36 00, extension 474, www.imta.gob.mx/tyca, fsalinas@tlaloc.imta.mx. Editor responsable, Nahún Hamed García Villanueva; Copyright No. 04-2013-121014514100-203, granted by the Instituto Nacional de Derechos de Autor. ISSN pending. Responsable for the latest update of this issue: Sub-Department of Dissemination and Circulation, Francisco José Salinas Estrada, Paseo Cuauhnáhuac 8532, Colonia Progreso, Jiutepec, Morelos, C.P. 62550.

Water Technology and Sciences is the traslation of *Tecnología y Ciencias del Agua*, which is the continuation of the following journals: *Irrigación en México* (1930-1946); *Ingeniería hidráulica en México* (1947-1971); *Recursos hidráulicos* (1972-1978), and *Ingeniería hidráulica en México*, second period (1985-2009).

Water Technology and Sciences

Vol. V, No. 1, January-February, 2014

For subscriptions, click here

Coordination for editorial comments, click here give

Home: inside the tunnel 1 conduction chute Hydroelectric Manuel Moreno Torres, Chicoasén, Chiapas, Mexico. Seismic effects are evaluated in underground structures with different approaches to those used for structures superficial. In general, surface structures are designed for inertial forces caused by the movement of its base. However, shares of design for structures underground are expressed in terms of deformations the structure imposed by the ground motion. See Article "seismic design criteria tunnel" of Luis Eduardo Pérez-Rocha and Javier Aviles (pp. 57-70).

Photo provided by Luis Eduardo Pérez Rocha.

Cascade River forming the Minatitlan (Marabasco), water from the Book Manantlan, Colima, Mexico.

Photo: Rubén Huerto.

Contents

Technical articles

Contenido

Artículos técnicos

Sedimentation in Navegation Channels under the context of Climate Change

• Mariano Re* •
Instituto Nacional del Agua, Argentina
*Corresponding Author

• Leandro D. Kazimierski • Ángel N. Menéndez •
Universidad de Buenos Aires, Argentina

Abstract

RE, M., KAZIMIERSKI, L.D. & MENÉNDEZ, A.N. Sedimentation in Navigation Channels under the Context of Climate Change. *Water Technology and Sciences* (in Spanish). Vol. V, No. 1, January-February, 2014, pp. 5-21.

A numerical modeling methodology for sedimentation in navigation channels is used to evaluate effects of Climate Change, through consideration of potential changes in the river discharge. This methodology, which is explained in detail, is illustrated through its application to a 'paso' of the Parana River (South America), validating its results with maintenance dredging data. It is shown that, keeping the present dredging elevations, the sedimentation volume would increase with the increment in discharge, and vice versa, with relative rates of change significantly larger than that of the discharge. If, on the contrary, the dredging elevations were adjusted to new reference levels, the trend would be the opposite, with relative rates of change only moderately larger than that of the discharge, in absolute value.

Keywords: sedimentation, navigation channels, dredging, Climate Change, Paraná River.

Resumen

RE, M., KAZIMIERSKI, L.D. & MENÉNDEZ, A.N. Sedimentación en canales de navegación en el contexto del cambio climático. Tecnología y Ciencias del Agua. *Vol. V, núm. 1, enero-febrero, 2014, pp. 5-21.*

Se utiliza una metodología de modelación numérica de la sedimentación en canales de navegación para evaluar efectos del cambio climático a través de la consideración de cambios potenciales en el caudal del río. Esta metodología, que se explica en detalle, se ilustra mediante su aplicación a un paso del río Paraná (Argentina), validándose sus resultados con datos de dragado de mantenimiento. Se muestra que si se mantuvieran las actuales cotas de dragado, el volumen sedimentado crecería con el incremento de caudal y viceversa, con tasas relativas de variación significativamente mayores que la del caudal, en valor absoluto. Si, en cambio, se ajustaran las cotas de dragado a nuevos niveles de referencia, la tendencia sería opuesta, con tasas relativas de variación de la sedimentación sólo moderadamente superiores a las de caudal, en valor absoluto.

***Palabras clave**: sedimentación, canales de navegación, dragado, cambio climático, río Paraná.*

Introduction

Climate change produces a series of consequences for river navigation. Changes in precipitation in a hydrographic basin alter the occurrence of extreme hydrological conditions and indirectly affect navigability (PIANC, 2008). Climate change can also alter the morphology of rivers (due to changes related to erosion and sedimentation processes), the maneuverability of ships and the operational efficiency of navigation structures (Hawkes *et al*., 2010).

Previous evaluations of the impacts of climate change on navigation have focused primarily on determining variations in water levels resulting from modifications in the hydrological variables of the basin (Sung *et al*., 2006; De Wit *et al*., 2007; Millerd, 2011). The problem of changes in the morphology of courses has been studied to a lesser extent (Verhaar *et al*., 2010).

This work presents a methodology to evaluate possible variations in maintenance dredging of navigation channels in the context of climate change. This is illustrated by its application to

the Parana River (Argentina), which has a sandy riverbed and is part of the navigation route through which a large amount of local agricultural exports and Argentine steel traffic travels.

Most of the 544 km of the Argentine sections of the Parana River is naturally navigable for ocean ships. Problems with little water depth occur in localized zones known as passages, requiring dredged artificial navigation passages. The natural tendency for sediment deposition in these channels requires periodic and systematic maintenance dredging, the yearly amount of which provides a vital indicator of the economic viability of guaranteeing a determined water depth.

Climatic and hydrological trends related to climate change are clearly observed in the Plata Basin (in which the Parana River is the main water course) (Barros *et al.*, 2006), impacting sedimentation in the navigation channels. Because of this climate change context, establishing the likely change in maintenance dredging is important to managing these channels. To illustrate the methodology proposed by this work , a section of the Parana River known as the Borghi Passage (Figure 1) was chosen for the analysis.

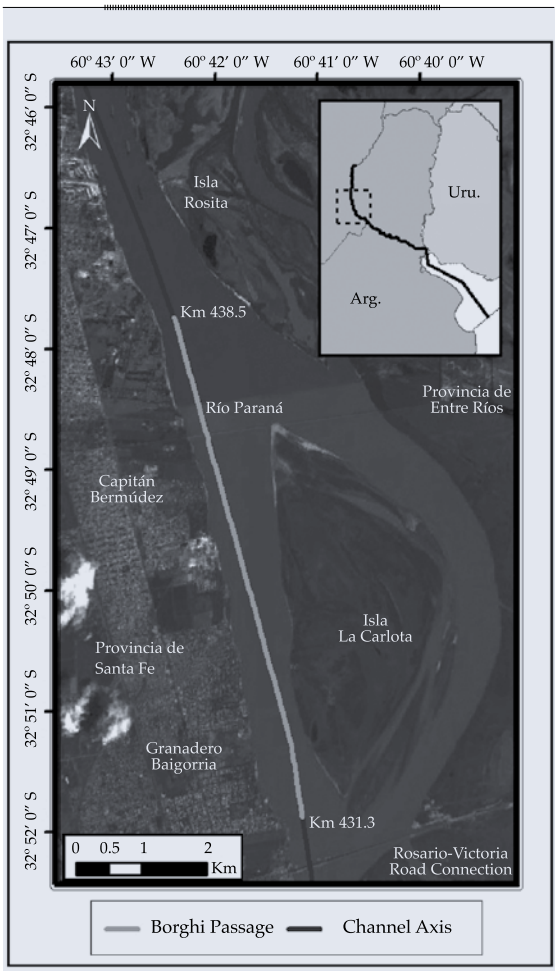

Figure 1. Study Zone.

Methodology

Model

This work calculates the sedimentation in the navigation channel using a 2D-V model implemented with the AGRADA numerical code developed by the National Water Institute (INA, Spanish acronym), Argentina (Menéndez, 1992, 1994; Kazimierski *et al.*, 2012). The model, whose analysis is based on the plane that is aligned with the current, includes several modules: hydrodynamic, riverbed sediment transport, suspended sediment transport and morphological evolution. Figure 2 shows the control volume on which the conservation equations are based . For the 2D-V model, to establish the orientation of the control volume and the intensity of the boundary condition for the water upstream, a 2D-H hydrodynamic model was used for the region of the navigation channel. This was implemented with the HIDROBID II numerical code also developed by the INA (Menéndez, 1990). The sedimentation model for channels will be briefly described next.

The hydrodynamic model solves the vertical profiles for both of the components of velocity (horizontal and vertical), the distribution of the shearing stress against the riverbed and the vertical profile of the turbulent mixing coefficient. Since changes in the level of the riverbed due to sedimentation processes occur over long time periods, compared to hydrodynamic variations, it can be assumed

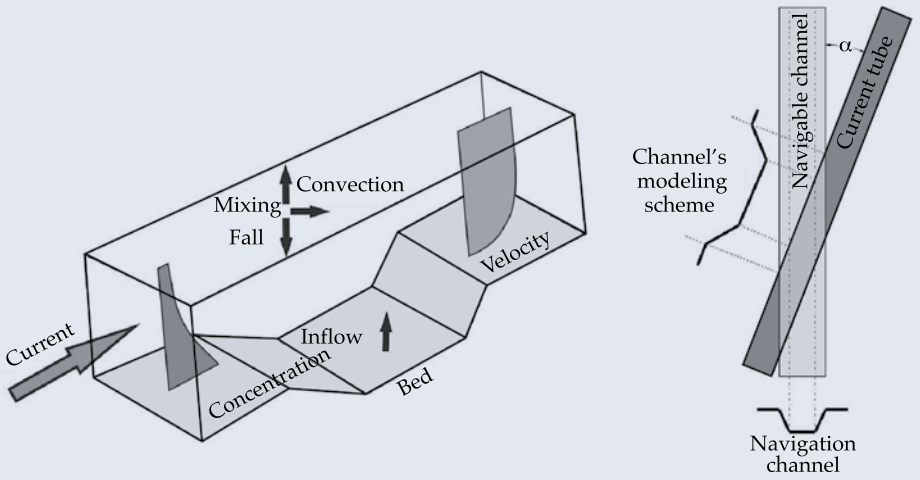

Figure 2. Control Volume for the 2D-V Model.

that the hydrodynamic conditions adapt instantaneously to those changes. The vertical profile of the horizontal component of velocity (x axis) is proposed as a parametric family of functions composed of a logarithmic and an tailcomponent (van Rijn, 1987):

$$u(x,z) = A_1(x)\cdot ln\left(z/z_0\right)\cdot u_h(x) + A_2(x)\cdot F(\eta)\cdot u_h(x)$$

where z is the vertical coordinate measured from the riverbed; z_0 is the height of the point of zero velocity; u_h, the free surface velocity; A_1 and A_2, are local parameters (independent of z); η, is the dimensionless vertical coordinate (varies from 0 to 1, while z varies from z_0 to the height of the free surface), and $F(\eta) = 2\,\eta^t - \eta^{2t}$, where t is another local parameter. The tail component is needed because when abrupt changes occur in the riverbed the vertical velocities profile move away from equilibrium conditions; for instance when a current crosses a dredged navigation channel. When the profile of the horizontal component of the velocity is known, the distribution of the vertical component W is obtained by numerically integrating the continuity equation over the vertical equation. The shearing stress against the riverbed is calculated by differentiating the profile of the vertical velocities. A parametric distribution is also proposed for the mixing coefficient (van Rijn, 1987).

When the current crosses the channel, a refraction effect which results in a change in direction (more alignment with the channel) and width (narrowing), producing a change in the intensity of the current. This effect can be determined based on abacus obtained from numerical simulations (van Rijn, 1991). Figure 3 shows the abacus for the local angle represented by the direction of the current and the channel axis, and for the relationship between local (mean vertical) and incident velocity, in function of the relationship between incident and local depth for different incident angles between the current and the channel. The change in the local width of the control volume with respect to the initial width occurs as a result of continuity.

Since the time scale associated with riverbed transport is much less than the hydrodynamic scale, this transport can be used to instantaneously adapt to local conditions. Therefore, it is not necessary to develop a temporal evolution equation for riverbed transport. A formula is sufficient. Nevertheless, since the velocities profile is not one of

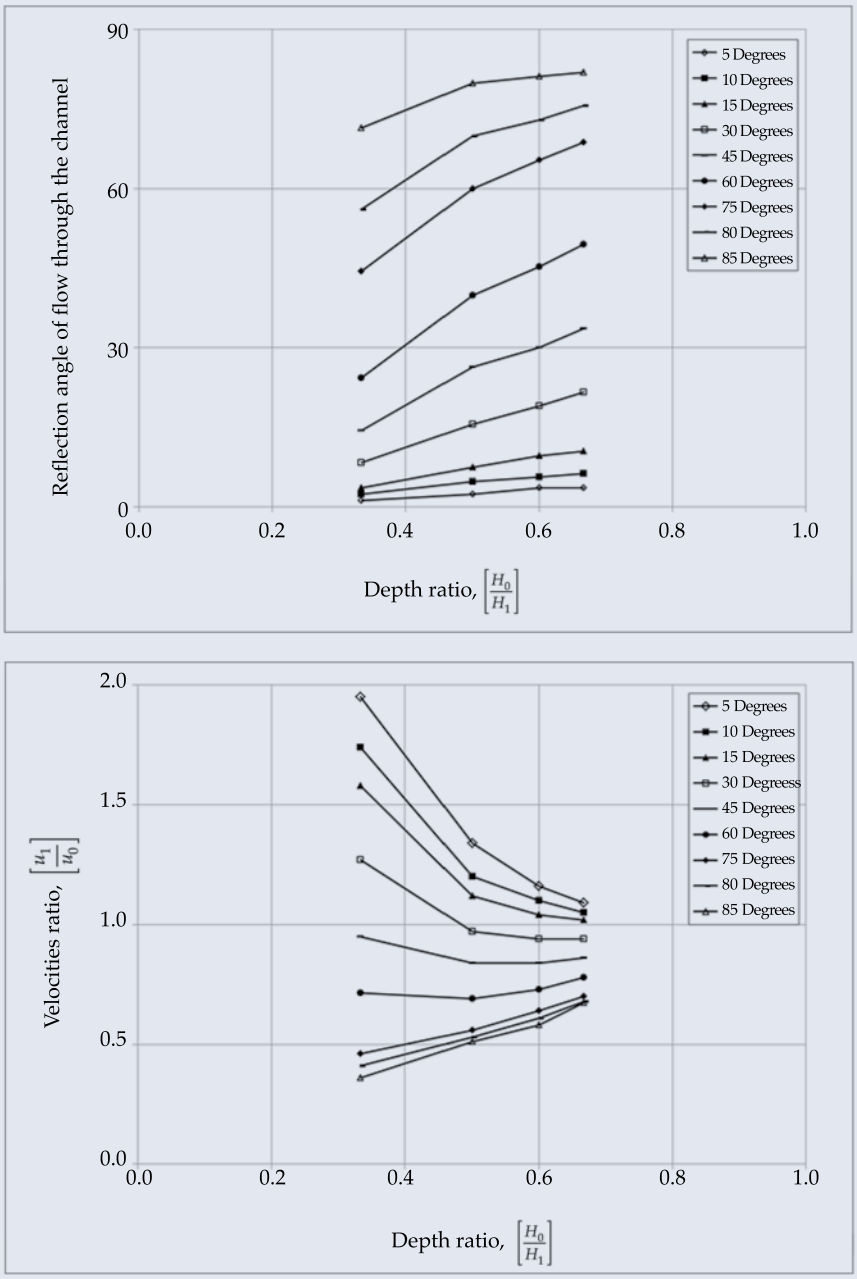

Figure 3. Abacusfor refraction effects: a) refraction angle in function of the depth ratio; b) velocities ratio in function of depth ratio (van Rijn, 1991).

equilibrium, it is useful to apply a more general transport formula than those normally used. The following proposal by van Rijn (1987) is used for the non-cohesive solid sediment flow transported as riverbed load (Q_{sf}):

$$\frac{Q_{sf}}{b \cdot d_{50} \cdot \left(g \cdot d_{50}\right)^{1/2}} = 0.053 \cdot \sqrt{\Delta} \cdot D_*^{-0.3} \cdot T_m^{2.1}$$

where d_{50} is the mean diameter of the particle; D_* is the dimensionless size of the particle; Δ,

its relative density; b the width of the control volume; g the acceleration of gravity, and T_m is the mean value of the denominator "state parameter" which is the excess in the shearing stress against the riverbed with respect to the critical value for the initiation of movement, dimensionless with the standard deviation of the statistical distribution of the shearing stress.

The riverbed transport over the slopes of the channel does not strictly follow the direction of the current since the action of gravity contains a weight component in the direction of the center of the channel, which generates a deviation. The angle of the deviation is calculated based on a formula proposed by Fredsoe (1978), which depends on the inclination of the slope and the internal friction angle.

The suspended sediment transport model includes the longitudinal advection (in the direction of the current), the effective vertical advection and turbulent diffusion according to the vertical (van Rijn, 1987):

$$\frac{\partial\left(b\cdot u\cdot c\right)}{\partial x}+\frac{\partial\left(b\cdot\left(w-w_s\right)\cdot c\right)}{\partial z}=\frac{\partial}{\partial z}\left(b\cdot\varepsilon_s\cdot\frac{\partial c}{\partial z}\right)$$

where c is the volumetric concentration of sediment; w_s is the velocity of falling sediment; and ε_s is the turbulent mixing coefficient in the vertical direction. This equation is solved numerically using the finite elements method with a mesh composed of square elements. As a bed boundary condition it is common to presume local equilibrium, that is, to consider that deposition is equal to re-suspension at that point. The resulting formula, which is compatible with the van Rijn (1987) for riverbed transport is:

$$C_a=0.03\frac{d_{50}}{a}\frac{\overline{T_m^{1.5}}}{D_*^{0.3}}$$

Zero sediment flow is imposed on the free surface, while a local equilibrium profile for the concentration is considered for the inlet surface of the control volume. When the concentration is known, the solid suspended transport flow (Q_{ss}) is calculated by numerically integrating its flow for the entire transversal section.

The model for the evolution of the riverbed uses the Exner equation (1925):

$$\frac{\partial\left(b\cdot z_f\right)}{\partial t}+\frac{1}{1-p}\cdot\frac{\partial Q_s}{\partial x}=0$$

where z_f is the level of the riverbed; t is the temporal coordinate, p the porosity, and $Q_s = Q_{sf} + Q_{ss}$ is total solid flow. This equation is numerically solved using the finite differences method based on the change in riverbed level, that is, the longitudinal distribution of total solid flow.

Baseline Information

The Borghi Passage was created (at the depth of the current water depth) between km 431.3 to km 438.5 along the route that crosses the Parana River (the coordinate increases downstream). Information was obtained pertaining to the bathymetric surveys and dredged volumes for this passage during the period April 12, 2008 to April 12 2009, provided by the Órgano de Control de Concesiones de Redragado y Señalización (Re-dredging and Signage Licensing Control Board) which is operated by the Sub-Ministry of Ports and Navigable Routes (SSPyVN, Spanish acronym) of the national government.

Figure 4 shows the maintenance dredging operations employed during the year of analysis, and indicates the segments (100 m in length) for each dredging operation and the dredged volumes for those segments. Note that most of the dredging tends to occur in two sections— the "Lower" Borghi passage (km 431.3 - km 433.9) and the "Upper" Borghi Passage (km 436.8 - km 438.5). Based on those data, the mean annual dredged rate was determined for each segment, resulting in the distribution shown in Figure 5.

In order to simplify the analysis, each of the sections of the Borghi Passage was divided into sub-sections. The lower passage contained four sub-sections (numbered 1 through 4, all 500 m, and the remaining sub-section was not included, 600 m long, called number 4*). The upper passage contained three sub-sections (numbers 5 though 7, a sub-section measuring 800 m and the other two 500 m). Figure 5 also shows the mean dredging rate per sub-section.

The mean annual maintenance dredging rate will be assumed to be representative of the mean annual sedimentation rate. This is considered to be a reasonable hypothesis since no direct determinations of sedimentation are available.

In addition, the time between dredging for each section was determined. Figure 6 shows the resulting annual average per section. Forty days was a typical period for a large portion of the lower section, and 60 days was common for the other sections, although there were also periods of roughly 90 days.

Results and Discussion

Current Situation

A hydrodynamic 2D-H model was applied from km 452 km on the navigation route (that is, 13.5 km upstream from the start of the Borghi Passage) to km 430.0 at the Rosario-Victoria Road Connection (that is, 1.3 km downstream from the end of the Borghi Passage). This region is shown in Figure 1. Detailed bathymetric information was used, which was obtained from an ad hoc measuring campaign (Guerrero *et al.*, 2011), based on which a Digital Elevation Model (DEM) was created containing square mesh cells measuring 40 m per side (the width of the river was roughly 1 000 m). To calibrate the hydrodynamic model, velocity data was measured with ADCP during the campaign (June 29 to July 3, 2009). These were also used to determine the flow of the river using integration, which resulted in a mean spatial-temporal value of 13 740 m^3/s, imposed as

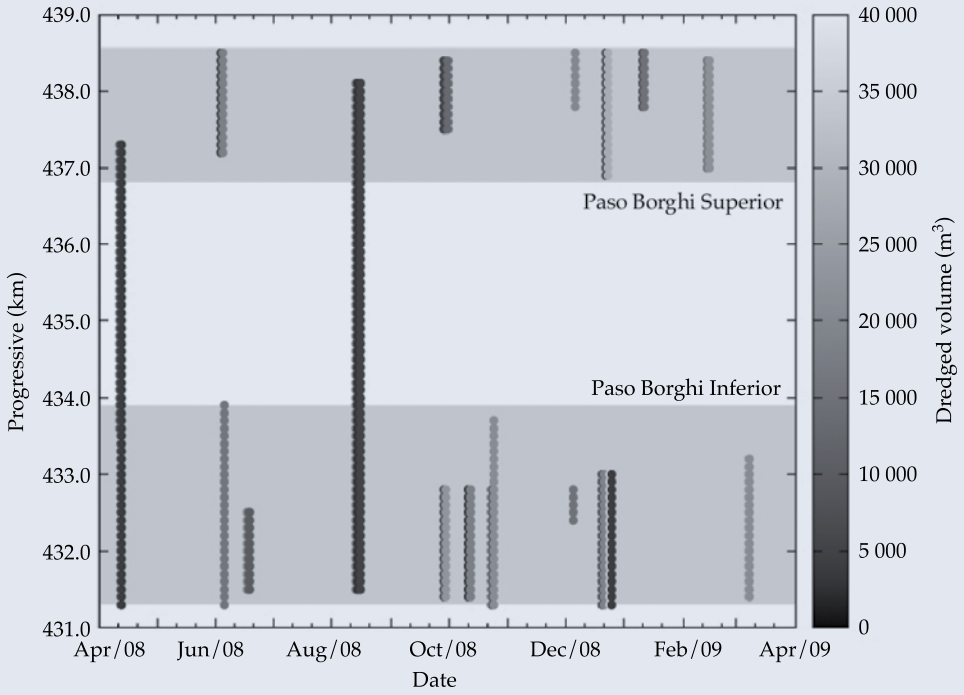

Figure 4. Date, location and maintenance dredging volume in 100 m segments from 2008-2009 in the Borghi Passage.

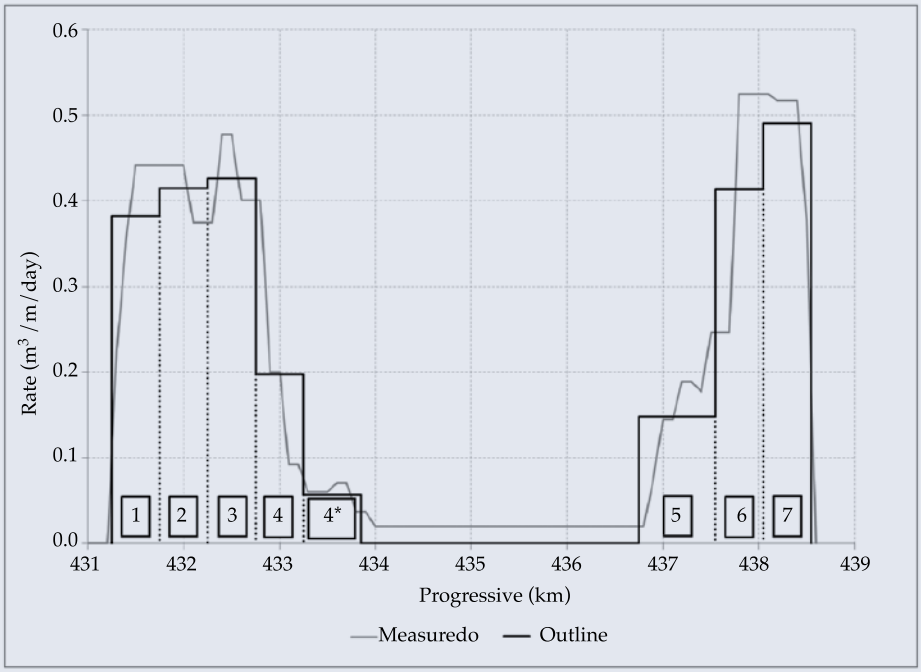

Figure 5. Longitudinal distribution of the annual mean maintenance dredging rate from 2008-2009 in the Borghi Passage.

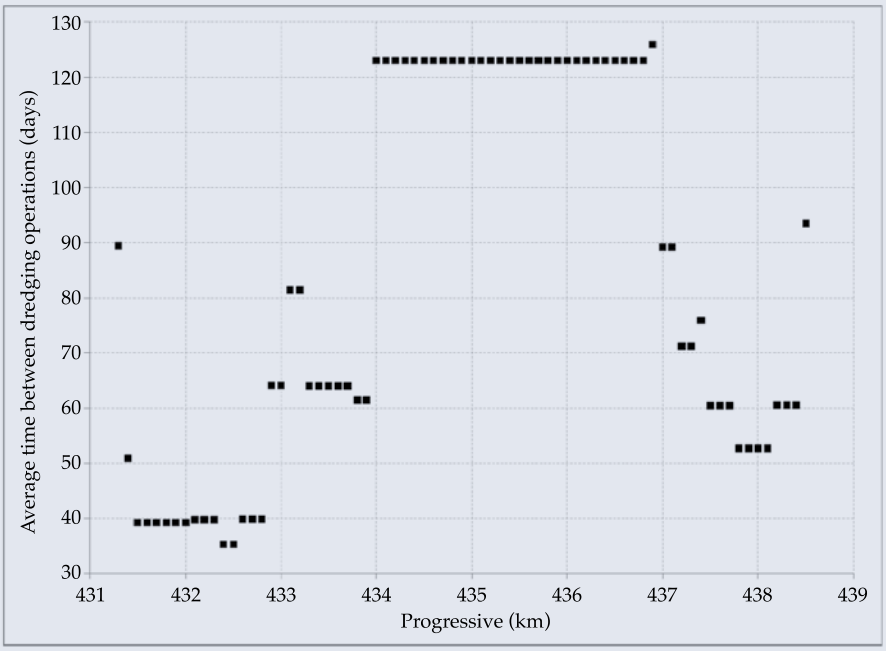

Figure 6. Mean period between maintenance dredging from 2008-2009 in the Borghi Passage.

a boundary condition upstream. The water level downstream was established (1.82 m above local zero). The calibration of the model consisted of fitting the value of the Manning roughness parameter to the riverbed, n, in order to obtain the best agreement possible with the current velocities measured, resulting in $n = 0.025$ (including the effect of the resistance of the dunes). Figure 7 presents one of the comparisons between the vertical mean velocities obtained from observations and those from the simulation, which shows satisfactory agreement. This hydrodynamic model generated the boundary conditions for the 2D-V hydrodynamic model (see below).

A model was built to calculate sedimentation for each of the sub-sections defined above. Based on the set of periodic surveys of cross-sections performed in the Borghi Passage during the study period (and after discarding some of those which showed inconsistencies), a profile representative of each sub-section was drawn for the design navigation channel (width of sill of 116 m and slopes of 1V:5H, according to indications by the navigation authority) and horizontally expanded on each side. This is shown in Figure 8. The identification of the dredged channel is not evident in the surveyed profiles. Therefore, the following criteria were established: for each side of the channel, the expanded level was taken to be the level that roughly corresponded to the upper third of the levels registered, while the level representing the lower third of the levels registered was selected for the riverbed level.

For all the models, a vertical discretization of 25 cells was adopted, with logarithmically distributed heights to obtain the highest resolution near the bed. The region begins 100 m upstream from the channel shoal (meeting point between the expanded area and the slope) and extends 300 m downstream from the following shoal. The longitudinal discretization adopted was 2 m.

To calculate the mean annual sedimentation in the navigation channel during the study period (April 12, 2008 to April 12, 2009) the corresponding annual mean flow was used, which resulted in 13 100 m^3/s. Based on the results of the 2D-H hydrodynamic model for this flow, flow tubes were built every 500 m^3/s (Figure 9). For each sub-section of each channel, one of the flow tubes were selected as representative (essentially the one that crosses the middle portion of the sub-section). This tube provides the incidence conditions for the control volume for the sedimentation model, including the width, water level and orientation of the velocity of the current with respect to the

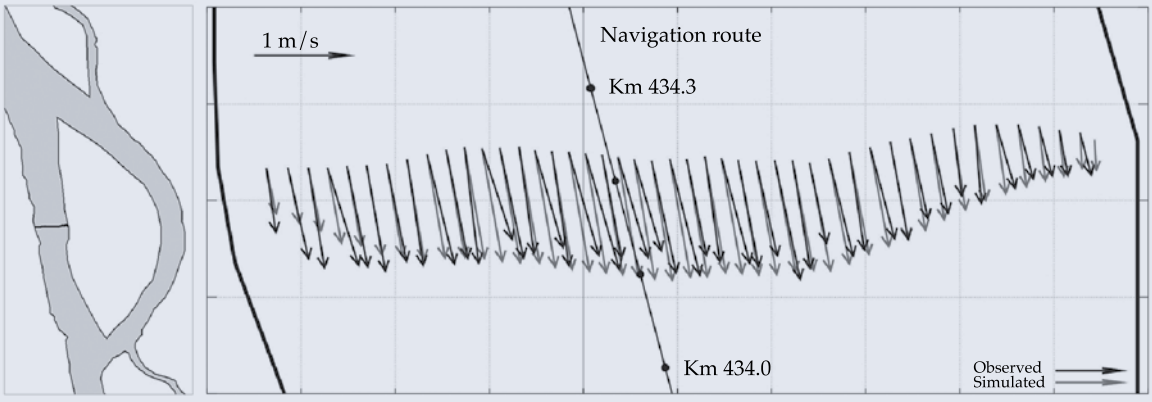

Figure 7. Observed and Simulated Velocities in the validation of the 2D-H model.

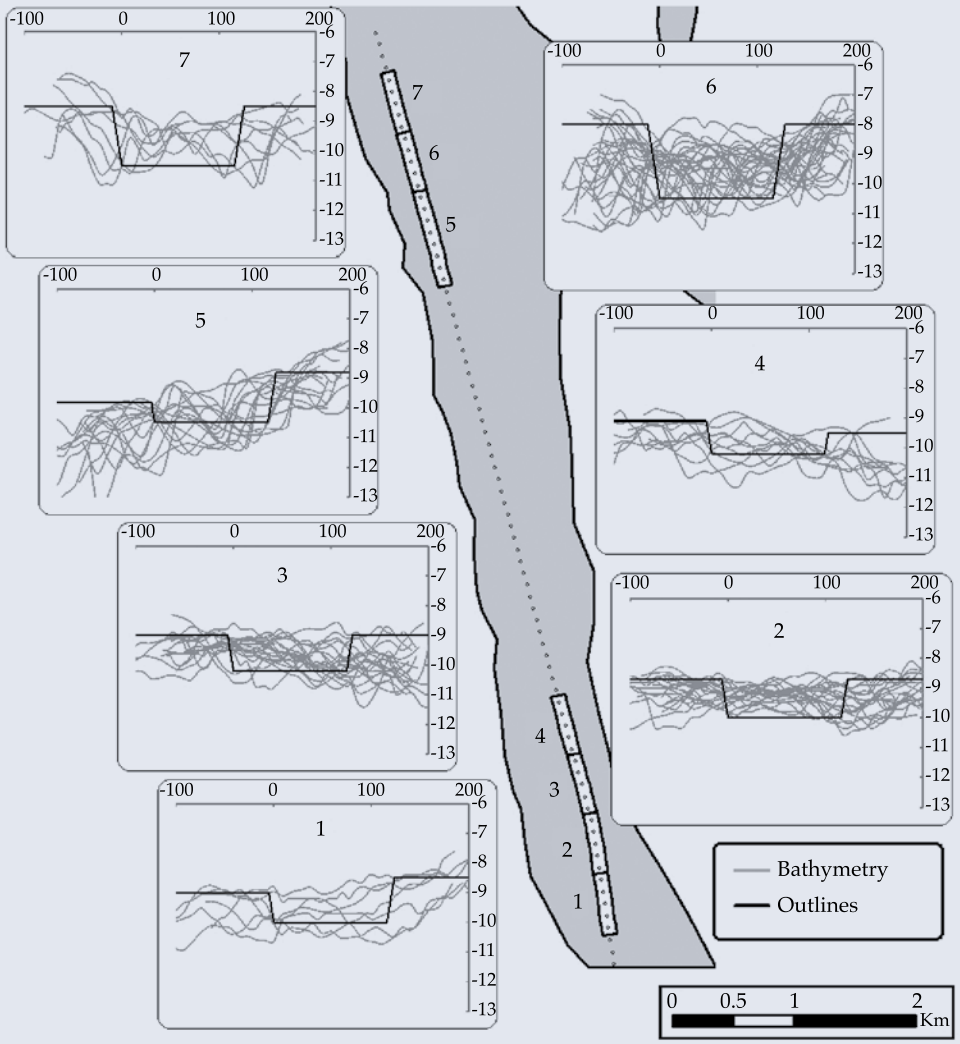

Figure 8. Outline of the dredged cross sections of the sub-sections.

axis of the sub-section, with which the values of all the hydrodynamic variables for the 2D-V modeling were established (Table 1).

The riverbed sediment of the Parana River is sand. Although transport of fine suspended material (washing load) occurs, it is deposited only in the inner harbors, access channels and locations where fluvial ports are maneuvered (Mangini *et al.*, 2003). Based on the available data along the navigation route (Menéndez, 2002), a mean (d_{50}) grain size of 260 μm was imposed. This is associated with a fall velocity of 3.7 cm/s, according to the formula by van Rijn (1987). It is relevant to mention that the granulometric distribution is concentrated such that the mean diameter size is sufficient ($d_{10} = 162$ mm and $d_{90} = 420$ mm). The porosity of the sand (which influences the *in situ* sediment volume) was taken to be 0.4. The concentration profile of the sediment in suspension that results from applying the model to the expanded zone (from upstream) was verified to be compatible with the measurements conducted for a vertical in a section located 30 kilometers downstream from the Borghi Passage, at km 406.5 (Royal Boskalis and Ballast Ham Dredging, 1992). Figure 10 shows this agreement for the case of all sub-sections.

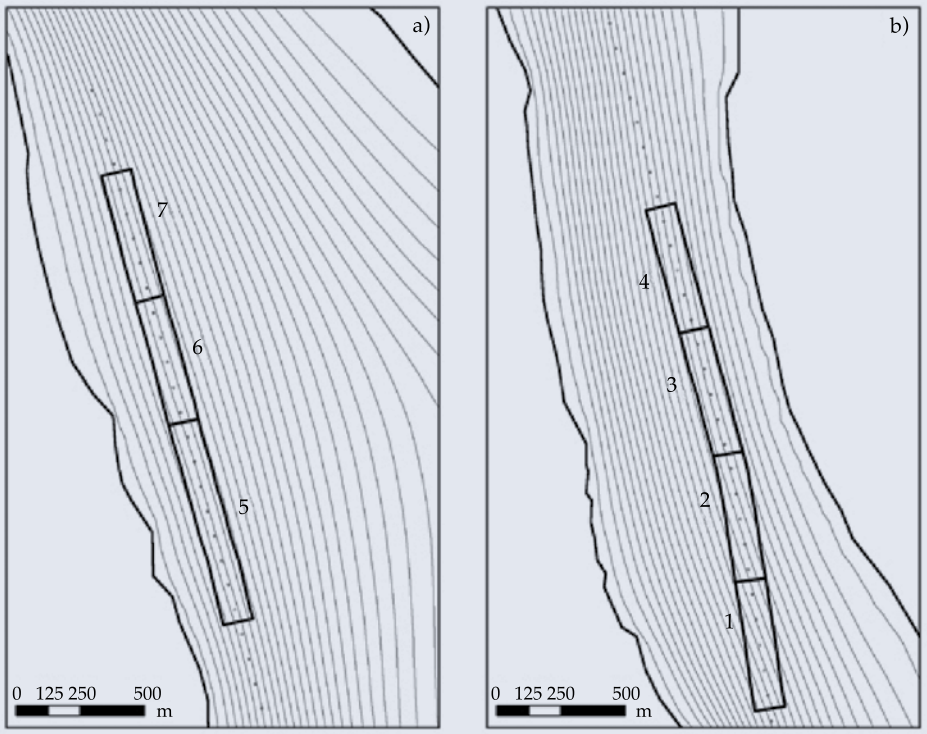

Figure 9. Flow tubes for the mean flow in a) Upper Borghi and b) Lower Borghi (tubes are shown every 500 m^3/s).

Table 1. Incidence values for the hydrodynamic parameters.

No.	Sub-section (km)	Specific flow ($m^3/m/s$)	Level over local zero (m)	Angle (°)
1	431.25 - 431.75	12.4	2.507	11.6
2	431.75 - 432.25	12.3	2.515	5.0
3	432.25 - 432.75	13.0	2.528	0.0
4	432.75 - 433.25	13.4	2.541	4.3
5	436.75 - 437.55	12.4	2.658	1.8
6	437.55 - 438.05	11.1	2.680	2.0
7	438.05 - 438.55	11.9	2.687	1.0

Table 2 presents the mean vertical concentration, <*c*>, and the resulting suspension and bed loads for each sub-section in the expanded area. The mean concentrations are compatible with those obtained by measurements taken in the zone (Guerrero *et al*., 2011). In addition, the bed load is observed to be 1/7 of the suspended sediment load, which is compatible with existing measurements (Szupiany *et al*., 2010).

With the currents crossing the navigation channel, the transport process increases as a result of sedimentation of the slope upstream (that is, from the point at which the current crosses) and decreases due to erosion of the slope downstream, which is called the "trap effect." The action of gravity on bed transport in the slopes generates a diffusion effect called "gravitational effect." For simplicity, these two effects have been calculated separately. In

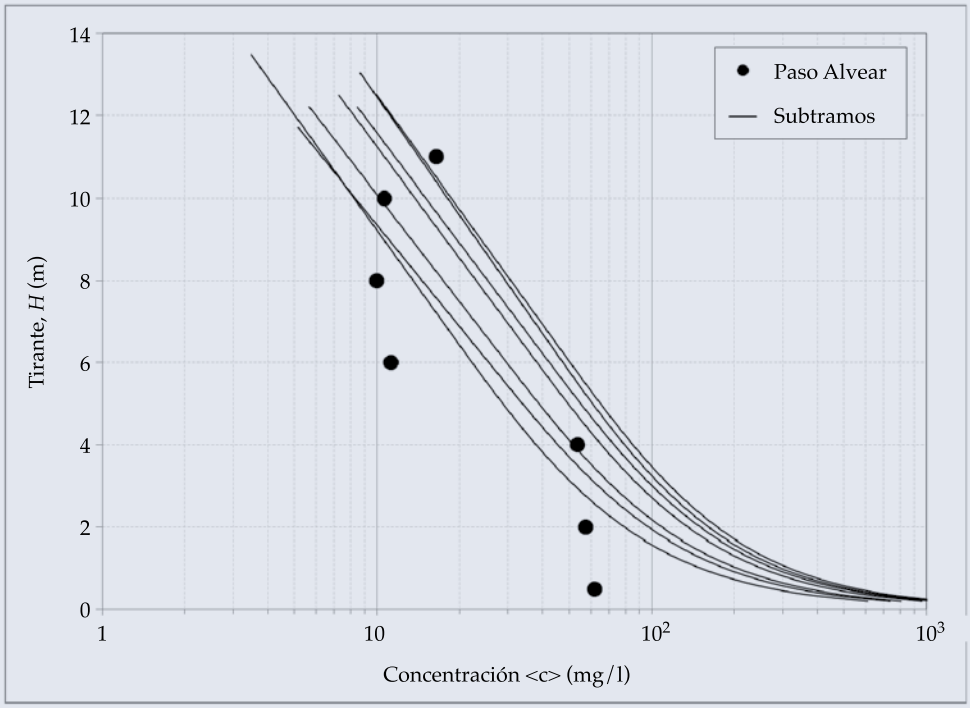

Figure 10. Vertical profiles of concentration calculated for the sub-sections analyzed (continuous lines) and measurements in the Alvear Passage – km 408 (points).

addition, the refraction angle corresponding to the middle point of each slope was used as representative in order to calculate the trap effect, and the deviation angle corresponding to the same points was used to calculate the gravitational effect. For example, Figure 11 shows how a portion of a sub-section of the channel evolves according to each one of the two effects. The time since dredging is indicated.

The sedimentation rates per unit length were determined for each sub-section based on the results for 1 month after dredging (representative time scale between maintenance dredging). To this end, the difference was determined between the riverbed level at the end and beginning of the simulation, integrating between shoals along the axis of the control volume and along its entire width (the origin of the sedimented volume of the control

Table 2. Values of incidence of the sedimentological parameters.

Sub-section	<c> (mg/L)	Q_{ss} (mg/m/s)	Q_{sf} (mg/m/s)	Q_{st} (mg/m/s)	Q_{ss}/Q_{sf}
1	69.5	889	126	1 015	7.0
2	78.2	1 004	142	1 147	7.1
3	88.6	1 212	167	1 379	7.2
4	80.4	1 298	177	1 475	7.3
5	39.1	471	67	538	7.0
6	52.4	577	86	663	6.7
7	56.9	672	98	770	6.9

volume), divided by the width of the projected control volume in the direction of the channel's axis (this is equal to directly integrating along the normal direction to the channel). This rate was calculated again using a timeframe of 2 months for some sub-sections, which resulted in little sensitivity.

Figure 12 shows the comparison between sedimentation rates per sub-section calculated using the model and those produced by the data from maintenance dredging. The agreement is considered satisfactory, in the sense that the rates have the same order of magnitude and essentially show similar spatial distribution trends, although the model tends toward overestimating. Therefore, in reality, the model could be calculated to improve the quantitative agreement per sub-section, which would be simple since a slight adjustment in the incidence angle of the current is all that is needed, to which the model is very sensitive given the that the current and the channel axis

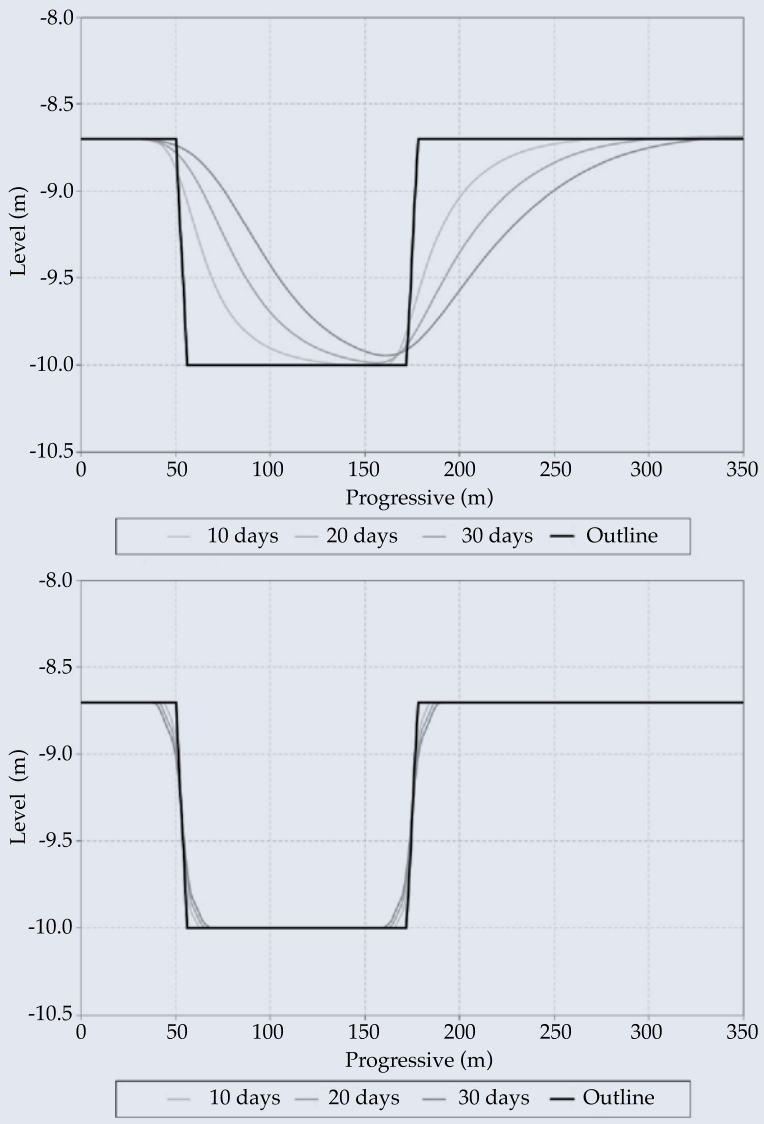

Figure 11. Evolution of the cross section (sub-section no. 2) with a) *trap effect* and b) *gravitational effect*.

are nearly parallel. Nevertheless, it was decided to maintain the values of that parameter— that is, to favor consistency between hydrodynamic and sedimentological models— since the objective of this work was not to obtain values that are ready for engineering actions but rather to calculate the relative change that can occur in the sedimentation rate, which only weakly depends on absolute values. This level of agreement is definitively considered sufficient to validate the calculation methodology.

These sedimentation rates represent a maintenance volume for the Borghi Passage of 792 000 m^3/year according to the model.

Future Scenarios

Given that there are no clear predictions for trends in the distribution of precipitation— and therefore of the flows of the rivers— in the Plata basin under the effects of climate change (Saurral, 2010), potential positive and negative changes in flow were considered for possible future scenarios. A mean year was used as a baseline scenario, defined as the "current" annual mean flow (during the period 1994-2010). For all these scenarios, the morphology of the Parana River was assumed to not be affected by changes in flow, that is, that the bed level would be maintained outside the dredged ("expanded") zones. In principle, this is not the case since a historical morphological evolution exists in the area on a 10-year time scale (Castro *et al*., 2007), which would also be influenced by changes in flow. Nevertheless, an evaluation by Nones *et al*. (2012) and Guerrero *et al*. (2013) of this effect throughout the Parana River using numerical modeling shows no net sedimentation or erosions trends in the study zone and, therefore, the approach is considered acceptable.

First, scenarios were developed based on the hypothesis that current dredged levels are maintained; that is, in spite of changes in

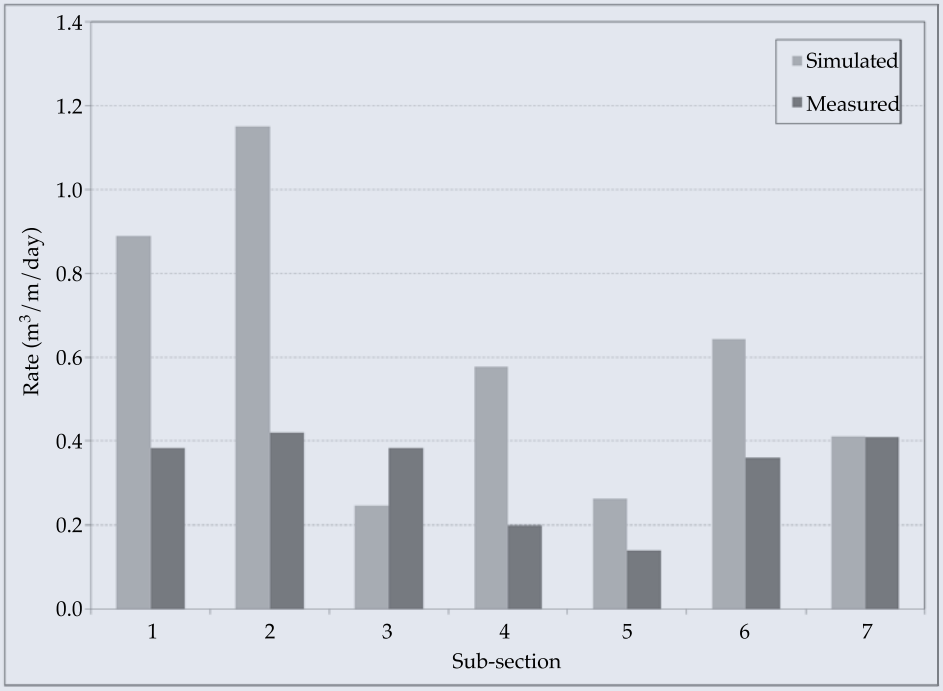

Figure 12. Comparison between calculated and maintenance dredging sedimentation rates (per unit of channel length).

mean flow, no changes were presumed in the reference level for defining the required water depth. This represents a situation in which the navigation management authority assumes no hydrological change. The results presented in Figure 13 show that the sedimented volume increases as the flow increases and vice versa, and that in absolute values, its relative rate of change is significantly greater than that of the flow, and increase with increased changes in flow.

Second, scenarios were considered in which the dredged level was adjusted to reflect the change in the reference level to define the required water depth according to the change in the mean flow (in this case the management authority would modify the regulations according to observed hydrological changes). This reference level was assumed to vary the same amount as the water level associated with the mean flow. These results are presented in Figure 14, which now shows an opposite trend; that is, the sedimented volume increases when the mean flow decreases (and vice versa), since the corresponding decrease in the water depth requires increasing the depth of the navigable channel, thereby increasing sedimentation. The relative rate of change in sedimentation is now, in absolute values, only slightly higher than that of the flow. For increases in flow over 10% of the mean flow, dredging would no longer be necessary in some of the sub-sections.

Conclusions

Los cambios hidrológicos que resulten The hydrological changes resulting from climate change will be observed through changes in the sedimentation rate in navigation channels, which will be indicative of the amount of dredging needed to keep them operating. To quantify the effects of hydrological changes, numerical modeling needs to be used as a method to calculate that sedimentation, as was presented in a relatively detailed manner by this work.

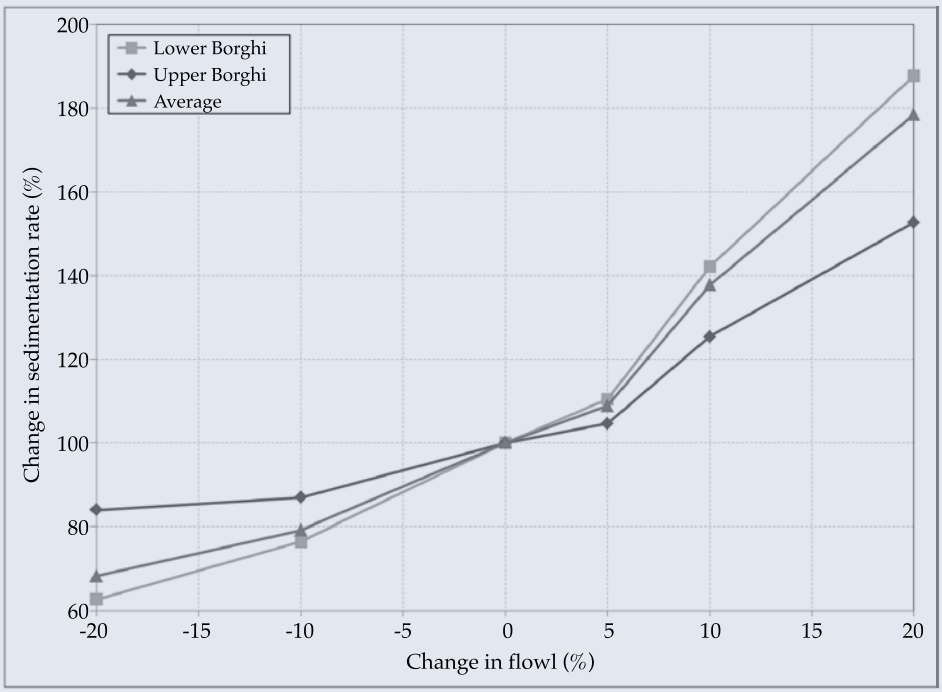

Figure 13. Change in sedimentation rate maintaining the dredged level.

This methodology was illustrated by its application to a passage (Borghi) in the Parana River, Argentina. The results were shown to satisfactorily agree with data from maintenance dredging without the use of calibration. With calibration, nearly complete quantitative agreement could be obtained by adjusting the incidence angle according to the current.

Since there are no clear predictions for the trend in the distribution of precipitation (and therefore of the flows of rivers) in the Plata Basin as a result of climate change effects, potential positive and negative changes in flow were considered for possible future scenarios. The results show that the rate of change in sedimentation is, in absolute values, always greater than that of flow. Specifically, if the current dredging levels were maintained (that is, if the regulations were not modified according to hydrological changes), the sedimented volume would increase as the flow increases and vice versa. Its relative rate of change, in absolute values, would be significantly greater than that of flow, and would increase with increased flow. On the other hand, if the dredged levels were adjusted to modify the regulations according to hydrological changes, the trend would be reversed; that is, the sedimented volume would increase as the mean flow decreases (and vice versa); the relative rate of change of the sedimentation would now be only slightly higher than that of flow, in absolute values.

For all of the scenarios, the morphology of the river was considered to not be affected by changes in flow. This effect, which is outside the scope of the present work, could be evaluated separately.

Acknowledgements

The research that provided these results was financed by Framework Programme No. 7 of the European Community (FP7/2007-2013), project number 212492 (*CLARIS LPB: A Europe-South America Network for Climate Change Assessment and Impact Studies in La Plata Basin)* . The Re-dredging

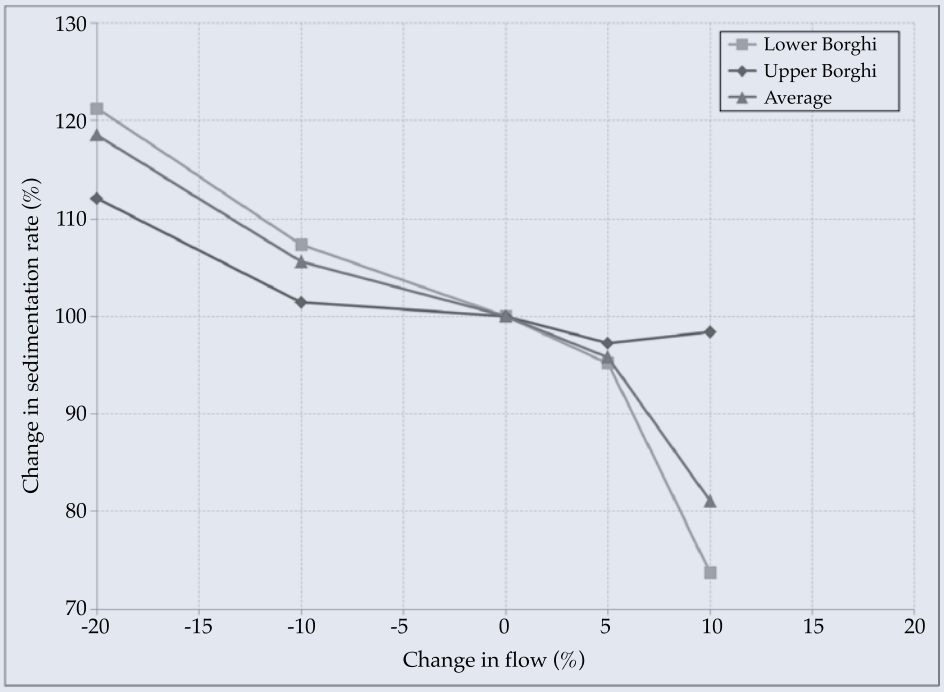

Figure 14. Change in sedimentation rate adjusting the reference dredging level .

and Signage Licensing Control Board (Órgano de Control de Concesiones de Redragado y Señalización) of the Sub-Secretary of Ports and Navigable Routes (SSPyVN) provided the information related to dredged volumes and bathymetric surveys, and the Civil Engineering Department-Hydraulic Sections of the University of Bolonia, Italy (DISTART-UNIBO) provided bathymetric information.

Received: 13/01/12
Accepted: 22/04/13

References

BARROS, V.R., CLARKE, R., and SILVA, P. *Introduction in Climate Change in La Plata Basin*. Buenos Aires: Ed. CIMA-CONICET/UBA, 2006, pp. 8-14.

CASTRO, S.L., CAFARO, E.D., GALLEGO, M.G., RAVELLI, A.M., ALARCÓN, J.J., RAMONELL, C.G., and AMSLER, M.L. *Evolución Morfológica del Cauce del Río Paraná en Torno a Rosario (km 456-406)*, Congreso Nacional del Agua (Conagua, 2007), Tucumán, Argentina, mayo, 2007.

DE WIT, M.J.M., VAN DEN HURK, B., WARMERDAM, P.M.M., TORFS, P.J.J.F., ROULIN, E., and VAN DEURSEN, W.P.A. Impact of climate change on low-flows in the river Meuse. *Climatic Change*. Vol. 82, No. 3-4, 2007, pp. 351-372.

EXNER, F.M. *Über die Wechselwirkung Zwischen Wasser und Geschiebe in Flüssen*, Sitzen berichte der Academie der Wissenschaften. Viena, Austria, Sec. IIA, 1925, pp. 134-199.

FREDSOE, J. *Sedimentation of River Navigation Channels*. *Journal of the Hydraulics Division*. New York: ASCE, February, 1978, pp. 223-236.

GUERRERO, M., NONES, M., SAURRAL, R., MONTROULL, N., SZUPIANY, R.N. Parana River sediment dynamics in the context of climate change. International *Journal of River Basin Management*. Special issue Impact Assessment of Climate Change on La Plata BasinWater resources (submitted, 2013).

GUERRERO, M., SZUPIANY, R.N., and AMSLER, M. Comparison of acoustic backscattering techniques for suspended sediments investigation. *Flow Measurement and Instrumentation*. No. 22, 2011, pp. 392-401.

HAWKES, P.J., PAULI, G., MOSER, H., ARNTSEN, Ø.A., GAUFRES, P., MAI, S., and WHITE, K. Impacts of climate change on waterborne transport. *Civil Engineering*. Vol. 163, 2010, pp. 55-63.

KAZIMIERSKI, L.D., RE, M. y MENÉNDEZ, A.N. *Sedimentación en canales de navegación: Paso Borghi*. Ezeiza, Argentina: Informe INA-CLARIS 01, 2012, Disponible en *World Wide Web*: http://laboratorios.fi.uba.ar/lmm/informes/SedimentacionPasoBorghi_2012.pdf.

MANGINI, S., PRENDES, H.H., HUESPE, J., and AMSLER, M. The importance of flocculation for suspended load sedimentation in the Paraná River, Argentina. *Hydraulic Engineering in Mexico*. Vol. 18, No. 3, July-September, 2003, pp. 55-69.

MENÉNDEZ, A.N. Sistema HIDROBID II para simular corrientes en cuencos. *Revista Internacional de Métodos Numéricos para Cálculo y Diseño en Ingeniería*. Vol. 6, núm. 1, 1990, pp. 25-36.

MENÉNDEZ, A.N. Simulación numérica de la sedimentación en canales de navegación. Informe LHA-INCYTH 102-001-92. Ezeiza, Argentina: INA, febrero, 1992.

MENÉNDEZ, A.N. Simulación numérica de la sedimentación en canales de navegación. *Información Tecnológica. Revista Latinoamericana*. Vol. 5, núm. 4, Chile, 1994.

MENÉNDEZ, A.N. *A Methodology to Scale Turbidity Plumes*. 2nd Int. Conf. New Trends in Water and Environmental Engineering for Safety and Life: Eco-compatible Solutions for Aquatic Environments, Capri, Italy, June, 2002.

MILLERD, F. The potential impact of climate change on Great Lakes international shipping. *Climatic Change*. Vol. 104, 2011, pp. 629-652.

NONES, M., DI SILVIO, G., GUERRERO, M., PASTORELLO, L. 1-D long term simulation of the Paraná River morphodynamics in the light of climate variability. *Proceedings of River Flow 2012*. Costa Rica, September 2012, Vol. 1, pp. 769-774, CRC Press/Balkema, Taylor & Francis Group, London, UK, 2012.

PIANC. *Waterborne Transport, Ports and Waterways: A Review of Climate Change Drivers, Impacts, Responses and Mitigation*. Report of PIANC EnviCom Task Group 3, Climate Change and Navigation. Brussels: World Association for Waterborne Transport Infrastructure, 2008.

ROYAL BOSKALIS AND BALLAST HAM DREDGING. *Ruta de Navegación de Ultramar San Martín-Océano*. Informe para la Licitación del Dragado de la Vía Navegable. Buenos Aires: Dirección de Vías Navegables, 1992.

SAURRAL, R.I. The Hydrologic Cycle of the La Plata Basin in the WCRP-CMIP3 Multimodel Dataset. *Journal of Hydrometeorology*. Vol. 11, No. 5, October, 2010, pp. 1083-1102.

SUNG, R.Y.J., BURN, D.H., SOULIS, E.D. A Case Study of Climate Change Impacts on Navigation on the Mackenzie River. *Canadian Water Resources Journal*. Vol. 31, No. 1, 2006, pp. 57-68.

SZUPIANY, R., HERNÁNDEZ, J., AMSLER, M., FORNARI, E., PARSONS, D., BEST, J.L., and TRENTO, A. *Comportamiento hidro-sedimentológico en bifurcaciones de un gran río*. XXIV Congreso Latinoamericano de Hidráulica, Punta del Este, Uruguay, Noviembre, 2010.

VAN RIJN, L.C.J. *Mathematical modelling of morphological processes in the case of suspended sediment transport*. Delft: Delft Hydraulic Communication 382, 1987.

VAN RIJN, L.C.J. Sedimentation of dredged channels and trenches. In: *Handbook of Coastal and Ocean Engineering*. John B. Herbich (editor). Chap. 9, Vol. 2, 1991, pp. 615-618.

VERHAAR, P.M., BIRON, P.M., FERGUSON, R.I., and HOEY, T.B. Numerical modelling of climate change impacts on Saint-Lawrence River tributaries Earth Surf Process. *Landforms*. Vol. 35, 2010, pp. 1184-1198.

Institutional Address of the Authors

Ing. Mariano Re
Leandro David Kazimierski
Dr. Ángel Nicolás Menéndez

Instituto Nacional del Agua
Laboratorio de Hidráulica
Au. Ezeiza-Cañuelas, tramo Jorge Newbery
Km 1620, Ezeiza, Buenos Aires, Argentina
Teléfono: +54 (11) 4480 4500
m.re@ina.gov.ar
leandrokaz@gmail.com
angel.menendez@speedy.com.ar

Universidad de Buenos Aires
Facultad de Ingeniería
Laboratorio de Modelación Matemática
Av. Las Heras 2214, 3er. piso
Buenos Aires, Argentina
Teléfono: +54 (11) 4514 3016

Click here to write the autor

Main Canal Imperial de Aragón, Spain.

Photo provided by Raúl Rivas Pérez.

Robust Fractional Order Controller Implemented in the First Pool of the Imperial de Aragón Main Canal

• Raúl Rivas-Pérez* •
Universidad Politécnica de La Habana "José Antonio Echeverría", Cuba
*Corresponding Author

• Vicente Feliu-Batlle • Fernando Castillo-García • Luis Sánchez-Rodríguez •
Universidad de Castilla-La Mancha, España

• Antonio Linares-Sáez •
ABEIMA, S.A., ABENGOA, España

Abstract

RIVAS-PÉREZ, R., FELIU-BATLLE, V., CASTILLO-GARCÍA, F., SÁNCHEZ-RODRÍGUEZ, L. & LINARES-SÁEZ, A. Robust Fractional order Controller Implemented in the First Pool of the Imperial de Aragón Main Canal. *Water Technology and Sciences* (in Spanish). Vol. V, No. 1, January-February, 2014, pp. 23-40.

This paper presents the design of a robust fractional order controller —which we denote as *FPI* controller since it can be regarded as a generalization of the standard *PI* controller— for effective control of water distribution in irrigation main canal pools characterized by time-varying dynamical parameters. Interest in such robust fractional order controller is justified by the fact that dynamical parameters of irrigation main canal pools may change drastically according to their operating discharge regimes. The *FPI* controller designed was installed in a *PLC SIMATIC S-7 300*, and was real-time implemented in the first pool of the Imperial de Aragon main canal, belonging to the Ebro Hydrographical Confederation (Spain). Real-time experiments were carried out with equivalent —in the sense of exhibiting the same closed loop dynamics for the nominal plant specifications— *FPI* and *PI* controllers. They showed a better performance and robustness of the *FPI* controller when large canal parameters variations were produced, that which facilitates to achieve a bigger speed of response, to satisfy in an operative way the demands of the users, as well as to minimize the losses for concept of operation of the available hydraulic resources.

Keywords: robust fractional order controller, real-time implementation, irrigation main canal, large time-varying dynamical parameters, efficient management of hydraulic resources.

Resumen

RIVAS-PÉREZ, R., FELIU-BATLLE, V., CASTILLO-GARCÍA, F., SÁNCHEZ-RODRÍGUEZ, L. & LINARES-SÁEZ, A. Controlador robusto de orden fraccional implementado en el primer tramo del canal principal Imperial de Aragón. Tecnología y Ciencias del Agua. Vol. V, núm. 1, enero-febrero, 2014, pp. 23-40.

En el presente trabajo se desarrolla el diseño de un controlador robusto de orden fraccional —el cual se denota como FPI*, debido a que constituye una generalización del controlador* PI *convencional— para el control efectivo de la distribución de agua en canales principales de riego caracterizados por presentar una amplia variación en sus parámetros dinámicos. El interés en esta clase de controladores se justifica por hecho de que la dinámica de los canales principales de riego puede cambiar de forma drástica con las variaciones de sus regímenes de descargas. El controlador* FPI *desarrollado se programó en un* PLC SIMATIC S-7 300 *y se implementó en tiempo real en el primer tramo del canal principal Imperial de Aragón, perteneciente a la Confederación Hidrográfica del Ebro, España. Se realizaron experimentos comparativos de funcionamiento en tiempo real del controlador* FPI *diseñado con otro controlador* PI *equivalente, en el sentido de exhibir ambos el mismo comportamiento dinámico en lazo cerrado para las especificaciones temporales de la planta nominal. Los resultados obtenidos de estos experimentos demuestran que cuando los parámetros dinámicos del tramo del canal presentan una amplia variación, el controlador* FPI *exhibe una mayor robustez, lo cual posibilita lograr una mayor velocidad de respuesta, satisfacer de forma operativa las demandas de los usuarios y minimizar las pérdidas por concepto de operación de los recursos hidráulicos disponibles.*

Palabras clave*: controlador robusto de orden fraccional, implementación práctica en tiempo real, canal principal de riego, parámetros dinámicos variables en el tiempo, uso eficiente de recursos hidráulicos.*

Introduction

Experience worldwide has shown that an important way to increase the effectiveness and efficiency of water distribution in main irrigation canals is to apply effective systems to automate control and assist with decision-making. These enable obtaining a strict correspondence between demand by various users and delivery of these resources, as well as reducing water loss due to operations as much as 90% (Clemmens, 2006; Feliu-Batlle *et al*., 2007; Kovalenko, 1983; Litrico and Fromion, 2009; Rivas-Pérez *et al*., 2003).

El objetivo fundamental del desarrollo e implementación práctica de sistemas efectivos de control automático de la distribución de agua en los canales principales de riego consiste en satisfacer, a pesar de las incertidumbres, las demandas de agua de los diferentes usuarios, garantizando que los volúmenes de agua extraídos desde la fuente de abasto se correspondan con las necesidades reales, así como que se minimicen las pérdidas por concepto de operación en todo el canal (Buyalski *et al*., 1991; Kovalenko, 1983; Rivas-Pérez, 1990).

The main objective of developing and implementing effective automated control systems to distribute water in main irrigation channels is to satisfy the water demands by the different users, in spite of uncertainty, thereby ensuring that water volumes extracted from the supply source correspond to actual needs, while also minimizing losses throughout the canal during operations (Buyalski *et al*., 1991; Kovalenko, 1983; Rivas-Pérez, 1990).Research conducted in different main irrigation canals shows that dynamic parameters vary widely when changes occur in discharge in the operating range [$Q_{mín}$, $Q_{máx}$] and /or in other hydraulic parameters (Corriga *et al*., 1989; Litrico and Fromion, 2009; Montazar *et al*., 2005; Rivas-Pérez *et al*., 2007). This type of canal is described as canals with time-varying dynamic parameters (Litrico *et al*., 2006; Rivas-Pérez *et al*., 2008b). Therefore, any controller that is designed should have a robust behavior in response to these types of variations (Deltour and Sanfilippo, 1998; Feliu-Batlle *et al*., 2009a; Litrico *et al*., 2006).

PID (proportional-integral-derivative) controllers are the most commonly used and are widespread in automation control systems for water distribution in main irrigation canals (Buyalski *et al*., 1991; Clemmens and Schuurmans, 2004; Litrico and Fromion, 2009; Malaterre *et al*., 1998; Schuurmans *et al*., 1999). Nevertheless, different studies show that when the main irrigation canals are subject to time-varying dynamic parameters, the application of conventional PID controllers is not effective because it results in a significant increase in establishment time and maximum peak of the response time of the control system. This decreases the effectiveness of water distribution in the canals, thereby resulting in the loss of the available water resources due to operations (Clemmens and Schuurmans, 2004; Litrico and Fromion, 2009; Feliu-Batlle *et al*., 2009b; Rivas-Pérez *et al*., 2002; Wahlin, 2004). Therefore, investigations related to the development of robust controllers for water distribution in main irrigation canals is of high scientific, technical and practical interest (Litrico and Fromion, 2009; Wahlin and Clemmens, 2006). The design of this type of controllers is a challenge and a crucial problem to improving the effectiveness and efficiency of water distribution in main irrigation canals.

In recent years, as result of improved understanding of fractional calculus and the market availability of a new electronic circuit known as fractal, fractional operators have been applied with satisfactory results to model and control processes with complex dynamic behavior, including processes with distributed parameters (Chen *et al*., 2004; Machado, 1997; Petras, 2002; Podlubny, 1999a; Vinagre *et al*., 2000). Fractional calculus is a field of mathematics involving non-whole (arbitrary) derivatives and integers, and generalizes standard differentiation and integration concepts (Podlubny, 1999a).

The application of fractional order controllers (FOC) enables broadening the control actions that can be developed for a variety of plants and/or processes, as well as contributing to the effective automation of processes whose dynamic behavior is described using non-whole models without using approximations (Podlubny, 1999a). One of the advantages of this type of controllers is that it makes it possible to design robust control systems for plants with dynamic parameters that vary widely or those subject to large disturbances (fluctuations in load), as well as for plants with long delay times, thereby maintaining the stability of the control system and providing simple, practical implementation (Feliu-Batlle *et al.*, 2009b; Monje *et al.*, 2004; Vinagre *et al.*, 2000).

The qualitative behavior of the PID controllers can be improved considerably by their generalization with a $PI^{\alpha}D^{\lambda}$ fractional order controller, which involves an α order integrator and a λ order differentiator (Podlubny, 1999b). Therefore, the use of $PI^{\alpha}D^{\lambda}$ controllers has been proposed and has received considerable attention (Barbosa *et al.*, 2004; Castillo *et al.*, 2010; Chen *et al.*, 2006; Djouambi *et al.*, 2005; Leu *et al.*, 2002; Monje *et al.*, 2004; Petras *et al.*, 2003; Podlubny *et al.*, 2002; Rivas-Pérez *et al.*, 2012; Wang *et al.*, 2005).

Works have recently been reported about the application of fractional order controllers to control water distribution in main irrigation canals (Castillo-García *et al.*, 2013; Feliu-Batlle *et al.*, 2011, 2009a, 2009b, 2007; Monje *et al.*, 2004; Rivas-Pérez *et al.*, 2008c; Sánchez *et al.*, 2007). Nevertheless, the results they offer are generally theoretical and not implemented in main irrigation canals that are in operation.

Different authors have reported that even though the problem with designing effective control systems for the distribution of water in main irrigation canals has been the object of many scientific publications, only a small number of these controllers has been successfully implemented in real-world conditions (Clemmens and Schuurmans, 2004; Litrico and Fromion, 2009; Schuurmans *et al.*, 1999; Wahlin and Clemmens, 2006).

The PI (proportional integral) controller is most often used to control the distribution of water in main irrigation canals because it is easier to correctly adjust than a PID, and the derivative portion of the PID is very sensitive to the noise of sensors, which creates problems with the stability of the control system (Baume *et al.*, 1999; Burt *et al.*, 1998; Rivas-Pérez *et al.*, 1998). The methods normally used to adjust the parameters of these controllers is trial and error (Deltour and Sanfilippo, 1998; Seatsu, 1999; Whalin and Clemmens, 2006), or optimization (Clemmens and Schuurmans, 2004). These methods generally are based on mathematical models for the nominal plant and do not take into account that the dynamic parameters of main irrigation canals can vary widely due to change in discharge and/or other hydraulic parameters. Therefore, PI controllers easily become unadjusted or can even cause instability in a control system (Litrico *et al.*, 2006; Rivas-Pérez *et al.*, 2007). Thus, the work herein explores the possible advantages of a FPI fractional order regulator versus a conventional PI regulator in terms of their robustness when the dynamic parameters of the canal vary and disturbances are present.

The objectives of this work include: a) the development of a robust fractional order FPI to effectively control the distribution of water in a section of a main irrigation canal (whose dynamic parameters vary widely). This enables decreasing establishment time and the maximum peak of the response time of the control system, which results in increasing the efficiency of water distribution, thereby reducing losses in the available water resources due to operations. And b) the practical implementation and validation of the designed FPI controller in the first section of the main Imperial de Aragón canal.

This work considers that it is possible to develop effective, decentralized control systems to distribute water in main irrigation canals by designing robust, independent

fractional order controllers for each section of the canal, with the addition of decouplers, in order to minimize the interaction between adjacent sections (Litrico and Fromion, 2009; Schuurmans *et al.*, 1999; Wahlin and Clemmens, 2006). Thus, this work focuses on the design of a FPI controller for one section of the main irrigation canal. Future investigations will analyze the problem to effectively control the distribution of water in adjacent sections or in entire canals with fractional order controllers.

The main contribution of this work is the practical implementation and validation (for the first time) of a robust fractional order controller (FPI) for water distribution in a section of a main irrigation canal that is in operation (first section of the main Imperial de Aragón canal), with very satisfactory results. This contribution offers a practical and relatively simple solution to the complex problem of designing robust controllers to distribute water in main irrigation canals with imprecise dynamic behavior (large amount of uncertainty) and demonstrates that the fractional order controllers (FOC) offer better results than conventional controllers (PI) for this type of application.

The results obtained are part of a research project conducted by the Castilla-La Mancha University and the Ebro Hydrographic Confederation (Spain) to model and control water distribution in the main Imperial de Aragón canal.

The work is organized as follows. A mathematical model is developed, aimed at controlling the dynamic behavior of the first section of the main canal of the Imperial de Aragón. The design is developed for the frequency domain of a robust fractional order controller (FPI) and a PI control with the same response time specifications for section of the canal under study based on a nominal operating regime. The experimental results from the implementation are analyzed for both controllers (FPI and PI) in the first section of the main Imperial de Aragón canal. Finally, the conclusions from the work are presented.

Mathematical Modeling to Control a Section of a Main Irrigation Canal

The need for mathematical models that adequately describe the more relevant dynamic behaviors in main irrigation canals is one of the difficulties of designing and implementing effective control systems for water distribution in main irrigation canals (Litrico and Fromion, 2009; Kovalenko, 1983; Rivas-Pérez *et al.*, 2008a). This type of models offers valuable information about the properties of dynamic systems, such as their response time, delay time, time constants, crossover frequency and maximum peak, among others.

The mathematical modeling of the dynamic behavior of main irrigation canals is usually performed using Saint-Venant equations, which are based on classical laws of conservation of mass and momentum (Chow, 1988; Kovalenko, 1983; Rivas-Pérez *et al.*, 2003). They represent non-linear equations with partial hyperbolic derivatives and complex restrictions and, therefore, their direct use in designing control systems presents serious difficulties (Litrico and Fromion, 2009). This leads to the need to obtain simple mathematical models for main irrigation canals that enable their direct application in the design of effective control systems.

Linear models are usually sufficient for capturing the primary dynamic properties of main irrigation canals needed to design control systems (Litrico and Fromion, 2009; Rivas-Pérez *et al.*, 2007). This type of model can be obtained by applying system identification tools (Rivas-Pérez *et al.*, 2011). The identification of systems makes it possible to obtain simple mathematical models that adequately describe the dynamics of complex plants for use in designing effective control systems (Ljung, 1999).

A typical main irrigation canal is made up of different sections separated by gates that are used to regulate the distribution of water in a section (see Figure 1 which shows a diagram of the first section of the Imperial de Aragón main canal). The opening of the gates varies

in order to maintain a determined water profile throughout the section. In general, in an automatically controlled main irrigation canal (by regulating water downstream with a remote level sensor), the controlled variable is the water level $y_i(t)$ measured at the end of the section, the controlling variable is the position of the gate $u_i(t)$ upstream and the main disturbances are lateral discharges , $q_i(t)$, where $i = 1, 2, ..., n$ is the number of the canal section (Kovalenko, 1983; Malaterre *et al*., 1998).

The data and results reported in this work were obtained from section 1 (origin) of the main Imperial de Aragón canal, known as Bocal. This canal is part of the Ebro Hydrographic Confederation, which is the largest hydrographic confederation on the Iberian peninsula (Pedregal *et al*., 2009). This canal receives its water from the Ebro River diversion.

The Bocal is 8 kilometers long with a depth between 3.1 and 3.6 meters, and a width between 15 and 26.9 meters. Its maximum flow (discharge) is $Q(t)$ = 30 m^3/s throughout its length. Figure 2 presents an upper view of a segment of the Bocal, showing large volumes of water transported through this section of the canal.

The level of water in the Bocal is controlled by 10 submerged gates by regulating water downstream with a remote level sensor. These gates are located in an enclosure called the Gate House. The measurements available for the Bocal include the water level upstream (Ebro River), $y_R(t)$, water level downstream, $y_{11}(t)$, remote water level downstream, $y_{12}(t)$ and the position (opening) of the gates upstream, $u_1(t)$. Figure 1 shows the 10 gates located in the Gate House through a single equivalent gate (Rivas-Pérez *et al*., 2008a).

In order to obtain the mathematical model to describe the dynamic behavior of the water distribution in the Bocal (plant), experiments were conducted using a stepped response. To this end, the position of the gates downstream remained fixed. The opening of four gates upstream was simultaneously increased 25 cm, equivalent to a total increase of 100 cm. The change in the remote water level of the water downstream was measured. The resulting response time of the dynamic behavior of the Bocal is presented in Figure 3.

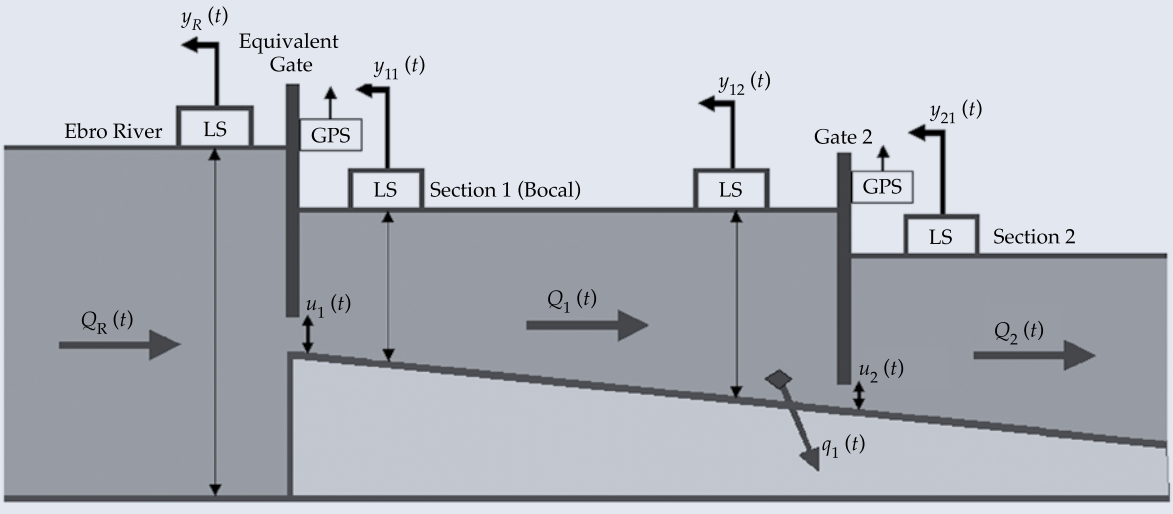

LS = Level Sensor.
GPS = Gate Position Sensor.

Figure 1. Diagram of Section 1 (Bocal) of the main Imperial de Aragón Canal.

This response shows that the dynamic behavior of the distribution of the water in the Bocal can be represented using the following second order transfer function with a time delay:

$$G(s) = \frac{\Delta y_{12}(s)}{\Delta u_1(s)} = \frac{K}{(T_1 s + 1)(T_2 s + 1)} e^{-\tau s} \qquad (1)$$

where $\Delta y_{12}(s)$ is the change in the remote water level downstream; $\Delta u_1(s)$ is the change in the opening of the equivalent gate; K is the static gain, T_1, T_2 are time constants and τ is the time delay. T_1 is taken as the predominant time constant (the largest, associated with the dynamics of the section of the canal), and T_2 is the smaller time constant which represents the secondary dynamic (motor + gate + level sensor). T_2 is usually much smaller than T_1 (Rivas-Pérez *et al*., 2007).

When the discharge $Q_1(t)$ through the gates upstream of the Bocal correspond to the nominal operating regime $Q_1(t) = Q_{nom}$, the nominal values of the parameters of the mathematical model (1) (nominal plant) are obtained. These parameters are represented as K_0, T_{10}, T_{20}, t_0, and their values are $K_0 = 0.055$, $T_{10} = 880.79$ s, $T_{20} = 81.27$ s, $t_0 = 360$ s. The results from validating the nominal linear model are presented in Figure 4, which shows good correspondence between the measured output and the predictions resulting from this model.

Figure 2. Upper View of a portion of the Bocal.

Nevertheless, when the discharge $Q_1(t)$ through the gates upstream from the Bocal do not correspond to the nominal operating regime, $Q_1(t) \neq Q_{nom}$,and present variations in the operating range $[Q_{min}, Q_{max}]$ changes result: in the water volume that accumulates in the section of the canal between minimum and maximum discharge; in the water level of waters downstream in the range $[H_{min}, H_{max}]$; as well as in the flow propagation, which is determined according to the celerity of the wave (C) and mean flow speed (V) (Chow, 1988; Kovalenko, 1983). As a result, the dynamic parameters of the Bocal vary widely (parametric uncertainties of the model):

$$\begin{aligned} 0.01 &\leq K(t) \leq 0.16 \\ 600 &\leq T_1(t) \leq 3\,000 \\ 50 &\leq T_2(t) \leq 200 \\ 300 &\leq \tau(t) \leq 360 \end{aligned} \qquad (2)$$

Therefore, any controller that is designed for the Bocal must guarantee, *a priori*, a specific level of minimum behavior for the entire range of variations in its dynamic parameters (uncertainties of the model). This is the problem when designing controllers with robust behavior.

Design of the Robust Fractional Order Controller (*FPI*)

This section describes the design in the frequency domain of a robust fractional order controller, *FPI*, for the distribution of water in the section of the main canal studied under nominal behavior. As previously mentioned, this controller can be considered to be a generalization of the PI controller. In addition, the robustness properties of the FPI controller are compared to those of a conventional, equivalent PI controller.

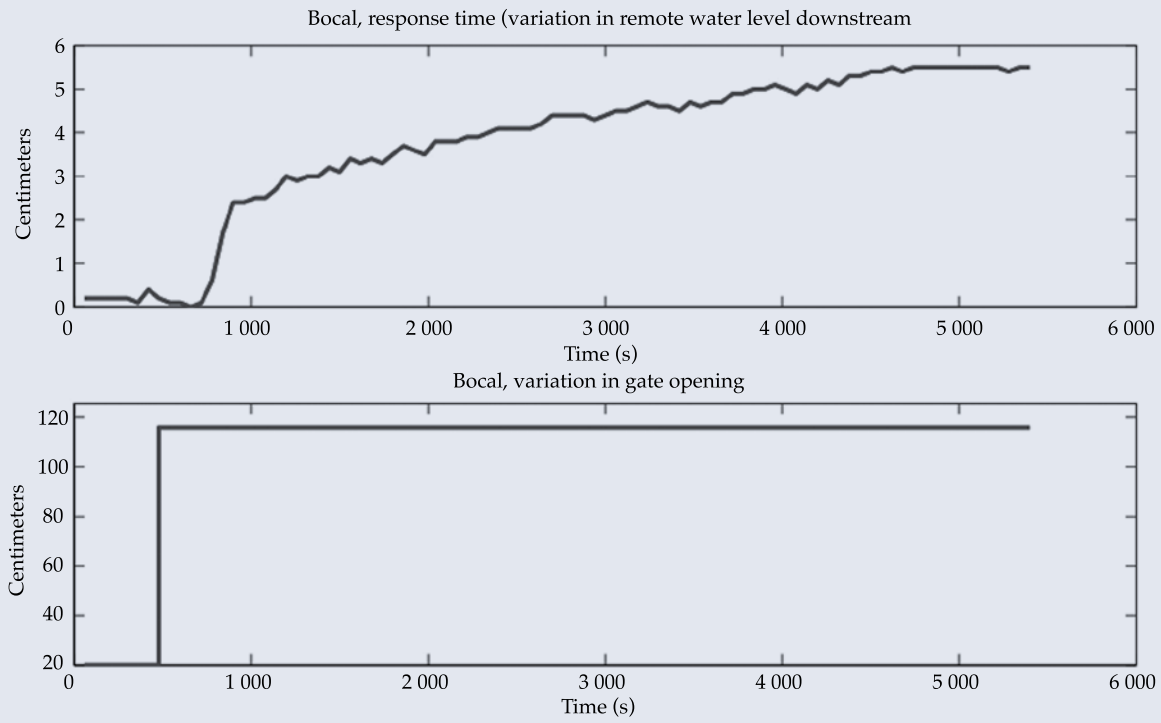

Figure 3. Time Response of the Bocal with a step signal for the gates upstream.

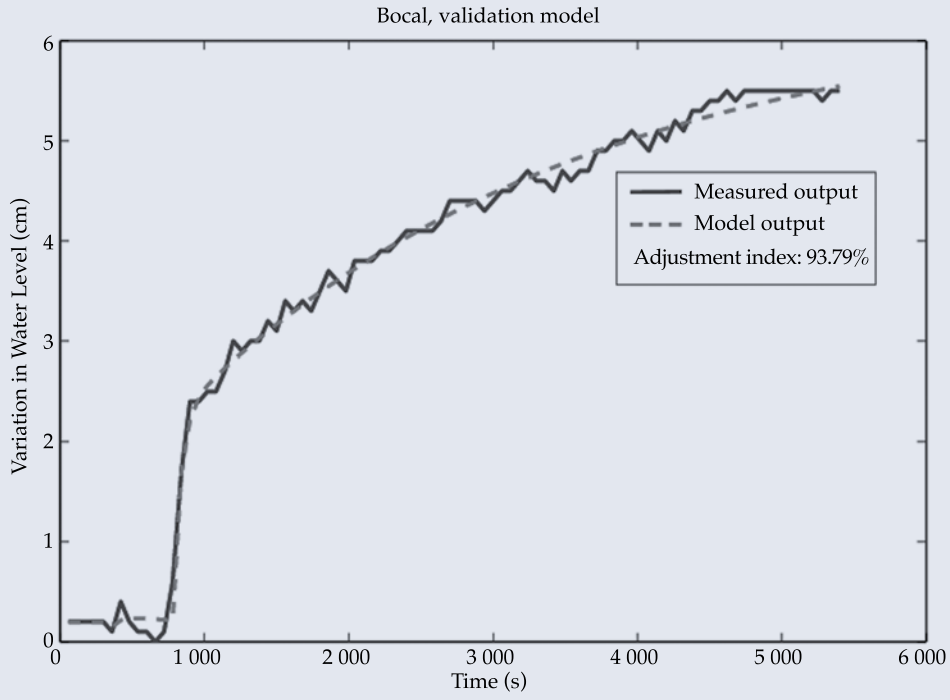

Figure 4. Results from Validating the Nominal Mathematical Model for the Water Distribution in the Bocal.

A *PI* controller was implemented in the Bocal. The advantages of this controller include its easy adjustability (tuning) and obtainment of an error when the regime is continuously null as a result of stepped changes in the reference, or step disturbances. As mentioned previously, the difficulty with these controllers is that they are very sensitive to changes in the dynamic parameters of the canal, they easily become unadjusted and can even destabilize the control system (Litrico and Fromiom, 2009; Rivas-Pérez, 1990).

The approach developed by this work includes designing a controller that exhibits the same behavior as a *PI* under the nominal dynamic behavior of the Bocal; that is, it is designed for the same specifications but with less sensitivity to changes in the dynamic parameters of the plant and, therefore, is more robust. Our innovate proposal consists of using an *FPI* fractional order controller, in which the α fractional order of the controller provides additional freedom by making it possible to increase robustness and obtain prefixed frequency behaviors. Therefore, our objective is to obtain a controller that behaves in a manner similar to the PI under a nominal regime and provides a better response time by the control system when changes occur in the discharge through the gates upstream from the Bocal, in the operating range [Q_{min}, Q_{max}], and/or when there are variations in other hydraulic parameters.

The *FPI* controller proposed is represented by the following transfer function:

$$R_{FPI}(s) = K_p \frac{1 + T_d s^{\alpha}}{s} \qquad (3)$$

where:

$$s^{\alpha} = (j\omega)^{\alpha} = \omega^{\alpha} e^{\frac{j\pi}{2}\alpha} \qquad (4)$$

$$0 \le \alpha \le 2$$

Note that the FPI controller (3) becomes a conventional PI controller when the fractional order parameter α = 1. This type of controller requires adjusting three parameters, K_p, T_d and α; that is, one more parameter than the conventional PI controller. The α fractional order parameter is used to meet the additional specification for the robust behavior of the control system.

Figure 5 shows the block diagram for the fractional order control system for the water distribution proposed for the Bocal. This diagram took into account disturbance $D(s)$, which represents lateral discharge from the section $q_i(t)$ (see Figure 1) and is modeled using a step signal that passes through a first order filter with the time constant $T_3 = 70$ s.

The method proposed to design the robust FPI controller is based on the following specifications of the frequency domain: a) the desired phase margin (f_m), which ensures the desired nominal damping of the response time (overdrive (M_p)), as well as the robustness of the control system under variations in delay time; b) crossover frequency of the desired gain (w_c), which ensures the desired nominal speed of the response time of the control system (establishment time (t_s)), *c*) zero error for static state. The last specification requires the controller to include an integer term. The parameters of the controller (3) that meet specifications a) through c) are calculated using the following algebraic procedures developed in the frequency domain.

In terms of the final value theorem (Ogata, 1993), specification c) implies that α > 0. The design specifications a) and b) given by a determined phase margin (f_m) and gain crossover frequency (w_c) can be expressed compactly using the following complex notation:

$$R_{FPI}(j\omega_c)G(j\omega_c) = e^{-(\pi - \phi_m)j} = -e^{j\phi_m} \qquad (5)$$

where $G(jw_c)$ represents the dynamic behavior (1) of the Bocal.

Based on (5), considering equations (3) and (4), we get:

$$R_{FPI}(j\omega_c) = K_p \frac{1 + T_d \omega_c^{\alpha} e^{j\frac{\pi}{2}\alpha}}{j\omega_c} = \frac{-e^{j\phi_m}}{G(j\omega_c)} \quad (6)$$

Considering:

$$(j\omega_c)^{\alpha} = \omega_c^{\alpha}\left(\cos\left(\frac{\pi}{2}\alpha\right) + j\sin\left(\frac{\pi}{2}\alpha\right)\right) \quad (7)$$

From equation (6) we get the control parameters K_p and T_d:

$$K_p = P_r - P_i \cot\left(\frac{\pi}{2}\alpha\right) \quad (8)$$

$$T_d = \frac{P_i}{\omega_c^{\alpha}\left[P_r \sin\left(\frac{\pi}{2}\alpha\right) - P_i \cos\left(\frac{\pi}{2}\alpha\right)\right]} \quad (9)$$

where:

$$P_r = \Re\left(-\frac{j\omega_c e^{j\phi_m}}{G(j\omega_c)}\right) \quad (10)$$

$$P_i = \Im\left(-\frac{j\omega_c e^{j\phi_m}}{G(j\omega_c)}\right) \quad (11)$$

$\Re()$ y $\Im()$ represent the real and imaginary parts of a complex number, respectively.

The design specifications of the *FPI* controller are as follows:

- Gain margin: the parameter that presents the greatest influence on the stability of the closed-loop control system is the static gain (K) of the plant. The results presented in the previous section (2) show that this parameter can vary up to three time the nominal value ($K_{máx} \approx 3\ K_0$).
- Therefore, the parameter α the fractional order *FPI* controller is used to improve the robustness of the control system closed, in the sense of stability to variations in the loop gain *K* of Nozzle; ie, to ensure that the profit margin (M_g) control system reaches its maximum value. In Figure 6 the variation margin depending on the parameter to be displayed. This figure shows that the maximum value of the markup $M_g \approx 4.47$ is achieved with $\alpha \approx 0.77$. This figure shows that the profit margin obtained with $\alpha = 1$ (standard *PI* controller) is $M_g = 3.6$, so that an improvement of 24% is achieved.
- Crossover frequency and establishment time: the establishment time of the opened-

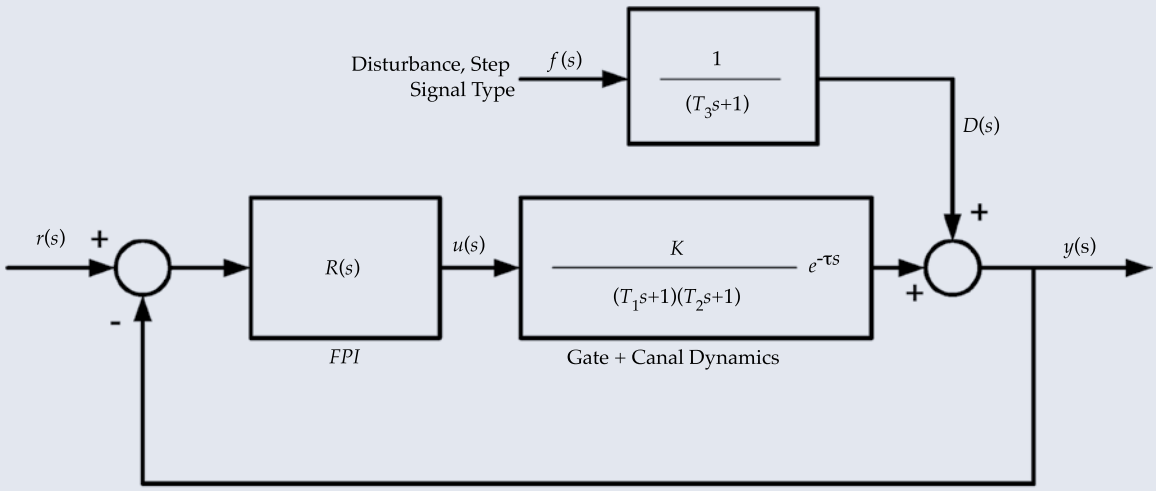

Figure 5. Block Diagram for the Fractional Order Control System for water Distribution in the Bocal

loop nominal plant is approximately $t^0_{OL} \approx 3T_{10} + \tau_0 = 3\,000$ s. It is desired that the closed-loop control system be twice as fast. To this end, the crossover frequency $w_c = 0.0033$ rad/s was chosen, which roughly corresponds to the establishment time $t_s \approx 5/w_c \approx 1\,500$ s. This latter expression is obtained from generally considering from the inverse relationship between the gain crossover frequency and the establishment time (Ogata, 1993).

- Phase margin: a phase margin of $\phi_m = 60^o$ is chosen, which is a standard value for this specification. For second order plants, the damping coefficient ξ is related to the phase margin by the expression $\xi = f_m = 60/100$ when $0 \leq \xi \leq 0.6$. Using the expression $M_p = \exp\left(-\pi\xi / \sqrt{1-\xi^2}\right)$ that relates the maximum overdrive M_p with the damping coefficient for second order plants results in the selected phase margin of $M_p \approx 10\%$, which is acceptable for this type of application. These expressions are often used as reasonable approaches for high-order plants (Ogata, 1993).

Using the design frequency specifications pair (ϕ_m, w_c) and the fractional order parameter α in expressions (8) and (9), the values of the *FPI* and *PI* controller parameters are obtained, represented respectively by the following expressions:

$$R_{FPI}(s) = 0.026\frac{1+255.7\,s^{0.77}}{s} \qquad (12)$$

$$R_{PI}(s) = 0.015\frac{1+134.6\,s}{s} \qquad (13)$$

Simulation Results

In order to confirm that the behavior of the water distribution control system for the Bocal improved, and that the FPI is more robust than the PI controller when there are variations in the dynamic parameters of the Bocal or external disturbances, different simulations of this system were performed with both controllers under the same operating conditions for the canal. Figure 7 and Table 1 present the comparative results obtained from the simulations, showing that when the behavior of the Bocal is nominal (nominal operating regime) both controllers behavior roughly the same. Nevertheless, when variations arise in the discharge of the Bocal in the operating range $[Q_{min}, Q_{max}]$, with the resulting value of the gain being different than that for nominal ($K \in [0.01, 0.16]$), the water level reference (320 cm) is reached much more quickly (less establishment time) and the maximum peak is smaller with the FPI controller than with the PI controller. In addition, the harmful effect of disturbances is more quickly reduced with the FPI controller than with the PI controller. Therefore, the FPI controller makes it possible to increase the effectiveness of the distribution of water in the Bocal and, thus, decrease losses in the available water resources due to operations.

As a consequence, the FPI controller is shown to have significant advantages over the PI controller when needing to control water distribution in a section of a main irrigation canal presenting dynamic time-varying parameters. The *FPI* controller behaves in a more robust manner throughout the range of variation in these parameters.

Results from the Practical Implementation of the *FPI* controller in the Bocal

The feasibility and robustness of the designed FPI controller was demonstrated through its real-time practical implementation in a Siemens SIMATIC S7-300 PLC installed in the control room of the Bocal, which is part of the centralized monitoring and control system of the Ebro Hydrographic Confederation. This PLC is compact (modular) and very powerful. Its real-time response speed is fast, it has high connectivity and offers various conveniences for managing software and hardware. In addition, it is highly immune to interferences produced by motors and can function in adverse conditions such as high temperatures and high humidity.

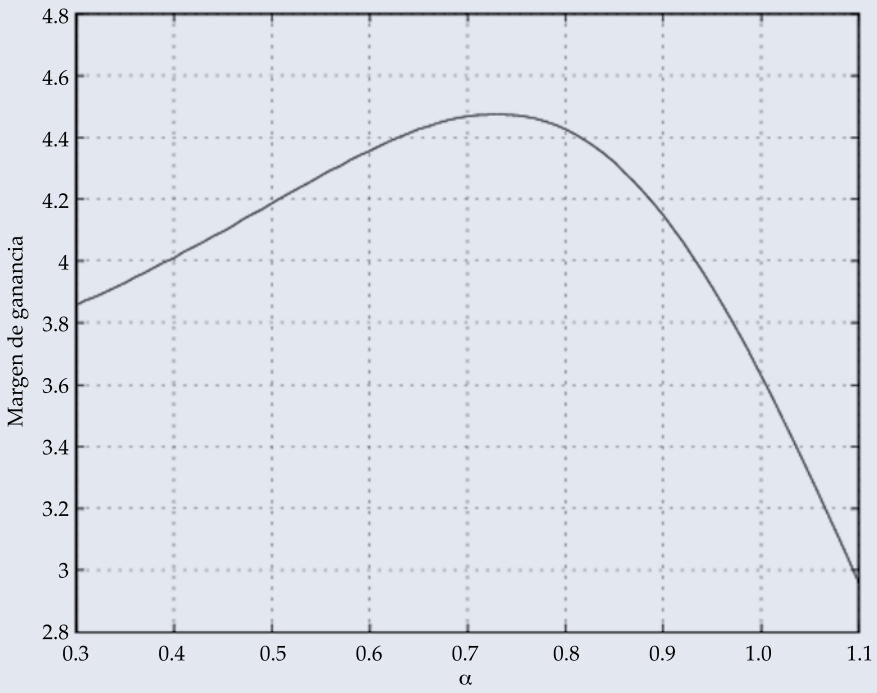

Figure 6. Variation in the Gain Margin of the Water Distribution Control System for the Bocal, as a function of the α parameter.

The PI controller (13) used to control the group of gates upstream from the Bocal (called the pilot regulator) was implemented in the Siemens SIMATIC S7-300 PLC mentioned. This controller sends its control signal $u_{PI}(t)$ to another internal controller (called the organ regulator), which is responsible for the discretization of the control signal $u_{PI}(kT)$ and the obtainment of the positioning (actual opening) of the group of gates upstream (located in the Gate House). Thus, the gates do not continually move and the mechanical wear resulting from ongoing movement is reduced. Figure 8 presents a functional block diagram of the water distribution control system in the Bocal, which shows the interaction between the pilot regulator and the organ regulator.

The designed FPI controller (12) was implemented in parallel with the PI controller (13) in the SIMATIC S7-300 PLC using an AWL program (list of instructions). The fractional order operator of the FPI controller (12) was implemented using an FIR discrete filter (Finite Impulse Response) obtained using its numerical approach based on the definition by Grundwald-Letnikov (Podlubny, 1999a; Vinagre *et al.*, 2000), in combination with the short-memory principle with a series of 500 terms ($N = 500$). The sampling period used was $T = 60$ s, providing enough time for the PLC to generate the control signals.

The criteria followed to implement the FPI controller (12) in the SIMATIC S7-300 *PLC* were: a) modular structure of the executable code routines in such a way that its functioning would have the highest degree of autonomy possible; b) high reliability, introducing into the *PLC* the specific executable code needed to implement the *FPI* controller in parallel with the PI controller; c) simple and quick commutation between *FPI* and *PI* controllers when some type of failure or poor functioning was detected; and d) availability of control signals for both controllers as well as for the controlled variable (remote water level downstream) to monitor and compare the functioning of both

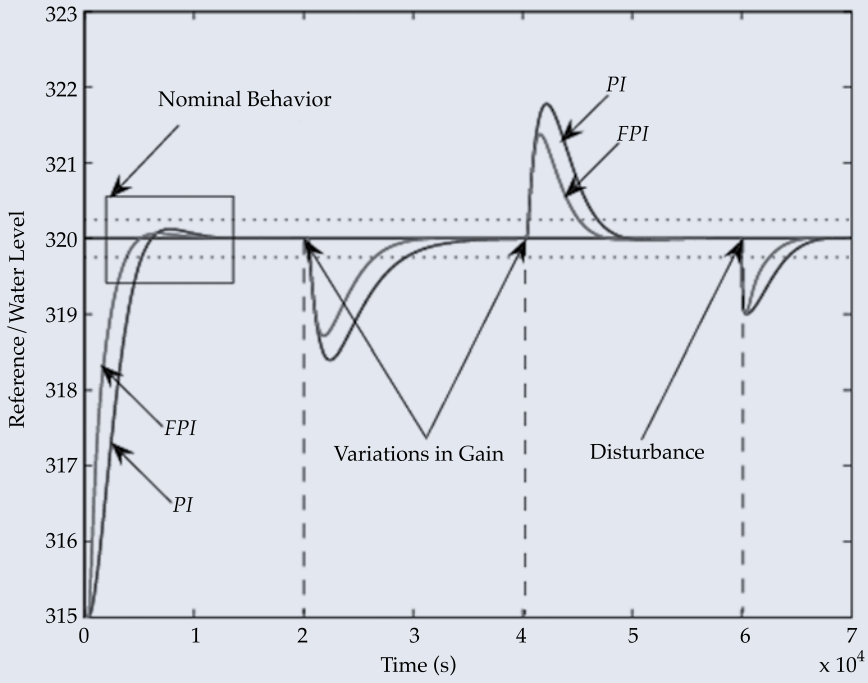

Figure 7. Comparative Simulation Results from the Time-response of the Water Distribution Control System in the Bocal with *FPI* and *PI* Controllers.

Table 1. Comparative Results from the Simulation of the Time-Response of the Water Distribution Control System for the Bocal with *FPI* and *PI* Controllers.

	Nominal Behavior		ΔK = -0.01		ΔK = 0.01		f(s) = -0.3/s	
Controller	M_p (%)	t_s (s)	M_p (%)	t_s (s)	M_p (%)	t_s (s)	M_p (%)	t_s (s)
FPI	0.03	3 480	0.4	6 488	0.3	5 120	0.3	2 500
PI	0.03	4 840	0.6	9 320	0.7	6 844	0.3	4 000

controllers. The executable code of the *FPI* controller (12) contains the following routines:

a) Routine to initialize internal data. This is executed only during start-up of the control system. It generates the weight vectors for the discrete Grundwald-Letnikov approximation as a function of the parameters of the *FPI* (12) controller and the sampling period.
b) Routine for instant sampling. This is executed cyclically. Its function includes choosing one of the two controllers (*FPI* or *PI*) and the instant of time at which to connect.
c) Calculation routine for the control signal. This is executed as requested by the previous routine. It is responsible for calculating the control signal.

Experimental Results

Two cases of comparative experimental results are shown for the real-time functioning of the water distribution control system with FPI and PI controllers in the Bocal. The value of the

Remote Downstream Water Level Reference Signal decreased with the FPI (decrease in the discharge through the gates upstream) and increased with the PI (increase in the discharge through the gates upstream). For each case, an experiment was developed first with the PI controller and then repeated with the FPI controller. It is necessary to take into account that because the experiments with the FPI and PI controllers were conducted separately in real-time operating conditions, it was very difficult to maintain the same conditions upstream (variations in the level of the Ebro River) during both experiments. In fact, these variations are one of the main disturbances in the control system in this section. In addition, the variations in the level of the Ebro River occurred randomly (Pedregal *et al*., 2009) and could not be controlled by our control system.

For the first case, Remote Downstream Water Level Reference Signal for the water control system in the Bocal) was reduced 8 cm, from 325 to 317 cm, maintaining the gates downstream in the same position. In this case, the discharge through the gates upstream decreased ($Q_1(t) < Q_{nom}$) and, therefore, the water level in the section also decreased. The graph at the top of Figure 9 shows the comparative results from the change in the level of the Ebro River (disturbance conditions), and the graph at the bottom and Table 2 presents the comparative results from the change in remote water level downstream (controlled variable) in the Bocal during the real-time experiments with FPI and PI controllers. The top graph in this figure shows that the water level in the Ebro River remained roughly the same but with small variations ($\Delta y_R(t) = \pm 5$ cm) during each of the experiments with the FPI and PI controllers, and therefore both experiments were conducted with similar disturbance conditions. The graph at the bottom of this figure and Table 2 show a region of error of 2 cm in the water level in the Bocal in relation to the reference level during both experiments. Nevertheless, the reference level was reached more quickly with the FPI controller (52.5 min) than with the PI controller (61.5 min), that is, roughly 9 minutes more quickly. At 120 minutes, the water level with the FPI controller had zero error in static state, while there was a 1 cm error with the PI controller.

For the second case, the reference signal was increased 10 cm, from 310 cm to 320 cm, while keeping the gates downstream in the same position. In this case, the discharge through the gates upstream increased ($Q_1(t) > Q_{nom}$) and therefore the water level in the Bocal also increased. The comparative experimental results from controlling the water distribution in the Bocal with the PI and FPI controllers is shown in Figure 10 and Table 2. The graph at

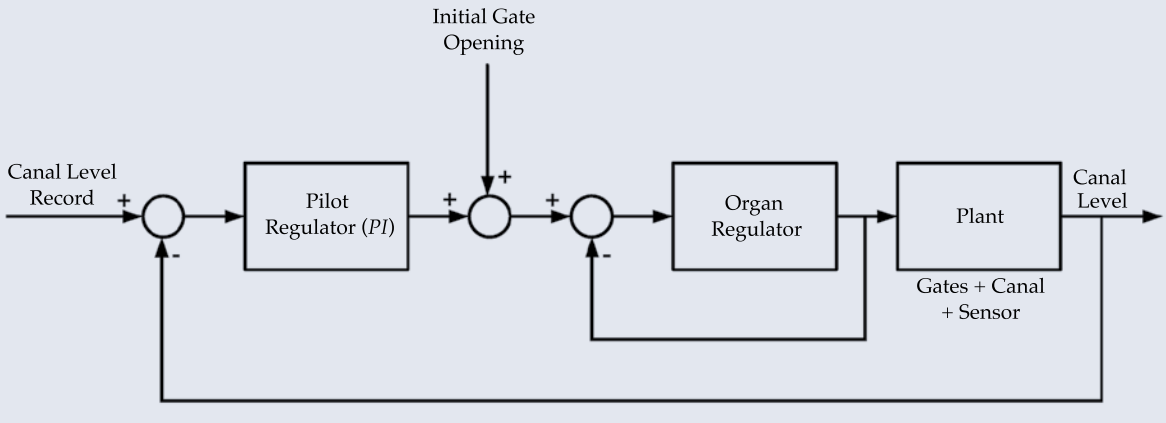

Figure 8. Functional Block Diagram for the Water Distribution Control System in the Bocal.

the top of this figure (disturbance conditions) shows an abrupt decrease in the level of the Ebro River during the experiment with the FPI controller. This decrease was produced by the start-up of a hydro power plant located on the opposite banks of the Ebro river, across from the Gate House. This strong disturbance caused the level of the Ebro River to decrease from 385 to 372 cm, that is, $\Delta y_R(t) = -23$ cm (roughly) in less than 2.5 minutes. During the experiment with the PI controller, the level of the Ebro River stayed roughly the same, with a small disturbance ($\Delta y_R(t) = \pm 5$ cm). Therefore, the experiment with the FPI controller was conducted with larger changes in the discharge through the gates upstream of the Bocal and with greater variations in the dynamic parameters of the section studied.

The graph at the bottom of Figure 10 and Table 2 show that the remote water level downstream has a region of error of ±1.0 cm in relation to the reference level during the experiments with both controllers, but the reference level was reached more quickly again (32 min) with the FPI controller than with the PI controller (48 min), that is 16 minutes more quickly. In addition, at 80.0 min, the water level in the Bocal had zero error in static state with the FPI controller and 0.8 cm with the PI controller.

These experimental results show that the FPI controller exhibits better dynamic behavior than the PI controller, in terms of roughly 25% less establishment time for the time-response of the control system (greater response speed) and more precise control. This makes it possible to increase the effectiveness of the water distribution in the canal, satisfy the demands of the users in a timely fashion and reduce water losses due to operations by 25% (Kovalenko, 1983; Litrico and Fromion, 2009).

In addition, more robustness with the FPI controller than the PI controller was observed because the time-response of the control system with the FPI controller behaved better than that of the PI controller under conditions with greater variations in the dynamic parameters of the Bocal, as well as with more aggressive external disturbances.

Thus, the comparative experimental results from the real-time functioning of the water distribution control system for the Bocal with FPI and PI controllers demonstrated the usefulness of implementing fractional order controllers when needing to effectively control main irrigation canals with dynamic time-varying parameters.

Conclusions

This work presented the design and real-time practical implementation of an FPI controller in a section of a main irrigation canal in operation, which behaves in a more robust manner than the equivalent PI controller (in terms of exhibiting the same dynamic closed-loop behavior for nominal plant specifications) when large variations in dynamic parameters occur, as well as when the plant generates high frequency noise. This result is particularly relevant to main irrigation canals with dynamic parameters that exhibit a wide variation as a result of changes in discharge in the operating range $[Q_{min}, Q_{max}]$.

An FPI controller designed with a SIMATIC S7-300 PLC was implemented based on criteria for simplicity, high autonomy and a reliable executable code.

Experiments were conducted to evaluate the real-time functioning of a control system using FPI and PI controllers to distribute water in a section of a main irrigation canal in operation which underwent wide variations in discharge.

These experiments showed that when variations in discharge ($Q_1(t) \neq Q_{nom}$) in the canal occurred, roughly 25% better establishment time for the time-response (greater response speed) of the control system was obtained with the FPI controller as well as more precise control. This translates into more effective water distribution in the canal, more quickly satisfying the demands of different users and significantly reducing losses (25%) in the available water resources due to operations.

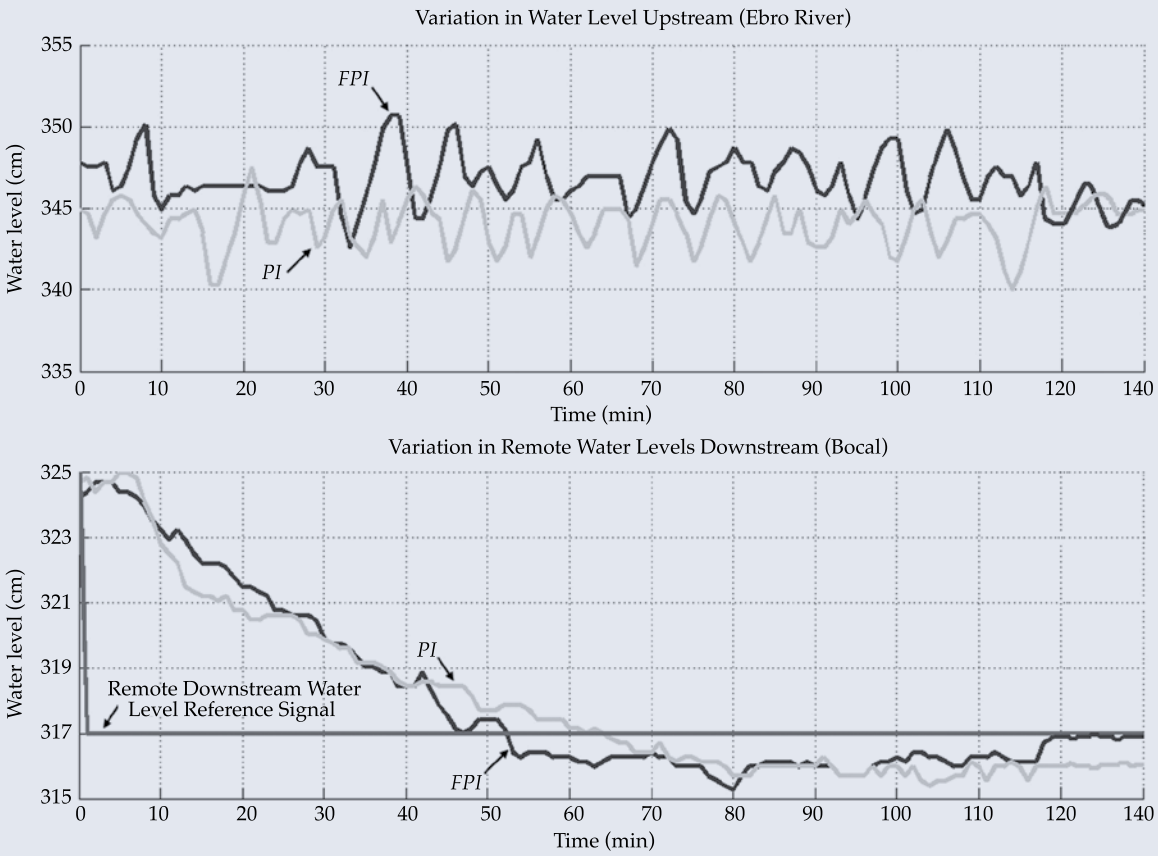

Figure 9. Comparative Experimental Results for the Real-time Functioning of the Water Distribution Control System in the Bocal with *FPI* and *PI* Controllers when Discharge Decreases.

Table 2. Comparative Experimental Results from the Real-time Functioning of the Water Distribution Control System with *FPI* and *PI* Controllers in the Bocal.

	First Experiment $Q_1(t) < Q_{nom}$			**Second Experiment** $Q_1(t) > Q_{nom}$		
Controller	t_s (min)	e_{ss} (cm)	Δy_R (cm)	t_s (s)	e_{ss} (cm)	Δy_R (cm)
FPI	52.5	0	± 5	32	0	- 23
PI	61.5	1	± 5	48	0.8	± 5

It is important to highlight that this work presents the first experiences with the practical implementation and comparative evaluation of a robust fractional order FPI controller in a section of a main irrigation canal in operation. The objective of the investigations to follow is to generalize the results obtained with this work to the overall control of a main irrigation canal made up of several sections with high interactions between the sections.

The benefits obtained by the robust and effective control of water distribution in a main irrigation canal include an immediate improvement in the management and use of the

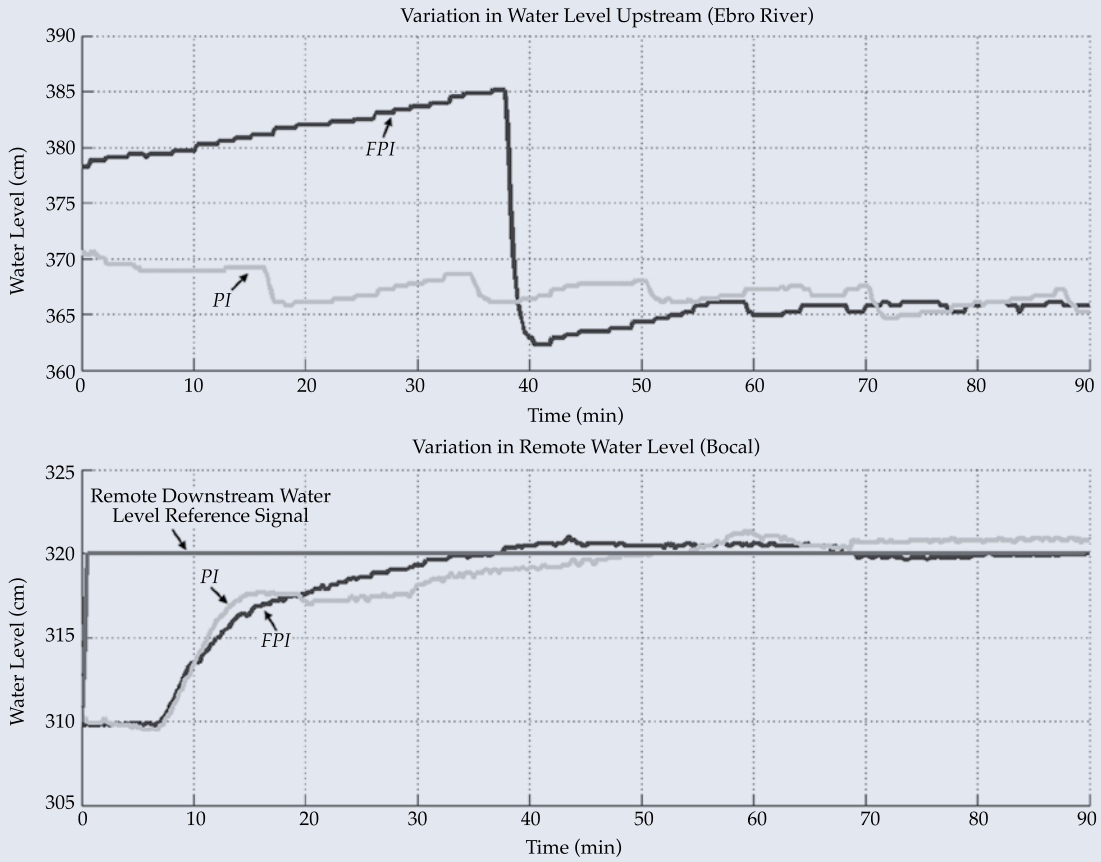

Figure 10. Comparative Experimental Results from the Real-time Functioning of the Water Distribution Control System in the Bocal with *FPI* and *PI* Controllers when Discharge Increases.

available water resources, as well as improved environmental protection by decreasing water losses resulting from operations.

Acknowledgements

This work is part of a scientific collaborative project between the Castilla La-Mancha University and the Ebro Hydrographic Confederation to model and control the main canal of the Imperial de Aragón. The authors wish to express their sincere thanks to the Ebro Hydrographic Confederation for their unconditional help and support.

Received: 27/07/10
Accepted: 07/03/13

References

BARBOSA, R.S., MACHADO, J.A.T., and FERREIRA, I.M. Controller tuning based on Bode's ideal transfer function. *Nonlinear dynamics*. Vol. 38, No. 1-4, 2004, pp. 305-321.

BAUME, J., MALATERRE, P., and SAU, J. Tuning of PI controllers for an irrigation canal using optimization tools. *Proceedings of Workshop on Modernization of Irrigation Water Delivery Systems*, Phoenix, Arizona, USA, 1999.

BURT, C., MILLS, R., KHALSA, R., and RUIZ, V. Improved proportional integral (PI) logic for canal automation. *Journal of Irrigation and Drainage Engineering*. Vol. 124, No. 1, 1998, pp. 53-57.

BUYALSKI, C., EHLER, D., FALVEY, H., ROGERS, D., and SERFOZO, E. Canal systems automation manual. Technical report. *A water resources technical publication*. Vol. 1, Denver: Department of Interior, Bureau of Reclamation, 1991, 113 pp.

CASTILLO-GARCÍA, F., FELIU-BATLLE, V., and RIVAS-PÉREZ, R. Time domain tuning of fractional order controllers combined with a Smith predictor for automation of water distribution in irrigation main channel pools. *Asian Journal of Control*. Vol. 15, No. 3, 2013, pp. 1-15.

CASTILLO, F., FELIU, V., RIVAS-PÉREZ, R., and SÁNCHEZ, L. Design of a class of fractional controllers from frequency specifications with guaranteed time domain behaviour. *Computers and Mathematics with Applications*. Vol. 59, No. 5, 2010, pp. 1656-1666.

CHEN, Y., DOU, H., VINAGRE, B., and MONJE, C. A robust tuning method for fractional order PI controllers. *Proceedings of 2nd IFAC workshop on fractional differentiation and its applications*, Porto, Portugal, 2006.

CHEN, Y., VINAGRE, B., and PODLUBNY, I. Using continued fraction expansion to discretize fractional order derivatives. *Nonlinear dynamics*. Vol. 38, No. 1-4, 2004, pp. 155-170.

CHOW, V.T. *Open-channels hydraulics*. New York: McGraw Hill Book Company, 1988, 680 pp.

CLEMMENS, A. Canal automation. *Resource Magazine*. Vol. 13, No. 1, 2006, pp. 7-8.

CLEMMENS, A., and SCHUURMANS, J. Simple optimal downstream feedback canal controllers: theory. *Journal of Irrigation and Drainage Engineering*. Vol. 130, No. 1, 2004, pp. 26-34.

CORRIGA, G., SANNA, S., and USAI, G. Estimation of uncertainty in an open-channel network mathematical model. *Applied Mathematical Modelling*. Vol. 13, 1989, pp. 651-657.

DELTOUR, J. y SANFILIPPO, F. Introduction of Smith predictor into dynamic regulation. *Journal of Irrigation and Drainage Engineering*. Vol. 124, No. 1, 1998, pp. 3-30.

DJOUAMBI, A., CHAREF, A., and BOUKTIR, T. Fractional order robust control and PI^{λ} D^{μ} controllers. *WSEAS transactions on circuits and systems*. Vol. 4, No. 8, 2005, pp. 850-857.

FELIU-BATLLE, V., RIVAS-PÉREZ, R., CASTILLO, F., SÁNCHEZ, L., and LINAREZ, A. Robust fractional order controller for irrigation main canal pools with time-varying dynamical parameters. *Computers and Electronics in Agriculture*. Vol. 76, No. 2, 2011, pp. 205-217.

FELIU-BATLLE, V., RIVAS-PÉREZ, R., CASTILLO, F., and SÁNCHEZ, L. Smith predictor based robust fractional order control: Application to water distribution in a main irrigation canal pool. *Journal of Process Control*. Vol. 19, No. 3, 2009a, pp. 506-519.

FELIU-BATLLE, V., RIVAS-PÉREZ, R., and CASTILLO, F. Fractional order controller robust to time delay variations for water distribution in an irrigation main canal pool. *Computers and electronics in agriculture*. Vol. 69, No. 2, 2009b, pp. 185-197.

FELIU-BATLLE, V., RIVAS-PÉREZ, R., and SÁNCHEZ, L. Fractional robust control of main irrigation canals with variable dynamic parameters. *Control Engineering Practice*. Vol. 15, No. 6, 2007, pp. 673-686.

KOVALENKO, P.I. *Automation of land reclamation systems*. Moscow: Kolos, 1983, 330 pp.

LEU, J., TSAY, S., and HWANG, C. Design of optimal fractional-order PID controllers. *Journal of the Chinese Institute of Chemical Engineers*. Vol. 33, No. 2, 2002, pp. 193-202.

LITRICO, X. and FROMION, V. *Modeling and control of hydrosystems*. London: Springer-Verlag, 2009, 409 pp.

LITRICO, X., FROMION, V., and BAUME, J. Tuning of robust distant downstream PI controllers for an irrigation canal pool: (II) implementation issues. *Journal of Irrigation and Drainage Engineering*. Vol. 132, No. 4, 2006, pp. 369-379.

LJUNG, L. *System identification - theory for the user*. Second edition. New Jersey: Prentice Hall PTR, 1999, 610 pp.

MACHADO, J. Analysis and design of fractional-order digital control systems. *Journal Systems Analysis-Modeling-Simulation*. Vol. 27, 1997, pp. 107-122.

MALATERRE, P., ROGERS, D., and SCHUURMANS, J. Classification of canal control algorithms. *Journal of Irrigation and Drainage Engineering*. Vol. 124, No. 1, 1998, pp. 3-10.

MONJE, C., VINAGRE, B., CHEN, Y., and FELIU, V. On fractional PI^{λ} controllers: some tuning rules for robustness to plant uncertainties. *Nonlinear Dynamics*. Vol. 38, No. 1-4, 2004, pp. 369-381.

MONTAZAR, A., OVERLOOP, P., and BROUWER, R. Centralized controller for the Narmada main canal. *Journal* of *Irrigation and Drainage Engineering*. Vol. 54, 2005, pp. 79-89.

OGATA, K. *Modern control engineering*. New Jersey: Prentice-Hall, Englewood Cliffs, 1993, 1013 pp.

PEDREGAL, D., RIVAS-PÉREZ, R., FELIU, V., SÁNCHEZ, L., and LINARES, A. A non-linear forecasting system for the Ebro River at Zaragoza, Spain. *Environmental modelling and software*. Vol. 24, No. 4, 2009, pp. 502-509.

PETRAS, I., GREGA, S., and DORCAK, L. Digital fractional order controllers realized by PIC microprocessor: experimental results. *Proceedings of international Carpathian control conference*, High Tatras, Slovak Republic, 2003.

PETRAS, I. Control of fractional order Chua's system. *Journal of Electrical Engineering*. Vol. 53, No. 7-8, 2002, pp. 219-222.

PODLUBNY, I., PETRAS, I., VINAGRE, B., O´LEARY, P. y DORCAK, L. Analogue realization of fractional order controllers. *Nonlinear Dynamic*. Vol. 29, 2002, pp. 281-296.

PODLUBNY, I. *Fractional differential equations*. San Diego: Academic Press, 1999a, 368 pp.

PODLUBNY, I. Fractional-Order Systems and $PI^{\lambda}D^{\mu}$ Controllers. *IEEE Transactions on Automatic Control*. Vol. 44, No. 1, 1999b, pp. 208-214.

RIVAS-PÉREZ, R., SOTOMAYOR, J., FELIU, V. y CASTILLO, F. Control robusto de orden fraccional de la presión del vapor en el domo superior de una caldera bagacera. *Memorias del XV Congreso Latinoamericano de Control Automático*, Lima, Perú, 2012.

RIVAS-PÉREZ, R., FELIU-BATLLE, V., CASTILLO, F., and LINAREZ, A. Control oriented model of a complex

irrigation main canal pool. *IFAC Proceedings Volumes (IFAC-PapersOnline)*. Vol. 18, No. PART 1, 2011, pp. 2919-2924.

RIVAS-PÉREZ, R., FELIU-BATLLE, V., SÁNCHEZ, L., PEDREGAL, D., and LINARES, A. Identification of the first pool of the Imperial de Aragón main irrigation canal. *Hydraulic Engineering in Mexico*. Vol. XXIII, No. 1, 2008a, pp. 71-87.

RIVAS-PÉREZ, R., FELIU-BATLLE, V., CASTILLO-GARCÍA, F., y LINAREZ, A. System identification for control of a main irrigation canal pool. *IFAC Proceedings Volumes (IFAC-PapersOnline)*, Vol. 17, No. 1, Part 1, 2008b.

RIVAS-PÉREZ, R., FELIU-BATLLE, V., SÁNCHEZ, L., CASTILLO, F. y LINAREZ, A. Computer based fractional order control system of water levels in irrigation main Canals. Patent No. ES 2277757, International classification G05 D 9/12, E02 B 7/36, Spain, 2008c.

RIVAS-PÉREZ, R., FELIU-BATLLE, V., and SÁNCHEZ, L. Robust system identification of an irrigation main canal. *Advances in Water Resources*. Vol. 30, No. 8, 2007, pp. 1785-1796.

RIVAS-PÉREZ, R., PERAN, J., PINEDA, B., and PÉREZ, S. Distributed control under centralized intelligent supervision in the Güira de Melena irrigation System. *Hydraulic Engineering in Mexico*. Vol. XVIII, No. 2, 2003, pp. 53-68.

RIVAS-PÉREZ, R., PRADA, C., PERAN, J., and KOVALENKO, P. Robust adaptive predictive control of water distribution in irrigation canals. *Proceedings of 15th IFAC World Congress*, Barcelona, Spain, 2002.

RIVAS-PÉREZ, R., BEAUCHAMP, G., RODRIGUEZ, D., and PÉREZ, S. Computer control of water distribution in irrigation systems. *Tropical Hydrology and Caribbean Water Resources Proceedings, Book Series: American Water Resources Association Technical Publication Series*. Vol. 98, No. 2, 1998, pp. 149-154.

RIVAS-PÉREZ, R. *Automatic control of water distribution in irrigation systems*. D.Sc. thesis, Kiev, Ukraine: Land Reclamation and Hydraulic Scientific Research Institute of Ukraine (UkrNIIGiM), 1990, 520 pp.

SÁNCHEZ, L., FELIU-BATLLE, V., RIVAS-PÉREZ, R., and RUIZ, M. Robust Control of a Laboratory Hydraulic Canal by Using a Fractional PI Controller. *Proceedings of the 2007 ASME international design engineering technical conferences*. Las Vegas, Nevada, USA, 2007.

SCHUURMANS, J., HOF, A., DIJKSTRA, S., BOSGRA, O., and BROUWER, R. Simple water level controller for irrigation and drainage canals. *Journal of Irrigation and Drainage*. Vol. 125, No. 4, 1999, pp. 189-195.

SEATZU, C. Design and robustness analysis of decentralized constant volume-control for open-channels. *Applied Mathematical Modelling*. Vol. 23, No. 6, 1999, pp. 479-500.

VINAGRE, B., PODLUBNY, I., HERNÁNDEZ, A., and FELIU, V. Some approximations of fractional order operators used in control theory and applications. *Journal of Fractional Calculus and Applied Analysis*. Vol. 3, No. 3, 2000, pp. 231-248.

WAHLIN, B. Performance of model predictive control on ASCE test canal 1. *Journal of Irrigation and Drainage Engineering*. Vol. 130, No. 3, 2004, pp. 227-237.

WAHLIN, B. and CLEMMENS, A. Automatic downstream water-level feedback control of branching canal networks: theory. *Journal of Irrigation and Drainage Engineering*. Vol. 132, No. 3, 2006, pp. 208-219.

WANG, Z., WANG, Z., CAO, G. y ZHU, X. Digital implementation of fractional order PID controller and its application. *Journal of Systems Engineering and Electronics*. Vol. 16, No. 1, 2005, pp. 116-122.

Institutional Address of the Authors

Dr. Raúl Rivas-Pérez

Catedrático
Universidad Politécnica de La Habana "José Antonio Echeverría" (CUJAE)
Departamento de Automática y Computación
Calle 114 # 11901, CUJAE, Marianao
19390 Ciudad de La Habana, Cuba
Teléfono: +53 (7) 2663 285
rivas@electrica.cujae.edu.cu
raul_rivas_perez@yahoo.es

Dr. Vicente Feliu-Batlle

Catedrático
Universidad de Castilla-La Mancha
Escuela Técnica Superior de Ingenieros Industriales
Campus Universitario s/n
13071 Ciudad Real, España
Teléfono: +34 (92) 6295 364
vicente.feliu@uclm.es

Dr. Fernando Castillo-García

Profesor titular
Universidad de Castilla-La Mancha
Escuela Técnica Superior de Ingenieros Industriales
Campus Universitario s/n
13071 Ciudad Real, España
Teléfono: +34 (92) 6295 300
fernando.castillo@uclm.es

Dr. Luis Sánchez-Rodríguez

Profesor Titular
Universidad de Castilla-La Mancha
Escuela Universitaria de Ingenieros Técnicos Industriales
Campus Tecnológico de la Antigua Fábrica de Armas s/n
45071 Toledo, España
Teléfono: +34 (90) 2204 100, extensión 3844
luis.sanchez@uclm.es

Ing. Antonio Linares-Sáez

ABEIMA, S.A., ABENGOA
Avda. La Buharia, 2
41018 Sevilla, España
Teléfono: +34 (95) 4970 587
antonio.linares@abeinsabd.abengoa.com

Click here to write the autor

Verification of Numeral Procedures for Simulation of Gate Maneuvers

• Gilberto de Jesús López-Canteñs* • Víctor Prado-Hernández •
Universidad Autónoma Chapingo, México
*Corresponding Author

• Benjamín de León-Mojarro •
Comisión Nacional del Agua, México

• Víctor Manuel Ruiz-Carmona •
Instituto Mexicano de Tecnología del Agua

• Mauricio Carrillo-García • Laura Ibáñez-Castillo • Eduardo Arteaga-Tovar •
Universidad Autónoma Chapingo, México

Abstract

LÓPEZ-CANTEÑS, J.G., PRADO-HERNÁNDEZ, V., DE LEÓN-MOJARRO, B. & RUIZ- CARMONA. V.M. Verification of Numeral Procedures for Simulation of Gate Maneuvers. *Water Technology and Sciences* (in Spanish). Vol. V, No. 1, January-February, 2014, pp. 41-54.

Applying Saint Venant equations in reaches of irrigation canals requires defining internal boundary conditions at the sites where they are located control structures like gates, considering the dynamic equation to transmit hydraulic information from one side of the structure to continue on the other. In this study three numerical procedures for maneuvering gates are tested to verify whether they represent the movement of these control structures, minimizing flow phase shifts after a maneuver. To this end, the Rehbock canal of the Autonomous University of Chapingo was used. Automated measurements of water depth and flow were taken. Results show that in progressive maneuvering with restart of water depth, flow through the gate and near it tends to be similar, while oscillations diminish over time, a phenomenon which is characteristic of water dynamics in canals. Moreover, when depth is the variable to be regulated it is advisable to use instantaneous or progressive maneuvering with restart of flow. On the other hand, if the variable is flow, progressive maneuvering with restart of depth is preferred. Simulation of progressive maneuvering with restart of depth is the procedure that best represents water dynamics in the structure.

Keywords: gates movement, simulation model, unsteady flow, control structures.

Resumen

LÓPEZ-CANTEÑS, J.G., PRADO-HERNÁNDEZ, V., DE LEÓN-MOJARRO, B. & RUIZ- CARMONA. V.M. Verificación de procedimientos numéricos de simulación de maniobras en compuertas. Tecnología y Ciencias del Agua. *Vol. V, núm. 1, enero-febrero, 2014, pp. 41-54.*

La aplicación de las ecuaciones de Saint Venant en los tramos de canales de riego requiere definir condiciones de frontera interna en los sitios donde se ubican estructuras de control como compuertas, considerando su ecuación dinámica para transmitir información hidráulica hacia ambos lados de la estructura, por lo que en el trabajo se verifican tres procedimientos numéricos de ejecución de maniobra de compuertas, con la finalidad de representar el movimiento de las estructuras de control, minimizándose el desfasamiento de caudales posteriores a una ejecución. Para ello se utilizó el canal Rehbock de la Universidad Autónoma Chapingo, México, realizándose de forma automatizada la medición de los niveles de agua y gasto, obteniéndose que en la maniobra progresiva con reinicialización de tirante, la tendencia del gasto en la vecindad y la compuerta es similar, atenuándose las oscilaciones en el tiempo, el cual se corresponde con la dinámica del agua en los canales; además, cuando la variable a regular es el tirante, se recomienda usar la ejecución de maniobra instantánea o la progresiva con reinicialización de gasto; pero si la variable es el gasto, es preferible la maniobra progresiva con reinicialización de tirante; además, el procedimiento de simulación de la maniobra progresiva con reinicialización de tirante es el que mejor representa la dinámica del agua en la estructura.

Palabras clave: *movimiento de compuertas, modelo de simulación, régimen no permanente, estructuras de control.*

Introduction

Piping and distribution systems are composed of a set of canals in which the necessary regulating structures are installed. The functioning of these systems is considered efficient if they operate without an excess or a lack of water and without greatly changing the flow of lateral extractions. The regulating structures need to be maneuvered in order to keep the water depths and flows within a certain range.

The configuration of canal systems is complex, since they contain different kinds of static (weirs) and dynamic (gates) control structures, important extraction structures such as lateral canals and a large amount of direct or farm intakes with small flows, as well as lateral supply structures. This set of elements can be conducted mathematically represented using a Saint Venant unsteady flow model that does not have an analytical solution (De León *et al*., 2002).

While unsteady flow equations are valid to study the maneuvering of water in irrigation canals, internal or external boundary conditions must be defined to represent control and measurement structures. Therefore, equations for these elements must be incorporated into the modeling process in order to take into account their functioning (Malaterre and Baume, 1998).

Manz (1998) mentions that the use of dynamic simulation models makes it is possible to predict hydraulic flow conditions at any point in an open canal system, as a function of the physical and operating characteristics. They can also be used to predict and evaluate the maneuvering sequence and time to be used in order to make those assignments. In addition, Manz indicates that these models simulate two basic types of hydraulic characteristics: the components of the open canals and the hydraulic control structures.

Most mathematical models adequately simulate the maneuvering of water in canals since they satisfy the technical criteria for conservation of mass, stability, precision, convergence and consistency (Clemmens *et al*., 1991; Goussard, 2000; CEMAGREF, 2000). Nevertheless, they present problems when simulating the flow propagation produced by the maneuvering of control structures, which can produce numerical oscillations that prolong the transition time between one permanent regime and another. They may also reflect the out-of-phase flow because of the lack of correspondence between the physical behavior and the numerical solution of the phenomenon.

Due to the above deficiencies, the temporal variations of the hydraulic characteristics induced by the maneuvering of control structures needs to be studied in more depth. De León *et al*. (2007) present three mathematical procedures that combine the Saint Venant equations in the vicinity of the gates with the equations at the structure in order to transmit hydraulic information to both sides. Therefore, the objective of this work is to verify the above numerical simulation procedures proposed to minimize flow shifts after maneuvering a radial gate.

Mathematical Representation of the Operations of Irrigation Canals

When the opening of gates or flow in lateral intakes vary, the water dynamics in a section of a free-surface irrigation canal restricted by control structures can be represented using the Saint Venant equations, which according to Chow (1994) are composed of the continuity equation:

$$\frac{\partial Q}{\partial x} + T\frac{\partial y}{\partial t} = q \qquad (1)$$

where T is the width of the free water surface (m); y is the water depth (m); Q is the flow (m^3s^{-1}); q is the flow of the lateral supply (+) or extraction (-)per unit canal length ($m^3s^{-1}m^{-1}$); X is the coordinate in the direction of the canal length (m); t is time (s).

And the dynamic equation, also called the momentum equation is:

$$\frac{\partial Q}{\partial t}+\frac{\partial\left(QV\right)}{\partial x}+gA\frac{\partial y}{\partial x}=gA\left(S_o-S_f\right)+kqV \quad (2)$$

where S_f is the friction slope (dimensionless); S_o is the bed slope of the canal (dimensionless); g is gravitational acceleration (ms^{-2}); V is the mean flow velocity (ms^{-1}); A is the hydraulic area (m^2); k a coefficient that takes the value zero if $q>0$ and one if $q<0$ (dimensionless).

The above equations make up a hyperbolic system of first-order, non-linear, partial differential equations for flow and water depth. It is a highly non-linear system that has no analytical solution and therefore numerical procedures are needed to solve them.

Equations (1) and (2) in the simulation models are generally solved using an implicit finite differences scheme. In effect, the discrete solution for each section of the canal and each time interval is the following linear recursive equation (Liggett and Cunge, 1975; CEMAGREF, 2000):

$$R_i\Delta Q_i+S_i\Delta y_i=T_i \quad (3)$$

where:

$$\Delta Q_i=A\Delta Q_{i+1}+B\Delta y_{i+1}+C \quad (4)$$

$$\Delta y_i=D\Delta Q_{i+1}+E\Delta y_{i+1}+F \quad (5)$$

R, S and T are coefficients that vary according to the boundary condition; A, B, C, D, E and F are coefficients that vary from one time interval to another and in each section of the integration domain; Δy and ΔQ are the unknowns in sections i and $i+1$; i is an index that defines the section calculated in the discretization space.

Equations (3), (4) and (5) are related to the water depth and flow variables at each time interval for two consecutive points (i, $i+1$) defined by the discretization of space. The recursive equation (3) can be easily solved using the double-sweep method. The first sweep is conducted from upstream to downstream to obtain the coefficients R_i, S_i and T_i in the discretization space using the type (3) equation in the following form:

$$R_{i+1}\Delta Q_{i+1}+S_{i+1}\Delta y_{i+1}=T_{i+1} \quad (6)$$

where:

$$R_{i+1}=R_iA_i+S_iD_i \quad (7)$$

$$S_{i+1}=R_iB_i+S_iE_i \quad (8)$$

$$T_{i+1}=T_i-R_iC_i-S_iF_i \quad (9)$$

With the second sweep, which is conducted from downstream to upstream in the section, the variations in water depth and flow in the section I are calculated by solving equations (4) and (5).

Boundary Conditions

To apply any of the methods to solve the equations for the unsteady regime, the initial and boundary conditions must be defined. The former is generally represented by the backwater curve at the initial instant $t=t_o$, which is obtained when the regime is permanently varied in a gradual manner (Arteaga, 1997). The second refers to the definition of the depth, velocity or flow at the upper and lower ends of the section, by including in the calculation all time intervals beginning with the initial time.

Liggett and Cunge (1975) and Husain *et al*. (1988) indicate that two types of boundary conditions exist—exterior located at the ends of the length of the canal under consideration, and interior (CF_i) located in the middle of the canals. These are caused by a geometric discontinuity or the presence of a control structure. De León *et al*. (2002) assert that the formulation and treatment of the initial (CF_{arr}) and final (CF_{ab}) external boundary conditions of a canal do not present difficulties when they are modeled. De León *et al*. (2007) and CEMAGREF (2000)

indicate that the boundary condition upstream is represented by the irrigation demand, which is an input hydrograph of the type $Q_o = f(t)$, and can be linearized using the following form in order to solve the Saint Venant model using the type (3) equation:

$$Q_0(t + \Delta t) - Q_0(t) = f_0(t + \Delta t) - f_0(t) \text{ or also:}$$
$$\Delta Q_0 = \Delta f(t)$$

where the sub-index 0 represents the beginning of the canal.

Having the boundary condition at the beginning of the canal (upstream), the first sweep is initiated to calculate the coefficients R_i, S_i and T_i, since the type (3) equation is recursive. Therefore the coefficients R_o, S_o and T_o at the beginning of the canal are:

$$R_o = 1.0,\ S_o = 0.0 \text{ y } T_o = Q_o(t + \Delta t) - Q_o(t)$$

For the first sweep, the end of the canal is reached with a system of two equations and two unknowns:

$$R_m \Delta Q_m + S_m \Delta y_m = T_m \qquad (10)$$

$$f(\Delta Q_m, \Delta y_m) \qquad (11)$$

where m is the last section of the canal to be discretized.

Equation (11) represents the boundary condition downstream, which generally is represented using a ratio known as the depth-flow, whose coefficients R_m, S_m and T_m from equation (3) take the following form (CEMAGREF, 2000; De León and Prado, 2006):

$$R_m = 1.0,\ S_m = -\frac{\Delta Q_m}{\Delta y_m} \text{ y } T_m = 0.0$$

Mathematical Representation of Control Structures

At sites where control structures are located, Saint Venant equations are not valid. It is therefore necessary to introduce two equations to transmit hydraulic information upstream (section 2) and downstream (section 3). One ensures the continuity of the flow and the other describes the dynamics of the gate (Figure 1). Therefore, the following system of equations for these points needs to be solved (Cunge, 1988):

$$R_2 \Delta Q_2 + S_2 \Delta y_2 = T_2 \qquad (12)$$

$\Delta Q_2 = \Delta Q_3$: continuity equation for the structure (13)

$f(Q_2, y_2, y_3, a) = 0$: dynamic equation for the structure (14)

where a is the gate opening (m); sub-index 2 represents the discretization section upstream from the gate and 3 downstream from the structure.

Equation (12) is the linear Saint Venant model, representing the hydraulic information upstream from the structure. The system of equations (12), (13) and (14) results in the equation that represents the information downstream from the structure (De León *et al.*, 2007):

$$R_3 \Delta Q_3 + S_3 \Delta y_3 = T_3 \qquad (15)$$

Coefficients R_3, S_3 and T_3 are obtained from the linearization of equation (14):

$$\frac{\partial f}{\partial t}(Q_2, y_2, y_3, a) = 0 \qquad (16)$$

Using an analysis at the site of the Saint Venant structures, De León (1990) obtained a second-order, ordinary differential equation that makes it possible to calculate the hydraulic behavior in the vicinity of the structure. This equation is expressed as:

$$\frac{1}{T}\left(\frac{dQ}{dy}\right)^2 - \frac{2Q}{A}\left(\frac{dQ}{dy}\right) + \frac{Q^2 T}{A^2} - gA = 0 \qquad (17)$$

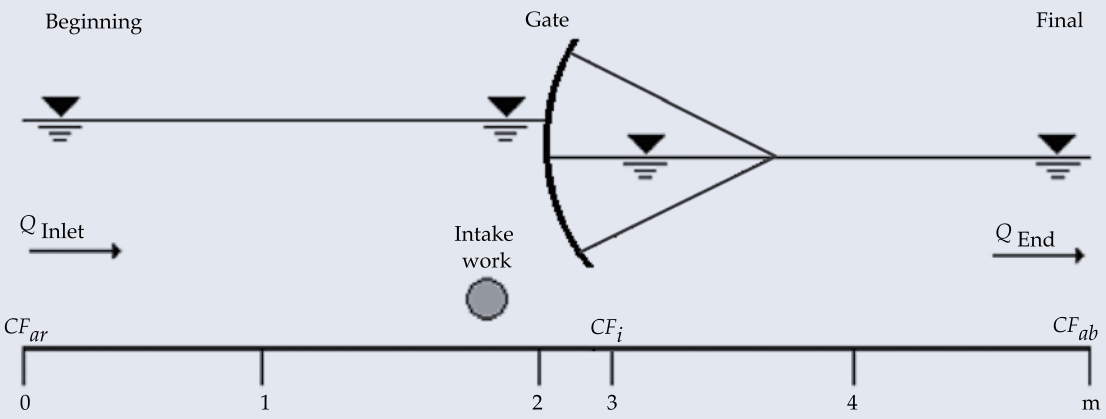

Figure 1. Discretization of a section of the irrigation canal.

The primary solution of the equation (17), in dQ/dy, is obtained when the structure moves, and is equal to the following equation:

$$\frac{dQ}{dy} = (v \pm c)T \tag{18}$$

where $c = (gA/T)^{1/2}$ is the celerity of the waves produced by the maneuvering of the structure (ms^{-1}).

In equation (18), the positive sign indicates the flow-depth ratio immediately downstream, while the negative sign refers to the ratio upstream.

Equation (17) serves as a basis to establish simulation procedures to execute maneuverings that minimize the flow propagation error. De León *et al*. (2007) proposes that at the points at which a singularity is located, equation (18) can be applied, which identifies the recursive equation (3) when $R_i = 1.0$, $S_i = -(v \pm c)T$ and $T_i = 0.0$. This equation represents the characteristic lines which are based on the hydraulic information upstream and downstream from the structure, and intercept the finite differences discretization mesh.

Execution of the Maneuvering of Gates in an Irrigation Canal Network

Regulating gates in an irrigation canal network need to be maneuvered in order to maintain the flow and depth values near previously defined reference values (Litrico and Fromion, 2006).

If the structure is static, a tangential approximation of the dynamic equation for the gate can be used to continue the solution downstream from the gate. Nevertheless, De León and Exebio (1990) indicate that when temporal variations are introduced into the opening of the gates, the tangential approximation leads to errors, which are accumulative, since for each time interval or instant of change the fitting error between the tangential approximation and the exact singularity function is added to the new value of the calculated variables (flow and water depth).

De León (1990) indicates that the tangential approximation problem requires a way to predict the change in levels upstream (dy_i) and downstream (dy_{i+1}) resulting from the change in irrigation demand in the structure (dQ). This is achieved using equation (18), applying the following procedure:

$$dy_i = \frac{dQ}{(v_i - c_i)T_i} \tag{19}$$

$$dy_{i+1} = \frac{dQ}{(v_{i+1} + c_{i+1})T_{i+1}} \tag{20}$$

thereby obtaining the new values for water depth $y_i^{n+1} = y_i^n + dy_i$ and $y_{i+1}^{n+1} = y_{i+1}^n + dy_{i+1}$,

where n represents the period of time before the change in flow.

The type (3) recursive equation represents a set of straight lines that describe the temporal variation of the water depth (dy) and flow (dQ) for each mesh in the discretization of space. By superimposing (dy, dQ) the previous straight lines and curves of the gate opening on a plane, as shown in Figure 2, De León *et al*. (2007) were able to analyze the trajectories characterizing different maneuvering procedures.

As in the type (3) equation, the temporal variation of the flow represents supply and the change in the water depth represents storage. The relationship "supply + storage = constant" should be met for each time interval.

According to the above relationship, three possibilities exist when maneuvering: a) change in storage and supply; b) change in storage and c) change in supply.

Figure 2 shows the trajectories characterizing the maneuvering simulation procedures, where run 13 corresponds to possibility (a), run 143 to possibility (b) and 123 to possibility (c).

According to De León and Prado (2006), the numerical treatment of these three possibilities generate two overall simulation procedures: instantaneous maneuvering obtained with possibility (a) and progressive maneuvering obtained with possibilities (b) and (c).

Progressive maneuvering is named as such because when a change in the irrigation demand occurs, the reference point (number 3) is reached during the time interval after the maneuvering.

Materials and Methods

Description of the Installations

The experimental phase was applied to the Rehbock canal in the Hydraulic Laboratory of the Irrigation Department at the Autonomous University of Chapingo (UACh), Chapingo, State of Mexico. The Rehbock canal is rectangular, has a metallic structure and glass walls, is 20 m long with a template of 0.6 m, a height of 1 m and a slope of 0.0005. It is fed by a 12" valve (0.305 m) leading to a holding pond to prevent turbulence at the canal inlet, where it is first restricted by a thin-walled weir without lateral contractions (and tall enough to not be drowned when operating) and a sliding gate.

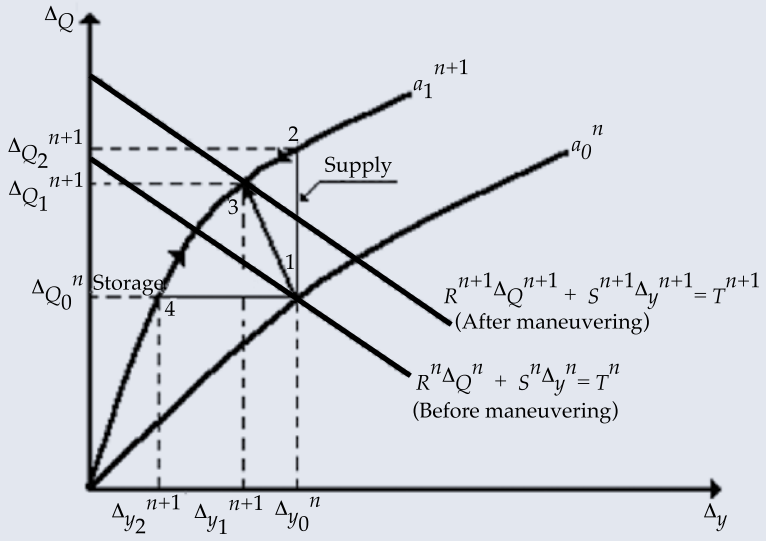

Figure 2. Representation of the maneuvering of a hydraulic structure.

A sliding gate is located at the end of the canal which functions as a movable rectangular weir and enables controlling the water level in the canal. A radial gate was installed and operated at 5.5 m from the beginning, measuring 0.75 m high and 0.60 m wide, with a gate radius of 0.9 m.

The water levels were measured with an automated system consisting of 6 continuous sensors— 5 located throughout the length of the canal and 1 upstream from the weir to determine the load in order to calculate flow at the inlet.

Gate Maneuvering Simulation Procedures

The maneuvering of a gate in an irrigation canal produces changes from an initial flow Q_o to a final flow Q_n . This occurs when the opening of a gate changes from its initial value a_o to a final value a_n.

Considering the above, De León and Prado (2006) and De León *et al*. (2007) proposed a methodology to simulate the maneuvering of regulating structures that causes flow propagations due to a change in demand. These methodologies consist of resetting the flow, opening and water depth values at the gate. Water depths values are only reset immediately upstream and downstream from the gate. In the rest of the sections, the general model propagates the effect of maneuvering. The methodology proposed by these authors is described in detail below.

Progressive Maneuvering with Resetting Flow

This procedure consists of resetting the flow in the structure, which corresponds to the change in demand as well as the value of the opening, while maintaining water depth upstream and downstream constant, as described next.

At an instant $t = n$, the hydraulic state of the gate (Δy_o^n, ΔQ_o^n, a_o^n) and the type (3) equation for the straight line that passes through that point are known. Then, as result of maneuvering, a flow can be established $Q_1 = Q_o + \Delta Q$ that requires passing from point (Δy_o^n, ΔQ_o^n, a_o^n) to point (Δy_1^{n+1}, ΔQ_1^{n+1}, a_1^{n+1}) (Figure 2).

The authors indicate that if only the flow value is reset and the water depth values are held constant, it really goes from point (Δy_o^n, ΔQ_o^n) to point (Δy_o^n, ΔQ_2^{n+1}), whose ordinate is greater than the desired value (ΔQ_1^{n+1}).

Point (Δy_o^n, ΔQ_2^{n+1}) corresponds to the intersection of the system represented by the following equations:

$$\Delta y_o^n = \text{constante} \tag{21}$$

$$\Delta Q_2^{n+1} = f\left(\Delta y_o^n, a_1^{n+1}\right) \tag{22}$$

Since the intersection of this system of equations does not correspond to the point of interest (Δy_1^{n+1}, ΔQ_1^{n+1}), the authors note that by resetting the flow at a value ΔQ_1^{n+1} less than ΔQ_2^{n+1}, the model is forced to decrease from point (Δy_o^n, ΔQ_2^{n+1}) to the point of interest (Δy_1^{n+1}, ΔQ_1^{n+1}) on the gate curve a_1^{n+1} .

With this procedure, the type (3) straight line shifts from point (Δy_o^n, ΔQ_o^n) to point (Δy_1^{n+1}, ΔQ_1^{n+1}) during a time interval. The evaluation of coefficients *R*, *S* and *T* enables transmitting downstream the information regarding the size of the maneuvering.

Progressive Maneuvering with Resetting the Water Depth

This procedure consists of resetting the values for the water depth upstream and downstream and the opening of the gate, while maintaining the value for the flow in the structure constant. The changes in water depth are calculated with equations (19) and (20).

As in the previous procedures, it is necessary to pass from point (Δy_o^n, ΔQ_o^n, a_o^n) to point (Dy_1^{n+1}, ΔQ_1^{n+1}, a_1^{n+1}) (Figure 2). The authors indicate that if the water depth values upstream and downstream from the gate are reset and the flow is held constant, it passes from point (Δy_o^n, ΔQ_o^n) to point (Δy_2^{n+1}, ΔQ_o^n), whose abscissa is less than the reset value (Dy_1^{n+1}).

Point $(\Delta y_2^{n+1}, \Delta Q_o^n)$ corresponds to the intersection of the system, represented by the equations:

$$\Delta Q_o^n = \text{constante} \quad (23)$$

$$\Delta Q_o^n = f\left(\Delta y_2^{n+1}, a_1^{n+1}\right) \quad (24)$$

The intersection of this system results in a flow that is lower than that demanded on the gate curve a_1^{n+1}. Then, since the water depth value is reset at a value Δy_1^{n+1} higher than the value Δy_2^{n+1}, the variables of point $(\Delta y_2^{n+1}, \Delta Q_o^n)$ shift to the point of interest $(\Delta y_1^{n+1}, \Delta Q_1^{n+1})$ on the gate curve a_1^{n+1}.

With this procedure, the type (3) straight line progressively shifts during a time interval (Δt) to point $(\Delta y_1^{n+1}, \Delta Q_1^{n+1})$. Likewise, the flow uniformly passes from value ΔQ_o^n to value ΔQ_1^{n+1} over a time interval.

Instantaneous Maneuvering

This procedure consists of simultaneously resetting the values for the flow and water depth in the structure, obtained with equations (19) and (20), as well as the gate opening. The authors indicate that this procedure is equal to instantaneously shifting the type (3) straight line from point $(\Delta y_o^n, \Delta Q_o^n)$ to the point of interest $(\Delta y_1^{n+1}, \Delta Q_1^{n+1})$ (Figure 2). This point corresponds to the intersection of the system of equations:

$$R^{n+1}\Delta Q^{n+1} + S^{n+1}\Delta y^{n+1} = T^{n+1} \quad (25)$$

$$\Delta Q_1^{n+1} = f\left(\Delta y_1^{n+1}, a_1^{n+1}\right) \quad (26)$$

where the coefficients in equation (25) are determined using equation (18).

The simulation process uses a distance interval of $\Delta x = 0.5$ m and a time interval of $\Delta t = 10$ s, which ensure a suitable representation of the dynamics of the system. In addition, considering the criteria for the time weighting factor discussed by Liggett and Cunge (1975), Saavedra and López (1996) and CEMAGREF (2000), a value of 0.66 was selected to ensure the convergence, accuracy and stability of the model.

Results and Discussion

Verification of the Numerical Simulation Procedures to Maneuver Gates

To verify the numerical procedures proposed by De León *et al*. (2007) for maneuvering control structures, experimental data from the Rehbock canal and an simulation unsteady flow model developed by Prado (2006) were used. First, the model was calibrated for a steady regime for an operating flow of 0.095 m^3s^{-1} in order to obtain the initial conditions. During the process, the values for the roughness conditions in the canal (0.009)and the coefficient for flow in the control structure (0.6) were fitted.

An analysis of the profile of the free water surface in Table 1 found that the measured and simulated residuals of the water depth throughout the canal were less than ± 0.004 m, while the largest percentage error was 0.67%, which was within the range of error considered acceptable by Arteaga (1997) and CEMAGREF (2000), of around 1%. Therefore, for the condition analyzed , the model can be considered to be capable of simulating the behavior of the water in the canal with sufficient accuracy.

In order to observe the behavior of the type (3) equation, the flow at the canal inlet was varied 0.023 m^3s^{-1} without any maneuvering of the structure, producing the family of parallel straight lines shown in Figure 3. This family of straight lines represents the change in flow and in water depth in the structure until reaching a new steady regime over 27 time intervals (4.5 min).

The straight lines resulting from the type (3) equation in the vicinity of the structure, superimposed on the load-flow curves for different openings make it possible to analyze the simulation procedures for the maneuverings, as proposed by De León *et al*. (2007), to satisfy changes in irrigation demand.

When the structures are maneuvered in order to satisfy changes in irrigation demand, the geometry and flow characteristics change, which makes it difficult to analyze the terms in the Saint Venant equations. Therefore, a global analysis was conducted of the phenomenon after maneuvering in the immediate vicinity of the gate.

When analyzing the phenomenon, taking into account choked discharge, the geometric and hydraulic characteristics in the structure and vicinity before maneuvering ($t = n$) were:

Opening = 0.19 m Water depth upstream = 0.694 m
Flow = 0.095 m^3s^{-1} Water depth downstream = 0.595 m

To satisfy a change in demand of 0.023 m^3s^{-1} in one time interval after maneuvering ($t = n + 1$), the following hydraulic geometric conditions were obtained:

Opening = 0.28 m Water depth downstream = 0.600 m
Water depth upstream = 0.667 m Type of discharge = choked

The gate opening was obtained using its dynamic equation, while water depth

1. Table 1. Calibration of the simulation model for the Rehbock Canal. Steady Regime.

Distance (m)	*n*	Water depth (m)		
		Measured	Simulated	Residual
0	0.009		0.689	
2.5	0.009	0.688	0.691	-0.003
4.5	0.009	0.694	0.691	0.003
5.5	0.009		0.692	
9	0.009	0.595	0.595	0
13.5	0.009	0.595	0.597	-0.002
18	0.009	0.595	0.599	-0.004
20	0.009		0.600	

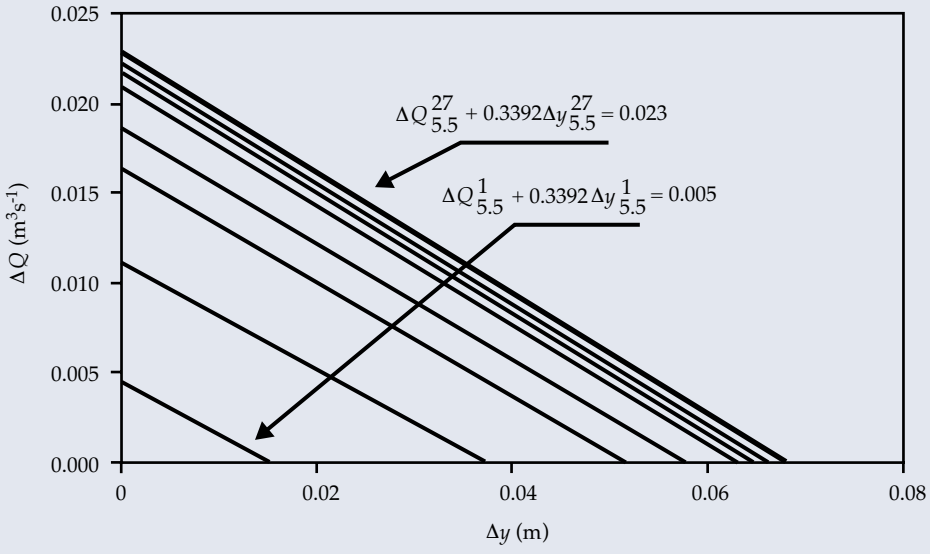

Figure 3. Family of straight lines for supply-storage in the structure.

upstream and downstream was calculated with equations (19) and (20).

Figure 4 was obtained by superimposing the family of straight lines for supply - storage with load-flow curves corresponding to the structure, which represents the trajectories for the methods used to execute the maneuvering of gates, as proposed by De León *et al*. (2007). The analysis of this figure shows that when the flow is reset and water depth remains constant (*a*), the intersection of equations (21) and (22) results in a flow of 0.141 m^3s^{-1} on the gate curve $a_1^{n+1} = 0.28$ m, which is higher than the reference (0.118 m^3s^{-1}). Nevertheless, by resetting the flow, the value demanded is imposed, requiring the model to decrease to the desired point, whose coordinates are $\Delta y = 0.067$ m and $\Delta Q = 0.118$ m^3s^{-1}, on the same gate curve during a time interval.

For the case in which the water depth is reset and flow remains constant (b), an intersection point is obtained with equations (23) and (24), which represents a load at the gate of 0.044 m, less than the reference value (0.067 m) on the gate curve $a_1^{n+1} = 0.28$ m. This results in a flow of 0.095 m^3s^{-1}, less than the flow demanded (0.118 m^3s^{-1}). The difference in flow is corrected by resetting the water depths, imposing the load needed to reach the reference point (0.067, 0.118) on the gate curve in a time interval.

When the maneuvering of the gate is instantaneous, flow and water depth are reset (c), and therefore the model is instantaneously shifted from the initial point (0.097, 0.095) on the gate curve $a_0^n = 0.19$ m to the location of the reference point (0.067, 0.118) on the gate curve $a_1^{n+1} = 0.28$ m.

Evolution of Flow with Progressive Maneuvering

Resetting Water Depth

When imposing the water depth in the calculation process during the simulation of the maneuvering of the gate, as observed in Figure 5, beginning at $t = 1$ min (the time at which the change occurs) the trend in the flow demand upstream and downstream and at the gate is the same, that is, the oscillations

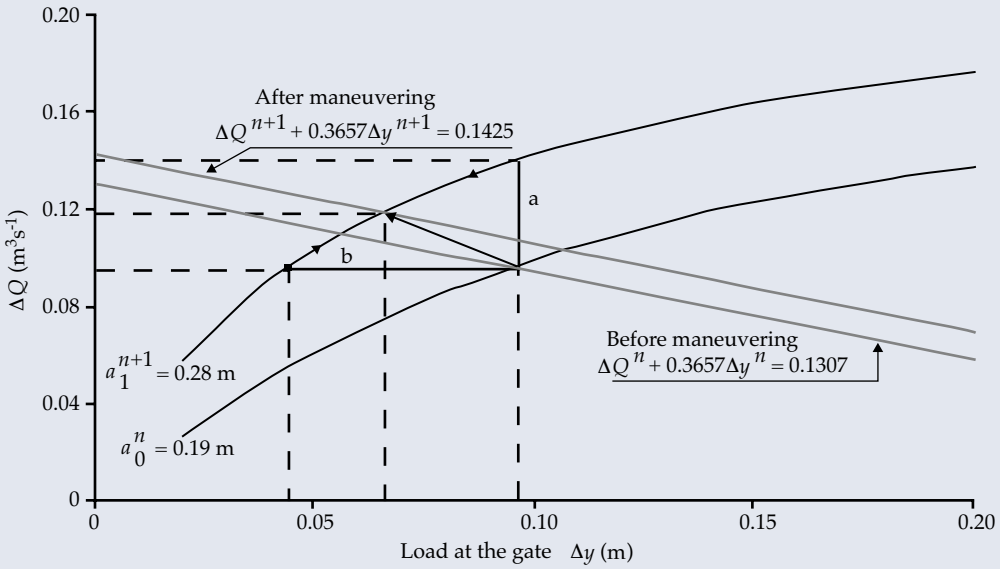

Figure 4. Run of the flow and water depth to maneuver the gate according to change in demand.

propagate at the same time and decrease in the same way. Nevertheless, the model calculates one time interval after the change in flow, 0.011 m^3s^{-1}, which is less than the 0.023 m^3s^{-1} corresponding to the change in demand. Therefore, the supply generated by the change in storage is underestimated. This behavior is similar to that reported by De León and Prado (2006) and De León *et al*. (2007).

The numerical oscillations in flow caused by maneuvering the gate were quickly reduced, since the time to reach a new steady regime was 1.8 min.

Resetting Flow

When the flow is reset in the simulation process, beginning at t = 1 min, the time at which the change in demand occurs, there is a shift in flow at the structure with respect to the near vicinity upstream and downstream, as seen in Figure 6. The maneuvering instantaneously affects the change in flow at the gate, while in the near vicinity the change occurs one time interval later, with the oscillations propagating themselves in phaseon both sides of the structure. In addition, a difference in flow of 0.011 m^3s^{-1} occurs between the gate and the sections upstream and downstream, which lessens after 1.8 minutes.

The changes in the flow behavior during a time interval for the sections analyzed are due to the incompatibility between the numerical scale and the physical scale of the propagation, similar to that reported by De León *et al*. (2007). This can be solved by reducing the time interval used in the simulation process, though it would create the disadvantage of increasing the computer processing time.

Evolution of Flow with Instantaneous Maneuvering

When flow and water depth are reset, as shown in Figure 7, as the unsteady regime begins (t = 1 min), the flows behave similarly to the progressive maneuvering that resets the flow, while the range of the oscillations is greater. As can be seen, the flow at the structure changes at the moment in which the maneuvering occurs, while upstream and downstream it changes one time interval later and propagates in phase; the numerical oscillations stabilize at 1.8 min.

Since the flow value is reset, the flow in the structure is expected to be equal to the demand at the time of maneuvering, as seen

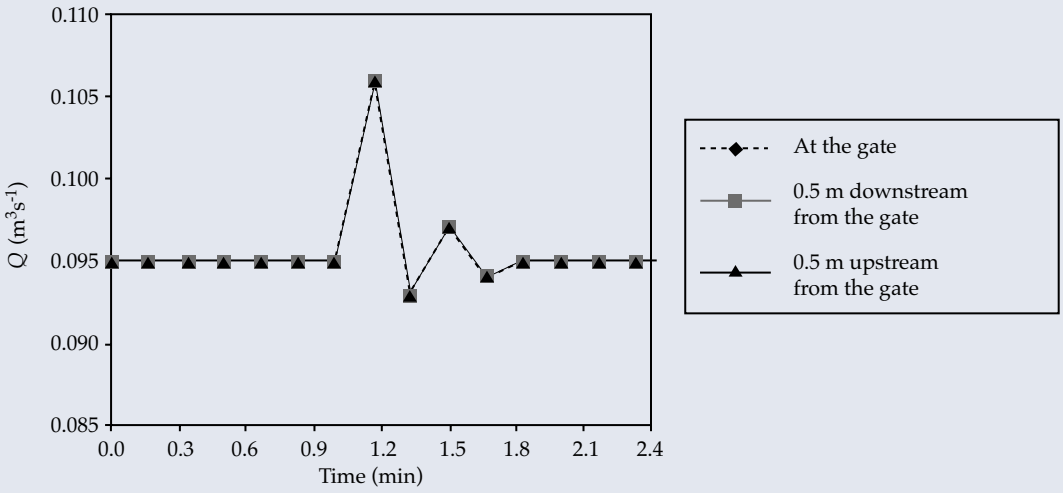

Figure 5. Progressive maneuvering with resetting the water depth and constant flow.

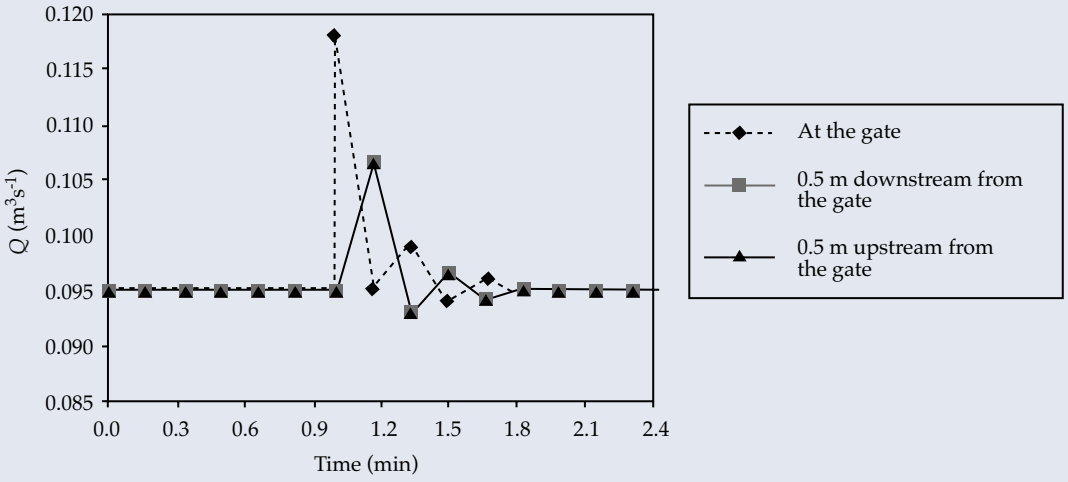

Figure 6. Progressive maneuvering with resetting water flow and constant water depth.

in Figure 7. Also observed is that this is the only maneuvering procedure in which the numerical oscillations disappear at the gate. Nevertheless, although the time in which the transient phenomenon occurs is the same for all three procedures, the numerical oscillations are greater with this procedure.

The three simulation procedures for gate maneuvering proposed by De León *et al*. (2007) were evaluated, which minimize the out of phase problem between the flow through the gates after the operation and the flow in the vicinity of the gates. In addition, these procedures can be integrated to execute the maneuvering of control structures with transient flow models. Nevertheless, the selection of the operating method will depend on the problem to be solved. When the variable to be regulated is flow, then progressive maneuvering with resetting water depth should be used, and when the variable to be regulated is water depth, then progressive maneuvering with resetting flow should be used.

By evaluating the behavior of the procedures to simulate gate operations (Figures 5, 6 and 7), it was possible to determine that progressive maneuvering with resetting the water depth reflect the best correspondence to the real functioning of a gate in an irrigation system, since the changes in flow in the structure and the near vicinity occur at the same time as the maneuvering.

Conclusions

The hypothesis proposed by De León *et al*. (2007) for the application of three simulation procedures for maneuvering of gates in irrigation canals was verified.

The procedures evaluated to simulate maneuvering minimize the problem of a shift in flow in the vicinity near the structures occurring as a result of changes in demand.

The simulation procedure with resetting the water depth best represents the flow dynamic when maneuvering of a gate occurs.

Received: 07/06/10
Accepted: 21/05/13

References

ARTEAGA, E. *Análisis y verificación de modelos matemáticos para el régimen impermanente en canales de riego*. Tesis de Doctor en Ciencias Técnicas. La Habana: Instituto Superior Politécnico José A. Echeverría, 1997, 121 pp.

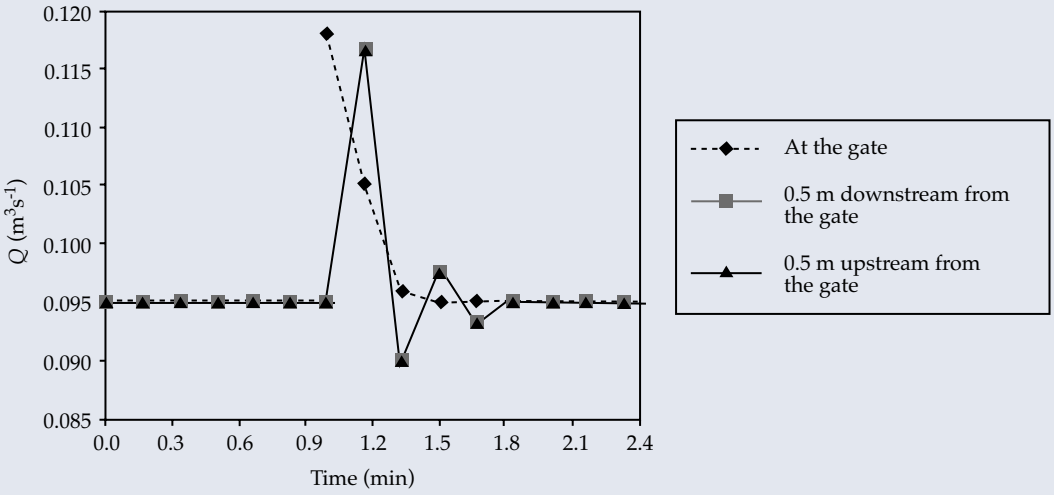

Figure 7. Instantaneous maneuvering with resetting water flow and water depth.

CEMAGREF. Simulation of irrigation canals. Volume II. *Theoretical concepts modeling approach*. Montpellier, France: CEMAGREF, 2000, 80 pp.

CHOW, V.T. *Hidráulica de canales abiertos*. Santafé de Bogotá, Colombia: Editorial McGraw Hill Interamericana S.A., 1994, pp. 513-543.

CLEMMENS, A.J., HOLLY, F.M., BURT, C.M., and DEVRIES, J.J. *Future needs for unsteady flow canal models*. ASCE National Conference on Irrigation and Drainage Engineering, Hawaii, 1991, pp. 501-507

CUNGE, J.A. *Simulation des ecolements non permanents dans les rivieres et canaux*. Grenoble: Ecole Nationale Supériore d'Hydraulique de Grenoble, 1988, 173 pp.

DE LEÓN, B. Modelación matemática de la maniobra de estructuras en una red de canales de riego. *Agrociencia*. Serie Agua-Suelo-Clima. Vol. 1, núm. 4, 1990, pp. 101-109.

DE LEÓN, B., PRADO, V., VERDIER, J. y FUENTES, C. Simulación numérica del movimiento de estructuras de control en canales de riego. *Agrociencia*. Vol. 41, núm. 1, 2007, pp. 75-86.

DE LEÓN, B. y PRADO, V. *Ejecución de la maniobra de compuertas en una red de canales de riego*. Documento Interno. Jiutepec: IMTA, 2006, 22 pp.

DE LEÓN, B., VERDIER, J., PIQUEREAU, A., RUIZ, V. y RENDÓN, L. Control of an Irrigation Canal Network. *Hydraulic Engineering in Mexico*. Vol. XVII, No. 4, October-December, 2002, pp. 21-34.

DE LEÓN, B. y EXEBIO, A. *La modelación matemática aplicada al estudio de la planeación de la operación de Unidades de Riego*. Montecillo, México: Centro de Hidrociencias, Colegio de Postgraduados, 1990, 14 pp.

GOUSSARD, J. *Modèles de Simulation du Fonctionnement des Canaux*. Grenoble, France: ICID-CIID, 2000, 28 pp.

HUSAIN, T., ABDERRAHMAN, W., KHAN, H., KHAN, S., KHAN, A., and EQNAIBI, B. Flow simulation using channel network model. *Journal of Irrigation and Drainage Engineering*. Vol. 114, No. 3, 1988, pp. 424-441.

LIGGETT, A. and CUNGE, J.A. Numerical methods of solution of the unsteady flow equations. Chapter 4 of "Unsteady flow in open channels". Vol. I. Edited by Mahmood, K. and Yevjevich, V. Ft. Collins, USA: Water Resources Publications, 1975, pp. 89-163.

LITRICO, X. and FROMION, V. Boundary control of linealized Saint Venant equations oscillating modes. *Automática*. Vol. 42, 2006, pp. 967-972.

MALATERRE, P.O. and BAUME, J.P. *Modeling and regulation of irrigation canals: existing applications and ongoing researches*. International Conference on Systems, Man and Cybernetics, California, USA, 1998, pp. 3850-3855.

MANZ, D.H. *Evaluación del funcionamiento de los sistemas de conducción de agua para riego, usando modelos de simulación dinámica*. Calgary, Canadá: Departamento de Ingeniería Civil, Universidad de Calgary, 1998, pp. 7-35.

PRADO, V. *Calibración de compuertas y simulación de la maniobra*. Documento Interno. Jiutepec, México: IMTA, 2006, 37 pp.

SAAVEDRA, Y. y LÓPEZ, J.L. Comparación de dos esquemas en diferencias finitas para la solución de ecuaciones de flujo no permanente en canales abiertos. En *Memorias del XII Congreso Latinoamericano de Hidráulica*, Guayaquil, Ecuador, 1996, pp. 97-108.

Institutional Address of the Authors

Dr. Gilberto de Jesús López Canteñs
Dr. Víctor Prado Hernández

Universidad Autónoma Chapingo
Km. 38.5 carretera México-Texcoco
56230 Chapingo, Estado de México, México
Teléfonos: +52 (595) 9521 680 y 9526 298
alelopez10@hotmail.com
vpradohdez@gmail.com

Dr. Benjamín de León Mojarro

Director de Conagua en Zacatecas
Comisión Nacional del Agua
Avenida Secretaría de la Defensa Nacional 90
Colonia Industrial
98604 Guadalupe, Zacatecas, México
Teléfono: +52 (492) 4914 951
felipe.deleon@conagua.gob.mx

Dr. Víctor Manuel Ruiz Carmona

Instituto Mexicano de Tecnología del Agua
Coordinación de Riego y Drenaje
Subcoordinación de Operación y Mantenimiento de Infraestructura Hidroagrícola
Paseo Cuauhnáhuac 8532, Colonia Progreso
62550 Jiutepec, Morelos, México
Teléfono: +52 (777) 3293 600, extensión 609
Fax: + 52 (777) 3293657
vmruiz@tlaloc.imta.mx

Dr. Mauricio Carrillo García
Dra. Laura Ibáñez Castillo
Dr. Eduardo Arteaga Tovar

Universidad Autónoma Chapingo
Km. 38.5 carretera México-Texcoco
56230 Chapingo, Estado de México, México
Teléfonos: +52 (595) 9521 649 y 9521 551
Fax: +52 (595) 9521 650
mauricio@correo.chapingo.mx
libacas@gmail.com
eatovar@correo.chapingo.mx

Click here to write the autor

Seismic Design Criteria of Tunnels

• Luis Eduardo Pérez-Rocha •
Instituto de Investigaciones Eléctricas, México

• Javier Avilés* •
Instituto Mexicano de Tecnología del Agua
*Corresponding Author

Abstract

PÉREZ-ROCHA, L.E. & AVILÉS, J. Seismic Design Criteria of Tunnels. *Water Technology and Sciences* (in Spanish). Vol. V, No. 1, January-February, 2014, pp. 55-68.

A revision and adaptation of the seismic design criteria established in the practice for straight tunnels of circular shape is presented. Two methods of analysis are considered: the free-field deformation method and the soil-structure-interaction method. The axial, flexural and ovaling deformations caused by the passage of seismic waves are analyzed, and practical expressions for computing the associated mechanical elements are given. The application of both methods is illustrated by solving the case of a typical tunnel in soft ground, which clearly shows the effect due to the stiffness contrast between the two elements.

Keywords: soil-tunnel interaction, free-field deformation, seismic response of tunnels.

Resumen

PÉREZ-ROCHA, L.E. & AVILÉS, J. Criterios de diseño sísmico de túneles. Tecnología y Ciencias del Agua. *Vol. V, núm. 1, enero-febrero de 2014, pp. 55-68.*

Se presenta una revisión y adaptación de los criterios de diseño sísmico establecidos en la práctica para túneles rectos de sección circular. Se consideran dos métodos de análisis: el método de deformación de campo libre y el método de interacción suelo-estructura. Se analizan las deformaciones axial, flexionante y de ovalamiento causadas por el paso de ondas sísmicas, y se dan expresiones prácticas para calcular los elementos mecánicos asociados. La aplicación de ambos métodos se ilustra con el caso de un túnel típico en suelo blando, que muestra claramente el efecto debido al contraste de rigidez entre los dos elementos.

Palabras clave: *interacción suelo-túnel, deformación de campo libre, respuesta sísmica de túneles.*

Introduction

Although underground structures are less vulnerable to seismic movement than surface structures, it is necessary to ensure the safety of these works in terms of the seismic movement of the construction area, whose geotechnical characteristics are usually very different.

The approaches used to evaluate the seismic effects on underground structures are different than those used for surface structures. In general, the design of surface structures takes into account inertial forces caused by movements in their foundation, whereas the design of underground structures addresses deformations imposed on the structure from the movement of the soil. For openings, seismic analysis methods are scarce and limited. Avilés and Pérez-Rocha (2011) recently developed a dynamic soil - opening interaction method, as well as design criteria based on calculating static shearing and moment values, multiplied by amplification factors that take into account the dynamic effect of the soil.

The simplest design approach is to ignore the interaction between the tunnel and the circumferential soil. In these conditions, free-field land deformations are first calculated and then the tunnel is designed to accommodate these deformations. This approach is satisfactory for tunnels that are more flexible than the land, but can be very conservative when the case is reversed. Therefore, soil-structure interaction effects need to be taken into account since the rigidity of the tunnel can considerably affect circumferential deformations.

This work presents a review and adaptation of the seismic design criteria established, in practice, for straight tunnels with circular sections (St. John and Zahrah, 1987; Hashash *et al*., 2001). The analysis methods include those for free-field deformations and soil-structure interactions to calculate maximum axial and flexural (curvature) deformations produced by different types of waves as well as axial stress, the flexural moment and design shear stress.

The seismic safety of tunnels must be demonstrated in terms of the capacity of the lining to resist three types of deformations: axial, curvature and ovaling. In straight tunnels, axial and curvature deformations occur (see Figure 1) when the seismic waves are propagated parallel or obliquely to the axis. In this case, the overall behavior of the tunnel is similar to that of an elastic beam subject to deformations imposed by the circumferential soil. The design conditions for this type of deformation apply to the longitudinal direction.

Ovaling deformations can occur when the seismic waves are propagated perpendicularly to the tunnel axis (see Figure 2), resulting in a distortion of the cross-section in the case of a flat deformation. In general, the vertical propagation of shear waves produces a critical ovaling deformation. The design considerations for this type of deformation apply to the transverse direction.

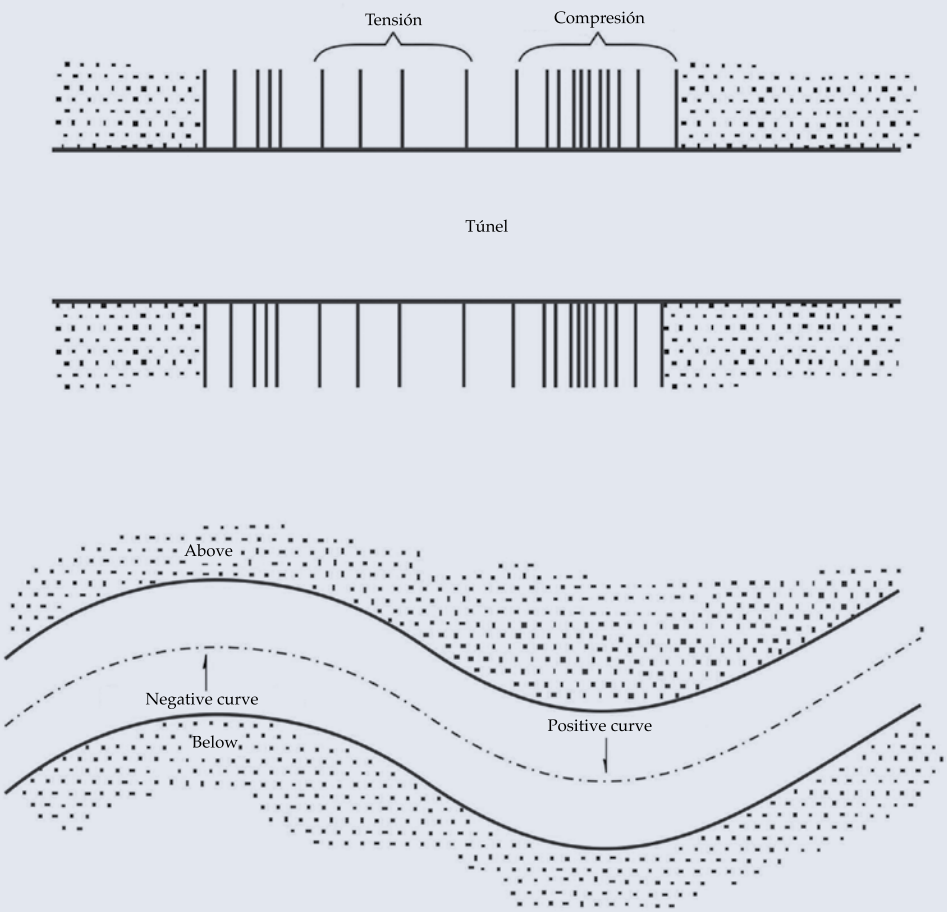

Figure 1. Axial and flexural deformations along the tunnel axis.

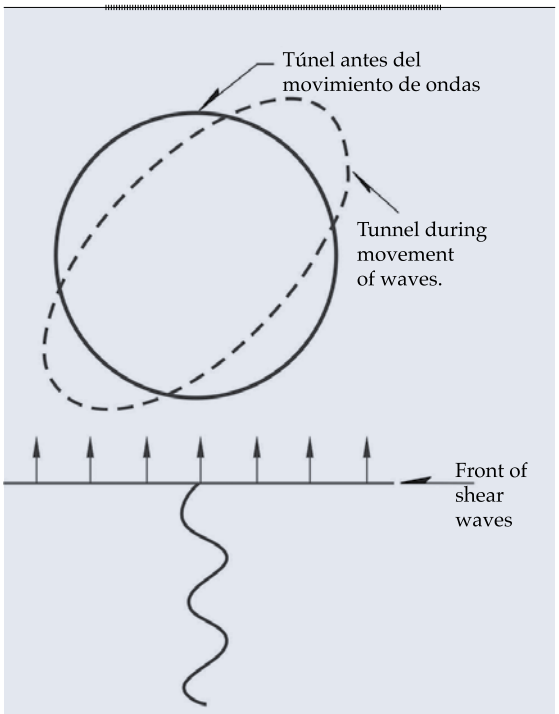

Figure 2. Ovaling deformation in a circular cross-section of the tunnel.

Method for Free-field Deformations

Free-field deformations refers to deformations in the land caused by the movement of seismic waves without the presence of a tunnel or excavation. This deformation ignores the soil-tunnel interaction, but in some cases it can provide a good representation of the expected structural deformation. This approach—which was adopted by the Seismic Design Manual produced by the Federal Electric Commission (MDS-CFE; 2008) and is based on piping design criteria (Flores and Vassilev, 1999)— overestimates or underestimates tunnel deformations depending on its rigidity with respect to the land.

Axial and Flexural Deformations

Figure 3 shows the movements of the land due to a harmonic shear wave at an oblique angle in relation to the tunnel axis. As can be observed, the transverse displacement depends on the incidence angle θ, the displacement angle *D* and the wavelength *L*, according to wave propagation theory.

The axial ε and curvature κ deformations can be expressed in terms of the incidence angle and the apparent horizontal propagation velocity ($C/\cos\theta$). For flat waves *S* and *P*, as well as Rayleigh waves propagated in an elastic medium (see Figure 4), we have the following expressions (Newmark, 1968):

$$\left.\begin{aligned}\varepsilon &= \frac{V_s}{C_s}\sin\theta\cos\theta \\ \kappa &= \frac{A_s}{C_s^2}\cos^3\theta\end{aligned}\right\}\text{; ondas de cortante } (S) \qquad (1)$$

$$\left.\begin{aligned}\varepsilon &= \frac{V_p}{C_p}\cos^2\theta \\ \kappa &= \frac{A_p}{C_p^2}\sin\theta\cos^2\theta\end{aligned}\right\}\text{; ondas de comprensión } (P) \qquad (2)$$

$$\left.\begin{aligned}\varepsilon &= \frac{V_R}{C_R}\cos^2\theta \\ \kappa &= \frac{A_R}{C_R^2}\cos^2\theta+\frac{A_R}{C_R^2}\sin\theta\cos^2\theta\end{aligned}\right\}\text{; ondas de Rayleigh} \qquad (3)$$

where:

V_s, V_p, V_R = maximum particle velocity of waves *S*, *P* and Rayleigh, respectively.

A_s, A_p, A_R = maximum particle acceleration of waves *S*, *P* and Rayleigh, respectively.

C_s, C_p, C_R = effective propagation velocity of waves *S*, *P* and Rayleigh, respectively.

The deformations produced by Rayleigh waves tend to be dominant only in the case of surface tunnels at sites far from the seismic source. Since it is difficult to define the incidence

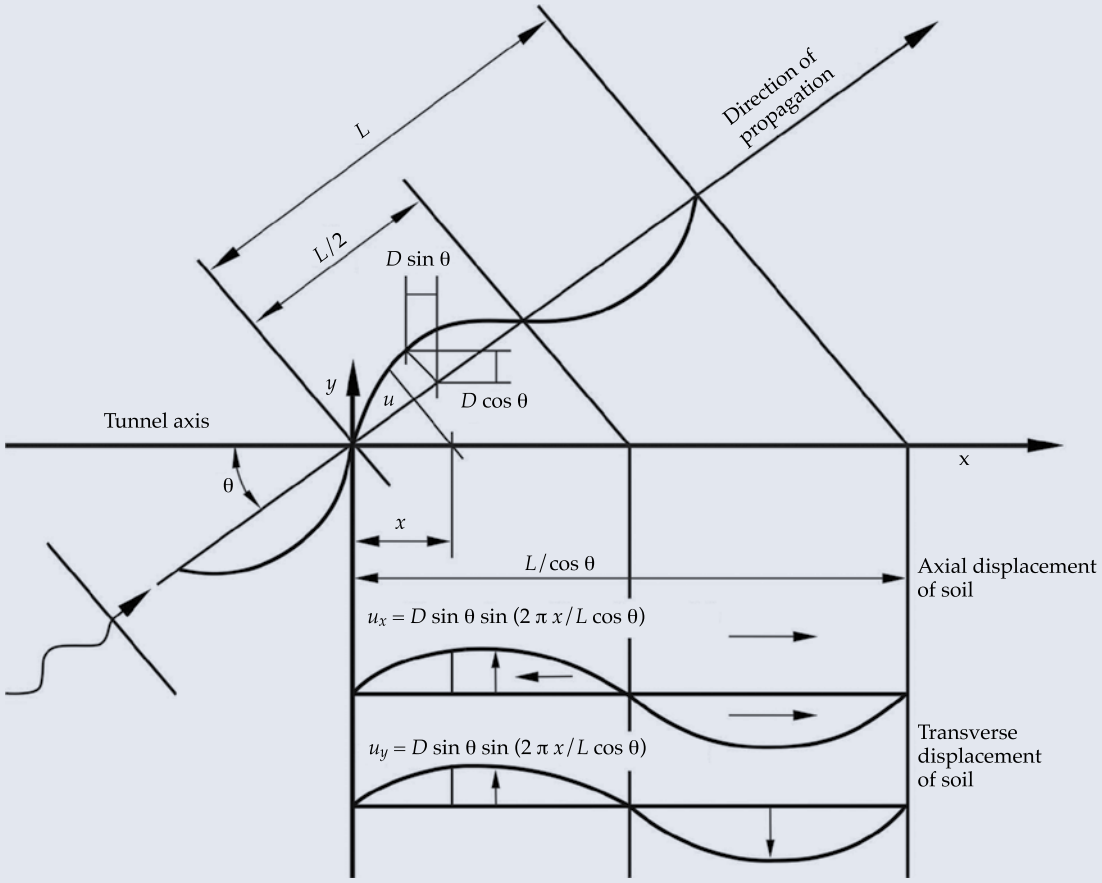

Figure 3. Effect of movement of shear waves along the tunnel axis.

angle, the design values proposed for ε and κ result in the maximums for the critical angles, that is:

$$\varepsilon_{máx} = \frac{V}{c_\varepsilon C} \tag{4}$$

$$\kappa_{máx} = \frac{A}{(c_\kappa C)^2} \tag{5}$$

where C is the effective wave propagation velocity, and V and A are the maximum velocity and acceleration of the land for the seismic design, respectively; c_ε and c_κ are the deformation and curvature coefficients, respectively, whose size depends on the type of wave and the critical incidence angle, as indicated in Table 1.

It is difficult to determine which type of waves are dominant in the earthquake design, and therefore an analysis is needed based on the observed evidence and engineering judgments. For design purposes, the combined axial and flexural deformation is calculated as follows:

$$\varepsilon_{tot} = \varepsilon_{máx} + r\kappa_{máx} \tag{6}$$

where r is the radius of the tunnel. The total deformation must be compared to the allowable deformation ε_{per} specified for the lining of the tunnel. With $\varepsilon_{tot} < \varepsilon_{per}$, the design is considered satisfactory.

The curvature more greatly affects the longitudinal deformation when the radius of the tunnel is larger. Nevertheless, the flexural deformation is generally relatively

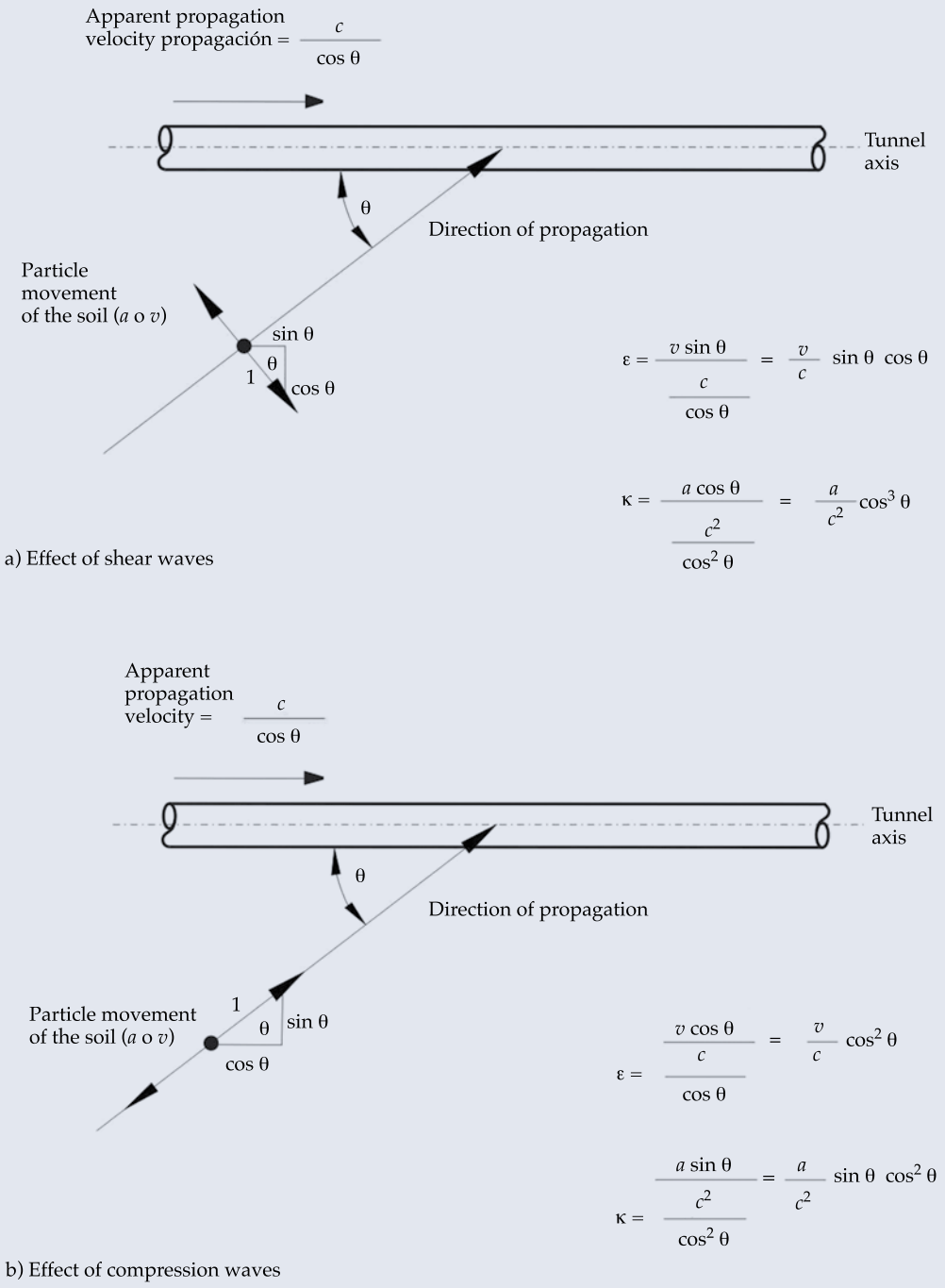

Figure 4. Deformations in the soil resulting from the oblique incidence of flat waves *S* and *P*.

Cuadro 1. Coeficientes de deformación y curvatura del terreno.

Tipo de coeficiente	Ondas *S*	Ondas *P*	Ondas de Rayleigh
c_ε	2 (θ = 45°)	1 (θ = 0)	1 (θ = 0)
c_κ	1 (θ = 0)	1.6 (θ = 35°)	1 (θ = 0)

small compared to the axial deformation. It is important to keep in mind the cyclical nature of the seismic response, since the lining can crack due to stress and the superimposing of dynamic and static compression stress can exceed the local lining capacity.

Ovaling Deformation

Distortions in the land from vertical incidence shear waves can be calculated for two conditions, as shown in Figure 5. With no excavation, the maximum diametral deformation is given by:

$$\frac{\Delta d}{d} = \pm \frac{\gamma_{máx}}{2} \qquad (7)$$

where $d = 2r$ is the tunnel diameter and $\gamma_{max} = V_s / C_s$ is the maximum shear deformation. With excavation, the maximum diametral deformation is given by:

$$\frac{\Delta d}{d} = \pm 2\gamma_{max}\left(1 - \nu_s\right) \qquad (8)$$

where ν_s is the Poisson ratio of the soil. The lining of the tunnel must be designed to support this deformation and be adjusted to changes in the cross-section.

Comparing equations (7) and (8), it can be deduced that when there is excavation, distortions are greater by a factor of 2 (for $\nu_s = 0.5$) to 3 (for $\nu_s = 0.25$). Equation (8) is a reasonable distortion criterion for tunnels that are less rigid than the circumferential soil, while equation (7) is appropriate when the rigidity of the lining is similar to that of the land. For tunnels that are more rigid than the circumferential soil, the distortions are even less than those obtained with equation (7) because of the soil-tunnel interaction.

Soil-Structure Interaction Method

The presence of the tunnel changes the free-field deformations, especially in soft soils. The analysis of the soil-structure interaction takes into account the rigidity of both the land and the tunnel. The coupled system is modeled as a beam on an elastic foundation subject to shear waves, ignoring inertial effects. When the tunnel is submitted to axial and flexural deformations due to the propagation of waves along the axis, the cross-section undergoes the following mechanical effects: a) axial stress Q, and 2) flexural moments M and shear stress V, as indicated in Figure 6.

Axial Stress

The axial stress generated by shear waves is at its maximum when $\theta = 45°$ and can be calculated as:

$$Q_{max} = \frac{\frac{K_a L_s}{2\pi}}{1 + 2\frac{K_a}{E_c A_c}\left(\frac{L_s}{2\pi}\right)^2} D_s \qquad (9)$$

where:

K_a = axial rigidity of the circumferential soil per unit length of the tunnel.
L_s = length of the dominant wave.
D_s = maximum displacement of the land.
E_c = elastic modulus of the lining.
A_c = area of the cross-section of the tunnel.

Calculating the maximum axial stress in this manner, it will not exceed the friction resistance of the soil, given by:

$$Q_{lim} = \frac{f L_s}{4} \qquad (10)$$

where f is the last friction force that can occur between the tunnel and the land, per unit length of tunnel.

Flexural Moment

The flexural moment generated by shear waves is at its maximum when $\theta = 0$ and can be calculated as:

$$M_{max} = \frac{K_l\left(\frac{L_s}{2\pi}\right)^2}{1 + \frac{K_l}{E_c I_c}\left(\frac{L_s}{2\pi}\right)^4} D_s \qquad (11)$$

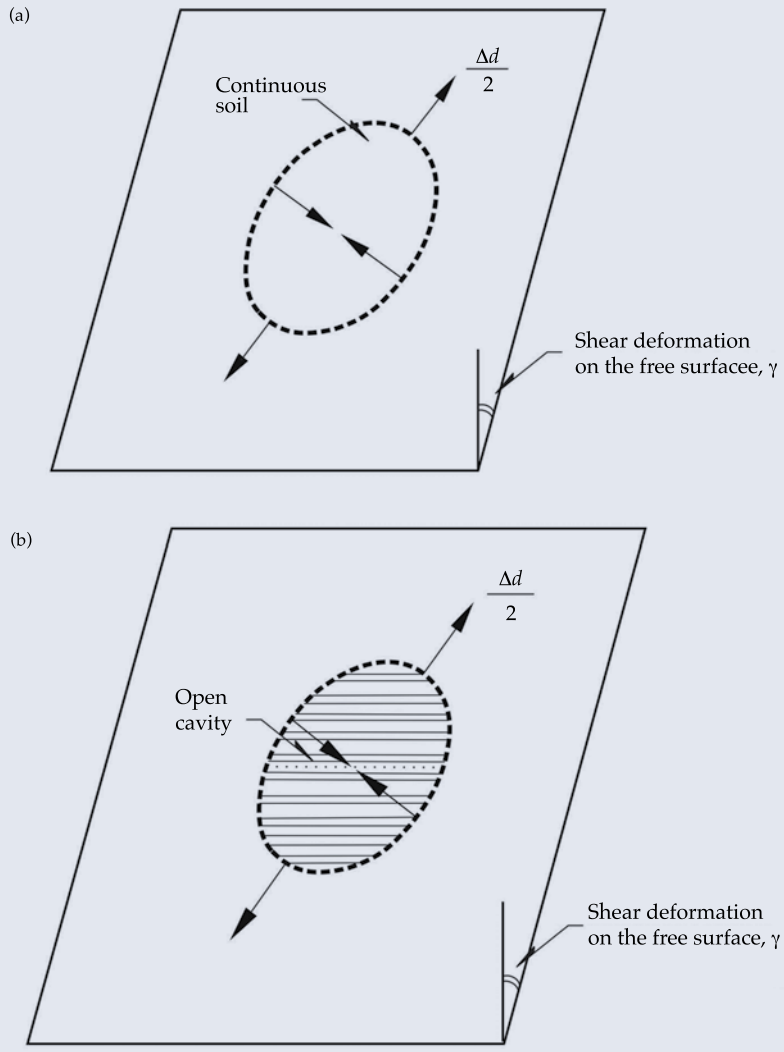

Figure 5. Free-field shear distortion in a medium without and with excavation.

Where:

K_l = lateral rigidity of the circumferential soil per unit of length of the tunnel.
L_s = dominant wavelength.
D_s = maximum displacement of the land.
E_c = elastic modulus of the lining.
I_c = inertial moment of the cross-section of the tunnel.

Equations (9) and (11) show that when the rigidity of the tunnel increases, represented by section modules $E_c A_c$ or $E_c I_c$, the axial stress and the flexural moment do not decrease. In fact, the tunnel attracts greater stress when it is more rigid. Therefore, a more flexible design that is adequately reinforced to provide sufficient ductility is sometimes more desirable.

Shear Stress

The maximum shear stress is obtained by:

$$V_{max} = \frac{2\pi}{L_s} M_{max} \qquad (12)$$

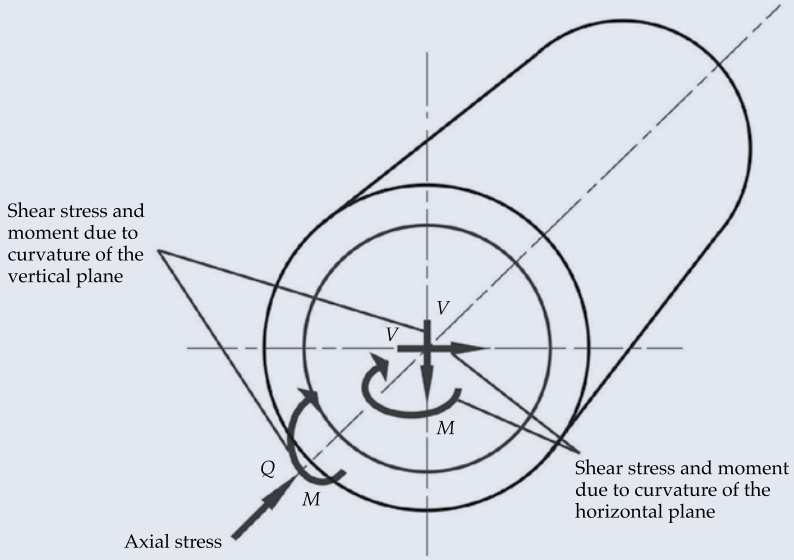

Figure 6. Longitudinal forces and moments caused by waves propagated along the tunnel axis.

To guarantee the structural safety of the tunnel, the following condition must be met:

$$F_C V_{máx} < F_R V_{res} \tag{13}$$

where F_C and F_R are load and resistance factors, respectively, V_{res} is the shear strength stress.

To calculate the sectional stresses, the dominant wavelength must be known. A reasonable calculation is given by:

$$L_s = T_s C_s \tag{14}$$

where T_s is the dominant vibration period and C_s is the effective propagation velocity of the soil. In addition, the axial and lateral rigidities of the soil springs can be calculated as:

$$K_a = K_l = \frac{16\pi G_s (1-\nu_s)}{3-4\nu_s}\frac{d}{L_s} \tag{15}$$

where:

G_s = shear modulus of soil.
ν_s = soil Poisson ratio.
d = tunnel diameter.
L_s = dominant wavelength.

Site Parameters

For a horizontally stratified medium (see Figure 7), the dominant vibration period can be estimated as:

$$T_s = 4\sqrt{\left(\sum_{n=1}^{N}\frac{h_n}{G_n}\right)\left(\sum_{n=1}^{N}\rho_n h_n\left(w_n^2 + w_n w_{n-1} + w_{n-1}^2\right)\right)} \tag{16}$$

where $w_o = 0$ in the basal rock and:

$$w_n = \frac{\sum_{i=1}^{n} h_i/G_i}{\sum_{i=1}^{N} h_i/G_i}; \quad n = 1,2,...,N \tag{17}$$

is a static approximation of the dominant vibration mode; h_n, G_n and ρ_n are the thickness, shear modulus and density of the nth stratum, respectively.

Once the value of the dominant period of the soil is known, the effective propagation

velocity of the shear waves can be represented by:

$$C_s = \frac{4H_s}{T_s} \tag{18}$$

where H_s is the depth of the soil deposit. The rigidity modulus for effective shear in the stratified medium is $G_s = \rho_s C_s^2$ where:

$$\rho_s = \frac{\sum_{n=1}^{N} \rho_n h_n}{H_s} \tag{19}$$

the mean density.

Axial and Flexural Deformation

For design purposes, the combined deformation that results from the axial stress and flexural moment is calculated as:

$$\varepsilon_{tot} = \varepsilon_{axial} + \varepsilon_{flexion} \tag{20}$$

where:

$$\varepsilon_{axial} = \frac{Q_{máx}}{E_c A_c} \tag{21}$$

$$\varepsilon_{flexion} = \frac{rM_{máx}}{E_c I_c} \tag{22}$$

and where r is the radius of the tunnel. The total deformation must be compared to the allowable deformation, ε_{per}, specified for the lining of the tunnel. With $\varepsilon_{tot} < \varepsilon_{per}$, the design is considered satisfactory.

Ovaling Deformation

The rigidity of the tunnel relative to the land is represented by the compressibility C and flexibility F coefficients, given by:

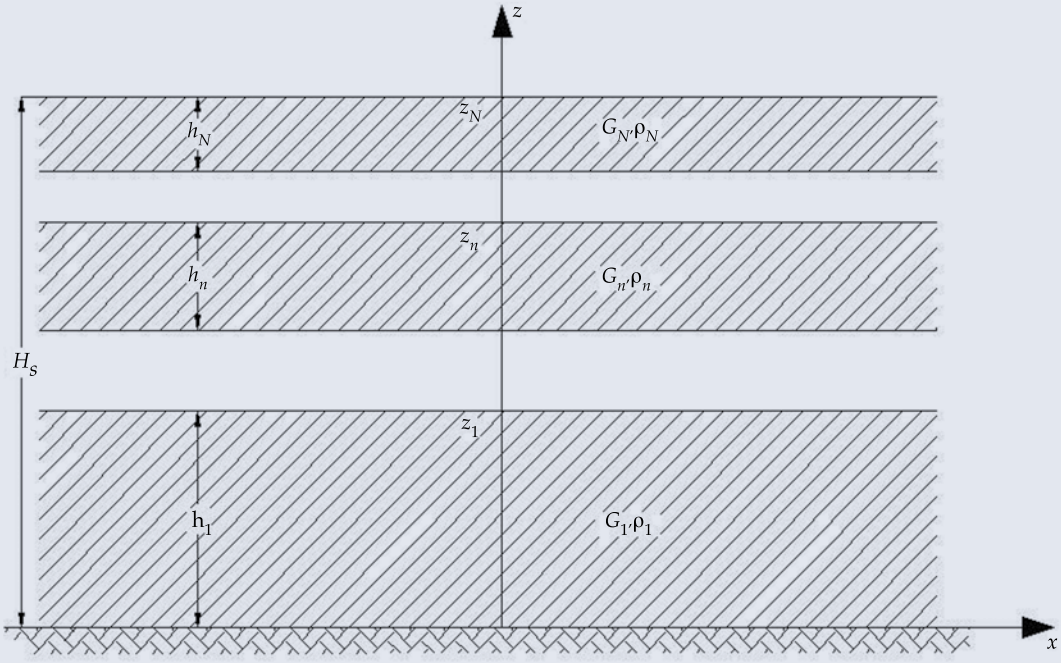

Figure 7. Horizontally stratified soil deposit.

$$C = \frac{E_s\left(1-\nu_c^2\right)r}{E_c t\left(1+\nu_s\right)\left(1-2\nu_s\right)} \tag{23}$$

$$F = \frac{E_s\left(1-\nu_c^2\right)r^3}{6E_c I_c'\left(1+\nu_s\right)} \tag{24}$$

where:

E_s = elastic modulus of soil.
ν_s = Poisson ratio of the soil.
E_c = elastic modulus of the lining.
ν_c = lining Poisson ratio.
t = lining thickness.
r = tunnel radius.
I_c' = inertial moment of the lining per unit width.

The C coefficient measures the radial rigidity of the tunnel-soil system, while coefficient F measures its ovaling rigidity. Based on these parameters and the maximum shear deformation, γ_{max}, the diametral deformation $\Delta d/d$ can be calculated (Figure 5) as well as the normal circumferential stress N_{max} and the flexural moment M_{max} (see Figure 8) that act on a strip of unit width b, by applying the following expressions:

$$\frac{\Delta d}{d} = \pm\frac{1}{3}K_1\gamma_{máx} \tag{25}$$

$$N_{máx} = \pm\frac{1}{2}K_2\frac{E_s}{(1+\nu_s)}r\gamma_{máx} \tag{26}$$

$$M_{máx} = \pm\frac{1}{6}K_1\frac{E_s}{(1+\nu_s)}r^2\gamma_{máx} \tag{27}$$

where:

$$K_1 = \frac{12\left(1-\nu_s\right)}{2F+5-6\nu_s} \tag{28}$$

$$K_2 = 1 + \frac{F\left(1-2\nu_s\right)\left(1-C\right)-\left(1-2\nu_s\right)^2/2+2}{F\left[\left(1-2\nu_s\right)\left(1+C\right)+2\right]+C\left(2.5-8\nu_s+6\nu_s^2\right)+6-8\nu_s} \tag{29}$$

The stress σ_{tot} and the deformation ε_{tot} resulting from the circumferential stress and moment are given by:

$$\sigma_{tot} = \pm\frac{N_{máx}}{A_c'} \pm \frac{M_{máx}t}{2I_c'} \tag{30}$$

$$\varepsilon_{tot} = \frac{\sigma_{tot}}{E_c} \tag{31}$$

where $A_c' = bt$ and $I_c' = bt^3/12$ are the area and the inertial lining moment.

Application Examples

The application of the design criteria presented is illustrated next, taking into account the following data:

Seismic Parameters

- Maximum ground acceleration, A_s = 150 cm/s^2.
- Maximum speed terrain, V_s = 45 cm/s.

Geotechnical Parameters

- Dominant soil period, T_s = 1.25 s.
- Effective propagation velocity, C_s = 200 m/s.
- Shear modulus of soil, G_s = 7 340 ton/m^2.
- Poisson ratio of soil, ν_s = 0.45

Structural Parameters

- Inside tunnel diameter, d = 7 m.
- Thickness of lining, t = 35 cm.
- Area of the cross-section of the lining, $A_c = \pi(3.5^2 - 3.15^2) = 7.31$ m^2.
- Inertial moment of the cross-section of the lining, $I_c = \pi(3.5^4 - 3.15^4)/4 = 40.53$ m^4.
- Area and inertial moment of the lining per unit width, $A_c' = 1 \times 0.35 = 0.35$ m^2 e $I_c' = 1 \times 0.35^3/12 = 0.0036$ m^4.

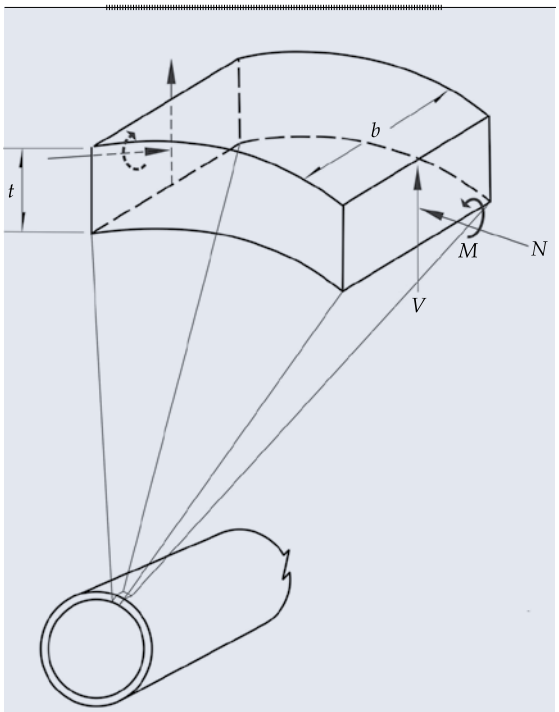

Figure 8. Circumferential stresses and moments caused by waves propagated perpendicular to the tunnel axis.

- Elastic modulus of the concrete, E_c = 250 000 kg/cm^2.
- Poisson ratio of the concrete, $\nu_c = 0.2$
- Allowable deformation of the concrete, $\varepsilon_{per} = 0.003$.

Analysis without Interaction Effects

To apply the method for the free-field deformation, the following steps are used:

1. Calculate the axial and flexural deformation, considering the critical effect of shear waves, with $c_\varepsilon = 2$ and $c_\kappa = 1$.

$$\varepsilon_{máx} = \frac{V_s}{c_\varepsilon C_s} = \frac{0.45}{2 \times 200} = 0.00113$$

$$r\kappa_{máx} = \frac{rA_s}{(c_\kappa C_s)^2} = \frac{3.5 \times 1.5}{(1 \times 200)^2} = 0.00013$$

The combined maximum axial and flexural deformation is:

$$\varepsilon_{tot} = \varepsilon_{máx} + r\kappa_{máx} = 0.00113 + 0.00013$$
$$= 0.00126 < \varepsilon_{per} = 0.003$$

Because of the cyclical nature of the seismic response, the lining must be adequately reinforced to prevent stress cracking. It is also necessary to review the superimposition of compression stresses from static load and seism. The latter equals 250 000 x 0.00126 = 315 kg/cm^2.

2. Calculate the ovaling deformation that the tunnel must support in monolithic conditions. The maximum shear deformation is:

$$\gamma_{máx} = \frac{V_s}{C_s} = \frac{0.45}{200} = 0.00225$$

Therefore, the maximum change in diameter (extension and compression) imposed on the tunnel is:

$$\Delta d = \frac{\gamma_{máx}}{2} d = \frac{0.00225}{2} \times 700 = 0.79 \text{ cm}$$

Analysis with Interaction Effects

To apply the soil-structure interaction method, the following steps are used:

Review of the axial and flexural deformations

1. Calculate the dominant wavelength:

$$L_s = T_s C_s = 1.25 \times 200 = 250 \text{ m}$$

2. Deduce the maximum land displacement such that the associated deformations are comparable to those calculated using the free-field deformation method. The purpose of this supposition is to clearly see the effect of the soil-tunnel interaction:

$$\frac{2\pi D_s}{L_s} = \frac{V_s}{c_\varepsilon C_s} \quad \therefore \quad D_s = \frac{250 \times 0.45}{4\pi \times 200}$$

= 4.48 cm, for axial deformation

$$\frac{4\pi^2 D_s}{L_s^2} = \frac{A_s}{(c_\kappa C_s)^2} \quad \therefore \quad D_s = \frac{(250)^2 \times 1.5}{4\pi^2 \times (200)^2}$$

= 5.94 cm, for flexural deformation

3. Calculate the axial and lateral rigidity of the soil, per unit length of the tunnel:

$$K_a = K_l = \frac{16\pi G_s(1-\nu_s)}{3-4\nu_s}\frac{d}{L_s}$$

$$= \frac{16\pi \times 7\,340 \times (1-0.45)}{3-4\times 0.45} \times \frac{7}{250} = 4\,734.84 \text{ ton/m}$$

4. Calculate the maximum axial stress and the corresponding longitudinal deformation:

$$Q_{máx} = \frac{\frac{K_a L_s}{2\pi}}{1+2\frac{K_a}{E_c A_c}\left(\frac{L_s}{2\pi}\right)^2} D_s$$

$$= \frac{\frac{4\,734.84 \times 250}{2\pi}}{1+2\times\frac{4\,734.84}{2\,500\,000\times 7.31}\times\left(\frac{250}{2\pi}\right)^2} \times 0.0448 = 4\,636.49 \text{ ton}$$

$$\varepsilon_{axial} = \frac{Q_{máx}}{E_c A_c} = \frac{4\,636.49}{2\,500\,000 \times 7.31} = 0.00025$$

5. Calculate the maximum flexural moment and the corresponding longitudinal deformation:

$$M_{máx} = \frac{K_l\left(\frac{L_s}{2\pi}\right)^2}{1+\frac{K_l}{E_c I_c}\left(\frac{L_s}{2\pi}\right)^4} D_s$$

$$= \frac{4\,734.84\times\left(\frac{250}{2\pi}\right)^2}{1+\frac{4\,734.84}{2\,500\,000\times 40.53}\times\left(\frac{250}{2\pi}\right)^4} \times 0.0594 = 3\,769.56 \text{ ton-m}$$

$$\varepsilon_{flexion} = \frac{rM_{máx}}{E_c I_c} = \frac{3.5 \times 3\,769.56}{2\,500\,000 \times 40.53} = 0.00013$$

6. Compare the combined axial and flexural deformation with the allowable deformation:

$$\varepsilon_{tot} = \varepsilon_{axial} + \varepsilon_{flexion} = 0.00025 + 0.00013$$

$$= 0.00038 < \varepsilon_{per} = 0.003$$

Note that this deformation is significantly less than that calculated using the free-field deformation method.

7. Determine the maximum shear stress due to the curvature resulting from flexion:

$$V_{máx} = \frac{2\pi}{L_s} M_{máx} = \frac{2\pi}{250} \times 3\,769.56 = 94.74 \text{ ton}$$

It is necessary to validate that the acting shear stress is less than the shear strength stress stipulated by regulations.

Review of Ovaling Deformation

1. Obtain the elastic modulus of soil:

$$E_s = 2(1+\nu_s)G_s = 2\times(1+0.45)\times 7\,340 = 21\,286 \text{ ton/m}^2$$

2. Determine the compressibility and flexibility coefficients of the tunnel-soil system:

$$C = \frac{E_s(1-\nu_c^2)r}{E_c t(1+\nu_s)(1-2\nu_s)}$$

$$= \frac{21\,286\times(1-0.2^2)\times 3.5}{2\,500\,000\times 0.35\times(1+0.45)\times(1-2\times 0.45)} = 0.56$$

$$F = \frac{E_s(1-\nu_c^2)r^3}{6E_c I_c'(1+\nu_s)}$$

$$= \frac{21\,286\times(1-0.2^2)\times 3.5^3}{6\times 2\,500\,000\times 0.0036\times(1+0.45)} = 11.19$$

3. Determine the system response coefficients:

$$K_1 = \frac{12(1-\nu_s)}{2F+5-6\nu_s}$$

$$= \frac{12\times(1-0.45)}{2\times 11.19+5-6\times 0.45} = 0.267$$

$$K_2 = 1+\frac{F(1-2\nu_s)(1-C)-(1-2\nu_s)^2/2+2}{F[(1-2\nu_s)(1+C)+2]+C(2.5-8\nu_s+6\nu_s^2)+6-8\nu_s}$$

$$= 1+\frac{11.19\times(1-2\times 0.45)\times(1-0.56)-(1-2\times 0.45)^2/2+2}{11.19[(1-2\times 0.45)(1+0.56)+2]+0.56(2.5-8\times 0.45+6\times 0.45^2)+6-8\times 0.45}$$

$$= 1.094$$

4. Calculate the ovaling deformation that the tunnel must support in monolithic conditions. The maximum shear deformation is:

$$\gamma_{máx} = \frac{V_s}{C_s} = \frac{0.45}{200} = 0.00225$$

Therefore, the maximum change in diameter (extension and compression) imposed on the tunnel is:

$$\Delta d = \frac{1}{3}K_1\gamma_{máx}d$$

$$= \frac{0.267\times 0.00225\times 700}{3} = 0.14 \text{ cm}$$

5. Calculate the maximum circumferential normal stress and maximum flexural moment:

$$N_{máx} = \frac{1}{2}K_2\frac{E_s}{(1+\nu_s)}r\gamma_{máx}$$

$$= \frac{1.094}{2}\times\frac{21\,286}{(1+0.45)}\times 3.5\times 0.00225 = 63.24 \text{ ton}$$

$$M_{máx} = \frac{1}{6}K_1\frac{E_s}{(1+\nu_s)}r^2\gamma_{máx}$$

$$= \frac{0.267}{6}\times\frac{21\,286}{(1+0.45)}\times 3.5^2\times 0.00225 = 18.01 \text{ ton-m}$$

6. Determine the circumferential stress and deformation resulting from the combined effect of N_{max} and M_{max}:

$$\sigma_{tot} = \frac{N_{máx}}{A'_c}+\frac{M_{máx}t}{2I'_c}$$

$$= \frac{63.24}{0.35}+\frac{18.01\times 0.35}{2\times 0.0036} = 1056 \text{ ton/m}^2$$

$$\varepsilon_{tot} = \frac{\sigma_{tot}}{E_c} = \frac{1\,056}{2\,500\,000} = 0.00042$$

Given the cyclical nature of the seismic response, the lining must be adequately reinforced in order to prevent stress cracking. It is also necessary to review the superimposition of compression stresses due to static load and seism.

Final Comments

This work discusses two approaches: free-field and soil-structure interaction. Free-field is a method that determines deformations in the land due to the movement of waves, and these deformations are later imposed on the structure to determine the stresses that it must support. To calculate these deformations, it is necessary to know the maximum particle velocities and accelerations produced by the movement of waves *S*, *P* and Rayleigh. Generally, free-field stresses are much higher than those that occur in the structure. In effect the presence of the structure changes the deformations imposed by the free field. As a result, both the soil and structure deformations are less. The soil-structure interaction is the approach that takes into account this reduction. This approach provides expressions to evaluate the stresses that occur in transverse and longitudinal sections of the tunnel. To determine these stresses, the characteristic wavelength must be known, which is evaluated based on the dominant vibration period and the shear wave

propagation velocity in the constructed area. Expressions are also provided to determine the deformations in the tunnel based on the those in the land caused by seismic excitation. Finally, an example is solved step-by-step, which illustrates the two types of analyses: free-field deformation versus soil-structure interaction deformations.

Certain considerations have been mentioned regarding the applicability of the expressions presented. In general, the seismic design criteria can be applied to the main, more definitive lining conditions, taking into account the actual thickness and the equivalent properties of the compound section. On the other hand, no criteria are given to take into account the connection between the tunnel with the rigid opening elements. Because of the complexity of the response in the tunnel-opening connection, the dynamic concentration of stresses that occurs at this junction are usually calculated using finite element models.

The design criteria presented are based on knowledge of the maximum movements of the land in the design seism and the use of sufficiently approximated simplified analysis methods. The maximum movement of the land must be calculated at the level of the tunnel given the reduced values at greater depths. Hashash *et al*. (2001) provide recommendations to calculate the maximum velocity and acceleration of the land in function of the size of the seism, the distance between the source and the site and the depth of the tunnel.

Received: 29/09/11
Accepted: 16/05/13

References

AVILÉS, J. y PÉREZ-ROCHA, L.E. Presiones dinámicas del suelo en lumbreras. *Revista de Ingeniería Sísmica*. Núm. 85, 2011, pp. 1-31.

FLORES, R. y VASSILEV, V. Seismicity in pipeline design. *Hydraulic Engineering in Mexico*. Vol. XIV, No. 2, May-August, 1999, pp. 49-64.

HASHASH, Y.M.A., HOOK, J.J., SCHMIDT, B., and YAO, J.I.C. Seismic design and analysis of underground structures. *Tunnelling and Underground Space Technology*. Vol. 16, 2001, pp. 247-293.

MDS-CFE. *Manual de diseño de obras civiles: diseño por sismo*. México, D.F.; Comisión Federal de Electricidad e Instituto de Investigaciones Eléctricas, 2008.

NEWMARK, N.M., Problems in wave propagation in soil and rock. *Proceedings of the International Symposium on Wave Propagation and Dynamic Properties of Earth Materials*. Albuquerque, 1968.

ST. JOHN, C.M. and ZAHRAH, T.F., Aseismic design of underground structures. *Tunnelling and Underground Space Technology*. Vol. 2, 1987, pp. 165-197.

Institutional Address of the Authors

Dr. Luis Eduardo Pérez-Rocha

Instituto de Investigaciones Eléctricas
Paseo de la Reforma 113
62490 Temixco, Morelos, México
Teléfono +52 (777) 3623 811, extensión 7578
lepr@iie.org.mx

Dr. Javier Avilés

Instituto Mexicano de Tecnología del Agua
Paseo Cuauhnáhuac 8532, colonia Progreso
62550 Jiutepec, Morelos, México
Teléfono: +52 (777) 3293 600, extensión 864
Fax: +52 (777) 3293 679
javiles@tlaloc.imta.mx

Click here to write the autor

Mechanisms that Release Arsenic to the Groundwater of the Laguna Region, States of Coahuila and Durango, Mexico

• Miguel Ángel Mejía-González* • Luis González-Hita •
Instituto Mexicano de Tecnología del Agua
*Corresponding Author

• Roberto Briones-Gallardo • Antonio Cardona-Benavides •
Universidad Autónoma de San Luis Potosí, México

• Pedro Soto-Navarro •
Comisión Nacional del Agua, México

Abstract

MEJÍA-GONZÁLEZ, M.A., GONZÁLEZ-HITA, L., BRIONES-GALLARDO, R., CARDONA-BENAVIDES, A. & SOTO-NAVARRO, P. Mechanisms that Release Arsenic to the Groundwater of the Laguna Region, States of Coahuila and Durango, Mexico. *Water Technology and Sciences* (in Spanish). Vol. V, No. 1, January-February, 2014, pp. 69-80.

In order to elucidate the processes that causes high concentrations of arsenic in the aquifer of the Comarca Lagunera were conducted geochemical studies of groundwater and sediment. The results of the sediment geochemistry indicate that arsenic is mainly adsorbed on amorphous and crystalline Fe oxides. The results of the groundwater geochemistry indicate: 1) Cation Exchange between calcium and sodium, 2) Dissolution of calcite due to cation exchange, 3) Increase in pH due to the dissolution of calcite, and 4) high concentrations of arsenic due to elevated pH values.

Keywords: groundwater, sediment, arsenic, Fe oxides, pH.

Resumen

MEJÍA-GONZÁLEZ, M.A., GONZÁLEZ-HITA, L., BRIONES-GALLARDO, R., CARDONA-BENAVIDES, A. & SOTO-NAVARRO, P. Mecanismos que liberan arsénico al agua subterránea de la Comarca Lagunera, estados de Coahuila y Durango, México. Tecnología y Ciencias del Agua. *Vol. V, núm. 1, enero-ebrero de 2014, pp. 69-80.*

A fin de dilucidar los procesos que dan origen a las altas concentraciones de arsénico en el acuífero de la Comarca Lagunera (México), se llevaron a cabo estudios geoquímicos del agua subterránea y los sedimentos. Los resultados de la geoquímica de los sedimentos indican que el arsénico disponible se encuentra principalmente adsorbido en los óxidos de Fe amorfos y cristalinos. Los resultados de la geoquímica del agua subterránea indican: 1) intercambio catiónico entre el calcio y el sodio; 2) disolución de calcita debido al intercambio catiónico; 3) aumento del pH debido a la disolución de la calcita, y 4) altas concentraciones de arsénico debido a elevados valores de pH.

Palabras clave: *agua subterránea, sedimento, arsénico, óxidos de fierro, pH.*

Introduction

In the early 1960s, Mexican health institutions reported health problems in people and animals in the Comarca Lagunera in the states of Coahuila and Durango, Mexico due to consumption of groundwater with high levels of arsenic. The water came from the alluvial aquifer that represented the main supply source for over two million people who lived in the area. Previous studies (Cinvestav, 1986; IMTA, 1992) identified extensive areas in the Lagunera region where arsenic concentrations were over 25 µg/l, the maximum level recommended by NOM-127-SSA1-1994 (modified in 2000) for water for human consumption.

Diverse hydrogeochemical and isotopic studies have been conducted in order to understand the geochemical behavior of arsenic and other groundwater components (SICYGSA, 2000; Ortega, 2003; Molina, 2004). Molina's work considers high arsenic values in groundwater to be a product of a combination of reactions involving the dissolution of Fe

oxide and desorption due to high pH values. SICYGSA's work suggests that desorption of AS as a function of the pH of groundwater is an important mobilization process since a good relationship was detected between dissolved As and pH. Research by Ortega in the Viesca lagoon found low arsenic values in the carbonate aquifer and high values in the water in the clay aquitard.

Those studies only analyze the chemical components of groundwater without addressing the geochemistry of the aquifer sediments. In this study, the geochemistry of both the sediments and the groundwater are analyzed in order to identify the mechanisms that influence the mobilization of arsenic.

Study Area

The study area is located in northern Mexico, in the southwestern portion of the state of Coahuila and in northeastern Durango, Mexico (Figure 1). It encompasses the Comarca Lagunera, located between 25° 15′ 00″ and 26° 15′ 00″ north latitude and the meridians 102° 40′ 00″ and 104° 00′ 00″ west of Greenwich.

The geological formations in the Comarca Lagunera range from the Paleozoic period (Rodeo Formation) to the Quaternary alluvium (Álvarez, 1961; Tamayo, 1982). The basin is made up of sedimentary deposits (limestone, dolomite, gypsum, clay sands and conglomerates) as well as igneous rocks

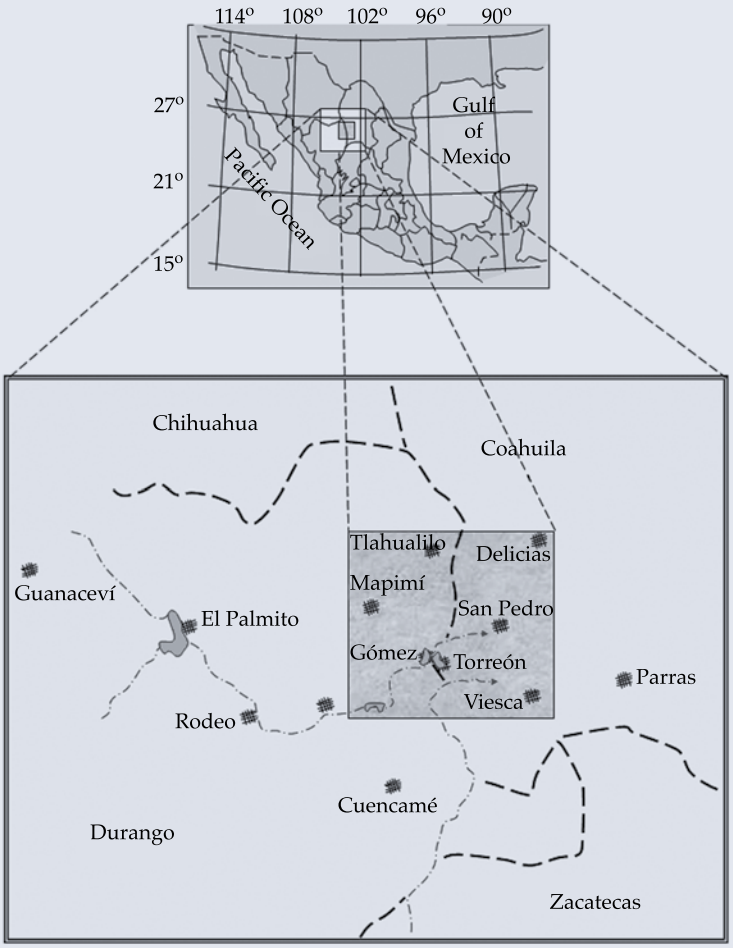

Figure 1. Location of the Study Area.

(volcanic deposits and granite). The geological succession (INEGI, 1988) is: (1) the Jurassic Formation, "Minas Viejas" with gypsum, lutites and limestone; (2) the Cretaceous Formation, "Aurora" with limestone and dolomites, "Indura" composed of lutites, limestone and limonites (Tardy, 1974), "Caracoal" with lutites, clays and sands; (3) the "Ahuichila" Tertiary Formation composed of limestone and conglomerates, and the "Santa Inés" also composed of limestone and conglomerates, with an impermeable clay matrix; and (4) the Quaternary alluvium that comprises the granular aquifer in the region (Figure 2).

The Comarca Lagunera is an endorheic basin fed by the Nazas and Aguanaval Rivers. The Nazas River, which is 220 kim long, drains the western region with a 60 000 km^2 basin located in the states of Coahuila and Durango. The mean annual flow is 1.1 x 10^9 m^3 and it is regulated by the Lázaro Cárdenas and Francisco Zarco dams (PIFSV-SARH, 1991). The Aguanaval River is 305 km long and drains the southeast portion with a 25 500 km^2 basin. The annual mean flow is 1.6 x 10^8 m^3 (PIFSV-SARH, 1991).

The rainy season is 4 months long, from June to September, with an annual mean precipitation of 200-300 mm (PIFSV-SARH, 1991). The mean annual temperature is 20.6 °C. The groundwater generally flows towards the northeast, from the mountains to the valley (Figure 3).

Methodology

Geochemistry of the Sediments

Four samples of sub-surface alluvial sediments were taken throughout the course of the Nazas River (Figure 4 and 5). The sampling was performed following the direction of the river channel, selecting those sites where it was possible to build a profile based on an unaltered alluvial wall that contained representative samples of alluvial deposition. The geographic coordinates (UTM) of the samples are indicated in Table 1 and represented with the letter *S*,

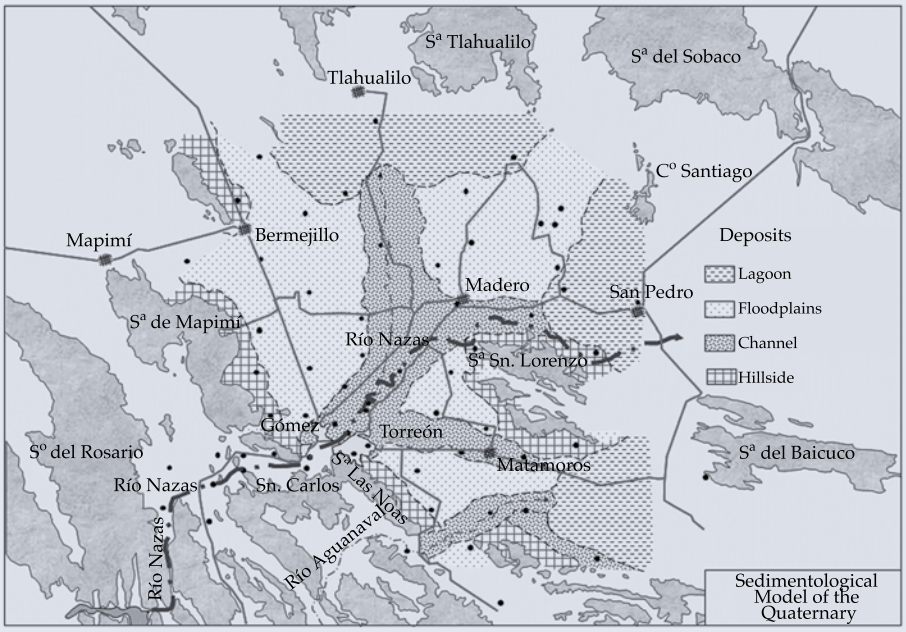

Figure 2. Sedimentological Model of the Quaternary Alluvium.

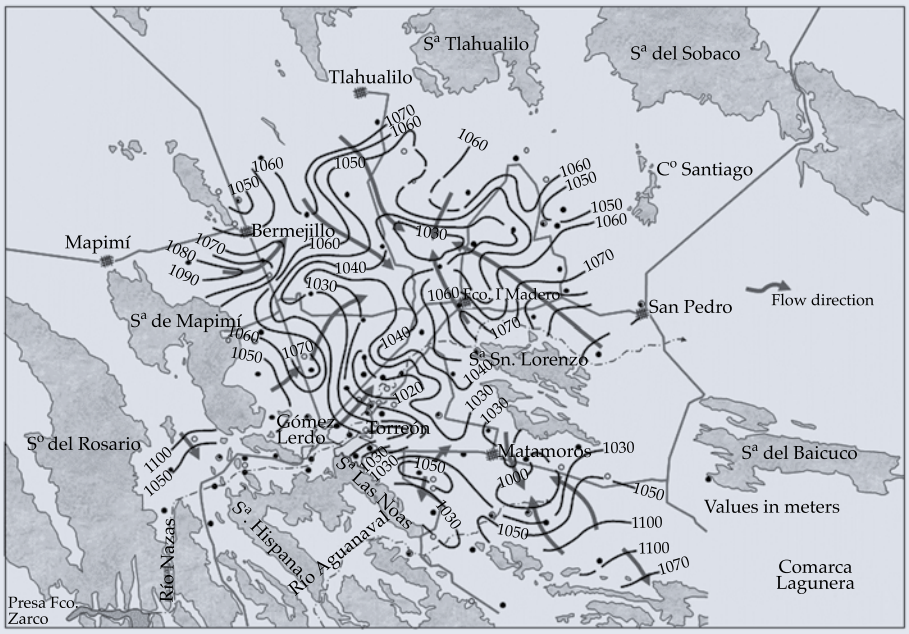

Figure 3. Groundwater flow.

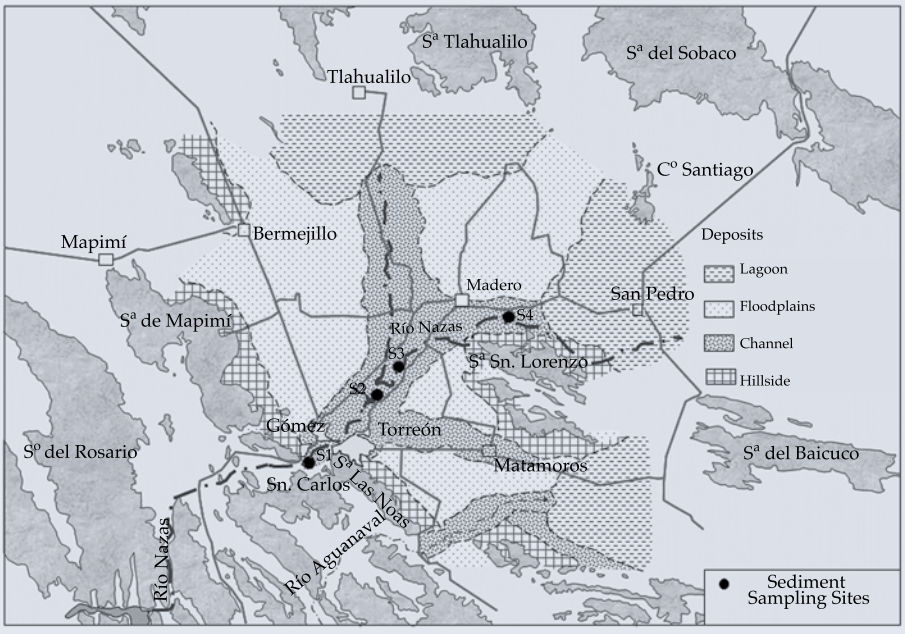

Figure 4. Sediment Sampling Sites in Channels.

followed by an Arabic number assigned in descending order with respect to the hydraulic load of the runoff.

The samples were dried in a stove at 35°C for 48 h. They were then homogenized, cracked and filtered with a 60 mesh (dp < 250 μm).

Table 1. Geographic Coordinates of the Sediment Sampling Points.

Code	Physical Reference	*X*	*Y*	*Z* (m)
S1	Domin. De Mexico Building Company	648733	2822764	1130
S2	Villa Unión Common Lands	658785	2835077	1116
S3	La Concha Common Lands	662286	2838006	1117
S4	Santa Mónica Common Lands	680734	2849560	1106

Figure 5. Profile of Sampling Point S2, Villa Unión Common Lands.

The sequential extraction of the arsenic was analyzed based on the granulometric fraction mentioned previously.

A 7-step sequential extraction (SE) procedure was applied to the samples to evaluate the arsenic (As) fraction and its mobilization potential. The protocol proposed by Vázquez (2007) was used, which is an adaptation of those by Keon *et al*. (2001) and Tessier *et al*. (1979). This protocol makes it possible to identify the following mineralogical fractions that could be associated with arsenic: soluble fraction (SOL), ionically bonded fraction (INTC), carbonate fraction (CAR), the fraction associated with the amorphous phases of Fe (INTA), Fe oxides and crystalline magnesium (OFM) fraction, organic matter and sulfur (MOS) fraction, and the residual fraction (RES).

After the sample was prepared, it was placed in a conical vial to begin the SE protocol using the following procedure. For the SOL fraction, the sample was placed in contact with deionized water for 20-min at a pH of 5.5. The supernatant was centrifuged and a chemical analysis was performed. The INTC included three sequential extractions of the sediment recovered from the soluble fraction with 0.5 M solutions of $NaNO_3$, $Mg(NO_3)_2$ and $MgCl_2$. The contact times for each extraction were 20 min. The supernatant was centrifuged and a chemical analysis was performed between each extraction. The result from this fraction was the sum of the concentrations obtained with each extracting agent. For CAR, the sediment recovered from the previous fraction was placed in contact with a solution of CH_3COONa (1 M) for 5 h at a pH of 5.0, adjusted with concentrated CH_3COOH. The supernatant was separated by centrifuging and the chemical analysis was conducted. For the INTA, the sediment recovered from the previous fraction was placed in contact with a solution of NaH_2PO_4 (1 M) for two 24-h cycles, centrifuging the supernatant and conducting the chemical analysis between each extraction cycle. To determine the OFM, the sediment recovered from the previous fractions was placed in contact with a NH_2OH*HCl (0.04 M) solution for 20-min, gauged with CH_3COOH at 25% v/v; this stage was performed in a water bath for 6 h at 96°C in a semi-closed reflux system. The supernatant was recovered by centrifuging and the chemical analysis was performed. For the MOS, the sediment recovered from the previous fraction was placed in contact with 30% H_2O_2 at a pH of 2.0 during two cycles. The first cycle was 2 h and the second 3 h at 85 °C. Later, an ammonium acetate solution was added, gauged with 20%

HNO_3 and agitated for 20-min. The supernatant was centrifuged and the chemical analysis was performed. Finally, for the RES, the sediment recovered underwent acid digestion in a microwave system using a solution of HNO_3/HCl with a 3:2 Vol/Vol ratio as an extracting agent.

To control the quality of the analysis, NIST 2710 standard reference material was used. The percentage of arsenic recovered during the different tests performed with the NIST 2710 standard reference was ~ 90%.

Geochemistry of the Groundwater

SWater samples were taken from wells located in the deposits of channels, given that the sediment samples analyzed corresponded to this type of deposit. The locations of the sampling points are shown in Figure 6.

The parameters measured in the field included water and air temperature (T), potential hydrogen (pH) and electrical conductivity. Metals, anions and perishable chemical parameters were analyzed in the laboratory.

The water samples for the laboratory analysis were collected from the wells' discharge train. Before measuring the field parameters and collecting the samples, the well was pumped (three times its volume) and the stabilization of the different parameters was ensured.

The water samples were placed in high-density polyethylene bottles, taking precautions so the samples did not come into contact with the air. For metals, the samples were acidified at a pH < 2 with highly-pure nitric acid. For anions, the samples were stored at 4 °C.

In order to limit changing the prevalent physiochemical properties of the groundwater to the greatest extent possible, the procedure used to measure the field parameters included isolation cells. Through hoses with small diameters, these devices connect to a valve in the wells' discharge train or to the direct charge, as in the case of wells with free discharge. Thus, the extracted water flows continuously without changing inside the cell, which makes it possible to introduce the respective measurement electrodes (T, pH, CE)

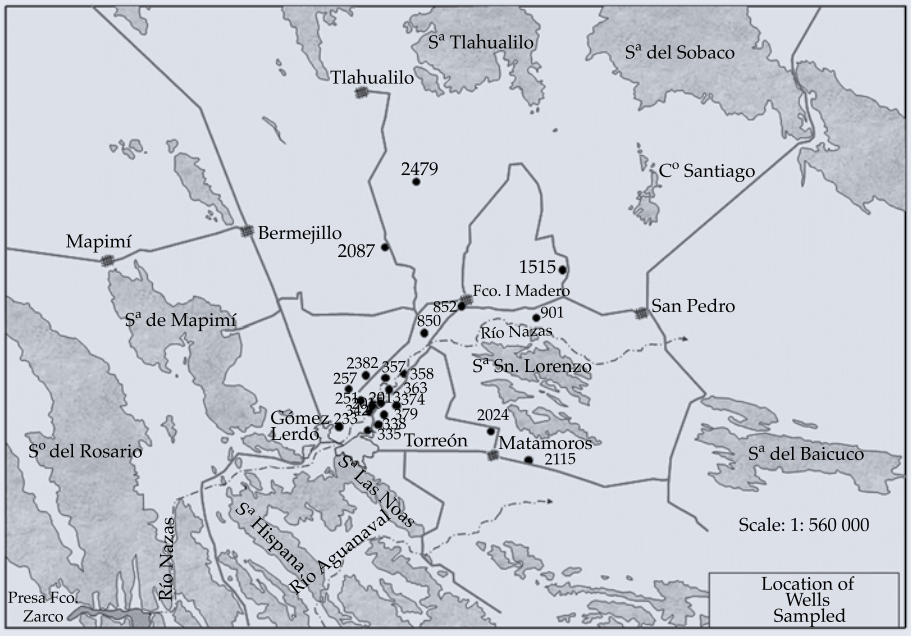

Figure 6. Location of Wells Sampled.

and conduct the measurements. This device also makes it easier to stabilize the readings, especially for pH.

Results and Discussion

Geochemistry of the Sediments

Figure 7 presents total As concentration, defined based on the sum of each of the fractions determined during the sequential extraction. An increase in arsenic can be seen from 11 to 22 mg/kg. Datta and Subramanian (1997) report arsenic concentration in sediments in the Bangladesh Rivers of 1.2 to 5.9 mg/kg. In terms of the affected population, the problem of arsenic in the groundwater in aquifers in Bangladesh is one of the most serious in the world. As can be observed in the data mentioned above, the arsenic contents in the Nazas River is higher than those in the Bangladesh Rivers.

Figure 8 shows the arsenic fraction. As can be observed, potential available arsenic increased from 36 to 55% and most was associated with amorphous Fe fractions (INTA) and iron and crystalline magnesium fractions (OFM).

Geochemistry of Groundwater

Table 2 shows the values of the physical and chemical parameters of the well water, measured in the field and laboratory.

Cation Exchange

Figure 9 presents the Piper diagram for the physical and chemical parameters. An evolution can be observed in the water from calcium to sodium. This process is known as cation exchange, in which the calcium from the groundwater exchanges with the sodium from the clay.

The surface of the clays is negatively charged, attracting cations in the outer, diffuse layer in dynamic equilibrium with the solution. The absorbed cations are weakly bonded and can be exchanged with other cations in the solution. This will occur when a cation in the water has a stronger adsorption and displaces others that were adhered to the clay. The

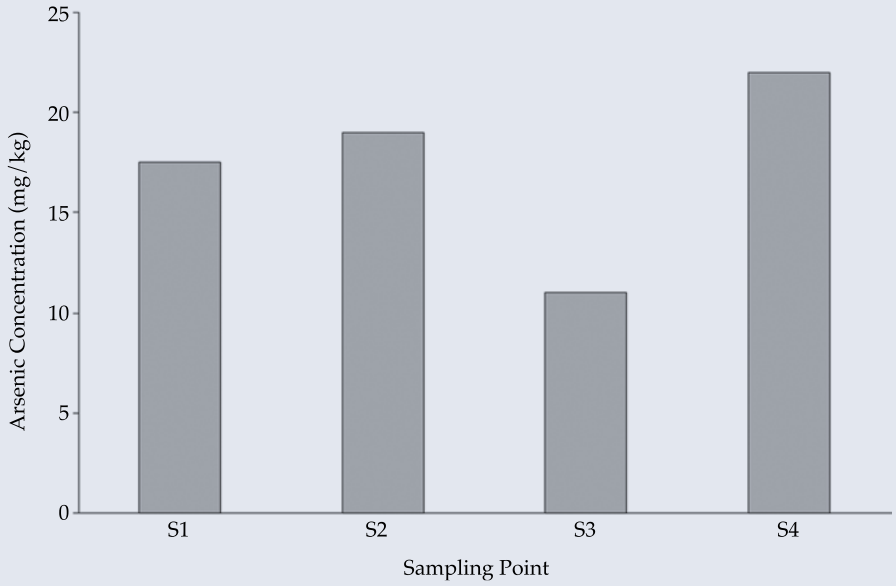

Figure 7. Total Arsenic Concentration in Sediments.

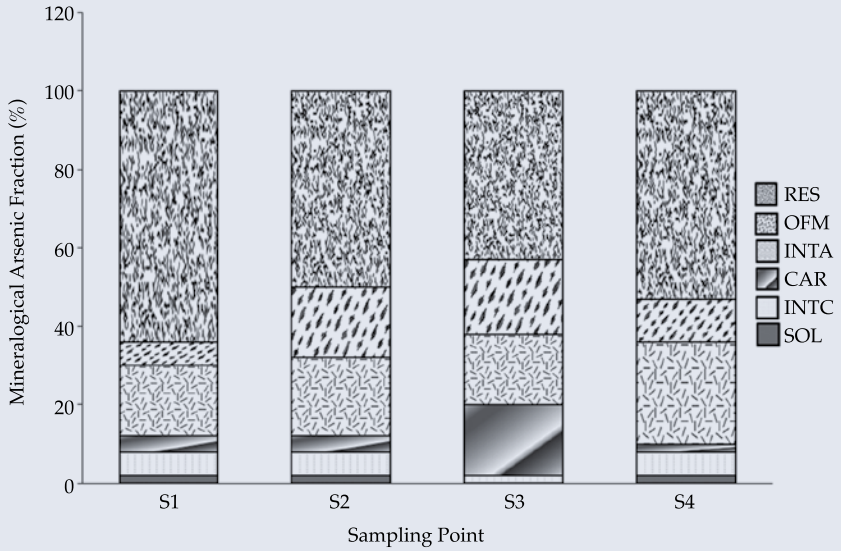

Figure 8. Arsenic Fraction per Mineralogical Fraction.

Table 2. Physical-Chemical Parameters of Groundwater in the Comarca Lagunera.

Well	pH	As (µg/l)	Na(mg/l)	Ca(mg/l)	Mg(mg/l)	SO^4(mg/l)	HCO^3(mg/l)	Temp (^{0}C)
233	8.04	16.27	49.3	120.95	19.3	306.4	122.1	28
251	7.7	2.58	42.7	84.55	8.85	185.07	124.44	23.9
257	8.04	5.34	63.1	231.6	22.77	580.9	95.2	26
331	8.65	304	128.7	3.73	1.25	44.4	259.86	28.8
336	7.92	2.43	45.2	73.4	11.3	143.78	173.24	23.5
338	7.96	4.7	36.8	49.35	5.13	92.19	168.36	22
342	7.92	4.58	40.1	95.95	8.64	74.43	262.57	24.9
357	7.85	25.3	41.2	28	2.4	49.5	151.28	27.8
363	7.9	25.1	32.7	28.36	1.76	29.37	146	26.1
368	8.11	52	50.9	21.61	0.72	35.55	161.1	29.2
374	7.68	2.96	44.8	63.1	6.7	146.07	141.52	25.1
379	8.08	4	39.8	55.41	6.13	96.53	132.98	25
504	8.05	13.9	98.1	95.6	6	236.28	112.24	27
520	7.92	6.43	44	34.68	4.91	76.03	194.1	24.3
852	7.93	27.3	51.8	25.99	0.77	66.26	131.8	28
1 125	8.13	108	107	29.96	1.76	213.6	131.76	30
1 515	8.11	165.2	244	43.97	1.73	272.12	90.3	35
2 016	8.24	198.5	96.8	27.74	2.62	80.87	226.9	27.4
2 024	8.12	142.2	225.5	117.2	14.79	529.62	136.6	26.1
2 087	8.13	35.36	62.4	21.68	0.67	74.4	124.5	30.6
2 115	8.16	97.65	163.4	40	4.56	304.76	112.2	30.9
2 382	7.89	3.4	43.7	66.76	6.64	83.91	168.36	24.6
2 479	8.28	175	88.8	15.25	0.6	84.85	146.4	30.5

Table 2 (continuation). Physical-Chemical Parameters of Groundwater in the Comarca Lagunera.

Well	Alkalinity (mg/l)	STD (mg/l)	K (mg/l)	F (mg/l)	Cl (mg/l)	Fe (mg/l)	NO_3 (mg/l)	% Ionic Balance Error
233	100	560	5.85	1.74	21.04	0.04	18.01	5.04
251	102	600	5.58	0.42	24.86	0.04	15.21	2.66
257	78	899	7.33	1.05	56.87	0.55	21.65	3.55
331	251	500	2.35	1.48	4.3	0.04	3.97	5.69
336	142	700	7.5	0.27	22.23	0.04	34.16	2.24
338	138	450	5.18	1.08	12.1	0.04	12.18	4.13
342	215	460	5.16	1.77	44.73	0.08	22.03	1.86
357	124	340	4.1	0.93	6.34	1.29	7.86	2.72
363	120	240	3.44	0.74	4.74	3.72	7.01	1.06
368	132	220	2.34	1.97	6.05	0.04	4.73	1.99
374	116	600	5.92	0.46	21.66	0.04	15.38	1.41
379	109	400	5.35	0.07	20.1	0.04	20.27	3.90
504	92	800	3.23	0.63	23.14	1.285	21.52	10.27
520	159	360	3.25	1.21	7.94	0.08	14.64	9.36
852	108	250	1.42	1.46	6.39	0.04	7.54	0.93
1 125	108	600	2.23	1.49	19.73	0.04	2.01	6.01
1 515	74	930	4.95	3.46	192.29	0.04	2.11	2.00
2 016	186	370	3.82	2.1	8.55	0.04	6.69	2.29
2 024	112	920	4.01	3.5	46.46	0.04	90.9	7.62
2 087	102	262	62.4	1.33	5.33	0.04	4.9	9.74
2 115	92	591	1.89	2.86	43.29	0.04	4.24	0.64
2 382	138	500	4.79	0.11	11.33	0.04	6.14	10.07
2 479	120	420	1.72	2.63	17.25	0.04	2.93	0.68

divalents are more strongly adsorbed than monovalents, and within each group those with a smaller ionic hydrated radius have more strength. The sequence from greater to lesser strength is $Ba^{2+} > Sr^{2+} > \mathbf{Ca^{2+}} > Mg^{2+} > K^{+} > \mathbf{Na^{+}} > Li^{+}$.

Dissolution of Calcite

For water in equilibrium with calcite, we have the following product:

$$(Ca^{++}) \cdot (CO_3^{=}) = K_{CaCO3}$$

When the calcium decreases, the product of the activity of the equation is less than the constant, which facilitates the dissolution of calcite.

The dissolution occurs through the following reaction:

$$CaCO_3 + H^{+} = Ca^{2+} + HCO_3^{-}$$

which consumes hydrogen ions, producing an increase in the pH since they are inversely proportional. Figure 9 shows that the decrease in calcium (circles) increases the pH.

Desorption of Arsenic

Arsenic versus pH values are shown in Figure 10. As can be seen, water samples with a pH value less than 8.1 have low arsenic contents. When the pH is over 8.1, the arsenic value increases considerably, exceeding the allowable limit (modified NOM-127-SSA1-1994) of 25 µg/l.

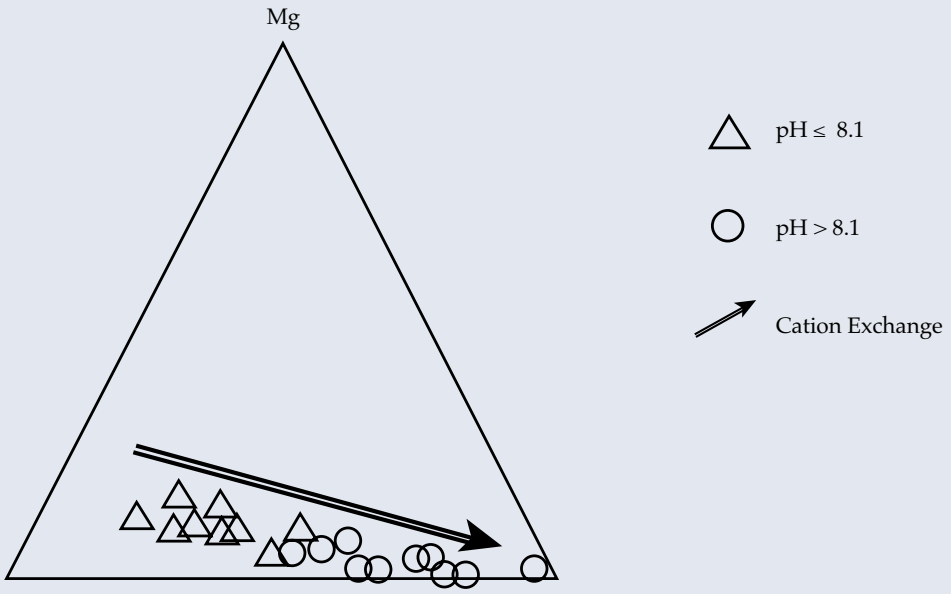

Figure 9. Piper Diagram of Chemical Parameters for Groundwater in the Comarca Lagunera.

Arsenic is adsorbed on the surface of a large variety of materials that are contained in aquifers, including Fe oxides, aluminum oxides and clay minerals (Dzombak and Morel, 1990). It is very strongly adsorbed on the surfaces of Fe oxides in acidic waters or those with a neutral pH (Waychunas *et al*., 1993; Dzombak and Morel, 1990) and unadsorbed when the pH is alkaline (Fuller and Davis, 1989; Dzombak and Morel, 1990). This occurs when the net charge of the surface of the Fe oxides changes from positive to negative as the pH increases (Dzombak and Morel, 1990). When the pH values are greater than ~8 , the net charge of the surface of Fe oxides becomes negative and negatively charged ions such as arsenic are repelled. As shown in Figure 8, the arsenic in the sediments of the channel are mostly adsorbed on the Fe oxides and are unadsorbed when the pH is greater than 8.1 (Figure 10).

Conclusions

The geochemical information regarding sediment and groundwater resulted in the following findings:

1. The sediments in the channel contained high amounts of arsenic (11-22 mg/kg).
2. In the sediments in the channel, the potentially available arsenic increased from 36 to 55%. Most of this amount was associated with amorphous Fe fractions (INTA) and crystalline Fe fractions (OFM).
3. The water samples changed from calcium to sodium due to cation exchange between the calcium in the water and the sodium in the sediment.
4. Calcite dissolved when the calcium in the water decreased, increasing the pH.
5. When pH values increased over 8.1, the net charge of the surface of the Fe oxides became negative and the arsenic ions (which are also negatively charged) were repelled.
6. It is concluded that pH is the mechanism that controls the release of arsenic into the groundwater from the sediments in the channel.

Acknowledgments

The study of the sediments was financed by the Fondos Sectoriales de Investigación y Desarrollo sobre el Agua

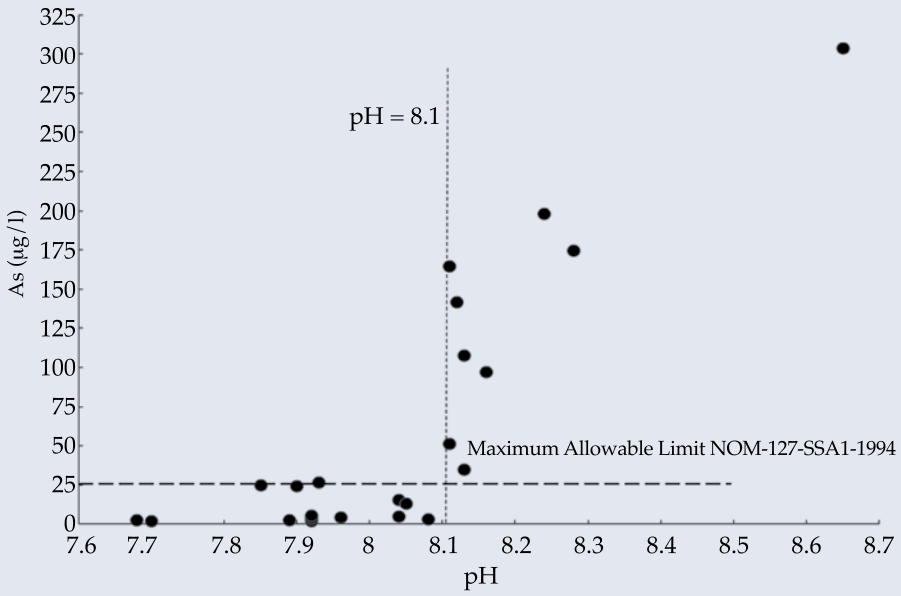

Figure 10. Arsenic Contents vs. pH Values.

(Water Research and Development Sectorial Funds) sponsored by Conacyt-Conagua.

Received: 24/04/12
Accepted: 19/05/13

References

ÁLVAREZ, J.M. Provincias fisiográficas de México. Sociedad Geológica Mexicana. Vol. 34, núm. 2, 1961, 17 pp.

CINVESTAV. *Estudio de calidad del agua para la identificación de compuestos arsenicales en la Comarca Lagunera*. Informe técnico. México, D.F.: Dirección de Calidad del Agua, Comisión Nacional del Agua, 1986.

DATTA, D.K., SUBRAMANIAN, V. Texture and mineralogy of sediments from the Ganges-Brahmaputra-Meghna river system in the Bengal basin, Bangladesh and their environmental implications. *Environ. Geol*. Vol. 30, 1997, pp. 181-188.

DZOMBAK, D.A. and MOREL, F.M. *Surface complexation modeling-Hydrous ferric oxide*. New York: John Wiley and Sons, 1990, 393 pp.

FULLER, C.C., and DAVIS, J.A. Influence of coupling of sorption and photosynthetic processes on trace element cycles in natural waters. *Nature*. Vol. 340, 1989, pp. 52-54.

INEGI. *Carta hidrológica de aguas subterráneas*. Torreón, México: Dirección General de Geografía del Territorio Nacional, 1988, G13-9 (escala 1/250 000).

IMTA, 1992. *Estudio hidrogeoquímico e isotópico del acuífero granular de la Comarca Lagunera*. Informe técnico. Jiutepec, México: Instituto Mexicano de Tecnología del Agua.

KEON, N.E., SWARTZ, C.H., BRABANDER, D.J., HARVEY, C., and HEMOND, H.F. Validation of an arsenic sequential extraction method for evaluating mobility in sediments. *Environmental Science & Technology*. Vol. 35, 2001, pp. 2778-2784.

MOLINA, A. *Estudio hidrogeoquímico en la Comarca Lagunera, México*. Tesis de Maestría en Ciencias de la Tierra. México, D.F.: Universidad Nacional Autónoma de México, 2004.

ORTEGA A. Origin and geochemical evolution of groundwater in a closed-basin clayey aquitard, Northern México. *Journal of hydrology*. Vol. 284, 2003, pp. 26-44.

PIFSV-SARH. *Estadística de la producción agropecuaria y forestal y su valor de los ciclos otoño-invierno y primavera-verano*. Cd. Lerdo, México: SARH Subdelegación de la Política y Concertación, Unidad de Información y Estadística, 1991.

SICYGSA. *Estudio de la contaminación difusa del acuífero de la Comarca Lagunera, Coahuila*. México, D.F.: Subdirección General Técnica, Gerencia de Aguas Subterráneas, Conagua, 2000.

TAMAYO, J.L. *Geografía moderna de México*. México, D.F.: Editorial Trillas, 1982.

TARDY, M. *Les grands traits structuraux du secteur transverse de Parras, Sierra Madre Oriental, Mexique*. Conference Géologique des Caraibes VII, Saint Francois, 1974, pp. 595-605.

TESSIER, A., CAMPBELL, P.G.C., and BISSON, M. Sequential extraction procedure for the speciation of particulate trace metals. *Analytical Chemistry*. Vol. 51, 1979, pp. 844-851.

VÁZQUEZ, R.G. *Movilización de elementos potencialmente tóxicos (EPT) en la rizósfera de Viguiera Dentata. Una especie vegetal tolerante, de suelos de Villa de La Paz, Matehuala, S.L.P*. Tesis de Maestría en Ciencias Ambientales. San Luis Potosí, México: Universidad Autónoma de San Luis Potosí, 2007.

WAYCHUNAS, G.A., REA, B.A., FULLER, C.C., and DAVIS, J.A. Surface chemistry of ferrihydrite - Part 1- EXAFS studies of the geometry of coprecipitated and adsorbed arsenate. *Geochimica et Cosmochimica Acta*. Vol. 57, 1993, pp. 2251-2269.

Institutional Address of the Authors

Dr. Miguel Ángel Mejía-González

Instituto Mexicano de Tecnología del Agua
Coordinación de Hidrología
Subcoordinación de Hidrología Subterránea
Paseo Cuauhnáhuac 8532, colonia Progreso
62550 Jiutepec, Morelos, México
Teléfono: +52 (777) 3293 600, extensión 217
Fax: +52 (777) 3293 682
mamejia@tlaloc.imta.mx

Fís. Luis González-Hita

Instituto Mexicano de Tecnología del Agua
Coordinación de Hidrología
Subcoordinación de Hidrología Subterránea
Paseo Cuauhnáhuac 8532, colonia Progreso
62550 Jiutepec, Morelos, México
Teléfono: +52 (777) 3293 600, extensión 805
Fax: +52 (777) 3293 682
lghita@tlaloc.imta.mx

Dr. Roberto Briones-Gallardo
Dr. Antonio Cardona-Benavides

Universidad Autónoma de San Luis Potosí
Dr. Manuel Nava 8
78290 San Luis Potosí, San Luis Potosí, México
Teléfono: +52 (444) 8262 330, extensión 2105

M.C. Pedro Soto-Navarro

Comisión Nacional del Agua, México
Av. Insurgentes Sur # 2416
Colonia Copilco el Bajo, delegación Coyoacán
04340 México, D.F., México
Teléfono: +52 (55) 5174 4000

Click here to write the autor

Distributed Hydrological Modeling based on Weather Radar

• Baldemar Méndez-Antonio •
Universidad de Sonora, México

• Gabriel Soto-Cortés* •
Universidad Autónoma Metropolitana, México
*Corresponding Author

• Fabián Rivera-Trejo •
Universidad Juárez Autónoma de Tabasco, México

• Ernesto Caetano •
Universidad Nacional Autónoma de México

Abstract

MÉNDEZ-ANTONIO, B., SOTO-CORTÉS, G., RIVERA-TREJO, G. & CAETANO, E. Distributed Hydrological Modeling based on Weather Radar. Water Technology and Sciences *(in Spanish). Vol. V, No. 1, January-February, 2014, pp. 81-98.*

In Latin America, the modernization of weather systems encourage the use of distributed hydrological models for forecasting and early warning. In this sense, remote sensing instruments, such as radar and weather satellites, become more important as basic elements in the generation of data for hydro-meteorological simulation. As a first step in this development process, radar is a key component for its ability to detect the spatial distribution of rainfall with an ideal resolution level for hydrological models. With this perspective, this paper presents the development of a hydrological simulation scheme based on the distributed model Modified Clark Unit Hydrograph, using radar data. In the paper the concepts underlying the model and illustrates its implementation, calibration and validation through a case study in an experimental catchment. The results show the ability of the radar-based distributed model to reproduce the runoff hydrograph in both volume and peak runoff value. The simulation shows that the lag time rainfall, compared against the peak runoff, opens a window of opportunity for decision-making and risk mitigation, safeguarding human lives and property. From the above it is concluded that distributed hydrological modelling based in radar has broad applicability in the implementation of early warning systems in addition to an adequate network of ground monitoring.

Keywords*: weather radar, rainfall-runoff models, distributed hydrological models, early warning systems.*

Resumen

MÉNDEZ-ANTONIO, B., SOTO-CORTÉS, G., RIVERA-TREJO, G. & CAETANO, E. Modelación hidrológica distribuida apoyada en radares meteorológicos. *Tecnología y Ciencias del Agua*. Vol. V, núm. 1, enero-febrero de 2014, pp. 81-98.

En América Latina, la modernización de los sistemas meteorológicos alentará el uso de modelos hidrológicos distribuidos con fines de pronóstico y alerta temprana. En este sentido, los instrumentos de percepción remota como los radares y satélites meteorológicos cobran mayor importancia como elementos básicos en la generación de datos para la simulación hidrometeorológica. En una primera etapa en este proceso de desarrollo el radar es pieza clave por su capacidad de detectar la distribución espacial de la lluvia a niveles de resolución ideales para modelos hidrológicos. Con esta perspectiva, en este trabajo se presenta el desarrollo de un esquema de simulación hidrológica basado en el modelo distribuido del hidrograma unitario de Clark modificado, alimentado con datos de radar. En el artículo se consideran los conceptos que sustentan el modelo y se ejemplifica su implementación, calibración y validación a través de un caso de estudio en una cuenca experimental. Los resultados muestran la capacidad del modelo distribuido basado en datos de radar para reproducir el hidrograma de escurrimiento tanto en su volumen como en el valor del escurrimiento pico. La simulación muestra que el valor del tiempo de retraso de la tormenta, comparado contra el tiempo pico del escurrimiento, abre una ventana de oportunidad para la toma de decisiones y la mitigación de riesgos, la salvaguarda de las vidas humanas y sus bienes. De lo anterior se concluye que la modelación hidrológica distribuida basada en datos de radar tiene amplias posibilidad de aplicación, principalmente en la implementación de sistemas de alerta temprana, en complemento a una red suficiente de monitoreo en tierra.

Palabras clave: radar meteorológico, modelos lluvia-escurrimiento, modelos hidrológicos distribuidos, sistemas de alerta temprana.

Introduction

Extreme weather phenomena regularly affect multiple sectors (urban, agricultural and health, among others). The impacts from this type of event often cause setbacks in the benefits created by development. The importance of these impacts are such that the countries signing the Millennium Development Objectives (UNISDR, 2010) concluded that these phenomena are among the main factors preventing countries from meeting their goals. Therefore, international entities have been created over the past decade to reduce the vulnerability and increase the resilience of countries that are more vulnerable to disasters caused by natural phenomena. What has been learned to-date is that increasing resilience is an investment, not a cost. In addition, the strategies to reduce disasters will be successfully implemented once governments and the citizens understand that disasters caused by natural threats occur not because of chance but rather due to a lack of foresight, and demonstrate our own carelessness (Informe ONU, 2004). Reducing risks of disasters and increasing the ability of different development sectors to respond to natural hazards can have multiplier effects and increase the achievement of the Millennium Development Objectives (UNISDR, 2010). With respect to this, the Global Assessment Report on Disaster Risk Reduction (United Nations, 2012) again proposes development, with an increased investment in disaster risk management and paying particular attention to droughts, which disproportionately affect poor rural homes.

In addition, 168 countries adopted the Hyogo Framework for Action (HFA) in 2005 to considerably reduce, by 2015, losses caused by disasters to life and property as well as the economy and environment of communities and countries (UNISDR, 2010). The HFA was adopted during the World Conference on Disaster Reduction, and was later supported by the United Nations General Assembly. The actions are focused on increasing the strength and resilience of nations and communities in the face of disasters.

The HFA establishes three strategic objectives in order to achieve its results:

1. Effectively include of risk of disasters in development policies, plans and programs at all levels, with special emphasis on preventing and mitigating disasters, preparedness for disaster cases and reducing vulnerability.
2. Develop and strengthen institutions, mechanisms and capacities at all levels to systematically contribute to increasing resilience to threats.
3. During the reconstruction phase of the affected communities, systematically incorporate risk reduction criteria in the design and implementation of programs to prepare for emergency situations, response and recovery.

The needed actions proposed to achieve these objectives are:

a) Ensure that disaster risk reduction is a national and local priority with a solid institutional base for its application.
b) Identify, evaluate and monitor the risks of disaster and strengthen early warning.
c) Use knowledge, innovation and education to establish a culture of safety and resilience at every level.
d) Reduce underlying risk factors.
e) Strengthen preparedness for disasters in order to ensure an effective response at every level.

In addition, in order to increase commitment by local decision-making authorities and urban leaders, the UNISDR and its partner organizations implemented the 2010 World Campaign "Making Cities Resilient: My City is Getting Ready!" (UN, 2012). The objectives of this campaign are to increase understanding and foster commitment of local and national governments so that reducing risks and

increasing resilience to disasters and climate change becomes a policy priority. In addition, the Hyogo Framework for Action is used as a reference to more closely address local needs (UN, 2012).

This campaign fosters the transmission of specialized knowledge and skills and technical support to achieve the objective of creating resilience based on "Ten Essentials for Making Cities Resilient." These are:

1. Put in place organization and coordination to understand and reduce disaster risk, based on participation of citizen groups and civil society. Build local alliances. Ensure that all departments understand their role to disaster risk reduction and preparedness.
2 Assign a budget for disaster risk reduction and provide incentives for homeowners, low-income families, communities, businesses and public sector to invest in reducing the risks they face.
3. Maintain up-to-date data on hazards and vulnerabilities, prepare risk assessments and use these as the basis for urban development plans and decisions. Ensure that this information and the plans for your city's resilience are readily available to the public and fully discussed with them.
4. Invest in and maintain critical infrastructure that reduces risk, such as flood drainage, adjusted where needed to cope with climate change.
5. Assess the safety of all schools and health facilities and upgrade these as necessary.
6. Apply and enforce realistic, risk compliant building regulations and land use planning principles. Identify safe land for low-income citizens and develop upgrading of informal settlements, wherever feasible.
7. Ensure education programs and training on disaster risk reduction are in place in schools and local communities.
8. Safeguard ecosystems and natural buffers to mitigate floods, storm surges and other hazards to which your city may be vulnerable. Adapt to climate change by building on good risk reduction practices.
9. Install early warning systems and emergency management capacities in your city and hold regular public preparedness drills.
10. After any disaster, ensure that the needs of the survivors are placed at the centre of reconstruction with support for them and their community organizations to design and help implement responses, including rebuilding homes and livelihoods.

To achieve these goals, the perception that the cost of disaster risk management competes with other priorities for scarce resources must be overcome. Risk reduction must be an integral part of local development. Comprehensive or holistic disaster risk management is more attractive when simultaneously responding to the needs of many participating partners and other competing priorities. In general, the incentives are greater when disaster risk management visibly contributes to improving economic and social wellbeing.

It is worth mentioning that in Mexico, hydrometeorological phenomena are responsible for over 95% of the direct and indirect losses (Figure 1) resulting from natural disasters. Therefore, taking increasingly better mitigation steps is to be expected.

As can be seen by the above, one of the disaster risk management actions to be reaffirmed is the development and implementation of early warning systems, which presumes the incorporation of real-time hydrometeorological models. Therefore this work presents the development and application of a distributed model, taking advantage of the increased infrastructure in the sector.

The development of distributed hydrological models has experienced a boon over the past three decades through the search to improve the prevention of disasters caused by extreme weather phenomena (Beven, 1985; Smith, 2004). An addition to current computing capabilities, these models facilitate a trend

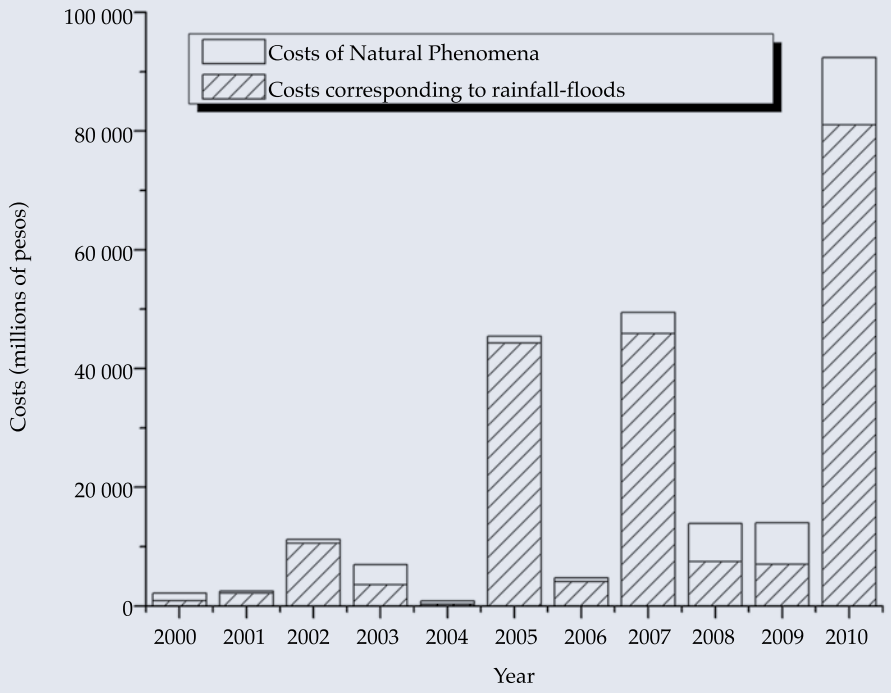

Figure 1. Costs of Natural Phenomena In Mexico (information from Cenapred, 2010).

toward operational (real-time) hydrological models. Using these models, the spatial and temporal variability of precipitation have a significant impact on the results of hydrological modeling (Faures *et al*., 1995; Morín *et al*., 1995; Guichard, 2004). Therefore, remote sensing instruments such as radars and weather satellites— because of their ability to calculate the spatial variability of precipitation— are ideal instruments for real-time hydrological modeling as part of early warning operating systems in order to forecast and prevent extreme events.

In Mexico, although the use of this technology is just emerging, significant growth in the sector is expected in the coming years. As recent as 2008, strategies to modernize the National Weather service were included in the National Water Plan (Conagua, 2008) in order to prevent risks related to meteorological phenomena. In addition, the prospective study of public policies for the Mexican water sector, called the "2030 Water Agenda" (Conagua, 2011) includes initiatives to ensure that settlements are safe from floods, with an estimated investment of 107 billion pesos (President of the Republic, 2012). Some of the actions planned include modernizing the structure, facilities and operations of the National Weather System, as well as measurement and observation networks, in order to take the necessary precautions and avoid catastrophes related to extreme meteorological phenomena. These investments are expected to be added to an infrastructure containing a National Data Center and a National Weather Forecasting Center, a network of 13 radars, a network of 8 land stations to receive satellite images, a network of surface observatories composed of 89 synoptic and 133 automatic stations, which are complemented by a number of networks to measure the quantity and quality of surface and groundwater (President of the Republic, 2012).

Thus, this work presents the development of a distributed hydrologic model, fed by

meteorological radar data, in order to develop a complete, real-time hydrological system that can be applied to an early flood warning system. The model was based on the Modified Clark Unit Hydrograph and applied to the Mixcoac River experimental basin located in Mexico City.

Distributed Hydrological Modeling

Traditional hydrological models take into account that the runoff from mountains into rivers is produced by excess precipitation. This flow component is called direct or surface runoff, and the proportion of precipitation volume it produces is called excess or effective precipitation (Horton, 1933). Using a transfer function, this volume is converted into direct runoff and, after adding the base flow, the total runoff hydrograph is obtained. A scheme such as this corresponds to hydrological models using concentrated parameters, which are based on spatial averages of the physiographic characteristics and the precipitation in the basin and only reproduce the temporal variability of the response at the outlet of the basin. On the other hand, distributed hydrological modeling takes into account the spatial variability of the physical properties and precipitation by dividing the basin into micro-basins, or cells. Naturally, development in the fields of remote sensing and geographic information systems has facilitated the management of spatially distributed information. Up to a few years ago, it was common practice to use aggregated representations and, therefore, it was not possible to generate a database to use in distributed models, mainly because of computing limitations or insufficient data.

According to Vieux (2001), the disadvantages associated with models aggregated by sub-basin include a) ignoring or averaging the variations in the properties of the sub-basins and b) and being cumbersome for managing data when there is a large number of sub-basins.

An advantage of distributed models is that they make it possible to analyze distinct elements that influence the hydrological response in the basin or part of the basin and that can be modified by human intervention— such as vegetation and land use. In addition, with suitable calibrations, distributed models enable calculating the changes resulting from these interventions in the hydrological response of the basin to extreme precipitation events. Distributed models can also simultaneously obtain flows at different points in a basin. In these cases, the model improves the evaluation of the risk of floods since by enabling the identification of the state of the system at any point in the drainage network. That is, distributed models explicitly take into account the spatial variation in precipitation, infiltration, losses and runoff, while these spatial variations are averaged or ignored by aggregate models.

General Characteristics of a Distributed Model for Operational Purposes

From an operating perspective, the model must be simple and agile to decrease execution times while not losing the physical representation of the system. Simplicity and agility in the operations of a model are key to using the model for operational (real-time) forecasting. Therefore, hydrological models that contain many parameters are not attractive for distributed modeling, especially in countries with little measurement history, such as Mexico. This is because all of the parameters for each one of the components of a system need to be determined in order to represent spatial variability (Vélez, 2001).

Although there is a belief that implementing geographic information systems (GIS) resolves the problem, they don't provide any improvements when the quality of rainfall data is poor or there is little data; they only facilitate processing and the determination of the physiographical parameters of a basin.

Because the field characterization of rainfall is crucial to distributed hydrological modeling, a network of rainfall graphs is not sufficient

since this equipment does not detect the most intense area of a storm, as required. Therefore, interpolated rainfall agrees very little with reality. For this reason, modelers have been greatly interested in calculating precipitation based on data from weather radars, which can provide a good alternative to resolving this problem since they calculate rainfall at the level of spatial detail required by distributed hydrological models. Thus, some initial steps have been taken to explore the possibility of using this type of data in models as popular as *HEC-HMS*, *SWAT*, *CEQUEAU*, *MIKE-SHE*, *TOP MODEL*, *MERCEDEZ*, *TOPKAPI*, among others (Lastoria, 2008).

Distributed Hydrological Model

A distributed hydrological model is composed of two conceptual sub-models. One generates or produces runoff and represents the production of the distinct runoff components for each of the variables that make up the distributed system. The other tracks the movement of the runoff downstream through the drainage network until it reaching the basin's outlet. Each of the sub-models are described below.

Runoff Production Sub-model

In the model, the hydrographic basin is represented by a set of rectangular cells, where each cell is considered a basic unit of runoff production. The runoff production in each one of the cells, or hydrological units, is obtained using a loss model. These hydrological losses are composed of initial losses and water that continues to infiltrate into the soil during a storm. The initial losses include water intercepted by vegetation, water stored in depressions on the surface (puddles) and water that infiltrates soil until it becomes saturated. It is necessary to consider that the methodology proposed does not explicitly quantify the evaporation volume, which could be considerable in arid and semi-arid regions as well as for storms in limited areas during hours with high solar radiation. This is because modeling is performed by events; this variable is included in continuous (long-term) hydrological models. Nevertheless, the modeling of events can include antecedent precipitation and, in the model presented herein, antecedent soil moisture.

The method by the Natural Resources Soil Conservation Service (SCS), or the curve number (CN), was used to determine runoff because of its simplicity (Frevert and Singh, 2002). This is one of the methods most often used to calculate runoff volumes. It is successful because, with one single parameter, it takes into account the main physical characteristics of the basin that produce runoff, such as the slope, land use and type. In addition to its easy application, this method has the advantages of predictability and stability. It is also represents a conceptual method to calculate direct runoff based on precipitation (Ponce and Hawkins, 1996).

To apply this model, after the basin is divided into square cells, the curve number for each cell is defined according to its soil properties, based on which its maximum storage is calculated. The water volume that does not run off infiltrates the sub-soil, where a portion is stored as moisture and the rest passes into underground storage, becoming the base flow.

The SCS method does not explicitly include an infiltration scheme, and therefore this was directly calculated from the accumulated surface runoff based on accumulated precipitation, the soil's storage capacity and initial losses. The hydrological surface model converts rainfall into essential runoff is based on the conservation of mass or hydric balance:

$$P = P_e + I_a + F_a \qquad (1)$$

where P is total precipitation (cm); P_e is effective precipitation (cm); I_a is initial infiltration (cm); F_a, accumulated infiltration (cm). I_a and F_a represent the losses and are quantified based on two basic hypotheses. The first establishes that the relationship between

the effective precipitation volume (P), or direct runoff, and maximum potential runoff ($P - I_a$) for an impermeable surface is equal to the relationship between real infiltration F_a and maximum potential infiltration S (equation (2)). The second hypothesis presumes that initial infiltration is directly proportional to potential retention (equation (3):

$$\frac{P_e}{P - I_a} = \frac{F_a}{S} \tag{2}$$

$$I_a = \lambda S \tag{3}$$

Combining equations (1) and (2):

$$P_e = \frac{(P - I_a)^2}{P - I_a + S} \tag{4}$$

Assuming $I_a = 0.2\ S$:

$$P_e = \frac{(P - 0.2S)^2}{P + 0.8S} \tag{5}$$

Given the value of S, in cm:

$$S = \frac{2\,540 - 25.4\,CN}{CN} \tag{6}$$

The value of P_e is obtained (Aparicio, 1994):

$$P_e = \frac{\left(P - \frac{508}{CN} + 5.08\right)^2}{P + \frac{2\,032}{CN} - 20.32} \tag{7}$$

where CN (curve number) is determined based on the use and type of soil, according to criteria by the US Soil Conservation Service. Equations (6) and (7) are valid for $P \geq I_a$. Parameter I_a is often seen as a regional parameter that depends on climatic and geological factors.

Hydrology is primarily interested in land use maps in order to model infiltration as a function of soil properties. Determining infiltration parameters based on soil properties requires some type of reclassification of soil units into representative parameters for the hydrological model. The Soil Conservation Service proposed criteria to determine effective precipitation in function of total precipitation and the characteristics of the soil through the classification of the latter, providing a table of curve number values for the type of soil (US Soil Conservation Service, 1957). For the particular case of Mexico, they hydrological classification of the soil texture and the curve number given by Domínguez and Gracia (1981) were used. Based on this criteria, equation (7) was used to obtain the runoff generated by the storm.

Runoff Movement Sub-Model

The movement of effective precipitation to the outlet of the basin is an interdependent component of the hydrological cycle. While a proportion of the rainfall is lost due to infiltration, excess rainfall generates surface runoff, which accumulates and drains through the network of courses toward the basin's outlet. The unit hydrograph is the most used method for this movement (Sherman, 1932), which was applied in this work.

To this end, the continuity equation was applied to each basin cell. The change in stored volume in one element of the drainage network during a time interval expresses the difference between stored volume at the end of the previous period V_{t_0} and stored volume at the end of the following period V_{t_1}. The change in storage, V_S is equal to the difference between the volume that enters V_I and the volume that leaves V_O during the same time interval Δt, that is:

$$V_S = V_I - V_O = \left(\bar{I}_t - \bar{O}_t\right)\Delta t \tag{8}$$

where $\bar{I}_t$ and $\bar{O}_t$ are mean inflows and outflows, respectively, during time interval Dt. Based on this, the movement of runoff from any point in the basin to the outlet is modeled

using a simple aggregate with the distributed unit hydrograph, or Modified Clark Unit Hydrograph (Kull and Feldman, 1998).

In the methodology developed by this work, the runoff produced in each cell is moved to the outlet of the basin after a time interval has passed equal to the travel time from the cell to the outlet, combining an isochron map with linear storage. In addition, surface runoff is considered to be the most important flow component when avenues are present while base flow and sub-surface runoff can be disregarded or included in linear storage (Vélez, 2001). Maidment (1993) observed the equivalent of this procedure with the application of a hydrograph of isochrones to each of the elements, called a distributed unit hydrograph of isochrones (Figure 2).

The Muskingum method is employed for the movement of runoff produced in each cell using the curve number method. This method uses the continuity equation (eq. (8)) and a relationship between storage V and the inflows and outflows of the section studied:

$$V = K\left[xI + (1-x)O\right] \tag{9}$$

where V is the storage in the section of the current; I is the inflow; O is the outflow; K the attenuation coefficient from storage and x is a weight factor associated with the storage inflows and outflows in the section of current.

Distributed Unit Hydrograph

In order to also use all the rainfall data obtained from weather radars, the Clark Unit Hydrograph adapted new technologies for use with distributed hydrological models, with its later application in real-time hydrological forecasting (Kull and Feldman, 1998). The conceptual model that uses this method with distributed models is shown in Figure 3.

This type of unit hydrograph is interpreted as the result of the combination of a pure movement process followed by another movement process involving linear storage. According to this scheme, the real travel time of a water particle is the time given by the time-area diagram plus the retention time in the linear storage (Vélez, 2001).

This method required the calculation of four parameters to determine the hydrograph of the basin: concentration time t_c; storage attenuation coefficient K; base flow recession constant R; a time-area histogram obtained using initial infiltration I_a and maximum potential infiltration S.

Concentration time t_c is defined as the time it takes for excess precipitation to reach the outlet of the basin from its most hydraulically remote point. This is a pure lag measurement without taking into account the storage effect (Figure 3). Various equations exist in the literature (Ponce, 1996) to calculate concentration time t_c; the study herein uses the Kirpich equation:

$$t_c = 0.000325\left(\frac{L^{0.77}}{\overline{S}^{0.385}}\right) \tag{10}$$

where t_c is the concentration time (hours), L is the length of the main channel (m) and $\overline{S}$ is the mean slope of the basin.

The storage attenuation coefficient (K) is the second parameter in this method and is a measurement of the lag caused by the effect of natural storage.

The recession constant (R) is a measurement of the decrease in the flow of the recession curve Q_i with respect to the previous interval Q_{i-1}. That is:

$$R = \frac{Q_i}{Q_{i-1}} \tag{11}$$

The fourth parameter, the time-area histogram, represents the area of the basin that contributes to the runoff at the outlet of the basin during a given a time. This area was obtained by generating an isochrones map based on the determination of the travel distance from each cell to the outlet of the

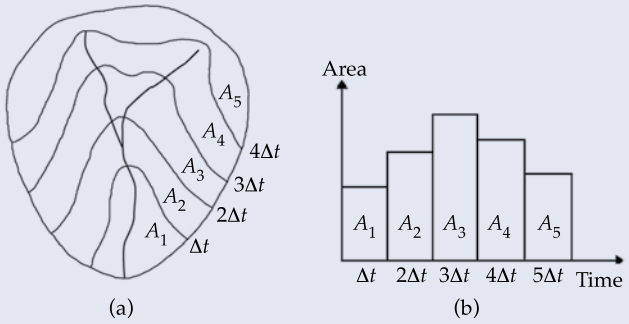

Figure 2. (a) Isochrones and (b) time-area histogram for a basin (adapted from Saghafian *et al*. 2002).

basin, calculated with equation (10). The time-area histogram of the basin is obtained by relating the areas between isochrones with the corresponding time interval. This parameter is very important to this methodology, since along with storage constant *K*, it reflects the basin's runoff response through to the outlet (Figure 3).

Case Study

The case study selected is the Mixcoac River experimental basin located in Mexico City, Mexico (Figure 4).

Mixcoac is a mountain river with low runoff during the dry season and sudden courses during rainy periods. It drains a portion of the Sierra de Las Cruces watershed located in the southwest portion of the valley of Mexico. It is elongated, runs southeast-northwest, and its drainage area is roughly 35 km^2. Its mean slope is 30%, though it varies greatly. The original characteristics of the basin have changed over the years; for example, with respect to land use. Nevertheless, it is still primarily forest (65%) with agricultural use (20%). The mean annual precipitation is 1 250 mm. The rainy season begins in March, reaches its peak in July and declines during the month of August. Rainfall is frequent in the area due to convection caused by the orography of the site (Magaña *et al*., 2003). The mean annual temperature varies according to the altitude from 10 to 15°C. This basin was selected because its type of response causes a large amount of damage and because runoff and precipitation data are available from 78 rain gauges and the Cerro Catedral weather radar located 35 km from the study basin (Figure 5). This availability of data made it possible to establish a relationship between rainfall and runoff to help to calibrate the hydrological model.

The basin was divided into cells with a spatial resolution of 1 x 1 km, so that they coincided with the geographic location and were equal to the mesh from the radar images (Figure 5). The precipitation mesh (*Z*) obtained from radar data corresponding to each period of analysis was calculated using the calibration equation obtained for the radar in the study zone (Méndez-Antonio *et al*., 2011):

$$Z = 300\,R^{1.3} \qquad (12)$$

where *R* is the intensity of precipitation and *Z* represent the radar reflectivity factor. It is important to mention that the process to calibrate the radar is a determinant of the quality of the modeling and depends on the existence of sufficient rain gauge data for this purpose. Thus, investing in a rain gauge network is a critical step that decision-makers need to consider for the use of real-time operational models (Mendez-Antonio *et al*., 2010s).

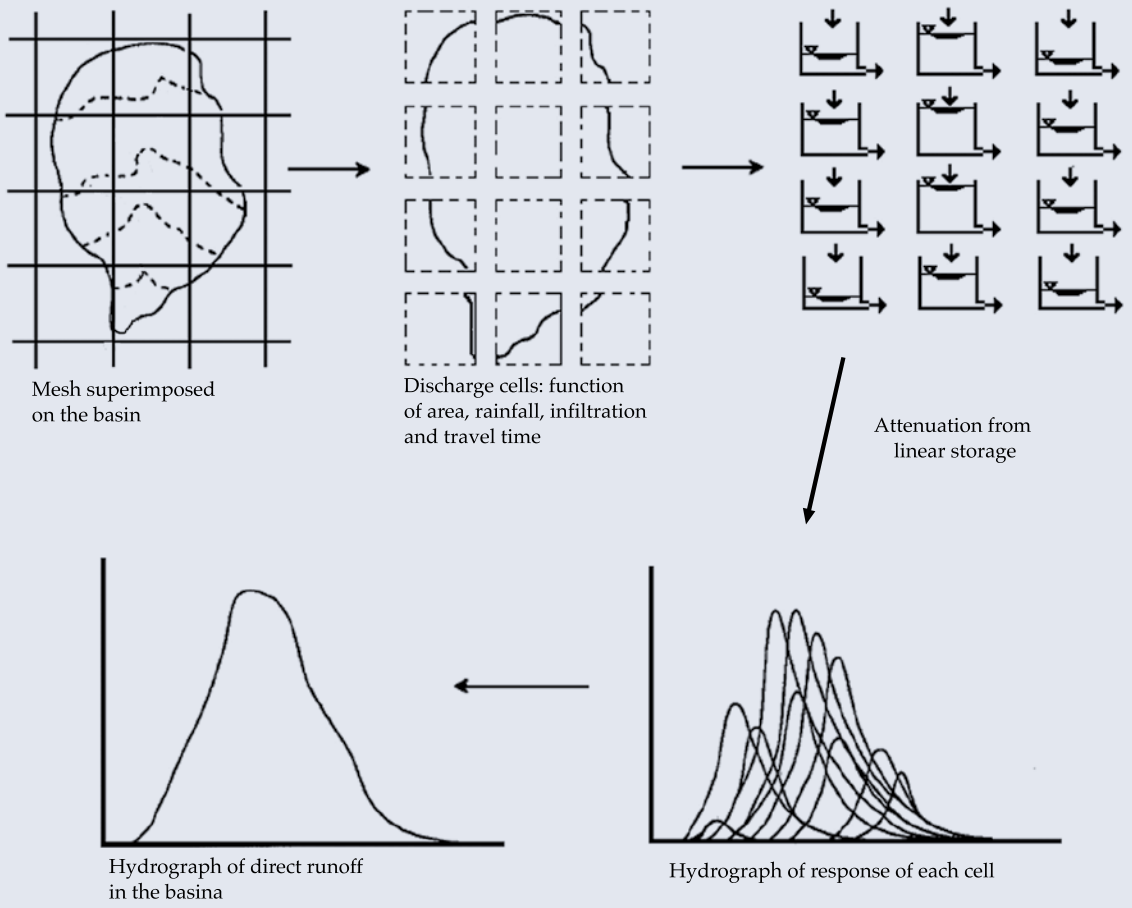

Figure 3. Conceptual Model of the Clark Method for Distributed Parameters (adapted from Kull and Feldman, 1998).

To calibrate the model, convective storms on July 28 and August 23, 1998 were selected, and precipitation meshes were obtained every 15 minutes. The period analyzed was from 18:00 to 00:00 on July 28 and 16:45 to 18:45 h on August 23. Figure 6 shows the meshes for the period of rainfall during the storm on August 23, 1998, with time intervals of 15 minutes. It presents the evolution of the storm as it nears the basin until it dissipates. These storms were selected because of the availability of radar precipitation data and runoff data through to the outlet of the basin, which made it possible to model the rainfall-runoff in the Mixocoac River experimental basin.

It is worth mentioning that the hydrological model used is a stimulus-response model (rainfall-runoff) rather than a statistical model such as the type requiring annual or inter-annual variability. Since the phenomena that produce the most precipitation are those that occur during the summer (intense precipitation during a short period of time), this type of model provides good results. Winter systems are associated with atmospheric and northern fronts. The precipitation in these systems is not intense and the periods are longer (one or two days), with mostly stratiform rainfall. The storms selected to calibrate the model presented in the work herein were convective.

The parameters records, in the form of a mesh, represents cells as sub-basins for the distributed modeling. Thus, based on the length of the current and the slope in each cell,

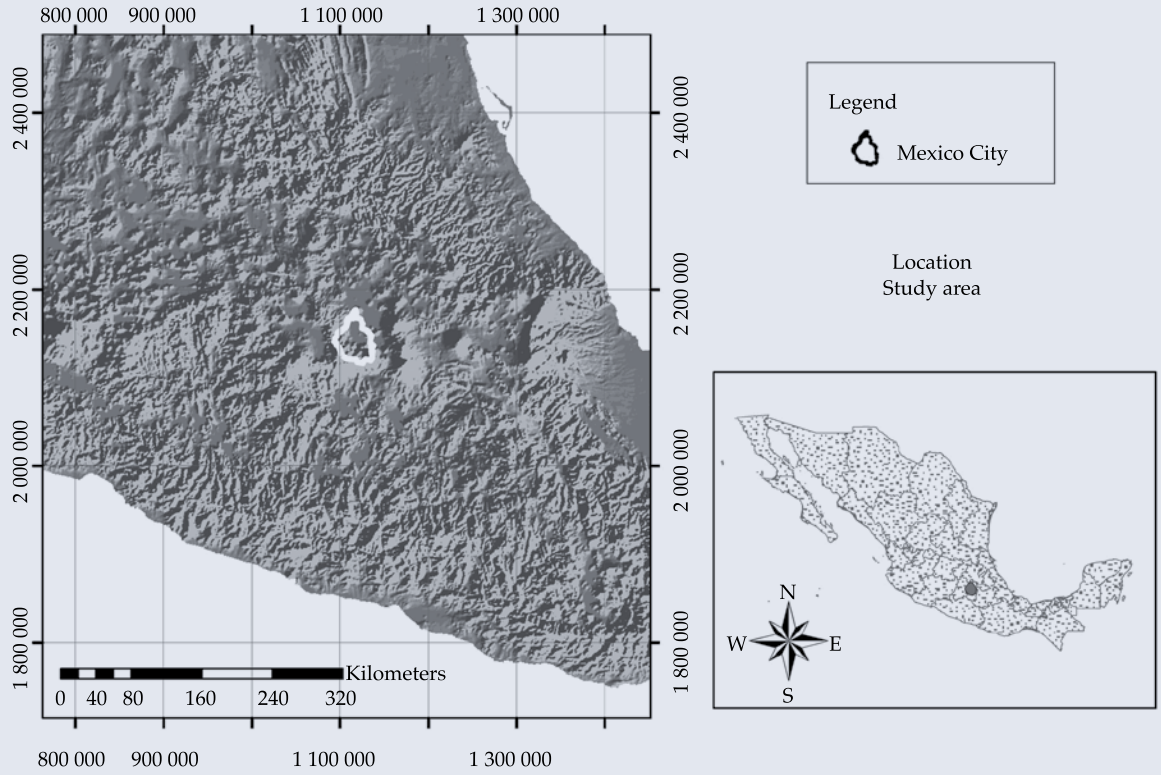

Figure 4. Location of the study basin.

the travel time to the outlet of the basin was calculated to create the isochrones required by the method in order to produce the area-time histogram and the movement of runoff (Figure 7).

The spatial variation of the curve number (*CN*) was determined using a geographic information system (GIS), with a raster map to verify that the study area and the data format agreed with the mesh representing precipitation from La Catedral weather radar. This format makes it possible to include the mesh with the CN for each cell as input in the model to generate runoff (Figure 8c). To obtain this mesh, land use and soil type maps were used (Figures 8a and 8b, respectively) for the study area. The degree of permeability was classified as Very High (Type A), Good (Type B), Average (Type C) and Low (Type D), based on the classification of the hydrological types of soil by Domínguez and Gracia (1981).

Finally, using the modified Clark method, the time-area histogram was generated with the sub-areas defined between the consecutive isochrones from the outlet of the basin to the furthest part. This histogram constitutes the basis for the transfer of rainfall into runoff and is determined by the convolution equation. The time interval used in the hydrograph of the response of the basin defines the travel time between two adjacent isochrones, which is defined according to Saghafian *et al.* (2002) as:

$$Q_j = \sum_{i=1}^{j} E_i A_{j-i+1} \qquad (13)$$

where j is the number of time intervals; Q is the flow to the outlet of the basin; E is the intensity

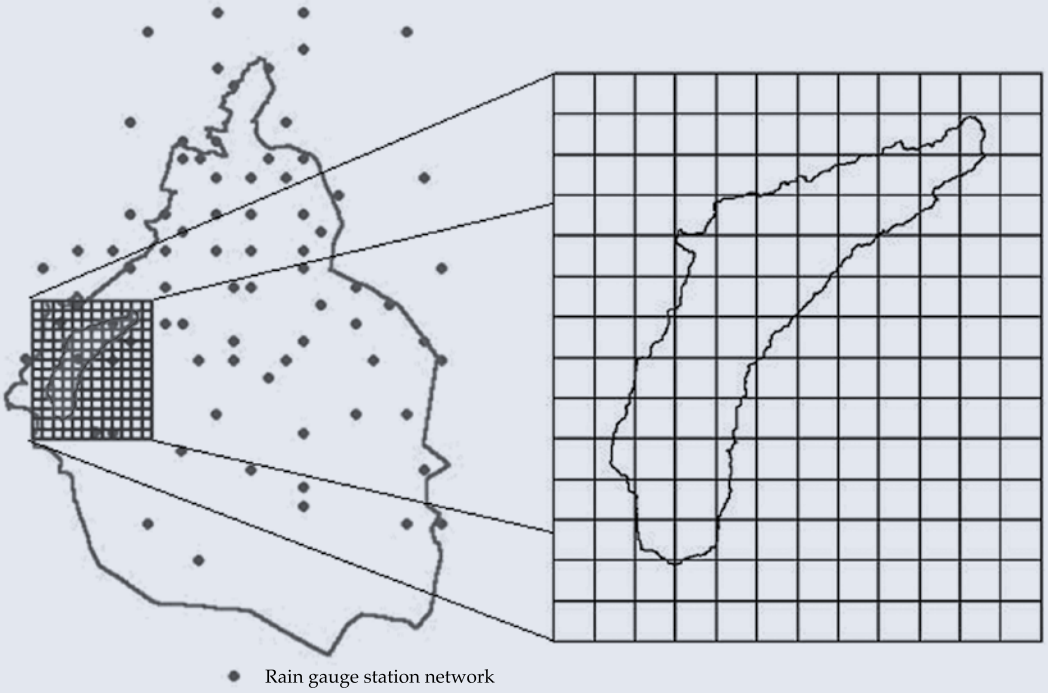

Figure 5. Study area and precipitation mesh (1 x 1 km grid) from weather radar.

of excess rainfall and A is the delimited area between isochrones. Using this method, the hydrological model was calibrated until the calculated hydrograph was comparable to the observed hydrograph of the selected storms. Observed rainfall and runoff data were used to calibrate the hydrological model.

Calibration Parameters

Table 1 presents seven parameters required to calibrate the model; initial infiltration (I_a) and potential retention (S) are influenced by antecedent soil moisture. Concentration time (t_c) and the storage coefficient (K) affect the shape of the hydrograph. Initial base flow (Q_{bi}), the recession constant (R) and threshold base flow (Q_u) are affected by the observed historical base flow. It is important to note that the three latter parameters can be obtained directly from the historical analysis, with the remaining four left for calibration.

The physical parameters of the basin that can be considered to be constants— watershed, slop and travel time— were obtained with *HEC-GeoHMS software. The variable parameters were determined with Runoff Forecasting Model software* (Domínguez *et al.*, 2008) *created expressly for a future hydrological operations model to encourage the use of radars and distributed hydrological models. This software is free and available to the academic community with an interest in distributed hydrological models. The software and its manual can be downloaded from the link at the National Autonomous University of Mexico's Engineering Institute* (http://aplicaciones.iingen.unam.mx/ConsultasSPII/Buscarpublicacion.aspx).

The usefulness of this model has been demonstrated in other basins in Mexico (project reports, limited circulation, Engineering Institute, National Autonomous University of Mexico) and its performance has been compared with the HEC-HMS Modified Clark (US Army Corps of Engineers, 2001) with good results.

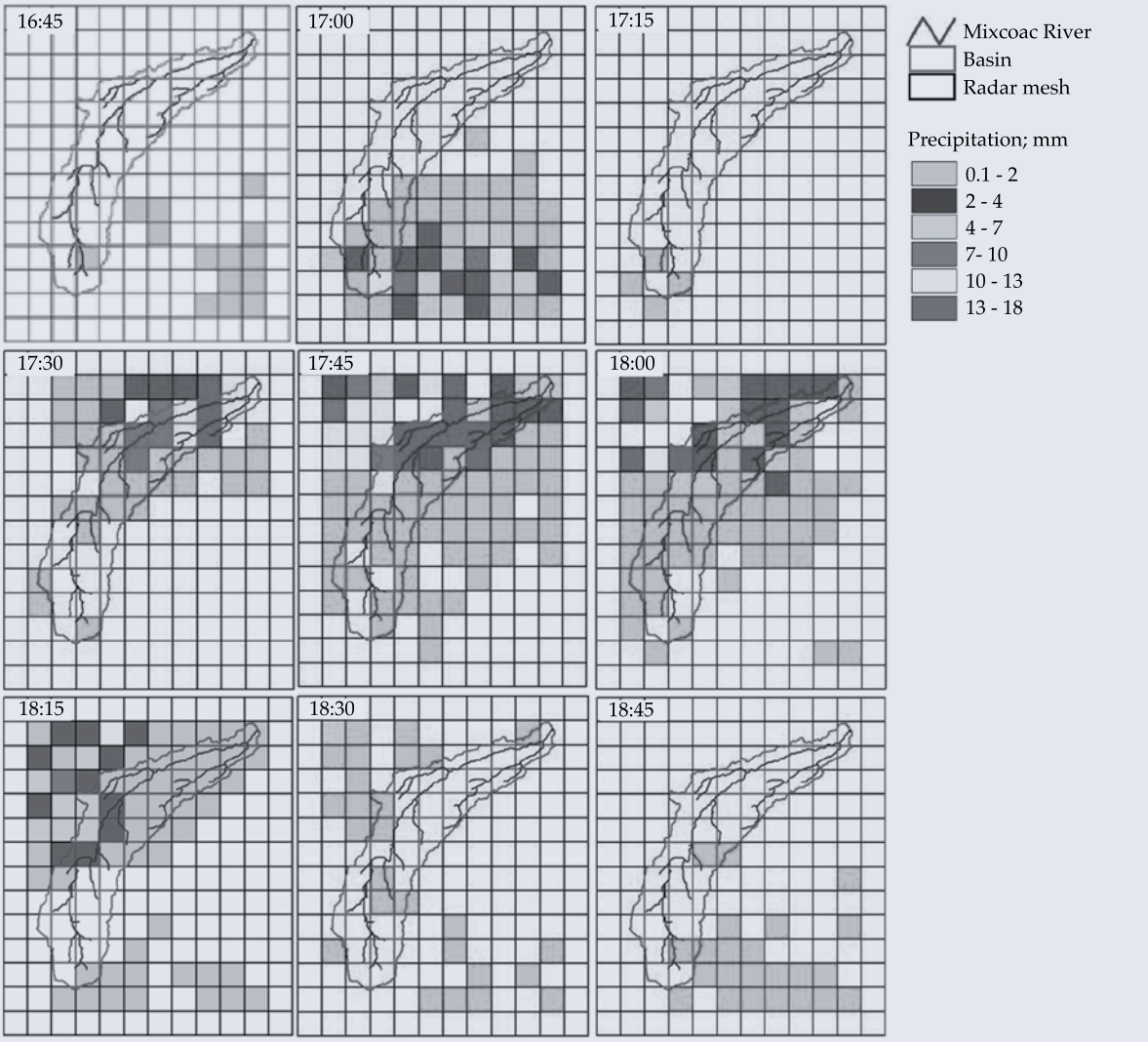

Figure 6 Precipitation mesh for August 23, 1998 (16:45 - 18:45 hours).

Results

Using the methodology described, the hydrological simulation of the case studies was performed. Figure 9 shows the main results, including the hydrographs which were calculated based on radar data, the data observed at hydrometric stations, histograms of total precipitation in the upper portion and calculated infiltration.

It is important to emphasize that variations in infiltration are observed when considering spatial variability, which would not be obtained with an aggregate model. For the study case analyzed, initial infiltration (I_a) and potential soil moisture (S) were calibrated with the runoff volumes present in the observed hydrographs. A variation from one storm to the other was observed only in the second case, primarily due to changes in antecedent moisture. For the storms selected, the infiltration parameters for the July 28 storm were less than the August 23 storm. This indicates that when a second storm occurs, the soil moisture is less than that of the first storm.

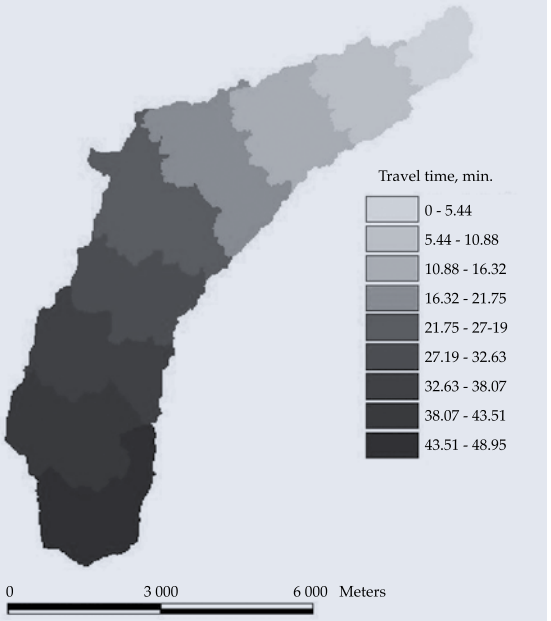

Figure 7. Isochrones map of the Mixcoac basin.

For the July 28 event, the difference in volume between the measured and observed hydrographs was 5%. For the August 23 event, the differences was 1%. The peak occurred with a lag of 30 minutes for the first case, and 30 minutes prior for the second case. This difference in volumes and time is due to the scarce availability of information to calibrate the model. The response of the model will improve if more events are available to calibrate it, which will be feasible once the modeling infrastructure increases.

Conclusions

Distributed models such as the one described herein make it possible to analyze the temporal spatial variability of storms and the spatial variability of the characteristics of the soil in a basin, in order to simulate a hydrograph that is more consistent with reality and with more meaningful physical characteristics.

Thus, weather radar is a good option to calculate the spatial variability of the precipitation that affects hydrological processes in a basin and influences its response. Radar can detect the spatial distribution of rainfall at resolution levels that are ideal for hydrological models. This is an important advantage, especially for zones with little rain gauge information, which offers an alternative to understand hydrological behavior at a regional scale in areas with little instrumentation.

These results demonstrate the feasibility of using weather radar to simulate the rainfall-runoff process with a distributed parameters

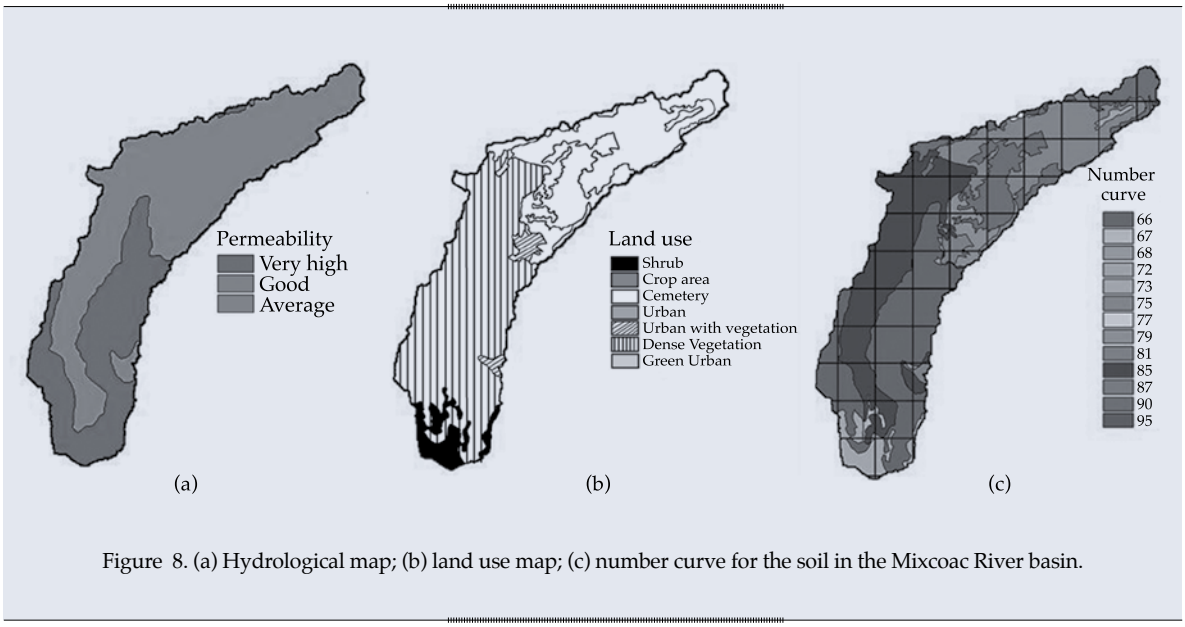

Figure 8. (a) Hydrological map; (b) land use map; (c) number curve for the soil in the Mixcoac River basin.

Table 1. Resulting Parameters for Each Storm.

Date	Basin model parameters						
	I_a (cm)	S (cm)	t_c (h)	K	Q_{bi} (m³/s)	R	Q_u (m³/s)
July 28, 1998	0.6	0.125	0.25	1.0	0.6	0.8	0.1
August 23, 1998	0.6	0.41	0.25	1.0	0.6	0.8	0.1

model, and shows the advantages of using radar as part of a real-time flood alert system, since the simulation time is less than the forecasting window, thereby allowing time to make decisions. The case study resulted in a suitable reproduction of the output hydrograph for the storms analyzed. For the 28 July storm, it underestimated runoff volume by 6% and peak flow by 1.3%, with a phase displacement of 30 min and base time of 4 h for an effective duration of 30 min. Given these observations, a window of opportunity exists to take important actions for both cases, when comparing the effective durations of the peak and base times of the runoff hydrograph. In semi-urban basins such as the Mixcoac River, this type of modeling is relevant to making decisions about mitigating hydrometeorological risks and safeguarding persons and their property. It is important to recalculate this forecasting window, which can be increased if the characteristics from radar are used to obtain immediate precipitation forecasts (nowcasting). This is a very valuable product for regions with urban basins and steep slopes, that have a rapid response.

Although the use of this technology is just emerging in Mexico, public policies are aimed at a significant and rapid growth in this sector, thereby reducing economic losses due to floods in various regions of our country (Figure 1). A variety of challenges will have to be addresses along as modernization progresses, including: the calibration of weather radar according to reflectivity z values (Méndez-Antonio *et al.*, 2011); steps to generate and implement regional meteorological models; including satellite data in rainfall calculations; and probably the most important conceptual challenge is the evaluation of antecedent moisture. It is worth highlighting that the above depends on significant investments in new information technologies and compiling hydrometeorological information, in addition to taking into account that distributed modeling based on radar is not a substitute for surface monitoring networks. On the contrary, this modeling requires a surface monitoring network with sufficient density to calibrate the model based on reflectivity (Méndez-Antonio *et al.*, 2006).

Acknowledgements

Thank you to the National Water Commission (Conagua, Spanish Acronym), through the National Weather Service and the Mexico City government, through the Mexico City Waters System, for the data provided and projects financed to develop and implement distributed hydrological models based on weather radar data. The World Meteorology Organization and Conagua for supporting studies regarding the management of water resources and prevention of disasters.

Received: 04/10/12
Accepted: 30/05/13

References

APARICIO, F. *Fundamentos de Hidrología de Superficie*. México, D.F.: Limusa.

BEVEN, K.J. Distributed models. In: *Hydrological forecasting*. Anderson, M.G. y Burt, T.P. (editors). Chichester: Wiley, 1985.

CENAPRED. *Características e impacto socioeconómico de los principales desastre ocurridos en la república mexicana en el año 2008*. Citado 11 de octubre de 2012. México, D.F.: Secretaría de Gobernación y Centro Nacional de Prevención de Desastres, 2012, 636 pp. Disponible para

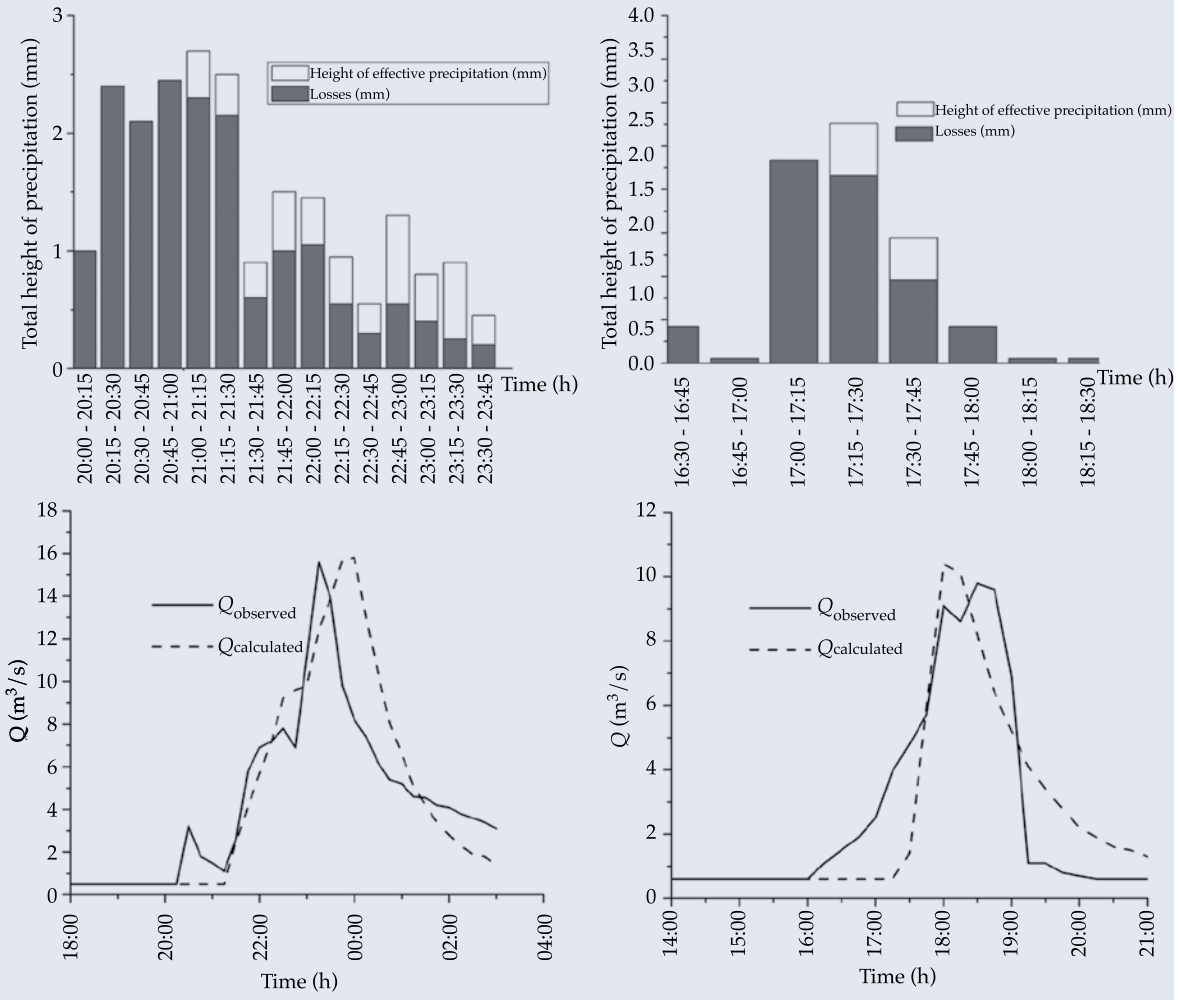

Figure 9. (a) Hydrograph of the outlet and histogram for the July 28, 1998 storm; (b) Hydrograph of the outlet and histogram for the August 23, 1998 storm.

World Wide Web: http://www.cenapred.unam.mx/es/Publicaciones/consultas/consulta2.html.

CENAPRED. *Características e impacto socioeconómico de los principales desastre ocurridos en la República Mexicana en el año 2010*. Citado el 11 de octubre de 2012. México, D.F.: Secretaría de Gobernación y Centro Nacional de Prevención de Desastres, 2012, 636 pp. Disponible para *World Wide Web*: http://www.cenapred.unam.mx/es/Publicaciones/consultas/consulta2.html.

CONAGUA. *Programa Nacional Hídrico 2007-2012*. México, D.F.: Secretaría de Medio Ambiente y Recursos Naturales, 2008, 158 pp.

CONAGUA. *Agenda del Agua 2030*. México, D.F.: Secretaría de Medio Ambiente y Recursos Naturales, 2011, 66 pp.

DOMÍNGUEZ, R. y GRACIA, J. *A.1.4. Manual de Diseño de Obras Civiles, Pérdidas*. México, D.F.: Comisión Federal de Electricidad, 1981.

DOMÍNGUEZ, R., ESQUIVEL, G., MÉNDEZ, B., MENDOZA, A., ARGANIS, M.L. y CARRIZOSA, E. *Manual del modelo para pronóstico de escurrimiento*. México, D.F.: Instituto de Ingeniería, Universidad Nacional Autónoma de México, 2008, 89 pp.

FAURES, J.M. GOODRICH, D.C. WOOLHISER, D.A., and SOROOSHIAN, S. Impact of small-scale rainfall variability on runoff Modeling. *Journal of Hydrology*. Vol. 173, 1995, pp. 309-326.

FREVERT, D.K. and SINGH, V.P. *Mathematical Models of Large Watershed Hydrology*. Chelsea, USA: WRP, 2002, 914 pp.

GUICHARD, D., GARCÍA R., FRANCÉS, F., DOMÍNGUEZ, R. Influencia de la Variabilidad Espacio-Temporal de la Lluvia Mediterránea en la Respuesta Hidrológica en Cuencas Pequeñas y Medianas. Memorias: *XXI Congreso Latinoamericano de Hidráulica.* Sao Paolo, Brasil, 2004.

HORTON, R.E. The role of infiltration in the hydrologic cycle. *Eos Trans*. Vol. 14, 1933, pp. 446-460.

KULL, D.W. and FELDMAN, A.D. Evolution of Clark's Unit Graphs Method to Spatially Distributed Runoff. *Journal of Hydrologic Engineering*. Vol. 3, 1998, pp. 9-19.

LASTORIA, B. *Hydrological Processes on the Land Surface: A Survey of Modelling Approaches*. Trento, Italy: Universidad de Trento, 2008.

MAGAÑA, V., PÉREZ, J., and MÉNDEZ, M. Diagnosis and prognosis of extreme precipitation events in the Mexico City Basin. *Geofísica Internacional.* Vol. 41, 2003, pp. 247-259.

MAIDMENT, D.R. Developing a spatially distributed unit hydrograph by using GIS. *Proceeding of HydroGIS'93*. Viena, Austria: IAHS Publ. No. 211, 1993 (citado por Saghafian, 2002).

MÉNDEZ-ANTONIO, B., DOMÍNGUEZ, M., MAGAÑA, R., CAETANO, E., and CARRIZOSA, E. Hydrological calibration of meteorological radars. *Hydraulic Engineering in Mexico.* Vol. XXI, No. 4, October-December, 2006, pp. 43-64.

MÉNDEZ-ANTONIO, B., DOMÍNGUEZ, R., SOTO-CORTÉS, G., MAGAÑA, V., CAETANO, E. Radars, an Alternative In Hydrological Modeling. Lumped Model. *Atmósfera*. Vol. 24, 2011, pp. 157-171.

MÉNDEZ-ANTONIO, B., SOTO-CORTÉS, G., RIVERA-TREJO, F., GUAYCOCHEA-GUGLIELMI, D. y CARRIZOSA-ELIZONDO, E. *Hacia la implementación de un modelo hidrológico operativo con fines de alerta contra inundaciones*. XXIV Congreso Latinoamericano de Hidráulica, Punta del Este, Uruguay, noviembre, 2010.

MORIN, J., ROSENFELD, D., and AMITAI, E. Radar rain field evaluation and possible use of its high temporal and spatial resolution for hydrological purposes. *Journal of Hydrology.* Vol. 172, 1995, pp. 275-292.

ONU. *Cómo desarrollar ciudades más resilientes, un manual para líderes de los gobiernos locales*. Ginebra, Switzerland: Organización de las Naciones Unidas, 2012, 103 pp.

ONU. *Vivir con el riesgo, informe mundial sobre iniciativas para la reducción de desastres*. New York, USA/Ginebra, Switzerland: Organización de las Naciones Unidas, 2004, 139 pp.

ONU. *Informe de evaluación global sobre la reducción del riesgo de desastres 2011. Revelar el riesgo, replantear el desarrollo*. Devon, United Kingdom: Organización de las Naciones Unidas, 2012. 190 pp.

PONCE, V.M. *Engineering Hydrology: Principles and practices*. Prentice Hall, 1996.

PONCE, V.M. and HAWKINS, R.H. Runoff curve number: has it reached maturity? *Journal of Hydrology Engineering*. Vol. 1, 1996, pp. 11-19.

PRESIDENCIA DE LA REPÚBLICA. *Sexto Informe de Gobierno* [en línea]. México: Servicio de Internet de la Presidencia, 2012 [citado el 01 de octubre de 2012]. Disponible para *World Wide Web*: http://www.informe.gob.mx/sexto_informe.html.

SAGHAFIAN, B., JULIEN, P., and RAJAIE, H. Runoff Hydrograph Simulation Based on Time Variable Isochrone Technique. *Journal of Hydrology*. Vol. 261, 2002, pp. 193-203.

SHERMAN, L.K. Stream Flow from Rainfall by the Unit Graph Method. *Engineering News-Record*. Vol. 108, 1932, pp. 501-505.

SMITH, M. NOAA Technical Report NWS 45. National Oceanic and Atmospheric Administration, 2004.

UNISDR. Reducción del riesgo de desastres: un instrumento para alcanzar los Objetivos de Desarrollo del Milenio, Kit de Cabildeo para Parlamentarios. Ginebra, Switzerland: United Nations International Strategy For Disaster Reduction and Unión Interparlamentaria, 2010, 53 pp.

U.S. ARMY CORPS OF ENGINEERS. *Hydrologic Modeling System HEC-HMS, User's Manual, V. 2.1*. EU: Hydrologic Engineering Center, 2001.

US SOIL CONSERVATION SERVICE. National Engineering Handbook. Sec. 4, Suplement A, Hydrology, Washington, D.C., 1956.

VÉLEZ, J. *Desarrollo de un Modelo Hidrológico Conceptual y Distribuido Orientado a la Simulación de Crecidas*. Tesis doctoral. Valencia: Universidad Politécnica de Valencia, 2001, 266 pp.

VIEUX, E.B. Distributed Hydrologic Model Using GIS. Kluwer Academic Publisher. *Water Science and Technology Library*. Vol. 38, 2001, 293 pp.

Institutional Address of the Authors

Dr. Baldemar Méndez-Antonio

Profesor investigador
Universidad de Sonora
Cerrada de los Escudos 1, colonia Real de Montejo
83224 Hermosillo, Sonora, México
Teléfono: +52 (662) 2165 942
baldemar.mendez@industrial.uson.mx

Dr. Gabriel Soto-Cortés

Profesor investigador
Universidad Autónoma Metropolitana, Azcapotzalco
Av. San Pablo 180, colonia Reynosa Tamaulipas
Azcapotzalco

02200 México, D.F., México
Teléfono: +52 (55) 5318 9065, extensión 114
gsc@correo.azc.uam.mx
Dr. Fabián Rivera-Trejo

Profesor investigador
Universidad Juárez Autónoma de Tabasco
Av. Universidad s/n
Col. Magisterial, Zona de la Cultura, Centro
86100 Cunduacán, Tabasco, México

Teléfono: +52 (993) 3581 500, extensión 6578
jose.rivera@daia.ujat.mx

Dr. Ernesto Caetano

Profesor investigador
Instituto de Geografía
Universidad Nacional Autónoma de México
Circuito Exterior s/n
Ciudad Universitaria
04510 México, D.F., México
Teléfono: +52 (55) 5622 4240, extensión 45459
caetano@unam.mx

Click here to write the autor

Variabilidad hidroclimática espacial y temporal en Durango, México

• José Návar* •
Centro Interdisciplinario de Investigación para el Desarrollo Integral Regional del Instituto Politécnico Nacional, Durango, México
*Autor de correspondencia

Resumen

NÁVAR, J. Variabilidad hidroclimática espacial y temporal en Durango, México. *Tecnología y Ciencias del Agua*. Vol. V, núm. 1, enero-febrero de 2014, pp. 99-120.

Este reporte presenta información sobre la variabilidad temporal hidro-climática y espacial para el estado de Durango, México. Datos de precipitación anual se ajustaron a las funciones de densidad de probabilidad gamma. La función de densidad de Gumbel- Fisher-Tipett proyectó la precipitación diaria máxima. La función de densidad log-Pearson Tipo III simuló la descarga anual máxima y los caudales máximos diarios. La evapotranspiración se estimó mediante la metodología de Thornthwaite. Más de 80 estaciones climatológicas con datos de más de 30 años se utilizaron para ajustar los parámetros de las funciones de densidad probabilística. Ecuaciones geográficas, por ejemplo, precipitación media anual = α + 1 (latitud) + β2 (longitud) + β3 (altitud) estimaron la variabilidad espacial de la precipitación, temperatura y evapotranspiración. Datos de series de tiempo reconstruidos con técnicas dendrocronológicas a largo plazo (1860-2004) de precipitaciones y caudales se analizaron mediante técnicas de regresión lineales y no lineales, y por medio de modelos ARIMA. Los resultados mostraron que la temperatura y la evapotranspiración promedio anual son variables que disminuyen con un incremento en la latitud y altitud. La precipitación media anual, por otro lado, aumenta con la latitud y la altitud, pero se reduce con la longitud. Esta tendencia se invirtió en la región fisiográfica del océano Pacífico. Los datos hidroclimáticos mostraron una falta de patrones monótonos lineales, lo que indica que las series de tiempo son estacionarias en el primer momento. Oscilaciones de varias escalas de tiempo: estacionales, interanuales, 3-7 años, y de 9 a 12 años se observaron consistentemente en las series de tiempo reconstruidas e instrumentales, el análisis de densidad espectral y los correlogramas para los datos de la precipitación anual y del caudal. Eventos climáticos sinópticos de gran escala, tales como los monzones estacionales, la variabilidad interanual, El Niño–Oscilación del Sur y La Oscilación Decadal del Pacífico parecían explicar las variaciones temporales. Se observó variabilidad hidroclimática espacial en mapas construidos utilizando técnicas SIG. Esta información espacial y temporal puede ser utilizada en la toma de decisiones en la gestión de los recursos del agua a las escalas espaciales locales y estatales, y en los estudios de productividad, los incendios forestales y las inundaciones del estado de Durango, México.

Palabras clave: recursos hídricos, el efecto del monzón, El Niño-Oscilación del Sur, Oscilación Decadal del Pacífico, variabilidad climática, aumento de consumo de agua, mapas tipo ráster y vectoriales.

Abstract

NÁVAR, J. Spatial and temporal hydro-climatic variability in Durango, Mexico. Water Technology and Sciences. *Vol. V, No. 1, January-February, 2014, pp. 99-120.*

This report presents information on the hydro-climate temporal and spatial variability for the State of Durango, Mexico. Annual rainfall data fitted the Gamma probabilistic density functions. The Gumbel-Fisher-Tipett density function fitted maximum daily precipitation. The log-Pearson Type III density function projected maximum annual discharge and daily maximum peakflows. Evapotranspiration was estimated by the Thornthwaite methodology. More than 80 climatic stations with data lasting longer than 30 years were used to fit probability density parameters. Geographical prediction equations; e.g. mean annual rainfall = α + β1 (Latitude) +β2 (Longitude) + β3 (Altitude) estimated the spatial variability of precipitation, temperature and evapotranspiration. Reconstructed and instrumental long-term (1860-2004) time series (precipitation and streamflow) data was temporally analyzed using ARIMA and linear and nonlinear regression techniques. Results showed mean annual temperature and evapotranspiration are spatially variable, diminishing with an increment in latitude and altitude. Mean annual precipitation on the other side increases with latitude and altitude but reduces with longitude. This trend was reversed for the Pacific Ocean physiographic region. Hydro-climatic data showed a lack of linear monotonic patterns indicating the time series are stationary in the first momentum. Oscillations of several time-scales: seasonal, inter-annual, 3-7 years; and 9-12-year were consistently noted on the modeled reconstructed and instrumental time series, spectral density analysis and correlograms for annual precipitation and streamflow data. Large-scale synoptic climate events such as the seasonal monsoon, the inter-annual variability, the El Niño Southern and the Pacific Decadal Oscillations appeared to explain temporal oscillations. Spatial variability was observed in hydro-climatic maps constructed using GIS techniques. This spatial and temporal information can be used in the decision making of water management resources at the local and State spatial scales; and in studies of productivity, forest wildfires, and floods of the State of Durango, Mexico.

Keywords*: water resources, monsoonal effect, El Niño-Southern Oscillation, Pacific Decadal Oscillation, climatic variability, increased water use, raster and vectorial maps.*

Introducción

La disminución de los recursos de agua por un incremento en la población, la agricultura y la industria, la deficiencia por la contaminación y la errática pero consistente escasez por las temporadas de sequía son problemas que la sociedad enfrentará en la actualidad y sin duda en el futuro durante los siguientes 50 años (Shiklomanov y Rodda, 2003; Postel y Wolf, 2001; Vorosmarty *et al*., 2000; Návar-Cháidez, 2011; Návar, 2012). Otros problemas actuales se deben a: mala administración, expansión de las áreas urbanas, desarrollo económico y malas decisiones sobre problemas del agua (CSIS, 2005). En consecuencia, en la mayor parte de del mundo árido y semiárido o en lugares con una temporada seca-húmeda bien definida existe en el presente un déficit entre el suministro y la demanda que es crítico para el desarrollo.

En general, las regiones del norte de México y en particular el estado de Durango se encuentran dentro del cinturón hemisférico boreal de las tierras áridas y semiáridas. Los ríos del estado en la actualidad corren secos en varios tramos debido a la prolongada temporada de sequías del 2010, junto con las asignaciones del flujo de ríos para la agricultura de riego, la industria y los sectores públicos. El agua subterránea se está agotando gravemente como resultado de las demandas crecientes de agua y el desarrollo no sustentable. En el presente, en la región de Durango cuatro acuíferos están clasificados como sobredrenados (FAO, 2005). Además, las temperadas de sequías de varias frecuencias de temporal están incrementando aún más la escasez de agua en la región (Návar, 2012); por ejemplo, el episodio precedente de sequía interanual que está impactando al norte de México es uno de los más agudos jamás registrados en los últimos 90 años (CNA, 2011).

A pesar de la disponibilidad a largo plazo de recursos de agua potable per cápita en el estado de Durango, México, estos son altamente variables en el espacio y en el tiempo. El estado tiene un intervalo de valores de descarga entre 13,000 a 15,000 M m^3 (11 800 M m^3 como flujo superficial y entre 1 000 y 3 000 M m^3 como descarga de acuíferos) por 1.5 M habitantes, lo cual se traduce a casi 10 000 m^3 por habitante por año (Návar, 2008). Esta cifra está muy por encima de la media actual mexicana, que se acerca a 4 500-5 000 m^3 por habitante por año. Sin embargo, la parte oriental

del estado es árida y semiárida con recursos de agua per cápita muy por debajo del promedio nacional, con una cifra que se compara con la de los países más pobres del Medio Oriente. Las temporadas de sequía de diferentes magnitudes y duración disminuyen la disponibilidad per cápita en más de un orden de magnitud. Los serranías altas de la cadena montañosa de la Sierra Madre Occidental, por otro lado, tiene la mayor disponibilidad de agua per cápita.

En tierras áridas, semiáridas, subtropicales y tropicales con una temporada seca bien definida, Postel (2000) y CSIS (2005) subrayan la necesidad de la implementación de prácticas sustentables de manejo de recursos para superar la crónica escasez de agua espacial y temporal. A pesar de estas recomendaciones, ocurre una falta consistente de información disponible públicamente para el desarrollo y puesta en práctica de proyectos hidrológicos. En virtud de que se requiere la información espacial y temporal sobre recursos de agua para entender mejor las potenciales fuentes inherentes de variabilidad, son necesarios sistemas de información geográfica, SIG, acoplados con el análisis estadístico de variables hidroclimáticas para exponer, manejar y pronosticar los datos. Esta información es útil para tomar las medidas apropiadas durante la presencia de temporadas de sequía en lugares con faltas consistentes de agua.

En este artículo, se analizó estadísticamente información hidroclimática y se compiló en un sistema SIG para el manejo sustentable de recursos hídricos en el estado de Durango, México, con el objetivo de administrar recursos de agua para el bienestar de las generaciones presentes y futuras. El objetivo de esta inves-

tigación fue a) analizar geográficamente las variables hidroclimáticas mediante ecuaciones de ajuste entre precipitación, temperatura y evapotranspiración y coordenadas (latitud y longitud), así como altitud sobre el nivel del mar; b) ajustar varias funciones de distribución de densidad, c) analizar estadísticamente si los datos hidroclimáticos (precipitación y descarga de ríos) muestran tendencias y oscilaciones temporales consistentes que pudieran relacionarse con el cambio climático y/o variabilidad; y d) discutir fuentes de pulsos y oscilaciones hidroclimáticas inherentes. La hipótesis nula intrínseca fue que las variables hidroclimáticas no presentan variabilidad espacial o temporal en el estado de Durango, México. La variabilidad espacial se probó formulando ecuaciones geográficas para predecir variables hidroclimáticas. La variabilidad temporal se evaluó ajustando modelos promedio de movilidad integrada autorregresivos, ARIMA, así como ecuaciones de regresión lineal para analizar estadísticamente las tendencias monótonas en el primer momento.

Materiales y métodos

Localización del área de estudio

El estado de Durango se localiza en la parte norcentral de México y cubre un área de aproximadamente 12.3 M ha (figura 1). Abarca 22º 35′ LN y 104º 50′ LO; 24º 44′ LN y 22º 58′ LO; 26º 83′ LN y 104º 27′ LO, y 23º 52′ LN y 107º 21′ LO. Tiene los estados vecinos de Chihuahua y Coahuila al norte y este; Coahuila y Zacatecas al este, Zacatecas y Nayarit al sur y Sinaloa y Nayarit al oeste. Caracterizan al estado cuatro regiones fisiográficas principales; a) las planicies occidentales del océano Pacífico, b) la cadena montañosa de la Sierra Madre Occidental, c) los valles centrales de Durango y Chihuahua, y d) el desierto de Chihuahua.

Métodos

Se contó con datos climáticos instrumentales de más de 80 estaciones del periodo de 1940-2004. De estas, 65 estaciones climáticas se ubicaron

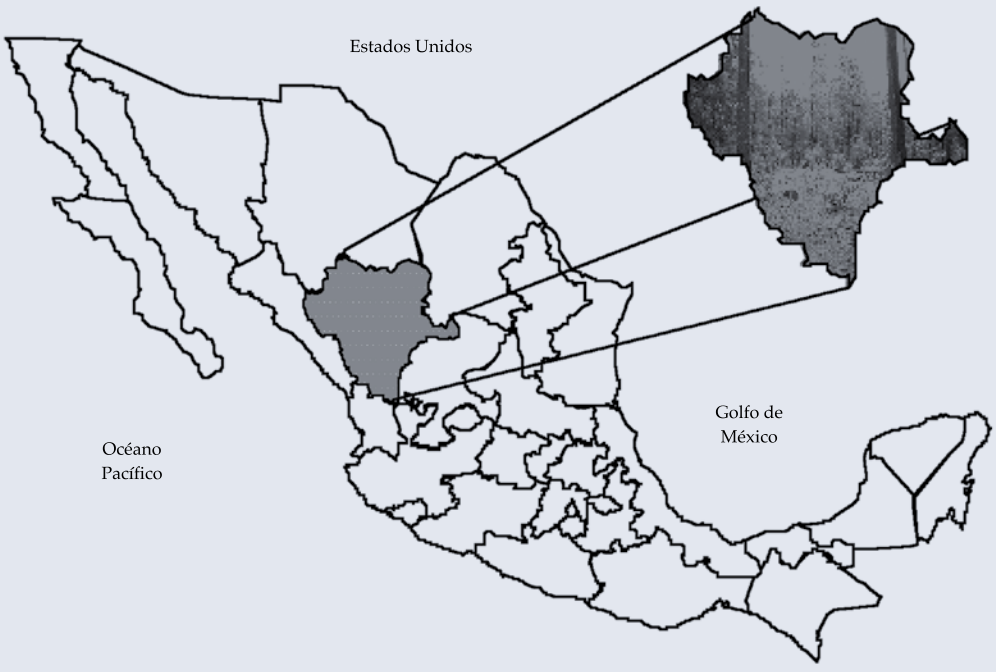

Figura 1. Localización del estado de Durango en México.

dentro del estado de Durango y el resto dentro del estado de Sinaloa, México. Además, se dispuso de datos de descarga diarios de más de 30 estaciones de medición ubicadas la mayor parte dentro del estado y varias de ellas justo a las afueras de los límites del mismo.

Precipitación anual

Los datos de precipitación anual se ajustaron a la función de densidad gamma con el fin de estimar la precipitación anual con probabilidades de 20, 50 y 80%. La función de densidad probabilística que describe la ecuación gamma está dada por el siguiente modelo (Haan, 2002):

$$px(x) = \lambda^{\eta} x^{\eta-1} e^{\lambda x} / \Gamma(\eta) \quad x, \lambda, \eta \rangle 0$$

Donde x es la variable aleatoria de interés; e es la función matemática exponencial; λ y η son los parámetros de forma y escala de la fdp; $\Gamma(\eta)$ es la función gamma y tiene las siguientes propiedades:

$$\Gamma(n) = (n-1)! \text{ para } n = 1,2,3,...$$

$$\Gamma(n+1) = n\Gamma(n) \text{ para } n > 0$$

$$\Gamma(n) = \int_0^{\infty} t^{n-1} e^{-t} dt \text{ para } n > 0$$

$$\Gamma(1) = \Gamma(2) = 1; \Gamma(1/2) = \sqrt{\pi}$$

Con el fin de ajustar esta función de densidad de probabilidad es necesario estimar los valores de los parámetros de forma y escala. Estos se evalúan con frecuencia utilizando la técnica de solución de máxima verosimilitud de Greenwood y Durand (1975) acoplada con un factor de corrección con el uso de las siguientes ecuaciones:

$$y = ln\bar{x} - \overline{ln\, x}$$

$$\eta = \left(.500876 + .1648852y - .0544274y^2\right)/y$$

$$FC = 3n/n$$

$$\hat{\lambda} = \hat{n}/\bar{x}$$

Donde ln es el logaritmo natural, x es la variable aleatoria de interés, por ejemplo, la precipitación mensual; λ y η son los parámetros de forma y escala de la fdp; FC = factor de corrección.

Curvas de precipitación-duración-frecuencia

La función de densidad de Gumbel-Fisher-Tippet se uso para calcular la precipitación correspondiente a una duración de 24 horas relativa a las frecuencias de 1, 2, 5, 10, 15, 25, 50 y 100 años. La fdp de valor extremo tipo I está dada por el siguiente modelo (Haan, 2002):

$$F(q) = exp\left[-exp\left(-\frac{X-u}{\alpha}\right)\right] -\infty \le X \le \infty$$

Donde u y α son los parámetros de la fdp; x es la variable aleatoria de interés, por ejemplo, la precipitación máxima anual para una duración de 24 horas; exp es la función exponencial. Los parámetros de esta fdp se estiman del modo siguiente:

$\alpha = \frac{\sqrt{6}}{\pi} Sx$; donde Sx es la desviación estándar de la variable aleatoria.

$u = m_x - 0.5772\alpha$; donde m_x es la media de la variable aleatoria.

El número anual promedio de días con precipitación medible también se calculó para cada una de las casi 80 estaciones climáticas.

Evapotranspiración potencial

La evapotranspiración potencial anual se estimó preliminarmente usando la metodología de Thornthwaite. El modelo empírico

desarrollado por Thornthwaite para estimar la evapotranspiración potencial está dado por la siguiente ecuación (Dunne y Leopold, 1978):

$$Et = 1.6\left[\frac{10T_a}{I}\right]^a$$

Donde Et = evapotranspiración potencial (cm); T_a = temperatura media del aire (°C); I = índice térmico anual = $\sum_{i=1}^{12}\left[\frac{T_{ai}}{5}\right]^{1.5}$, y a = 0.49 + 0.0179 I -0.0000771 I^2 +0.000000675 I^3.

Flujo base y flujo directo

Los flujos diarios base y directo se separaron utilizando el software *RORA* (Rutledge, 1998) para las 33 estaciones de medición. Los datos de descarga diaria registrados en todas las estaciones de medición se reportaron en el programa *BANDAS*.

Valores hidrológicos máximos

Los flujos del caudal diarios también se estimaron para diversas probabilidades de ocurrencia utilizando la función de densidad Log Pearson Tipo III. Esta última fdp se ha recomendado ampliamente para estos propósitos (USGS, 2002). La fdp está dada por la siguiente ecuación:

$$p(y) = \frac{\lambda^{\beta}\cdot(y-\varepsilon)^{\beta-1}\cdot\exp\left[-\lambda\cdot(y-\varepsilon)\right]}{\Gamma(\beta)}$$

Las ecuaciones que se resuelven para los parámetros de la fdp Log Pearson por medio de la metodología de momentos son las siguientes:

$$\lambda = \frac{\sqrt{\beta}}{\sigma_y};\ \beta = \left(\frac{2}{C_y}\right)^2;\qquad \varepsilon = \mu_y - \frac{\beta}{\lambda}$$

Donde:

$$\mu_y = \frac{\sum_{i=1}^{n} ln(x_i)}{n};\quad \sigma_y = \sqrt{\frac{\sum_{i=1}^{n}\left(ln(x_i)-\mu_y\right)^2}{n-1}};$$

$$C_y = \frac{n^2\cdot\sum_{i=1}^{n}\left(ln(x_i)-\mu_y\right)^3}{n-1\cdot n-2\cdot\sigma^3}$$

Este sistema de ecuaciones se resuelve simultáneamente con la ayuda de programas de computadora.

Reconstrucción de la precipitación anual y los datos de descarga

La precipitación anual y los datos de descarga se relacionaron con el incremento radial anual de árboles empleados por lo común en el análisis dendrocronológico. Las dendrocronologías de Banderas, Las Bayas y El Gato reportadas por González-Elizondo *et al*. (2005) se emplearon para relacionar el incremento radial de árboles con la precipitación anual y la descarga. En consecuencia, las ecuaciones de regresión reconstruyeron los parámetros de clima y de descarga más allá de los registros instrumentales usando el incremento radial pasado de árboles (Stahle *et al*., 1999). En general los datos hidrológicos se reconstruyeron hasta 1860. Esto es, las series de tiempo reconstruida e instrumental datan de 1860 a 2004.

Pruebas para tendencias monótonas

En este reporte, para las variables de precipitación y descarga anuales, se supone que los patrones monótonos lineales acoplados con las oscilaciones son indicaciones de cambio climático y variabilidad, respectivamente. Esto es, la precipitación o descarga anuales deben ser controladas por el cambio climático, y las series de tiempo no deben ser estacionarias en el primer momento. En consecuencia, un ecuación de regresión lineal simple (*por ejemplo*, $P = a \pm Bt$) prueba la estacionariedad fijando la

hipótesis nula $B = 0$. Por ejemplo, los patrones cuadráticos de las ecuaciones polinomiales de segundo grado pueden ser mejores indicadores de variabilidad climática. El argumento contra la hipótesis nula podría ser que cualquier patrón lineal o cuadrático es parte de variabilidad climática de escala de tiempo más larga. Sin embargo, en este tiempo para registros instrumentales y reconstruidos no se dispone de otra técnica estadística para aislar los efectos del cambio climático y la variabilidad climática en variables hidroclimáticas. Los modelos ARIMA con tendencias lineales y cuadráticas se ajustan las series de datos continuos y brutos , respectivamente. Con el fin de observar más de cerca las tendencias a largo plazo, se ajustaron de ecuaciones polinomiales de primero y segundo grado a los datos brutos reconstruidos e instrumentales (1860-2000). Además, el análisis de densidad espectral y las funciones parciales de autocorrelograma mejoraron nuestro entendimiento sobre ciclos y patrones de precipitación y descarga que se asocian con variabilidad climática y el cambio climático para el manejo de recursos naturales.

Sistema de información geográfica

Se desarrollaron mapas hidrológicos utilizando precipitación anual y mensual, temperatura, evapotranspiración, precipitación relativa a una duración de 24 horas para varias frecuencias prediciendo la distribución espacial de estos valores utilizando coordenadas de latitud y longitud y altitud como variables independientes. Un conjunto de ecuaciones de predicción se reportan preliminarmente en este artículo como la entrada principal en mapas de actualización futura que desplegarán espacialmente esta información.

Resultados

Modelos geográficos

La variabilidad hidroclimática espacial se observó en mapas SIG. Ejemplos de los modelos geográficos desarrollados para predecir variable hidroclimáticas se reportan en el cuadro 1. Las ecuaciones de predicción se dividieron en dos conjuntos en virtud de que la cadena montañosa de la Sierra Madre Occidental divide al estado en dos provincias climáticas principales; el océano Pacífico y los valles centrales incluyendo el desierto chihuahuense, cada uno con un conjunto único de gradientes climáticos.

Los mapas y geográficos a escala estatal mostraron gran variabilidad, la cual se redujo de manera parcial dividiendo climáticamente el estado en dos regiones fisiográficas, donde serranías altas de la cadena montañosa de la Sierra Madre Occidental son ambas la división continental y la hidroclimática. Dentro de la región fisiográfica, Et y la temperatura disminuyen con la latitud y la altitud, aunque aumentan con la longitud. El gradiente térmico es 1.1 °C por cada 1 000 metros, disminuyendo desde el desierto de Chihuahua hasta serranías superiores de la cadena una montañosa de la SMOc. Todas las variables de precipitación aumentan con la latitud y altitud, pero disminuyen con la longitud. Esto es, las cuencas colectoras en tierras altas noroccidentales interiores son más húmedas en las serranías de las cadenas montañosas de la SMOc.

En la región fisiográfica del océano Pacífico, Et y la temperatura disminuyen con la longitud y la altitud pero aumentan con la latitud. El gradiente térmico promedio es de 6 °C por cada 1000 m, disminuyendo desde las costas del océano Pacífico hasta las serranías superiores de las cadenas montañosas de la Sierra Madre Occidental hasta casi 12 °C. Todas las variables de precipitación se incrementan con la longitud y la altitud, pero disminuyen con la latitud. Es decir, el intervalo más húmedo se ubica en las serranías superiores de las tierras altas de las cuencas colectoras surorientales del estado de Durango.

La precipitación anual media es de 645, 583, y 575 mm cuando se evaluó mediante los polígonos aritméticos de Thiessen (figura 2) y las metodologías de isoyetas, respectivamente.

Cuadro 1. Ejemplos de ecuaciones de predicción geográfica de variables climáticas como una función de coordenadas y altitud para el estado de Durango, México.

Pendientes occidentales de la cadena montañosa de la Sierra Madre Occidental				
Parámetro climático	**Ecuación**	R^2	*Sx*	*CV*
Et	-3 748.8559-98.53 134*lt+67.39 232*lg-0.0670*al	0.35	94 mm	9
Temp M	-70.13988-1.4669*lt+1.18664*lg-0.0011*al	0.50	0.99 °C	4
Pt ≤ 20%	13 543+74.31406*lt-138.88607*lg+ 0.00728*al	0.11	204 mm	40
Pt ≤ 50%	20 221+117.70681*lt-209.2767*lg+0.00990*al	0.23	193 mm	27
Pt ≤ 80%	29 700+189.97134*lt-311.80979*lg+0.01809*al	0.30	225 mm	22
Pt M	22 021+128.4657*lt-227.66175*lg+0.04216*al	0.30	193 mm	23
Número de días lluviosos	1 550.1540+8.11432*lt-15.81674*lg+0.00461*al	0.42	12 No.	21
Pt RP 1 y	480.57920+4.45236*lt-5.11338*lg+0.0001563*al	0.03	11 mm	25
Pt RP 2 y	797.87780-2.7107*lt-6.03389*lg-0.00384*al	0.52	8 mm	10
Pt RP 5 y	1 087.84307-9.23365*lt-6.88060*lg-0.00748*al	0.59	14 mm	12
Pt RP 10 y	1 275.2190-13.60427*lt-7.38623*lg-0.00990*al	0.57	19 mm	14
Pt RP 25 y	1 515.60199-19.08744*lt-8.0681*lg-0.01296*al	0.55	26 mm	15
Pt RP 50 y	1 691.26833-23.1804*lt-8.54348*lg-0.01519*al	0.54	31 mm	16
Pt RP 100 y	1 869.4952-27.2171*lt-9.05694*lg-0.0174*al	0.53	37 mm	17
Pendientes orientales de la cadena montañosa de la Sierra Madre Occidental, los valles centrales y el desierto de Chihuahua				
Et	4 099.3558+44.06216*lt-36.7461*lg-0.2496*al	0.77	80 mm	10
Temp M	92.6339+0.5124*lt-0.7324*lg-0.0060*al	0.73	1.9 °C	12
Temp Mn	71.23053+0.3547*lt-0.5796*lg-0.0059*al	0.61	2.4 °C	35
Temp Mx	112.8249+1.3058*lt-1.0218*lg-0.0060*al	0.73	2.3 °C	9
Pt ≤ 20%	-3 120.5348-42.8920*lt+40.6139*lg+0.0844*al	0.45	84 mm	32
Pt ≤ 50%	-3 620.793-56.4930*lt+48.9796*lg+0.1281*al	0.54	92 mm	24
Pt ≤ 80%	-4 548.905-71.0450*lt+62.0633*lg+0.1637*al	0.62	100 mm	18
Pt M	-8 580.6623-176.0496*lt+123.8427*lg+0.2033*al	0.73	162 mm	27
Número de días lluviosos	-844.8399-14.2974*lt+11.7323*lg+0.0092*al	0.74	11 No.	18
Pt RP 1 y	-244.7799-4.42932*lt+3.52068*lg+ 0.00348*al	0.57	5 mm	19
Pt RP 2 y	-76.4611-4.0371*lt+1.92483*lg+0.00732*al	0.48	6 mm	14
Pt RP 5 y	-237.39352-5.77008*lt+4.04752*lg+0.00527*al	0.29	11 mm	19
Pt RP 10 y	-243.2048-6.4875*lt+4.3781*lg+0.00507*al	0.21	15 mm	22
Pt RP 25 y	-444.2397-9.5201*lt+7.0755*lg+0.00649*al	0.27	18 mm	22
Pt RP 50 y	-487.1182-10.6039*lt+7.8261*lg+0.00662*al	0.23	22 mm	24
Pt RP 100 y	-725.195-11.7571*lt+10.3221*lg+0.01184*al	0.30	24 mm	24

Donde: Et = evapotranspiración (mm): Temp = temperatura; Pt = precipitación (mm); M = media; Mn = mínimo; Mx = máximo; RP = periodo de retorno o frecuencia (años); lt = latitud; lg = longitud; al = altitud; y = año. Las unidades para latitud y longitud son grados en coordenadas UTM y la altitud está en metros sobre el nivel del mar.

La precipitación de monzón del verano es típica en la región, ya que más del 65% de la lluvia anual está restringida al periodo de julio-septiembre. El número de días con precipitación medible está en el promedio de 64 (± 4), aunque aumenta hasta 94 (± 12) en la cadena montañosa de la SMOc y disminuye hasta 46 (± 9) en el desierto de Chihuahua (figura 3). El número promedio de días lluviosos para el estado de Durango, México, se ilustra en la figura 3.

La precipitación anual bruta, datos promedio de movimiento uniforme y los

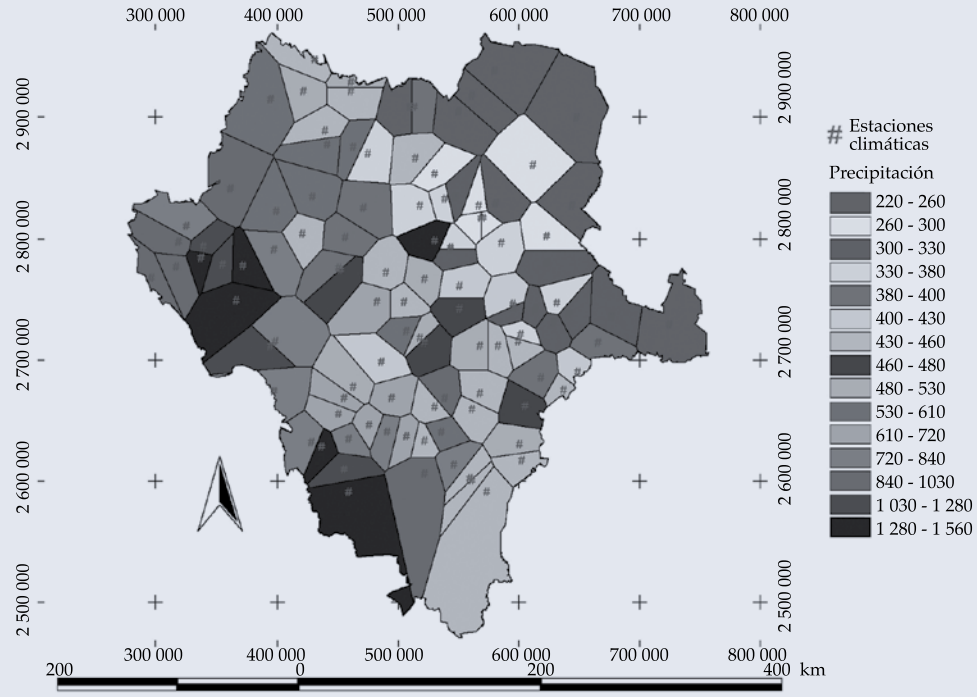

Figura 2. La metodología de Thiessen para estimar la precipitación anual promedio del estado de Durango, México.

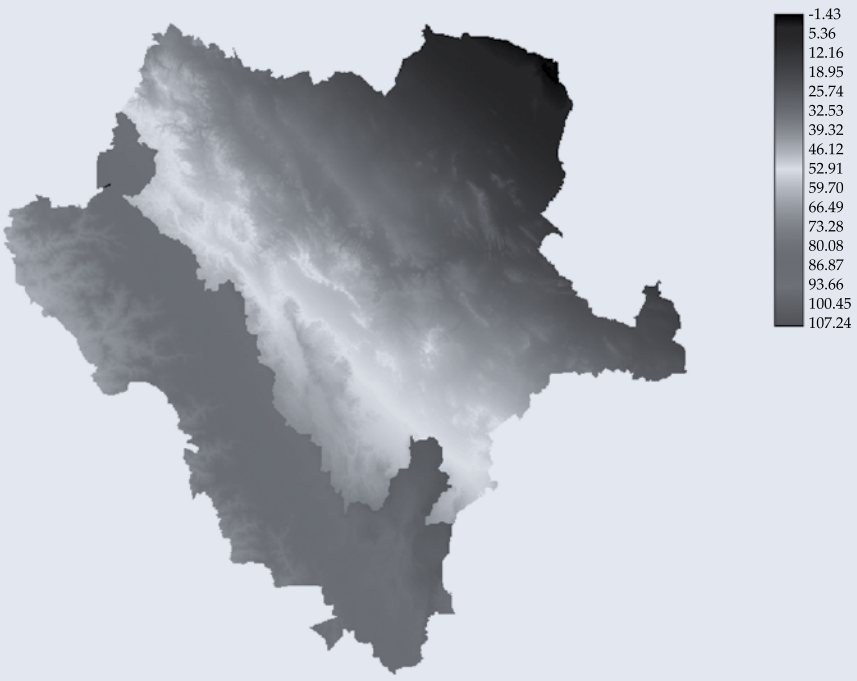

Figura 3. El número promedio de días lluviosos por año para el estado de Durango, México.

modelos ARIMA ajustados se describen en las figuras 4, 5 y 6. Si bien la precipitación anual disminuye monótonamente en las planicies del océano Pacífico, la cadena montañosa de la Sierra Madre Occidental y los valles centrales de Durango, con la excepción del desierto de Chihuahua (figuras 4, 5 y 6), las ecuaciones polinomiales de primer grado no tienen significancia estadística. Es decir, las series de tiempo son estacionarías en su primer momento. Las ecuaciones polinomiales de segundo grado se ajustan mejor a la precipitación anual de las estaciones climáticas Fco. I. Madero, Guanaceví, Rosario y Potrerillos. Las tendencias son disminuir (Fco. I. Madero, Rosarioy Potrerillos) e incrementar (Guanaceví) mostrando la falta de consistencia de los efectos del cambio climático sobre la precipitación anual y los cambios monótonos no significativos que se presentan es más probable que se deban a la variabilidad climática a escala de tiempo más larga. Es decir, la variabilidad climática parece ser una regla al explicar las tendencias cuadráticas, ya que resultan contrastantes en estas estaciones climáticas.

Los modelos ARIMA tienen consistentemente un parámetro autorregresivo simple para la precipitación anual reconstruida e instrumental en la mayor parte de las estaciones climáticas con excepción a las ubicadas en o cerca del desierto de Chihuahua (Cuencamé, San Juan de Guadalupe, Simón Bolívar, Francisco I. Madero, Guanaceví, Tepehuanes), las cuales requirieron dos parámetros autorregresivos para explicar más del 50% de la variabilidad de la precipitación anual.

La precipitación anual es consecuentemente más variable en el desierto de Chihuahua y en los valles centrales de Durango y Chihuahua y menos variable en la cadena montañosa de la Sierra Madre Occidental y las regiones fisiográficas del océano Pacífico.

Los modelos ARIMA con un solo parámetro autorregresivo resultan suficientes para predecir las series de tiempo anual continuas. Los ciclos del proyecto pronosticados en un dominio de tiempo diferente pero de análisis de densidad espectral indican que la serie de tiempo muestra picos en las bandas de frecuencia de los ciclos de 2 años; 3-6 años; y 9-11 años, respectivamente (figura 7). Estos sitios son consistentes a través de regiones fisiográficas, lo que indica la similitud de grandes eventos sinópticos que controlan la variabilidad del clima regional a través de las regiones fisiográficas.

Las estaciones climáticas Francisco I. Madero y Guanaceví (sotavento oriental) y Potrerillos, y Rosario (lado del ala occidental) presentan significancia estadística en las ecuaciones polinomiales de segundo grado ajustadas. Sin embargo, ninguna de las estaciones climáticas analizadas presenta significancia estadística en la ecuación polinomial de primer grado. Es decir, oscilaciones mayores que 70 años parecen explicar las ecuaciones cuadráticas con significancia estadística. En los Estados Unidos, Knight *et al*. (2006) vinculan esta variabilidad a largo plazo con la oscilación multidecadal del Atlántico. En este análisis falta el efecto monótono del cambio climático potencial, puesto que el primer momento de la serie de tiempo cambia de forma cuadrática.

Los modelos ARIMA para las series de tiempo reconstruidas y las precipitaciones anuales registradas instrumentalmente que representan cuatro episodios de sequía mayores pueden observarse durante el último siglo; a) en los años de 1900, b) en los años de 1920, c) en los años de 1950 y d) en los años de 1990; con una temporada seca intermedia de una duración más corta en los años de 1980.

La temperatura aritmética del aire tiene un valor medio (± intervalos de confianza) de 17.3 °C (± 0.9 °C). Aumenta hasta 19 °C en el desierto de Chihuahua y en las regiones fisiográficas del océano Pacífico, pero disminuye hasta 13.2 °C en la cadena montañosa de la Sierra Madre Occidental (figura 8).

El gradiente térmico se aproxima a 0.11 °C y a 0.60 °C por cada 100 m de altitud sobre el nivel del mar en el océano Pacífico y en el desierto de Chihuahua hasta las serranías

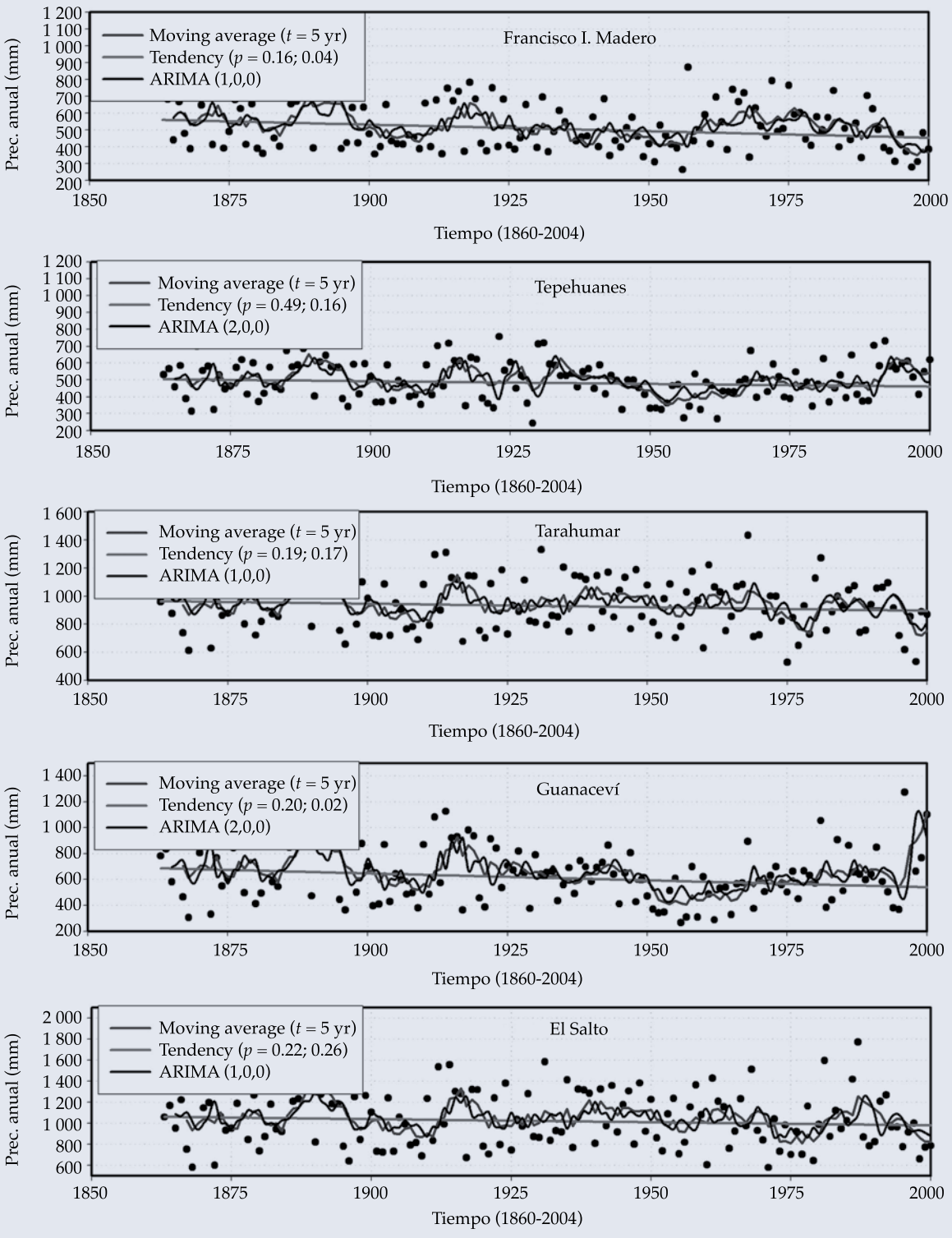

Figura 4. Patrones de datos de precipitación anual instrumentales registrados (1940 -2004) y reconstruidos (1860 -1940) para estaciones climáticas ubicadas en el área fisiográfica de la cadena montañosa de la Sierra Madre Occidental y los valles centrales de Durango y Chihuahua del estado de Durango, México. La probabilidad de ajustar una ecuación polinomial de primero y segundo grado también se representa en las leyendas de la figura.

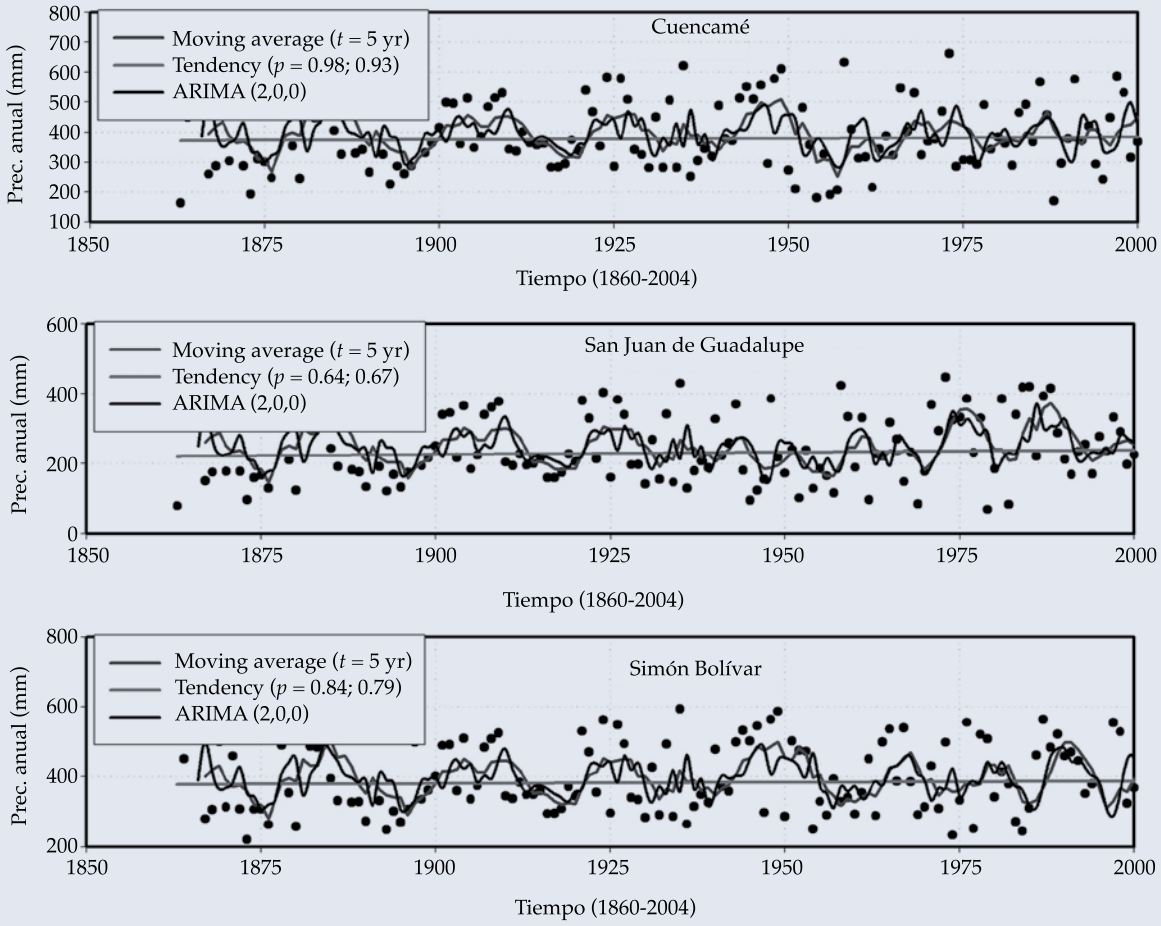

Figura 5. Patrones de datos de precipitación anual registrados (1940 -2000) y reconstruidos (1860 -1940) para tres estaciones climáticas ubicadas en el área fisiográfica del desierto de Chihuahua del estado de Durango, México. La probabilidad de ajustar una ecuación polinomial de primero y segundo grado también se representa en las leyendas de la figura.

superiores de la cadena montañosa de la Sierra Madre Occidental, respectivamente. La diferencia en ambos gradiente se explica por medio del efecto local del océano Pacífico sobre la temperatura de las tierras bajas occidentales de la cadena montañosa de la Sierra Madre Occidental.

Las variaciones temporales de la temperatura media anual correspondiente a las 3 regiones fisiográficas del estado de Durango, México, se presentan en la figura 9.

Las temperaturas medias anuales no están cambiando transitoriamente en el área de la SMOc (máxima con $p = 0.43$, media con $p = 0.11$, mínima con $p = 0.83$). Esto es, están ausentes las tendencias monótonas que muestran que las series de tiempo de temperatura media anual son estacionarías y se ubican también en esta región fisiográfica. Es decir, está ausente el efecto del cambio climático en la temperatura anual media. En el área del océano Pacífico, la temperatura anual media está disminuyendo con significancia estadística ($p = 0.0001$), aunque esta observación requiere de evidencia adicional antes de que pueda discutirse aún más como una estación climática que fue reubicada en los años 90. En el desierto de Chihuahua, la temperatura máxima normal

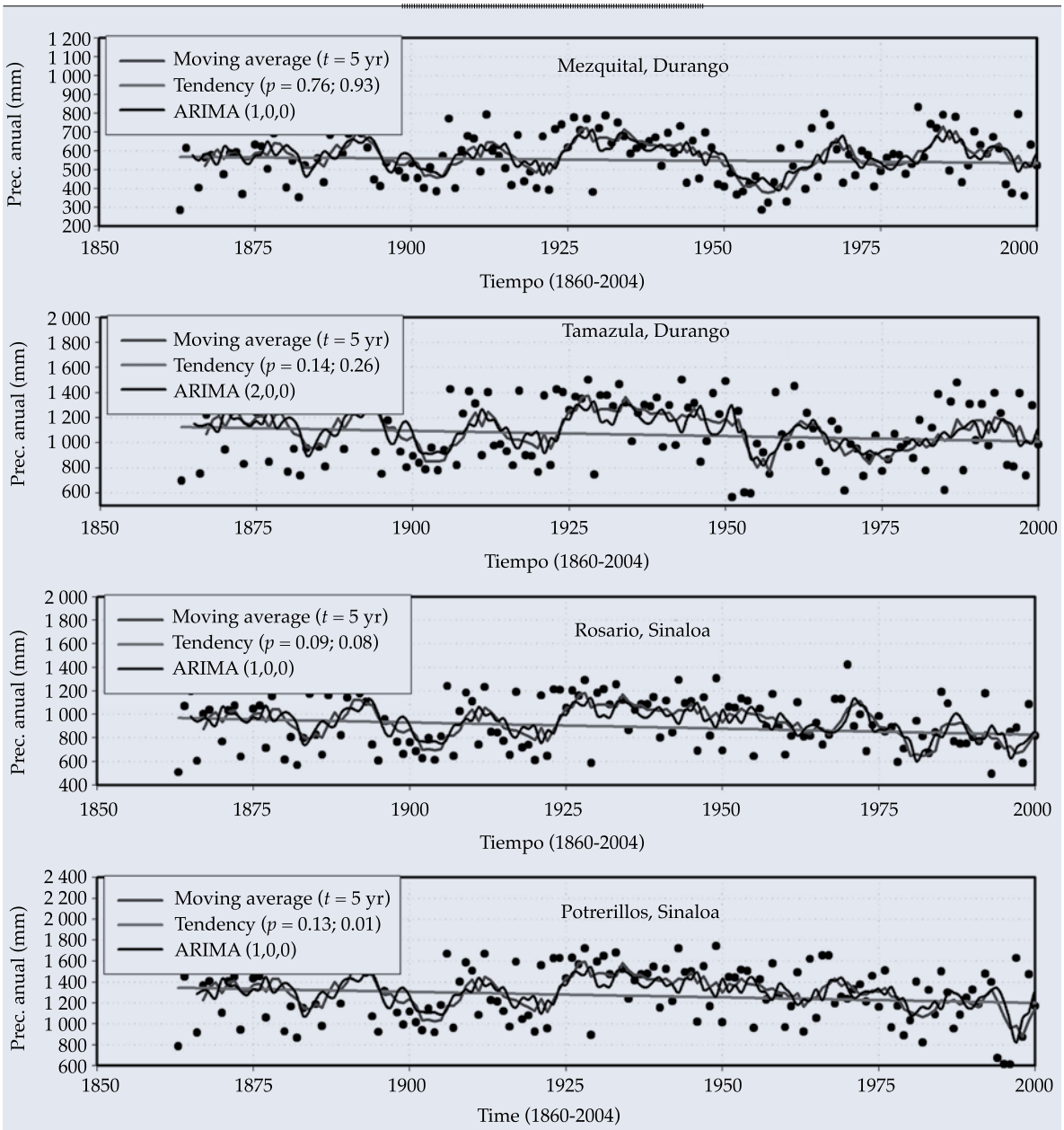

Figura 6. Patrones de datos de precipitación anual registrados (1940 -2000) y reconstruidos (1860 -1940) para cuatro estaciones climáticas ubicadas en el área fisiográfica de las pendientes occidentales de la cadena montañosa de la Sierra Madre Occidental del estado de Durango, México. La probabilidad de ajustar una ecuación polinomial de primero y segundo grado también se representa en las leyendas de la figura.

está creciendo estadísticamente (p = 0.009), la temperatura media o anual también está aumentando (p = 0.001), pero el mínimo medio no está cambiando de manera significativa (p = 0.99).

Descarga del río

La descarga anual tienen valores medio y de intervalo de confianza de 583 Mm^3 y 220 Mm^3, respectivamente, de acuerdo con los datos

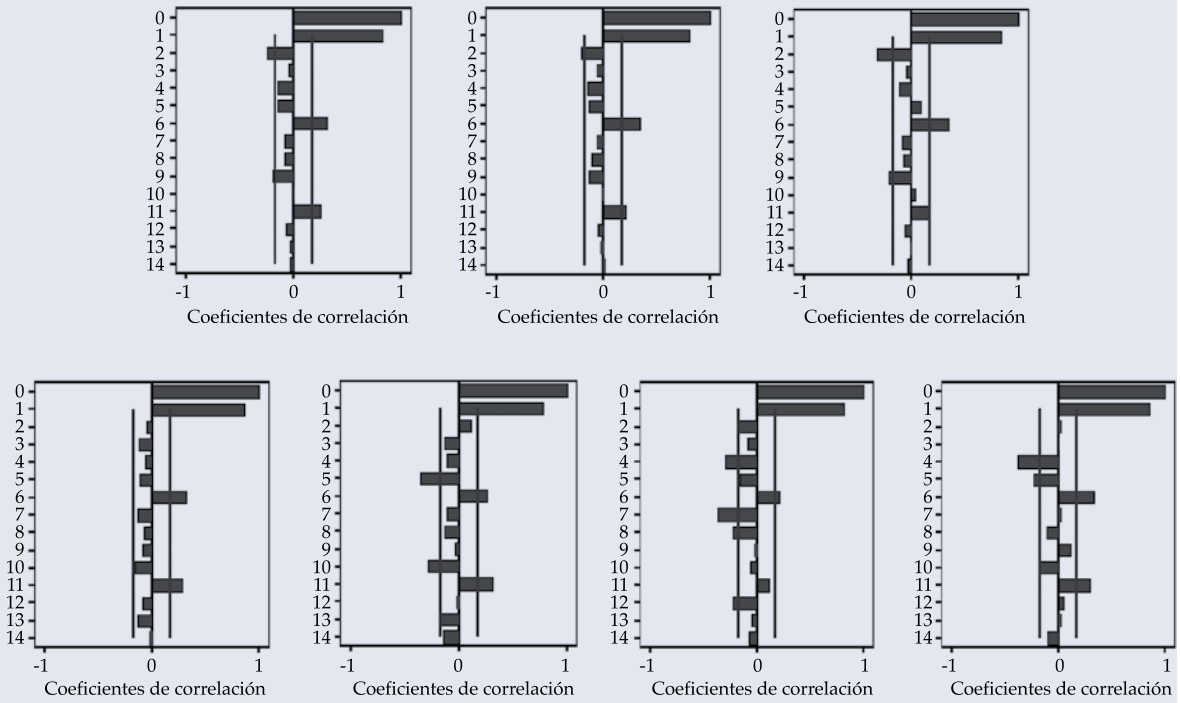

Figura 7. Funciones de autocorrelación parciales para la descarga anual (figuras superiores) para las estaciones de medición de: (a) San Pedro; (b) Acaponeta; y (c) Salomé Acosta; así como para la precipitación anual (figuras inferiores) para las estaciones climáticas de (a) Tepehuanes; (b) El Salto; (c) Cuencamé y (d) Tamazula para series de tiempo reconstruidas e instrumentales (1860 -2004) del estado de Durango, México.

del flujo del río en 25 estaciones de medición situadas en el estado. La variación a largo plazo es cercana a 50% de la descarga media anual acentuando el efecto de las sequías y la presencia de huracanes o ciclones. Resulta claro que el drenaje de los ríos hacia el océano Pacífico es el más grande y que el drenaje de los ríos hacia el interior del desierto de Chihuahua produce las descargas anuales más pequeñas (cuadro 2).

Las estaciones de medición situadas en los ríos que drenan hacia el océano Pacífico producen el flujo más grande y las que se ubican en los ríos que descargan hacia las cuencas interiores en el desierto de Chihuahua producen los caudales diarios más pequeños para la mayoría de las probabilidades (cuadro 3).

El análisis de separación hidrográfica utilizando datos de descargas diarias indica que el flujo base y el flujo directo corresponden en promedio a 36 y 64%, respectivamente, en las 17 estaciones de medición (cuadro 4). Las bajas cifras de flujo base son el resultado de suelos poco profundos perturbados y los eventos de lluvia erráticos e intensos. Durango es un estado con las lluvias más grandes y más pequeñas, ya que 65% de la precipitación anual está compuesta por lluvias de poca profundidad que no produce escurrimientos significativos y el restante 35% está compuesta por lluvias que producen tanto la recarga de acuíferos como escurrimientos superficiales.

Los datos de descarga no están disminuyendo monótonamente a lo largo del tiempo en la mayor parte de las estaciones de medición del estado de Durango (figuras 10 y 11). Las series de tiempo son estacionarías en el primer momento faltando el efecto del cambio climático sobre las variables que producen el

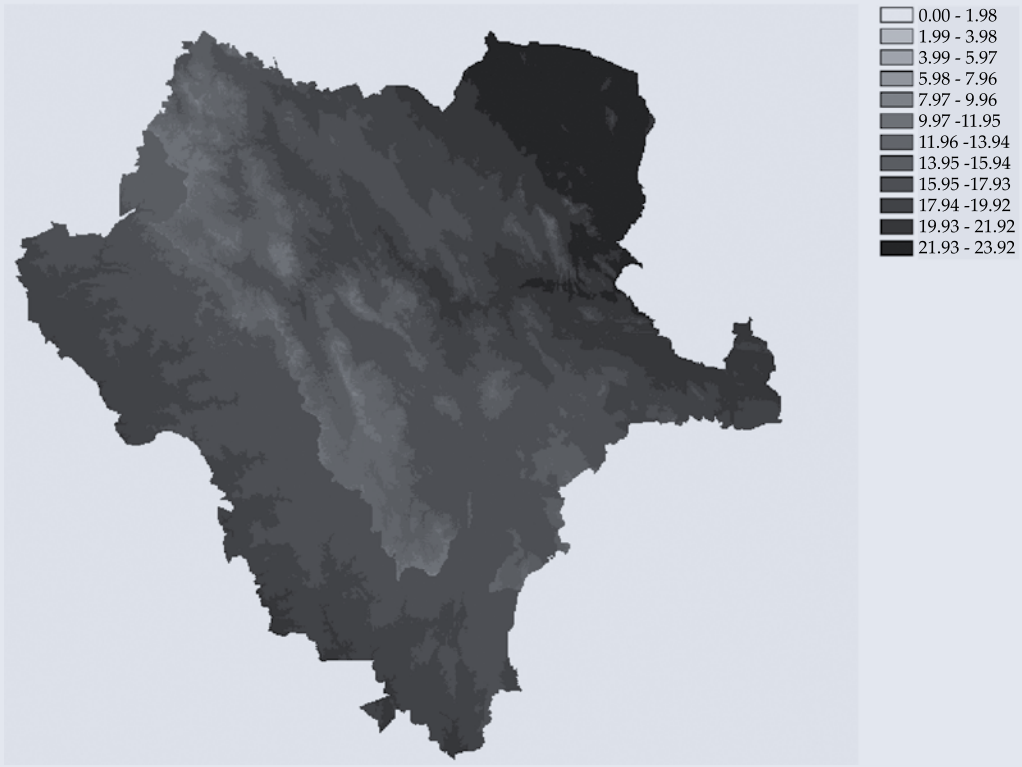

Figura 8. Temperatura del aire media anual para el estado de Durango, México.

flujo en los arroyos. De hecho, la tendencia de la descarga normal es altamente errática debido a la presencia-ausencia de lluvias promotoras de escurrimientos tales como ciclones, huracanes, depresiones tropicales y eventos de alta precipitación no estacionales en el área que enmascaran cualquier control potencial de cambio climático en esta variable. También son variables que operan a lo largo del tiempo las diversas prácticas inducidas por la actividad humana que controlan la descarga de ríos, tales como la construcción de presas y embalses, los cambios en el uso de la tierra y las prácticas de pastoreo excesivo, así como otras fuentes de variabilidad climática inherente.

Los modelos ARIMA ajustados explican un poco más del 50% de los datos de descarga anual continua (t = 3 años) y estos modelos estocásticos incluyen consistentemente dos parámetros autorregresivos para la mayor parte de las estaciones de medición que muestran que la descarga anual es más variable que la precipitación anual para el estado de Durango, México. El primer parámetro autorregresivo (retraso 1) es positivo, lo que demuestra el efecto potencial de dos años de la variabilidad anual de lluvias intensas y temporadas de sequías en la descarga anual en el área. Sin embargo, el segundo (retraso 2) es negativo demostrando que la descarga anual vuelve a sus condiciones previas después de la presencia de temporadas de sequía interanuales o altas tasas de descarga interanual.

Los ciclos de descarga anual de 2-3 años, 4-6 años y 9-10 años también se advierten en las series de tiempo (1860-2004), correlogramas, análisis de densidad espectral y modelos ARIMA. Se describen ciclos similares más tempranos para la precipitación anual.

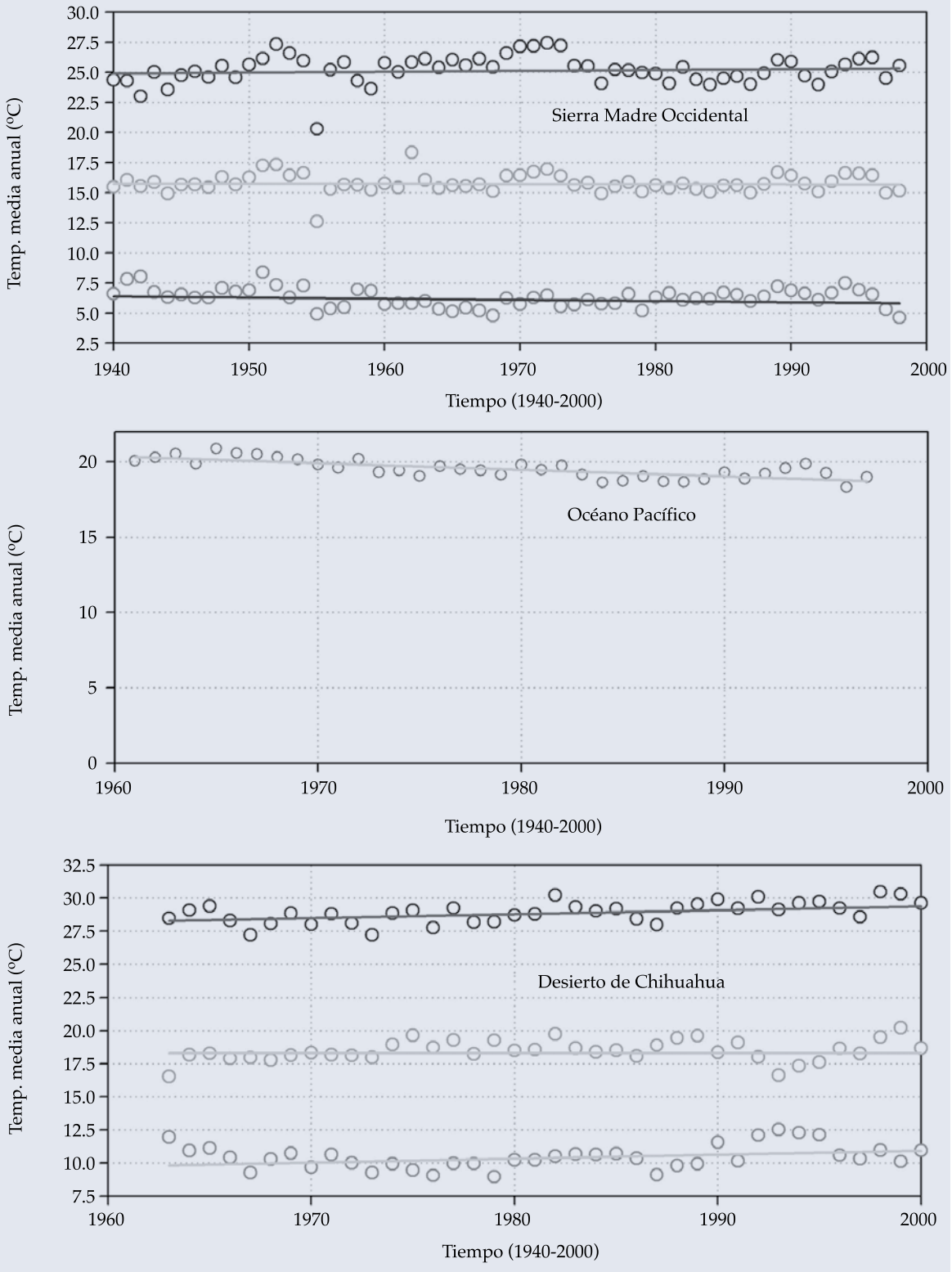

Figura 9. Patrones de temperatura de aire anual para tres regiones fisiográficas del estado de Durango, México.

Cuadro 2. Descarga anual para 25 estaciones de medición con varias probabilidades estimadas empleando la función de densidad Log Pearson Tipo III.

Estación de medición	Descarga anual (Mm^3) con una probabilidad de ocurrencia ($P(x \leq X)$)											Media
	10%	20%	30%	40%	50%	60%	70%	80%	90%	95%	99%	
Acaponeta	547	688	818	948	1 093	1 262	1 474	1 779	2 313	2 905	4 544	1 359
Acatitan	44	77	115	162	224	311	440	665	1 171	1 886	4 641	394
Baluarte	615	795	965	1 139	1 337	1 573	1 875	2 323	3 141	4 092	6 935	1 760
Guatenipa	435	596	756	927	1 129	1 380	1 715	2 232	3 233	4 460	8 394	1 611
Huites	1 379	1 795	2 194	2 610	3 090	3 674	4 439	5 599	7 793	10 437	18 758	4 196
Ixpalino	516	691	859	1 036	1 238	1 484	1 803	2 280	3 160	4 186	7 234	4 196
Tecusiapa	235	309	381	458	546	655	800	1 023	1 455	1 990	3 763	761
Sta. Cruz	285	441	611	805	1 047	1 364	1 808	2 532	4 020	5 950	12 549	1 669
Las Habitas	688	897	1 095	1 300	1 534	1 816	2 181	2 727	3 742	4 946	8 673	1 972
La Bayona	23	34	46	59	76	99	132	191	330	551	1 658	123
Las Tortugas	54	79	105	133	167	210	268	359	536	756	1 467	237
Tamazula	229	296	360	425	499	588	701	867	1 168	1 510	2 498	636
La Huerta	250	353	457	571	708	879	1 109	1 469	2 171	3 034	5 795	1 067
Agustín Melgar	396	519	639	766	913	1 094	1 333	1 699	2 405	3 271	6 089	1 179
El Palmito	151	242	349	484	670	942	1 379	2 223	4 444	8 235	28 120	1 015
El Pino	4	6	7	9	11	14	19	28	50	87	285	10
El Saltito	13	24	38	56	82	121	183	302	602	1 082	3 305	225
Fdez. II	543	646	743	844	963	1 114	1 324	1 671	2 427	3 504	7 916	1 191
N. Mendoza	6	9	12	16	21	28	37	53	85	128	285	34
Peña Águila	5	9	14	21	30	45	69	118	249	477	1 705	93
Salomé Acosta	92	142	195	256	331	428	562	777	1 210	1 757	3 548	550
San Felipe	3	7	12	20	32	53	90	172	425	932	4 311	96
San Pedro	1 076	1 374	1 650	1 931	2 245	2 617	3 089	3 779	5 023	6 448	10 644	2 773
V. Guerrero	1	3	5	8	13	20	33	61	140	286	1 135	31
Sardinas	62	103	151	208	283	386	539	805	1 405	2 270	5 795	530

Discusión

El clima mexicano se extiende desde las condiciones secas del desierto sonorense en el noroccidente, donde la precipitación promedio anual es menor a 100 mm, hasta los climas húmedos tropicales que caracterizan las regiones forestales del sur de México, donde la precipitación anual promedio puede alcanzar más de 2000 mm (Livermann, 1999). El estado de Durango se ubica justo en el centro de este gradiente hidroclimático. Este intenso gradiente de precipitación se origina en las bandas latitudinales de la circulación atmosférica, las cuales varían estacionalmente. Los vientos del occidente traen precipitación al norte de México en el invierno (Cavazos y Hastenrath, 1990). Los niveles altos subtropicales asociados con condiciones estables y la zona de convergencia intertropical y los vientos alisios liberan lluvia de verano en las regiones central y sur del país. Otras influencias clave en la precipitación son los huracanes del otoño en las costas tanto del Caribe como del Pacífico, los monzones de verano en el norte y la alta presión del verano que interrumpe el flujo de aire húmedo y crea

Cuadro 3. Flujos máximos diarios estimados mediante la función de densidad Log Pearson Tipo III para 11 diferentes probabilidades correspondientes a 17 estaciones de medición ubicadas sobre ríos del estado de Durango, México.

Estación de medición	Flujos máximos diarios ($m^3 s^{-1}$) con una probabilidad de ocurrencia (%) ($x \leq X$)													
	99.5	99	95	90	80	50	20	5	2	1	0.5	0.2	0.10	0.05
A. Melgar	872	697	439	323	251	176	142	127	123	122	121	120	119	119
El Palmito	3 738	3 285	2 370	1 747	1 274	634	278	112	67	47	33	21	16	12
Fernández II	462	388	268	205	163	113	85	69	64	61	58	56	55	54
La Huerta	2 206	1 974	1 492	1 158	895	515	273	138	94	72	56	41	33	26
N. Mendoza	194	123	47	24	13	6	3	2	2	2	1	1	1	1
P. del Águila	2195	1 472	572	257	118	25	5	1	0	0	0	0	0	0
R. Salcido	436	396	294	214	147	56	15	3	1	1	0	0	0	0
Río el Oro	1 005	988	920	821	691	394	152	40	17	9	5	2	1	1
S. Acosta	1 257	1 152	909	725	566	320	157	70	44	31	23	15	11	8
San Felipe	793	663	411	256	154	48	11	2	1	0	0	0	0	0
V. Guerrero	178	154	107	76	54	25	10	4	2	1	1	1	0	0
Acaponeta	10 987	7 985	4 021	2 435	1 586	779	439	286	238	214	196	178	167	159
Acatitan	11 298	8 891	4 786	2 690	1 475	391	81	14	5	3	1	1	0	0
Las Habitas	20 247	17 358	10 959	6 626	3 681	833	110	9	2	1	0	0	0	0
San Pedro	6 088	5 069	3 370	2 455	1 846	1 102	685	450	368	323	289	253	231	212
Santa Cruz	4 842	3 936	2 410	1 597	1 073	490	214	94	61	45	35	25	19	15

Cuadro 4. Flujo directo y base para 17 estaciones de medición ubicadas sobre ríos principales del estado de Durango, México.

Cuencas colectoras	Estación de medición	Años	Descarga total	Desviación	Flujo base	Flujo directo	Flujo base	Flujo directo
			(Mm^3)		(%)		(Mm^3)	
Sinaloa	La Huerta	28	1 094.5	561.1	26	74	284.6	809.9
Nazas	Agustín Melgar	29	1 179.4	502.0	23	77	271.3	908.1
Pre-Sanped	El Saltito	34	236.9	218.7	22	78	52.1	184.8
Nazas	Fernández II	31	1 190.6	505.7	23	77	273.8	916.8
Nazas	El Palmito	19	1 361.3	580.5	21	79	285.9	1 075.5
Pre-Sanped	N. Mendoza	36	31.9	18.7	66	33	21.1	10.5
Pre-Sanped	P. del Águila	43	94.9	103.9	55	45	52.2	42.7
Pre-Sanped	R. Salcido	54	58.9	51.2	53	47	31.2	27.7
Nazas	S. Acosta	25	500.2	275.4	25	75	125.1	375.2
Pre-Sanped	V. Guerrero	38	30.7	27.91	58	42	17.8	12.9
Sinaloa	Santa Cruz	50	1 651.3	682.5	84	16	1 387.1	264.2
Sinaloa	Tamazula	36	633.9	223.2	25	75	158.5	475.4
Pre-Sanped	El Bejuco	36	150.0	54.5	24	76	36.0	114.0
Pre-Sanped	Los Habitas	18	2 030.4	774.2	29	71	588.8	1 441.6
Pre-Sanped	San Pedro	50	2 760.9	1 003.3	26	74	717.8	2 043.1
Pre-Sanped	Acaponeta	50	1 358.9	514.5	26	74	353.3	1 005.6
Río Culiacán	Guatenipa II	31	1 568.0	665.3	24	76	376.3	1 191.7

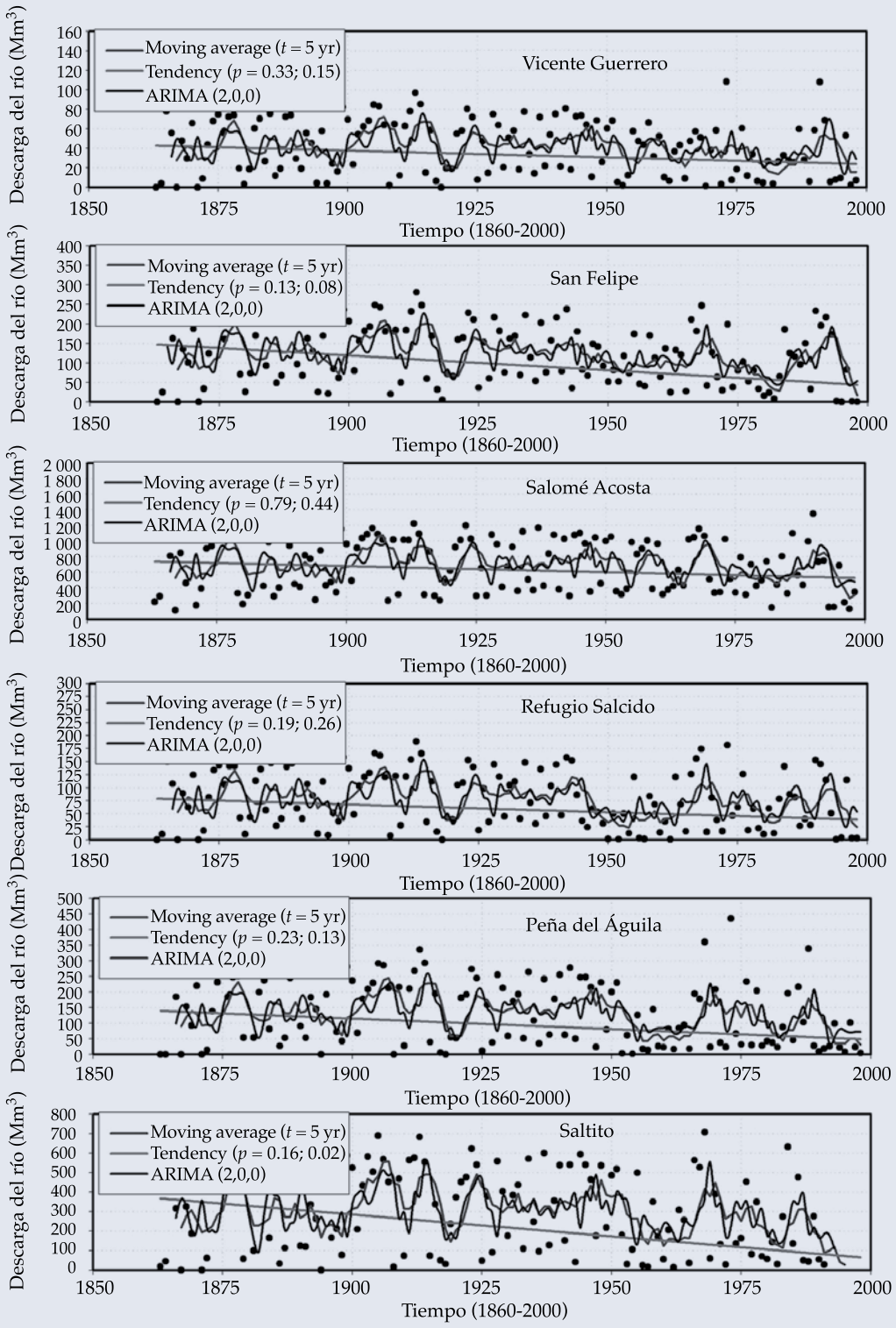

Figura 10. Patrones de datos de descarga anual registrados (1940 -2000) y reconstruidos (1860 -1940) para seis estaciones de medición a lo largo de las cuencas colectoras del Mezquital y Nazas dentro de las regiones fisiográficas de la Sierra Madre Occidental y el desierto de Chihuahua del estado de Durango, México.

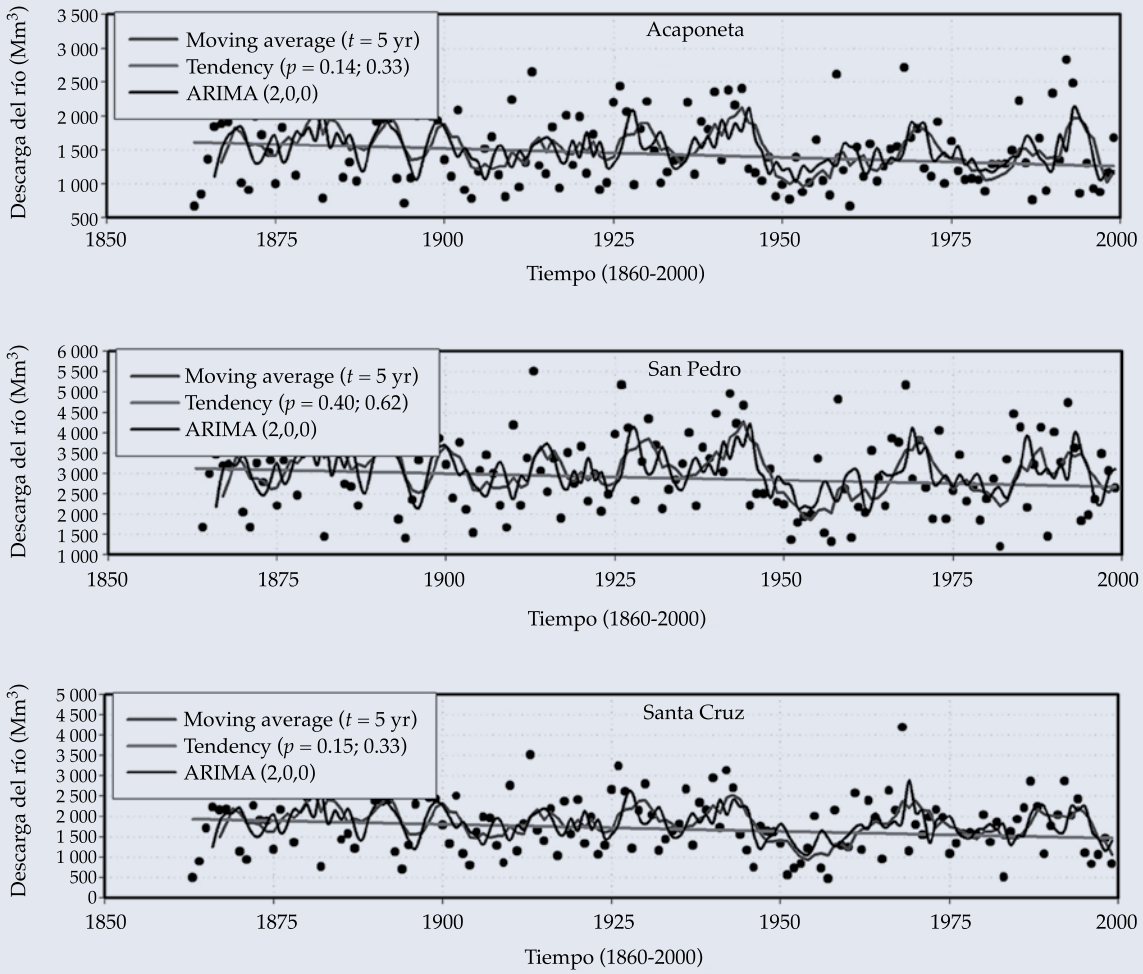

Figura 11. Patrones de datos de descarga anual registrados (1940 -2000) y reconstruidos (1860 -1940) para tres ríos principales de las tierras bajas del océano Pacífico en los estados de Durango y Sinaloa, México.

un periodo de condiciones secas conocido como sequía de medio verano. Las montañas y topografía variada de México dominan otras influencias climáticas.

La mayor parte del estado de Durango, México, con excepción de la punta más alta oriente se ubica dentro de la región llamada monzonal, la cual se extiende a lo largo de la Sierra Madre Occidental en el México noroccidental y sigue la división continental a través de la Arizona oriental, la mayor parte de Nuevo México y se extiende hacia el sur de Colorado en los Estados Unidos (Comrie and Glenn, 1998). Esta área se caracteriza por la intensa precipitación máxima de media a tardía con una precipitación considerablemente menor durante el resto del año. La estrecha frontera sur de la región monzónica con mayor probabilidad se mezcla en la zona de convergencia intertropical, ZCIT, precipitación relacionada con el México central y del sur. Las tormentas que provocan precipitación durante el invierno provienen del occidente y avanzan de norte a sur mientras que la precipitación de verano tiende a progresar de sur a norte como un sistema monzónico o real (Dettinger *et al.*, 1998; Higgins *et al.*, 1999). Sin embargo, el área controlada por el monzón es muy errática y parcialmente responsable de las oscilaciones estacionales y potencialmente interanuales

en la precipitación y descarga en las cuencas colectoras del estado de Durango, México.

Varias tendencias y oscilaciones climáticas que contribuyen a la variabilidad monzonal son El Niño-Oscilación del Sur, ENSO, la Oscilación Decadal del Pacífico, PDO, la oscilación del Atlántico Norte, NAO y la Pequeña Edad de Hielo. La precipitación reconstruida de Durango, México, empleando análisis dendrocronológico (1380-2000) mostró que el índice de lluvia tropical (ILLT) se correlaciona bien con la precipitación de invierno instrumental y reconstruida (r = 0.49 y 0.55, respectivamente), reflejando la fuerte modulación ENSO del clima de temporada fría sobre el norte de México (Cleaveland *et al*., 2003). Los índices ENSO y PDO se asociaron estadísticamente con la variabilidad hidroclimática a largo plazo sobre la cadena montañosa de la Sierra Madre Occidental (Návar, 2012). Debido a la falta de información a largo plazo, NAO y la Pequeña Edad de Hielo no se han teleconectado con la variabilidad hidroclimática en la región. Los estudios a largo plazo enfatizan que el clima es más variable en el norte de México debido a todas las fuentes e interacciones de variabilidad descritas antes. En consecuencia, el norte y el sur de México muestran a menudo señales climáticas opuestas. El análisis de sedimentos de lagos del centro de México mostró que las condiciones de clima húmedo del Pleistoceno-Holoceno tardío prevalecieron alrededor de 6 000 años AP, con grandes oscilaciones entre 6 000 y 5000 años AP y un periodo de marcada aridez en el centro de México cerca de 1 000 años AP (Metcalfe *et al*., 2000).

El Niño-Oscilación de sur, PDO, NAO, y la Pequeña Edad de Hielo se han teleconectado previamente con la variabilidad monzónica (Cavazos y Hastenrath, 1990). Sin embargo, para elucidar físicamente en mayor detalle los mecanismos controladores potenciales de la variabilidad monzonal, debe estudiarse más el papel de la circulación Hadley y la función de la zona de convergencia intertropical en la forma e intensidad de la circulación tropical sobre la región, entre otros aspectos (Comrie y Glenn, 1998). Cavazos y Hastenrath (1990), y Woodhouse (1997) discuten también como los anticiclones subtropicales y los asociados a serranías superiores centradas sobre la región y los océanos Atlántico y Pacífico adyacentes ejercen una influencia dominante de alrededor de un año, modulada por el papel de la circulación de media latitud occidental en el invierno y el monzón de Norteamérica en el verano.

El efecto del cambio climático monótono está ausente por la estacionariedad de las series de tiempo, aunque la modelación del efecto del cambio climático sobre el flujo en ríos y la precipitación por el IPCC (2007) pronostica que el norte de México supuestamente disminuirá la descarga y la precipitación de 0-25% con el calentamiento global. Villers-Ruiz y Trejo-Vázquez (1997) modelaron también la expansión por el cambio climático de los climas secos y la descarga consecuente en la mayor parte de los ecosistemas mexicanos. Mulholland *et al*. (1997) y el IPCC (2007), utilizando modelos de circulación general, predijeron que el norte de México, en particular la banda más baja del Río Bravo/Río Grande, recibiría 10% menos de lluvia con las crecientes temperaturas por el calentamiento global. Información adicional en el futuro cercano aclararía el efecto del cambio climático sobre la variabilidad hidro climática en la región estudiada.

Otras causas de la variabilidad de la descarga sobre la abstracción espacio-temporal de los recursos de agua directamente de ríos y acuíferos para irrigación agrícola, población e industria expandidas del estado de Durango. El mal manejo de los recursos naturales, en específico los recursos de plantas y sus suelos que conducen a la compactación de suelos y a la reducción de la cobertura de plantas, parece desempeñar también un papel en la disminución de la descarga a lo largo del tiempo, ya que en varios manantiales se están viendo reducidos los flujos base en la región.

Conclusiones

El hidroclima es altamente variable en el estado de Durango, México, en virtud de que la mayor parte de dicho estado se ubica dentro de la región de actividad monzonal. Este clima se caracteriza por oscilaciones erráticas que se han asociado con variabilidad estacional, interanual, ENSO y PDO, y potencialmente también con NAO y la Pequeña Edad de Hielo. El papel de la circulación de Hadley, la zona de convergencia intertropical, la migración de los anticiclones subtropicales y los sistemas de altas presiones de niveles superiores asociados, modulados por el papel de la circulación occidental de latitud media, parecen ejercer una fuerte influencia en la variabilidad hidroclimática en el invierno y el monzón de Norteamérica en el verano. Para abarcar de manera preliminar esta gran variabilidad, el manejo sustentable de los recursos hídricos es una práctica alternativa que puede alcanzar crecimiento económico, estabilidad social y compatibilidad ambiental, y debe implementarse para alcanzar el bienestar de las generaciones presente y futuras. Son bienvenidos otros proyectos dirigidos a incrementar la disponibilidad de agua en la región.

Agradecimientos

El autor de este reporte desea agradecer al fondo SIP por otorgar una beca mediante el proyecto 2011. Los mapas SIG fueron elaborados por el Dr. Armando Cortes. El autor es investigador de COFAA.

Recibido: 27/03/12
Aceptado: 22/04/13

Referencias

CAVAZOS, T. and HASTENRATH, S. Convection and rainfall over Mexico and their modulation by the Southern Oscillation. *J. Climatol*. Vol. 10, 1990, pp. 377-386.

CLEAVELAND, M.K., STAHLE, D.W., THERRELL, M.D., VILLANUEVA-DÍAZ, J., and BURNS, B.T. Tree-ring reconstructed winter precipitation and tropical teleconnections in Durango, Mexico. *Climate Change*. Vol. 59, 2003, pp. 369-388.

COMRIE, A.C. and GLENN, E.C. Principal components-based regionalization of precipitation regimes across the southwest United States and northern Mexico, with application to monsoon precipitation. *Climate Research*. Vol. 10, 1998, pp. 201-215.

CSIS. *Center for International and Strategic Studies. Addressing our Global Water Future*. New Mexico, USA: Sandia National Laboratories, 2005.

DETTINGER, M.D., CAYAN, D.R., DIAZ, H.F., and MEKO, D.M. North-south precipitation patterns in western North America on interannual-to-decadal timescales. *Journal of Climate*. Vol. 11, 1998, pp. 3095-3111.

FAO. *Aquifers under threat*. Rome: Food and Agriculture Organization, 2005.

GREENWOOD, J.A. and DURAND, D. Aids for fitting the gamma distribution by maximum likelihood. *Technometrics*. Vol. 2, No, 1, 1975, pp. 55-65.

GONZÁLEZ-ELIZONDO, M., JURADO, E., NÁVAR, J., GONZÁLEZ-ELIZONDO, S., VILLANUEVA, J., AGUIRRE, O.A., and JIMÉNEZ, P.J. Tree rings and climate association for five chronologies of Douglas fir from Durango and Zacatecas, México. *Forest Ecology and Management*. Vol. 213, 2005, pp. 39-53.

HAAN, C.T. Stochastic Models in Hydrology. Second edition. Iowa: Iowa State University Press, 2002, 450 pp.

HIGGINS, R.W., CHEN, Y., and DOUGLAS, A.V. Interannual variability of the North American warm season precipitation regime. *Journal of Climate*. Vol. 12, 1999, pp. 653-680.

IPCC. *Intergovernmental Panel on Climate Change. Impacts, adaptation, and vulnerability. Summary for Policy Makers*. Cambridge, UK: Cambridge University Press, 2007, 17 pp.

KNIGHT, J.R., FOLLAND, C.K., and SCAIFE, A.A. Climate impacts of the Atlantic Multidecadal Oscillation. *Geophysical Research Letters*. Vol. 33, LI7706, 2006, doi: 10.1029/2006GL026242.

LIVERMANN, D.M. Vulnerability and adaptation to drought in Mexico. *Natural Resources Journal*. Vol. 99, 1999, pp. 1-35.

METCALFE, S.E., O´HARA, S.L., CABALLERO, M., and DAVIES, S.L. Records of late Pleistocene-Holocene climate change in Mexico – a review. *Quaternary Science Reviews*. Vol. 19, 2000, pp. 699-721.

MULHOLLAND, P.J., BEST, G.R., COUTANT, C.C., HORNBERGER, G.M., MEYER, J.L., ROBINSON, P.J., STENBERG, J.R., TURNER, R.E., VERA-HERRERA, F., and R.G. WETZEL. Effects of climate change on freshwater ecosystems of the Southeastern United States and Gulf of Mexico. *Hydrological Processes*. Vol. 11, 1997, pp. 949-970.

NÁVAR, J. *Atlas Hidrológico del Estado de Durango*. Inédito. 2008, 220 pp.

NÁVAR-CHÁIDEZ, J.J. Water scarcity and degradation in the Rio San Juan watershed of northeastern Mexico. *Frontera Norte*. Vol. 23, No. 46, 2011, pp. 125-150.

NÁVAR, J. Modeling annual discharge for six Mexico's northern subtropical rivers. *Ambiente & Agua. An Interdisciplinary Journal*. Vol. 7, 2012, pp. 36-50, doi:10.4136/1980-993X.

POSTEL, L.S. Entering an era of water scarcity: the challenges ahead. *Ecological Applications*. Vol. 10, No. 4, 2000, pp. 941-948.

POSTEL, S. and WOLF, A.T. Dehydrating conflict. *Foreign Policy*. September/October, 2001, pp. 2-9.

RUTLEDGE, A.T. Computer programs for describing the recession of ground-water discharge and for estimating mean ground-water recharge and discharge from streamflow data - Update: U.S. *Geological Survey Water-Resources Investigations Report*. Vol. 98, No. 4148, 1998, 43 pp.

SHIKLOMANOV, I.A. and RODDA, J. *World Water Resources at the Beginning of the 21st Century*. Paris: UNESCO, 2003.

STAHLE, D.W., CLEAVELAND, M.K., THERRELL, M.D., and VILLANUEVA-DÍAZ, J. *Tree ring reconstruction of winter and summer precipitation in Durango, Mexico, for the past 600 years*. 10th Symp Global Change Studies, American Meteorological Society. Dallas, 1999, pp. 205-211.

USGS. 2002, http://pubs.usgs.gov/of/2007/1033/pdf/Appendix3_web.pdf

VILLERS-RUIZ, L. and TREJO-VÁZQUEZ, I. Assessment of the vulnerability of forest ecosystems to climate change in Mexico. *Climate Research*. Vol. 9, 1997, pp. 87-93.

VOROSMARTY, C.J., GREEN, P., SALISBURY, J., and LAMMERS, R.B. Global water resources: vulnerability from climate change and population growth. *Science*. Vol. 289, No. 5477, 2000, pp. 284-288.

WOODHOUSE, C.A. Winter climate and atmospheric circulation patterns in the Sonoran Desert Region. *USA. Int J. Climatol*. 17, 1997, pp. 859-873.

Dirección institucional del autor

Dr. José Návar

Profesor de Manejo de Recursos Naturales
Centro Interdisciplinario de Investigación para el Desarrollo Integral Regional del Instituto Politécnico Nacional (CIIDIR-IPN), Unidad Durango
Sigma núm. 119, Fracc. 20 de Noviembre II
34220 Durango, Dgo., México
Teléfono y fax: +52 (618) 8142 091
jnavar@ipn.mx
josedejesusnavar@yahoo.com.mx

Click here to write the autor

Obtainment of Empirical Equations for Design Floods Estimation in the Hydrological Region No. 10 (Sinaloa) of Mexico

• Daniel Francisco Campos-Aranda* •
Profesor jubilado de la Universidad Autónoma de San Luis Potosí
*Corresponding Author

Abstract

CAMPOS-ARANDA, D.F. Obtainment of Empirical Equations for Design Floods Estimation in the Hydrological Region No. 10 (Sinaloa) of Mexico. *Water Technology and Sciences* (in Spanish). Vol. V, No. 1, January-February, 2013, pp. 121-139.

Floods designing (Q_{Tr}) is the most common hydrological estimation, because it is basic to sizing and reviewing all types of hydraulic works. Its estimation in watersheds without annual maximum flow data is based on regional methods, which use such information from a region or geographical area, in order to obtain results that apply within it. There are two types of regional procedures: those related to the index flood and those that develop empirical equations. The first type is based on the homogeneity of the region, hence its predictability; whereas the second method allows some degree of heterogeneity, which is taken into account in the regression models generated. Four empirical equations were established, using as prediction variables: the watershed area (*A*), the main channel length (*Lcp*) and predictions of maximum daily rainfall (*PMD*). Only two equations were selected for each of the six return periods established. 23 records of maximum annual flow were processed to obtain values of Q_{Tr} based on the General Extreme Values distribution. To obtain the fit coefficients of each equation three methods were used: the least-squared residuals in the logarithmic domain, their bias correction and the numerical optimization minimizing an objective function. Six empirical equations for each of the six return periods analyzed were obtained. The regularity of the estimations was tested by numerically contrasting results from six gauging stations (not used in the derivation of the equations) and six of those processed (those with the longest period of record). Such analysis allowed to point out the predictive ability of the empirical equations developed. It is highly recommended to apply the proposed procedure in other regions to find such empirical equations for design flood estimation, because of their very simple application.

Keywords: multiple linear regression, relative error, performance indices, Rosenbrock algorithm.

Resumen

CAMPOS-ARANDA, D.F. Obtención de ecuaciones empíricas para estimación de crecientes de diseño en la Región Hidrológica Núm. 10 (Sinaloa) de México. *Tecnología y Ciencias del Agua*. Vol. V, núm. 1, enero-febrero de 2013, pp. 121-139.

*Las crecientes de diseño (Q_{Tr}) son la estimación hidrológica más frecuente debido a que son básicas para dimensionar y revisar todo tipo de obras hidráulicas. Su estimación en cuencas sin datos de gasto máximo anual se basa en los métodos regionales, que emplean tal información de una región o zona geográfica para obtener resultados que son aplicables dentro de ella. Los procedimientos regionales son de dos tipos: los similares al índice de crecientes y el desarrollo de ecuaciones de empíricas. Los primeros se basan y deben su capacidad de predicción a la homogeneidad de la región; en cambio, el segundo método permite cierto grado de heterogeneidad, la cual es tomada en consideración en los propios modelos de regresión generados. Empleando como variables predictivas el área de cuenca (*A*), la longitud del cauce principal (*Lcp*) y las predicciones de lluvia máxima diaria (*PMD*), se establecieron cuatro ecuaciones empíricas, seleccionando dos, según sus índices de desempeño, para cada uno de los seis periodos de retorno establecidos. Se procesaron 23 registros de gastos máximos para obtener los valores de Q_{Tr} con base en la distribución general de valores extremos. Para la obtención de los coeficientes de ajuste de cada ecuación se emplearon tres métodos: el de mínimos cuadrados de los residuos en el dominio logarítmico, su corrección por sesgo y el de optimización numérica minimizando una función objetivo. Se obtuvieron seis ecuaciones empíricas para cada uno de los seis periodos de retorno analizados. El contraste numérico en seis estaciones hidrométricas no utilizadas en la deducción de las ecuaciones y en seis de las procesadas, las de mayor periodo de registro, indica una regularidad en las estimaciones y destaca la capacidad predictiva de las ecuaciones empíricas desarrolladas. Se recomienda aplicar el procedimiento propuesto en otras regiones para encontrar este tipo de ecuaciones, que permiten estimar las crecientes de diseño de manera sumamente fácil.*

Palabras clave*: regresión lineal múltiple, error relativo, índices de desempeño, algoritmo de Rosenbrock.*

Introduction

Design floods are the most common hydrological estimates sinc , during planning and design, they serve as a basis to determine the size of all types of hydraulic infrastructure works. They also make it possible to evaluate the safety of these works after they are built, regardless of whether they are exploitation or control works (reservoirs), protection (dikes and channels) or crossings (sewers and bridges). The most reliable procedure to estimate design floods consists of fitting a probabilistic model to available maximum annual flow records, in order to obtain estimates or predictions for a range of flood probabilities, whose reciprocal is the return period or average interval, in years, between occurrences of an equal or greater event. The procedure cited is generally called a flood frequency analysis (FFA), which currently use as prescribed probabilistic models: log-Pearson type III distribution, Generalized Extreme Values and Generalized Logistic, fitting these using moments, maximum likelihood and *L* moments.

The main disadvantage of the FFA is the lack of flood records from the sites of interest. Therefore, a regional flood frequency analysis (RFFA) is used with available information related to maximum annual flows in a region or zone that can be considered hydrologically homogeneous. RFFA techniques jointly use the cited information and their results are applicable to any site located within a homogeneous region. Therefore, the RFFA makes it possible to estimate design floods in ungauged watersheds. Included among the classic RFFA methods are the season-years technique, floods index, fitting probabilistic models based on regional statistical parameters and obtaining potential regressions that relate the design floods obtained in gauged watersheds with certain physiographic climate characteristics (Cunnane, 1988; GREHYS, 1996a; Escalante-Sandoval and Reyes-Chávez, 2002).

GREHYS (1996a) shows that a clear distinction can be made among RFFA techniques—between methods similar to the floods index and those related to empirical regression. The former are based on the homogeneity of the region, which contributes to their predictive capacity and requires defining homogeneous regions. The second method allows a certain degree of heterogeneity, which is taken into account by the regression models designed. Thus, if the study region can be characterized as highly homogeneous, methods similar to the flood index are preferable, whereas if there is uncertainty when defining homogeneous regions or the study zone is composed of various sub-regions and there are not enough hydrometric information for these sub-regions to be analyzed independently, the use of empirical equations with an RFFA would be a better option.

The objective of this work is to develop a regional method using empirical regression equations for Hydrological Region No. 10 (Sinaloa), Mexico. This region is composed of either two sub-regions (one in the north and the other in the south) (Escalante-Sandoval (1998)) or three sub-regions (north, mountains and coastal plains) (Gutiérrez-López *et al.*, 2004; Campos-Aranda, 2008a). Twenty-three maximum annual flow records were processed ranging 19 from 65 years, with a mean value of 36 years. Four types of empirical equations were developed, each one for six return periods. They were all generated using two basic fitting methods— least-squares residuals in the logarithmic domain and unrestricted multivariate numerical optimization, applied using the Rosenbrock algorithm. Since the equations obtained with least–squares were corrected for bias, a total of 72 empirical equation were generated. Of these, the 36 with the best performance indicators were selected and tested in six hydrometric stations that were not used to obtain them and in six that were processed, the ones containing the most records. The conclusions highlight the consistency of the estimated predictions and suggest recommending this type of empirical

model be developed in other regions in the country, based on the following three proposals for fitting. These empirical equations make it possible to easily estimate design floods for other geographic regions in the country.

Development

Potential Regression and Fitting

Empirical equations are commonly used in hydrological engineering to perform estimates for sites where no hydrometric information exists. In terms of the estimate of design floods, the potential regression model has been used most to describe the relationship between the prediction (Q_{Tr}) and certain physiographic and climatic characteristics (X_i) of the watersheds from which the estimates are derived. Therefore, for a certain region considered homogeneous, we have (McCuen *et al.*, 1990; GREHYS, 1996a):

$$Q_{Tr} = b_0 \cdot X_1^{b_1} \cdot X_2^{b_2} \cdots X_m^{b_m} \cdot \varepsilon \qquad (1)$$

where $b_0, b_1, \ldots, b_m$ are fit parameters and ε is the multiplicative error of the model. To calculate the parameters, b_i, a common practice has been to linearize equation (1), taking logarithms and then estimating the coefficient of the multiple linear regression (MLR) model:

$$\log Q_{Tr} = \log b_0 + b_1 \cdot \log X_1 + b_2 \cdot \log X_2 + \cdots + b_m \cdot \log X_m + \log \varepsilon \qquad (2)$$

Setting $y = \log Q_{Tr}$, $a_0 = \log b_0$, $a_i = b_i$ and $x_i = \log X_i$, with $i = 1, 2, \ldots, m$, the MLR equation is obtained:

$$y = a_0 + b_1 \cdot x_1 + b_2 \cdot x_2 + \cdots + b_m \cdot x_m + \varepsilon \qquad (3)$$

(whose matrix solution of least-squares residuals (LSR) can be found in any text on numerical methods, for example, Campos-Aranda (2003)). The coefficient b_0 is equal to 10^{a_0} or e^{a_0}, depending on whether decimal or natural logarithms are used. The other coefficients have a direct correspondence. When the error in equation (1) is given by the sum, the MLR cannot be used to calculate the fit parameters and, therefore, numerical optimization is employed.

Correction for Bias to Fit MLR

Since the early 1970s, methods began to be developed to use an MLR equation to correct the results from fitting equation (1), since fitting the least-squares residuals minimizes the residuals in the logarithmic domain, employing the logarithms of the predictive variables (X_i) and the dependent variables (Q_{Tr}), as established in equation (2). The above implies that the determination coefficient (R^2) found is evaluated in the logarithmic domain and, therefore, is referred to as log R^2.

McCuen et al. (1990) present and apply three procedures to correct the b_0 coefficient, also called the ordinate due to the similarity between equation (3) and the straight line formula. The first method corrects most of the bias and consists of calculating the unbiased coefficient b_0 by making the residuals (e_i) equal to zero in the real domain, that is:

$$\sum_{i=1}^{n} e_i = 0 = \sum_{i=1}^{n} (\hat{y}_i - y_i) = \sum_{i=1}^{n} \hat{y}_i - \sum_{i=1}^{n} y_i$$

$$= f_0 \cdot \sum_{i=1}^{n} \left(x_1^{b_1} \cdot x_2^{b_2} \cdots x_m^{b_m} \right)_i = \sum_{i=1}^{n} y_i \qquad (4)$$

The calculation sought is:

$$f_0 = \frac{\sum_{i=1}^{n} y_i}{\sum_{i=1}^{n} \left(x_1^{b_1} \cdot x_2^{b_2} \cdots x_m^{b_m} \right)_i} \qquad (5)$$

To obtain f_0 it is accepted to correct the bias only by fitting b_0, but that does not result in unbiased b_i population coefficients; actually, only b_0 is unbiased for the sample used. This

procedure to correct for bias does not alter the value of the determination coefficient. The other procedures to fit b_0 presented by McCuen *et al.* (1990) are based on logarithmic residuals.

Empirical Equations to be Tested

The potential regressions that have been tested and provided satisfactory results to estimate design floods (Q_{Tr}) have used the watershed area (A) as a key physiographic variable, which is related to size and all hydrological variables. In addition to the size of the watershed, the length of the main channel (Lmc) has also been used to determine size, where an inverse relationship exists between its length and amount of flooding (McCuen *et al.*, 1990; Tasker *et al.*, 1996; GREHYS, 1996b; Pandey and Nguyen, 1999). The use of both variables creates a multicollinearity problem, since a correlation between them is common (Montgomery *et al.*, 2002).

With respect to climatic and meteorological variables, maximum annual daily rainfall (MDR_{Tr}) predictions have generally been included because of the large coverage of rain gauge stations and the ease in obtaining these data compared to, for example, rain gauge records. Based on the above, the four equations proposed for the purpose of investigation are:

$$Q_{Tr} = b_0 \cdot A^{b_1} \tag{6}$$

$$Q_{Tr} = b_0 \cdot A^{b_1} \cdot Lcp^{b_2} \tag{7}$$

$$Q_{Tr} = b_0 \cdot A^{b_1} \cdot MDR_{Tr}^{b_3} \tag{8}$$

$$Q_{Tr} = b_0 \cdot A^{b_1} \cdot Lcp^{b_2} \cdot MDR_{Tr}^{b_3} \tag{9}$$

The first two equations are compared to determine whether there is a statistical improvement when using two predictive variables, whereas the second two equations are compared to define the most useful result associated with the third predictive variable.

Performance Indices for Empirical Equations

When there are several MLR equations, the most useful one can be chosen based on several indicators pertaining to the residuals (Montgomery *et al.*, 2002); that is, differences between the observed (y) and estimated variables ($\hat{y}$) with the MLR equation to which it is compared. When working with the logarithms of the variables, indicators such as the determination coefficient (R^2) or the Mallows statistic (C_p) are not reliable since the residuals are evaluated in the logarithmic domain, as previously indicated.

Therefore, all the potential empirical equations obtained with the MLR are evaluated using the following three indices of average performance, calculated in the real domain (Pandey and Nguyen, 1999):

1. MAD is the *mean absolute deviation* in m^3/s:

$$MAD = \frac{1}{n - nfp} \sum_{i=1}^{n} \left| \hat{Q}_{Tr}^i - Q_{Tr}^i \right| \tag{10}$$

where Q_{Tr}^i and $\hat{Q}_{Tr}^i$ are the observed and estimated flow predictions, calculated using the potential empirical equation; n is the number of data used for each variable in this study (23) (see Table 1) and nfp is the number of fit parameters, which vary from 2 to 4..

2. *MSE is the mean standard error* in m^3/s:

$$MSE = \left[\frac{1}{n - nfp} \sum_{i=1}^{n} \left(\hat{Q}_{Tr}^i - Q_{Tr}^i \right)^2 \right]^{1/2} \tag{11}$$

3. *RMSE is the relative mean standard error* (without units):

$$RMSE = \left[\frac{1}{n - nfp} \sum_{i=1}^{n} \frac{\left(\hat{Q}_{Tr}^i - Q_{Tr}^i \right)^2}{\left(Q_{Tr}^i \right)^2} \right]^{1/2} \tag{12}$$

Three specific performance indices will also be evaluated, which are the maximum

relative error (*RE*max), minimum relative error (*RE*min) and median relative error (*RE*med). The relative error equation is:

$$RE_i = \frac{\left(\hat{Q}_{Tr}^i - Q_{Tr}^i\right)}{Q_{Tr}^i} \qquad (13)$$

When *RE* is negative, this indicates that ($\hat{Q}_{Tr}^i$) is less than the observed prediction or calculated design flood (Q_{Tr}^i, Table 2). Logically, when *RE* is positive the opposite occurs.

Processed Hydrometric Information

Table 1 presents the general characteristics of the 22 hydrometric stations processed, whose maximum annual flow data were obtained with the BANDAS system (IMTA, 2002). The stations are presented in order of decreasing watershed size. The data related to the San Francisco stations is from Boletín Hidrológico No. 36 (SRH, 1970, 1975). The annual data from these stations range from 19 to 56 years, with a mean of 36 years. The physiographic properties of the watershed area (*A*) and the length of the main channel (LMC) presented in Table 1 are taken from Appendix A in Escalante-Sandoval and Reyes-Chávez (2002). The last part of Table 1 shows another 5 hydrometric stations which are used for comparisons. Their records are not reliable and were integrated with the *BANDAS* system with values presented by Escalante-Sandoval and Reyes-Chávez (2002). Figure 1 shows the watersheds containing the 28 hydrometric stations in Hydrological Region No. 10 (Sinaloa) that were studied.

Annual Maximum Flow Predictions (Q_{Tr})

The six return periods for the design floods to be calculated using the empirical equations to be developed are 5, 10, 25, 50, 100 and 500 years. These recurrence intervals cover most of those that are used for the hydrological sizing and evaluations of the different hydraulic works.

In order to obtain reliable predictions, the statistical quality of the 23 records processed was tested by verifying that they had no deterministic components. Table 2 presents the maximum annual flow predictions (Q_{Tr}) obtained based on the fit of the Generalized Extreme Value (GEV) distribution, using the following four methods (Campos-Aranda, 2001): moments, sextiles, maximum likelihood and *L* moments. The results with the smallest standard fit error were adopted (Kite, 1977).

Maximum Daily Rainfall Predictions (MDR_{Tr})

Campos-Aranda (2008a) processed the maximum annual daily rainfall records for 67 rain gauge stations in Hydrological Region No. 10 (Sinaloa) and presented predictions for return periods of 2, 5, 10 and 100 years. Since there is no correspondence between these return periods and those selected for the maximum annual flow predictions, the 100-year maximum rainfall was used for the first flow recurrence intervals and the 100-year rainfall frequency for the following three (equations (8) and (9)). The processed rain gauge stations were located in each of the 29 watersheds containing the hydrometric stations used, and their average prediction was obtained. Logically, the small watersheds have only one rain gauge station which is located at the hydrometric stations, that is, at the outlet of the watershed, as in the case of Bamícori, La Tina, Pericos and Choix. In other cases, such as Badiraguato, Naranjo and Guamúchil, two rain gauge stations were located within the watershed. Lastly, three or more rain gauge stations were located in the medium and large watersheds. The values calculated for each watershed are shown in the last two columns of Table 2.

Empirical Equations Obtained using LSR

Tables 3 and 4 present the fit parameters obtained in the logarithmic domain using LSR

Table 1. Overall Characteristics of the 29 Hydrometric Stations Processed in Hydrological Region No. 10 (Sinaloa).

No.	Name	River or Stream	*BANDAS* Code	Length WG	Latitude N	*A** (km²)	*Lmc*** (km)	Years of Records*** (available)
1	Huites	R. Fuerte	10037	108° 22′	26° 54′	26 057	267	1942-1992 (51)
2	San Francisco	R. Fuerte	–	108° 07′	26° 54′	17 531	246	1941-1973 (33)
3	San Ignacio	R. San Miguel	10094	107° 51′	26° 53′	10 920	209	1967-1985 (19)
4	Santa Cruz	R. San Lorenzo	10040	106° 57′	24° 28′	8 919	180	1944-2002 (52)
5	Guatenipa II	R. Humaya	10112	107° 13′	25° 21′	8 252	178	1969-2001 (32)
6	Jaina	R. Sinaloa	10036	108° 01′	25° 54′	8 179	177	1942-1998 (56)
7	Palo Dulce	R. Chinipas	10077	108° 26′	27° 02′	6 439	184	1958-1986 (21)
8	Ixpalino	R. Piaxtla	10065	106° 36′	23° 57′	6 166	174	1953-1999 (45)
9	La Huerta	R. Humaya	10113	106° 42′	25° 22′	6 149	117	1970-1999 (28)
10	Toahayana	R. Petatlán	10110	107° 42′	26° 10′	5 281	131	1958-1987 (27)
11	Chinipas	R. Oteros	10064	108° 32′	27° 25′	5 098	131	1965-2002 (24)
12	Tamazula	R. Tamzula	10087	106° 58′	24° 56′	2 241	58	1963-1999 (32)
13	Naranjo	A. Ocoroni	10029	108° 28′	25° 48′	2 064	107	1939-1984 (45)
14	Acatitán	R. Elota	10070	106° 39′	24° 02′	1 884	115	1955-2002 (43)
15	Guamúchil	R. Mocorito	10031	108° 05′	25° 28′	1 645	65	1940-1971 (32)
16	Choix	R. Choix	10066	108° 19′	26° 44′	1 403	82	1956-2002 (38)
17	Badiraguato	R. Badiraguato	10079	107° 32′	25° 20′	1 018	59	1974-1999 (26)
18	El Quelite	R. Quelite	10083	106° 30′	23° 30′	835	42	1961-2001 (33)
19	Zopilote	A. Cabrera	10034	108° 21′	25° 44′	666	68	1939-2001 (56)
20	El Bledal	A. El Bledal	10027	107° 08′	24° 48′	371	31	1938-1994 (56)
21	Pericos	A. Pericos	10086	107° 41′	25° 07′	270	31	1961-1992 (30)
22	La Tina	A. Sibajahui	10078	108° 37′	26° 13′	254	30	1960-1983 (24)
23	Bamícori	A. Barotén	10057	108° 29′	26° 22′	223	20	1951-1983 (33)
I	Piaxtla	R. Piaxtla	–	106° 25′	23° 56′	5 307	142	1958-1973 (16)
II	Urique II	R. Urique	10100	107° 50′	27° 20′	4 000	127	1968-2002 (29)
III	Tecusiapa	R. Petatlán	10137	107° 22′	25° 51′	3 773	90	1959-1981 (23)
IV	Cazanate	A. Álamos	10098	108° 46′	26° 36′	1 813	93	1968-1985 (19)
V	Los Molinos	A. Los Molinos	–	107° 21′	25° 42′	501	35	1958-1970 (13)
VI	Chico Ruiz	A. Mezcales	10090	107° 45′	25° 09′	391	25	1977-2002 (19)

* Watershed Area.
** Length of main channel.
*** Annual Maximum Flow.

with equations (6) to (9) and each one of the six return periods analyzed. Therefore, the first performance indicator is the determination coefficient, indicated by log R^2. These tables also present other indices for average and specific performance (equations (10) to (13)). The observed and calculated predictions, as well as the relative errors obtained from each of the 23 hydrometric stations processed during the minimum and maximum return periods analyzed (5 and 500 years) are shown in Tables 5 and 6.

Empirical Equations Obtained using LSR with Correction for Bias

Tables 7 and 8 show the results from the application of equation (5) to calculate the corrected b_0 coefficient, that is f_0 from the four empirical equations proposed for the six return periods analyzed. The log R^2 is not shown since it is equal to that indicated in Tables 3 and 4. Tables 7 and 8 also present the performance indicators defined in equations (10) to (13). The observed and estimated prediction as

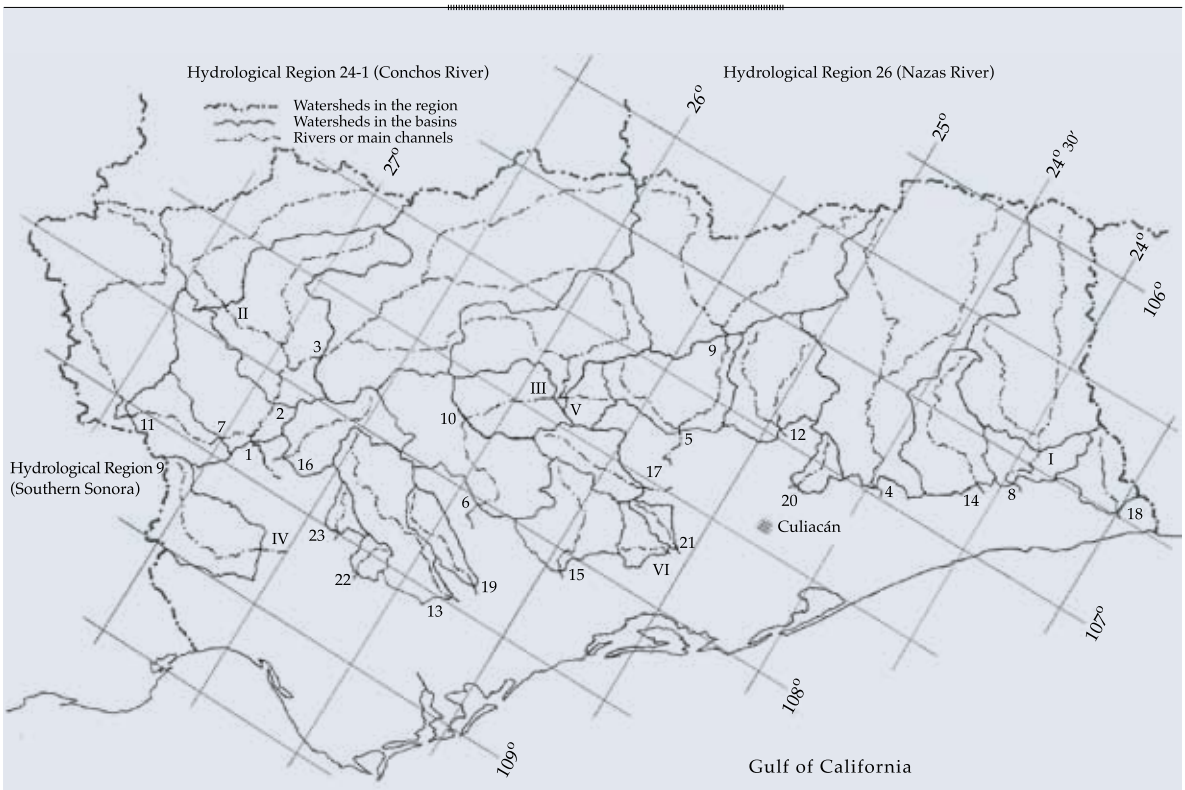

Figure 1. Location of the 29 hydrometric stations processed in the basins in Mexico Hydrological Region No. 10.

well as the relative errors obtained for each of the 23 hydrometric stations processed during the minimum and maximum return periods analyzed are shown in Tables 9 and 10.

Empirical Equations Obtained with Numerical Optimization

Since the early 1990s (McCuen *et al.*, 1990; GREHYS, 1996a), the use of numerical optimization has been suggested to fit potential regression models (equation (1)) in the real domain and thereby avoid the inconvenience of logarithmic transformation. Also since then, its use has been suggested to minimize the sum of squared errors using the algorithm for multiple unrestricted variables (Rosenbrock, 1960; Kuester and Mize, 1973; Campos-Aranda, 2003).

In order to address the number of fit parameters (*nfp*), which changes from two to four in equations (6) to (9), the use of the relative mean standard error (*RMSE*) as the objective function (OF) was considered to be appropriate, whose expression is:

$$ERCM = \frac{\sum_{i=1}^{n}\left[\frac{\left(\hat{Q}_{Tr}^{i} - Q_{Tr}^{i}\right)}{Q_{Tr}^{i}}\right]^{2}}{\left(n - npa\right)} \qquad (14)$$

For the Rosenbrock algorithm, the two following initial conditions were used according to each of the equations (6) to (9), minimizing the objective function (OF): (1) b_0 and the respective b_i and (2) changing only b_0 to f_0. Tables 11 and 12 present the new values of the fit coefficients, as well as other factors associated with the Rosenbrock algorithm, such as the initial and final objective function,

Table 2. Annual Flow Predictions (Q_{Tr}) in m^3/s for the 29 Hydrometric Stations Indicated in Hydrological Region No. 10 and Maximum Daily Rainfall (*MDR*) Predictions in Millimeters in their Respective Watersheds.

No.	Name	ASE* (m^3/s)	Return Periods (*Tr*) in years of Q_{Tr}						*Tr* of the *MDR*	
			5	10	25	50	100	500	10	100
1	Huites	1 021.6	4 134	6 166	10 030	14 266	20 144	44 215	95	140
2	San Francisco	376.6	2 292	3 258	4 925	6 593	8 732	16 355	80	125
3	San Ignacio	256.4	2 065	2 607	3 435	4 173	5 030	7 605	102	150
4	Santa Cruz	406.0	1 434	2 104	3 258	4 410	5 883	11 118	133	213
5	Guatenipa II	246.9	2 466	3 247	4 285	5 093	5 930	8 001	121	179
6	Jaina	311.1	1 347	2 029	3 309	4 692	6 589	14 199	117	183
7	Palo Dulce	895.5	1 274	1 913	3 252	4 858	7 267	18 597	110	157
8	Ixpalino	346.4	1 557	2 201	3 333	4 485	5 982	11 455	143	298
9	La Huerta	96.3	1 431	1 718	2 027	2 223	2 393	2 709	110	186
10	Toahayana	158.1	1 557	2 019	2 653	3 164	3 709	5 123	98	148
11	Chinipas	139.0	1 231	1 626	2 209	2 714	3 283	4 919	110	157
12	Tamazula	145.0	770	1 009	1 390	1 745	2 173	3 543	145	235
13	Naranjo	156.3	909	1 353	2 105	2 842	3 775	7 009	107	126
14	Acatitán	226.9	1 227	1 779	2 654	3 459	4 422	7 458	150	309
15	Guamúchil	234.9	948	1 351	2 038	2 717	3 579	6 599	108	149
16	Choix	99.9	461	650	979	1 312	1 741	3 294	98	150
17	Badiraguato	1 077.2	1 374	2 283	4 244	6 664	10 381	28 652	177	371
18	El Quelite	86.7	707	987	1 414	1 795	2 238	3 568	150	270
19	Zopilote	48.5	558	738	977	1 161	1 351	1 817	121	168
20	El Bledal	64.0	401	565	834	1 090	1 404	2 446	138	247
21	Pericos	28.5	354	457	601	719	846	1 184	136	271
22	La Tina	86.2	144	229	393	573	824	1 860	128	231
23	Bamícori	52.3	270	391	591	782	1 020	1 815	110	202
I	Piaxtla	909.8	1 672	2 585	4 442	6 613	9 796	24 180	143	298
II	Urique II	35.2	456	549	660	740	817	983	75	121
III	Tecusiapa	173.6	1 542	2 083	2 861	3 516	4 240	6 241	97	139
IV	Cazanate	419.6	722	1 123	1 907	2 792	4 049	9 427	105	125
V	Los Molinos	12.6	226	260	293	312	328	355	105	156
VI	Chico Ruiz	27.7	329	413	510	576	637	761	136	271

* Adjusted Standard Error.

number of stages and evaluations of the objective function. When working with equations (6) and (7), most of the time the fit coefficients from the MLS resulted in the lowest objective function (Table 11). Whereas when processing equations (8) and (9), the second initial conditions led to a better objective function in half of the cases (Table 12).

Analysis and Selection of Empirical Equations

Table 3 compares the performance of equations (6) and (7), showing that in the logarithmic domain, the determination coefficient (R^2) is slightly higher in equation (7). The performance indices for MAD and MSE are also slightly higher in equation (7), perhaps because of the larger number of fit parameters. The dimensionless RMSE index (equation (12)) indicates better performance with equation (6) for the first three return periods, and for equation (7) the performance was better for the second three return periods. The same can be said for the comparison of equations (8) and (9) shown in Table 4, while equation (8) is only recommended for the first two return periods, that is, for 5 and 10 years. The fit coefficients for the selected empirical equations are shown in Tables 3, 4, 7, 8, 11 and 12.

Table 3. Fit Coefficients and Performance Indices for the Indicated Empirical Equations adjusted by LSR (logarithmic domain) for Flood Designs (Q_{Tr}) in Hydrological Region No. 10.

Fit Coefficients and Performance Indices	Return Periods (*Tr*) in Years of Flow (Q_{Tr})					
	5	10	25	50	100	500
$Q_{Tr} = b_0 \cdot A^{b1}$						
b_0	17.8007	26.7186	41.1347	54.4500	70.4608	122.2585
b_1	0.5121	0.5036	0.4981	0.4965	0.4962	0.4973
log R^2	0.8437	0.8300	0.7927	0.7487	0.6936	0.5460
MAD	273.8	415.8	704.5	1 076.5	1 681.4	4 674.3
MSE	365.2	587.2	1 118.8	1 817.2	2 915.7	8 346.5
RMS	0.3485	0.3237	0.3270	0.3644	0.4339	0.7150
*RE*max	1.1066	0.8969	0.6507	0.8629	1.2336	2.4565
*RE*min	–0.5505	–0.6172	–0.6948	–0.7455	–0.7891	–0.8664
*RE*med	–0.0023	–0.0082	0.0732	0.0203	0.0295	–0.0087
$Q_{Tr} = b_0 \cdot A^{b1} \cdot Lmc^{b2}$						
b_0	17.5616	25.3697	37.3631	47.9470	60.2210	97.7937
b_1	0.4974	0.4474	0.3938	0.3586	0.3259	0.2552
b_2	0.0283	0.1084	0.2012	0.2660	0.3285	0.4670
log R^2	0.8438	0.8308	0.7952	0.7528	0.6995	0.5554
DAM	287.0	432.5	735.3	1 103.1	1 723.6	4 833.8
EEM	375.6	609.1	1 166.0	1 894.8	3 037.6	8 664.5
EREM	0.3578	0.3327	0.3318	0.3637	0.4266	0.6877
*ER*máx	1.1094	0.9078	0.6683	0.7483	1.0653	2.0921
*ER*mín	–0.5505	–0.6168	–0.6942	–0.7449	–0.7884	–0.8658
*ER*med	0.0019	0.0005	0.0772	0.0244	0.0165	–0.0532

With respect to the comparison shown in Table 7, and according to the *RMSE* performance index, it is concluded that equation (6) with f_0 is better for the first four return periods and equation (7) for the last two return periods, that is, in 100 and 500 years. For the comparison in Table 8 with respect to the RMSE index, equation (8) with f_0 is recommended only for the two first return periods and equation (9) for the remaining ones.

he Rosenbrock algorithm functioned in all cases and minimized the initial objective function (equation (14)), defined based on the results from the LSR or the bias-corrected LSR (Tables 11 and 12). The results— that is, equations (6) to (9) fitted to each one of the six return periods— are submitted to a selection process and, in this case, the one providing a better RSME or lower objective function was adopted. In Table 11, equation (6) is best for the three first return periods and equation (7) for the following three. With respect to Table 12, equation (8) is best for the first two return periods and equation (9) for the following four, that is, for recurrence intervals of 25, 50, 100 and 500 years.

Table 13 presents 36 empirical equations obtained with the three following methods: (1) least-squares residuals (LSR) in the logarithmic domain, (2) bias-corrected LSR and (3) numerical optimization of an objective function (*OF* = *RMSE*).

Numerical Comparisons of the 36 Empirical Equations Selected

Two numerical comparisons are performed. The first among the six hydrometric stations

Table 4. Fit Coefficients and Performance Indices for the Indicated Empirical Equations adjusted by LSR (logarithmic domain) for Flood Designs (Q_{Tr}) in Hydrological Region No. 10.

Fit Coefficients and Performance Indices	Return Periods (*Tr*) in Years of Flow (Q_{Tr})					
	5	**10**	**25**	**50**	**100**	**500**
$Q_{Tr} = b_0 \cdot A^{b1} \cdot MDR_{Tr}^{b3}$	MDR_{10}			MDR_{100}		
b_0	0.2490	0.2335	0.1966	1.2051	1.1086	0.8310
b_1	0.5618	0.5588	0.5604	0.5616	0.5671	0.5825
b_3	0.8116	0.9011	1.0158	0.6271	0.6832	0.8213
log R^2	0.8722	0.8657	0.8370	0.7923	0.7417	0.6004
MAD	313.6	474.1	787.5	1 173.0	1 834.4	5 082.7
MSE	402.8	644.4	1 209.5	1 878.5	2 999.2	8 517.4
RMS	0.3372	0.3161	0.3279	0.3749	0.4517	0.7505
*RE*max	0.9911	0.7827	0.6737	0.9279	1.3174	2.6118
*RE*min	–0.4079	–0.4798	–0.5686	–0.6388	–0.6912	–0.7888
*RE*med	–0.0781	–0.0445	–0.0207	–0.0061	0.0763	0.0526
$Q_{Tr} = b_0 \cdot A^{b1} \cdot Lmc^{b2} \cdot MDR_{Tr}^{b3}$	MDR_{10}			MDR_{100}		
b_0	0.2482	0.2271	0.1859	0.9893	0.8717	0.5936
b_1	0.5563	0.5126	0.4671	0.4065	0.3781	0.3181
b_2	0.0107	0.0889	0.1793	0.3010	0.3666	0.5130
b_3	0.8113	0.8983	1.0102	0.6359	0.6940	0.8364
log R^2	0.8722	0.8662	0.8390	0.7977	0.7491	0.6117
MAD	329.9	499.8	830.5	1 230.9	1 936.5	5 447.8
MSE	413.7	668.4	1 261.3	1 976.6	3 151.2	8 895.2
RMS	0.3464	0.3224	0.3257	0.3647	0.4313	0.6999
*RE*max	0.9936	0.7919	0.5550	0.7957	1.1243	2.1997
*RE*min	–0.4074	–0.4797	–0.5686	–0.6360	–0.6883	–0.7859
*RE*med	–0.0775	–0.0536	0.0105	0.0611	0.0880	0.1448

indicated at the end of Tables 1 and 2 were not used to obtain the empirical equations because their records were not reliable. For the second comparison, the hydrometric stations with the largest number of maximum annual flow records were used, which ranged from 45 to 56. The Huites station was eliminated because part of its watershed area was outside the expectations of the application of the empirical equations in Hydrological Region No. 10. Since six empirical equations were selected for each of the six return periods processed, the median value was obtained to define the estimated prediction and compare it to the observed.

Table 14 presents the results from the first comparison. The observed predictions from the Piaxtla station are considered to be extremely high— higher than those observed at the Ixpalino station, which has a 16% larger watershed area. Therefore, the predictions from the empirical equations are more consistent with the likely values. The opposite occurred in the Urique II station, whose observed predictions are extremely low, as can be seen when comparing them with those from Chinipas, an adjacent watershed with 27% more area. Again, the predictions obtained with the empirical equations are considered more consistent with the likely floods.

All of the predictions obtained based on the empirical equations from the Tecusiapa and Cazanate stations are below those observed but within the order of magnitude. The opposite, and much more noticeable occurred in the last

Table 5. Relative Errors for Return Periods of 5 Years calculated for the 23 Hydrometric Stations in Hydrological Region No. 10. The Indicated Empirical Equation was adjusted by LSR (logarithmic domain).

No.	Name	Observed Predictions	$Q_5 = 17.8007 \cdot A^{0.5121}$	Relative Error (*RE*)	*RE* ordinate
1	Huites	4 134	3 249.613	–0.2139	–0.5505
2	San Francisco	2 292	2 653.714	0.1574	–0.3101
3	San Ignacio	2 065	2 081.665	0.0081	–0.2687
4	Santa Cruz	1 434	1 876.696	0.3087	–0.2139
5	Guatenipa II	2 466	1 803.461	–0.2687	–0.2108
6	Jaina	1 347	1 795.274	0.3328	–0.1670
7	Palo Dulce	1 274	1 588.301	0.2467	–0.1158
8	Ixpalino	1 557	1 553.452	–0.0023	–0.1094
9	La Huerta	1 431	1 551.257	0.0840	–0.0815
10	Toahayana	1 557	1 434.961	–0.0784	–0.0784
11	Chinipas	1 231	1 409.277	0.1448	–0.0243
12	Tamazula	770	925.120	0.2015	–0.0023
13	Naranjo	909	886.951	–0.0243	0.0081
14	Acatitán	1 227	846.459	–0.3101	0.0511
15	Guamúchil	948	789.652	–0.1670	0.0840
16	Choix	461	727.856	0.5789	0.1448
17	Badiraguato	1 374	617.596	–0.5505	0.1574
18	El Quelite	707	557.998	–0.2108	0.2015
19	Zopilote	558	496.979	–0.1094	0.2467
20	El Bledal	401	368.310	–0.0815	0.3087
21	Pericos	354	312.996	–0.1158	0.3328
22	La Tina	144	303.356	1.1066	0.5789
23	Bamícori	270	283.794	0.0511	1.1066

two stations— Los Molinos and Chico Ruiz. For the former, its maximum annual flow records have already been demonstrated to have values that are not consistent with the size of the watershed (Campos-Aranda, 2008b). Predictions are larger for the Chico Ruiz, the watershed adjacent to Pericos, which is 31% smaller, implying that the highest values may not yet have been reported by the short-term records from Chico Ruiz, while the lowest values may have been reported (1991 with 10 m^3/s and 1999 with 17 m^3/s). With respect to Table 14, the predictions obtained from the empirical equations are considerably more consistent with reality than those derived from the records, which are not reliable. The numerical applications shown in Table 14 illustrate the benefits of the regional methodology that was developed.

With respect to the results in Table 15, overall, it is concluded that there is an excellent approximation between the observed and estimated predictions for return periods of less than 100 years. Relative errors over 20% due to defect for return periods of more than 50 years were found only in the Narajanjo station. In the rest of the hydrometric stations studied, the relative errors due to excess are not significant since the maximum is 38%, which was obtained in Santa Cruz with the

Table 6. Relative Errors for Return Periods of 5 Years calculated for the 23 Hydrometric Stations in Hydrological Region No. 10. The Indicated Empirical Equation was adjusted by LSR (logarithmic domain).

No.	Name	Observed Predictions	$Q_{500} = 0.5936A^{0.3181}\,Lmc^{0.5130}\,MDR_{100}^{0.8364}$	Relative Error (*RE*)	*RE* ordinate
1	Huites	44 215	16 520.40	–0.6264	–0.7859
2	San Francisco	16 355	12 701.47	–0.2234	–0.6264
3	San Ignacio	7 305	11 704.96	0.6023	–0.4822
4	Santa Cruz	11 118	13 630.15	0.2260	–0.4694
5	Guatenipa II	8 001	11 431.49	0.4288	–0.3973
6	Jaina	14 199	11 578.39	–0.1846	–0.2802
7	Palo Dulce	18 597	9 628.99	–0.4822	–0.2234
8	Ixpalino	11 455	15 773.59	0.3770	–0.1846
9	La Huerta	2 709	8 667.87	2.1997	–0.0696
10	Toahayana	5 123	7 228.64	0.4110	0.0084
11	Chinipas	4 919	7 509.80	0.5267	0.0394
12	Tamazula	3 543	5 334.19	0.5056	0.1448
13	Naranjo	7 009	4 224.03	–0.3973	0.2090
14	Acatitán	7 458	9 016.47	0.2090	0.2260
15	Guamúchil	6 599	3 501.33	–0.4694	0.3770
16	Choix	3 294	3 770.87	0.1448	0.4110
17	Badiraguato	28 652	6 133.80	–0.7859	0.4288
18	El Quelite	3 568	3 708.53	0.0394	0.5056
19	Zopilote	1817	2 971.44	0.6354	0.5267
20	El Bledal	2 446	2 275.79	–0.0696	0.6023
21	Pericos	1 184	2 222.87	0.8774	0.6354
22	La Tina	1 860	1 875.68	0.0084	0.8774
23	Bamícori	1 815	1 306.51	–0.2802	2.1997

return period of five years. The Ixpalino and El Beldal stations had the lowest errors in all predictions; the error due to excess was lowest in the former and due to defect in the latter, both under 8.5%.

Conclusions

Only four types of potential equations were sought for design floods with return periods of 5, 10, 25, 50, 100 and 500 years using as predictive variables two physiographic properties (the watershed area and the length of the main channel) and a climatic characteristic (the maximum daily precipitation for return periods of 10 and 100 years). Nevertheless, only two equations were selected for each recurrence interval— those with the best statistical performance. By using three procedures to obtain the fit parameters, a total of 36 empirical equations were obtained, as shown in Table 13.

The first two fit methods (least-squares residuals in the logarithmic domain and its corrected version in the real domain) result in four empirical equations for each return period, which are unique. With the third fit procedure, based on numerical optimization (Rosenbrock algorithm), many empirical equations can be obtained by changing only the objective function (OF) to be minimized. In the present work, only the relative mean standard error was applied as an OF.

The two comparisons that were performed– the first with six hydrometric stations not used to obtain the empirical equations and the second with the six gauged stations containing the most records— demonstrate the consistency of the estimated predictions, whose median value is considered an acceptable approximation of the likely values of the design floods for any

Table 7. Fit Coefficients and Performance Indices for the Indicated Empirical Equations adjusted by bias-corrected LSR (logarithmic domain) for Flood Designs (Q_{Tr}) in Hydrological Region No. 10.

Fit Coefficients and Performance Indices	Return Periods (*Tr*) in Years of Flow (Q_{Tr})					
	5	**10**	**25**	**50**	**100**	**500**
$Q_{Tr} = f_0 \cdot A^{b1}$						
f_0	18.3055	27.7196	43.5402	59.0646	78.9490	153.4207
b_1	0.5121	0.5036	0.4981	0.4965	0.4962	0.4973
MAD	281.0	432.0	745.3	1 128.9	1 791.7	5 029.8
MSE	362.6	579.8	1095.9	1 766.9	2 813.8	7 910.6
RMS	0.3638	0.3439	0.3619	0.4215	0.5277	1.0002
*RE*max	1.1664	0.9680	0.7472	1.0208	1.5027	3.3376
*RE*min	–0.5378	–0.6028	–0.6769	–0.7240	–0.7637	–0.8323
*ER*med	0.0260	0.0290	0.1360	0.1068	0.1535	0.2440
$Q_{Tr} = f_0 \cdot A^{b1} \cdot Lmc^{b2}$						
f_0	18.0685	26.3414	39.5923	52.0804	67.5652	122.8478
b_1	0.4974	0.4474	0.3938	0.3586	0.3259	0.2552
b_2	0.0283	0.1084	0.2012	0.2660	0.3285	0.4670
MAD	295.7	472.3	788.8	1 173.8	1 860.7	5 247.5
MSE	372.8	601.7	1 141.4	1 841.7	2 931.8	8 224.2
RMS	0.3737	0.3692	0.3682	0.4227	0.5226	0.9733
*RE*max	1.1703	1.0259	0.7678	0.8991	1.3171	2.8842
*RE*min	–0.5375	–0.5931	–0.6760	–0.7229	–0.7626	–0.8314
*RE*med	0.0308	0.0625	0.1415	0.1127	0.1405	0.1893

site and any watershed in Hydrological Region No. 10 (Sinaloa), Mexico. Therefore, it is recommended to apply and develop the procedures followed to obtain potential equations to calculate maximum annual flow predictions or design floods in other regions or geographic areas to obtain these hydrological calculation tools (empirical equations), which are very simply to apply.

Received: 19/07/12
Accepted: 23/05/13

References

CAMPOS-ARANDA, D.F. *Introducción a los métodos numéricos: software en Basic y aplicaciones en hidrología superficial*. Capítulo 5, Ajuste de curvas, y capítulo 9: Optimización numérica. San Luis Potosí, México: Librería Universitaria Potosina, 2003, pp. 93-127 y 172-211.

CAMPOS-ARANDA, D.F. Contraste de cinco métodos de ajuste de la distribución GVE en 31 registros históricos de eventos máximos anuales. *Ingeniería Hidráulica en México*. Vol. XVI, núm. 2, abril-junio de 2001, pp. 77-92.

CAMPOS-ARANDA, D.F. Estudio de la precipitación máxima diaria anual en la Región Hidrológica No. 10 (Sinaloa), con base en Distancias Euclidianas. *Investigaciones Geográficas*. Núm. 65, abril-junio, 2008a, pp. 56-67.

CAMPOS-ARANDA, D.F. Calibración del método Racional en ocho cuencas rurales menores de 1,650 km² de la Región Hidrológica No. 10 (Sinaloa), México. *Agrociencia*. Vol. 42, núm. 6, 2008b, pp. 615-627.

CUNNANE, C. Methods and merits of regional flood frequency analysis. *Journal of Hydrology*. Vol. 100, 1988, pp. 269-290.

ESCALANTE–SANDOVAL, C. Multivariate extreme value distributions with mixed Gumbel marginals. *Journal of the American Water Resources Association*, Vol. 34, No. 2, 1998, pp. 321-333.

ESCALANTE-SANDOVAL, C. y REYES–CHÁVEZ, L. *Técnicas Estadísticas en Hidrología.* Capítulo 8: Análisis

Table 8. Fit Coefficients and Performance Indices for the Indicated Empirical Equations adjusted by bias-corrected LSR (logarithmic domain) for Flood Designs (Q_{Tr}) in Hydrological Region No. 10.

Fit Coefficients and Performance Indices	Return Periods (*Tr*) in Years of Flow (Q_{Tr})					
	5	10	25	50	100	500
$Q_{Tr} = f_0 \cdot A^{b1} \cdot MDR_{Tr}^{b3}$	MDR_{10}			MDR_{100}		
f_0	0.2567	0.2424	0.2078	1.2975	1.2312	1.0285
b_1	0.5618	0.5588	0.5604	0.5616	0.5671	0.5825
b_3	0.8116	0.9011	1.0158	0.6271	0.6832	0.8213
MAD	308.4	476.6	802.6	1 227.6	1 966.0	5 554.8
MSE	398.4	635.1	1 185.2	1 833.0	2 905.4	8 105.0
RMS	0.3534	0.3360	0.3611	0.4257	0.5375	1.0213
*RE*max	1.0526	0.8507	0.7690	1.0757	1.5736	3.4702
*RE*min	–0.3896	–0.4600	–0.5441	–0.6112	–0.6571	–0.7386
*RE*med	–0.0495	–0.0080	0.0351	0.0701	0.1954	0.3028
$Q_{Tr} = f_0 \cdot A^{b1} \cdot Lmc^{b2} \cdot MDR_{Tr}^{b3}$	MDR_{10}			MDR_{100}		
f_0	0.2556	0.2358	0.1966	1.0651	0.9680	0.7329
b_1	0.5563	0.5126	0.4671	0.4065	0.3781	0.3181
b_2	0.0107	0.0889	0.1793	0.3010	0.3666	0.5130
b_3	0.8113	0.8983	1.0102	0.6359	0.6940	0.8364
MAD	324.6	502.7	846.5	1 299.4	2 112.1	5 953.0
MSE	409.4	658.9	1 236.8	1 932.9	3 062.6	8 522.5
RMS	0.3624	0.3429	0.3598	0.4156	0.5168	0.9620
*RE*max	1.0530	0.8606	0.6445	0.9333	1.3589	2.9205
*RE*min	–0.3897	–0.4598	–0.5438	–0.6081	–0.6539	–0.7357
*RE*med	–0.0500	–0.0174	0.0686	0.1424	0.2082	0.4134

regional hidrológico y Apéndice A. México, D.F.: Facultad de Ingeniería de la UNAM, 2002, pp. 157-202 y 291-298.

GREHYS (GROUPE DE RECHERCHE EN HYDROLOGIE STATISTIQUE). Presentation and review of some methods for regional flood frequency analysis. *Journal of Hydrology*. Vol. 186, 1996a, pp. 63-84.

GREHYS (GROUPE DE RECHERCHE EN HYDROLOGIE STATISTIQUE). Inter-comparison of regional flood frequency procedures for Canadian rivers. *Journal of Hydrology*. Vol. 186, 1996b, pp. 85-103.

GUTIÉRREZ-LÓPEZ, A., LEBEL, T. y DESCROIX, L. Reflexiones sobre el concepto de cuencas hidrológicamente homogéneas. *Memorias del XXI Congreso Latinoamericano de Hidráulica*, Sao Paulo, Brasil, 2004, 10 pp.

IMTA. *Banco Nacional de Datos de Aguas Superficiales (BANDAS)*. Ocho CD. Jiutepec, México: Comisión Nacional del Agua-Secretaría de Medio Ambiente y Recursos Naturales-Instituto Mexicano de Tecnología del Agua, 2002.

KITE, G.W. *Frequency and Risk Analyses in Hydrology*. Chapter 12: Comparison of frequency distributions. Fort Collins, USA: Water Resources Publications, 1977, pp. 156-168.

KUESTER, J.L. and MIZE, J.H. *Optimization Techniques with Fortran*. ROSENB algorithm. New York: McGraw Hill Book Co., 1973, pp. 320-330.

McCUEN, R.H., LEAHY, R.B., and JOHNSON, P.A. Problems with logarithmic transformations in regression. *Journal of Hydraulic Engineering*. Vol. 116, No. 3, 1990, pp. 414-428.

MONTGOMERY, D.C., PECK, E.A., y VINING, G.G. *Introducción al Análisis de Regresión Lineal*. Capítulo 10: Multicolinealidad. México, D.F.: Compañía Editorial Continental, 2002, pp. 291-342.

PANDEY, G.R. and NGUYEN, V.T.V. A comparative study of regression based methods in regional flood frequency analysis. *Journal of Hydrology*. Vol. 225, 1999, pp. 92-101.

ROSENBROCK, H.H. An automatic method of finding the greatest or least value of a function. *Computer Journal*. Vol. 3, 1960, pp. 175-184.

SRH. *Boletín Hidrológico No. 36. Tomos I y VI.* Región Hidrológica No. 10 (Sinaloa). México, D.F.: Secretaría de

Table 9. Relative Errors for Return Periods of 5 Years calculated for the 23 Hydrometric Stations in Hydrological Region No. 10. The Indicated Empirical Equation was adjusted by LSR and corrected for bias (logarithmic domain).

No.	Name	Observed Predictions	$Q_5 = 18.3055 \cdot A^{0.5121}$	Relative Error (*RE*)	*RE* ordinate
1	Huites	4 134	3 341.767	–0.1916	–0.5378
2	San Francisco	2 292	2 727.941	0.1902	–0.2906
3	San Ignacio	2 065	2 140.698	0.0367	–0.2479
4	Santa Cruz	1 434	1 929.917	0.3458	–0.1916
5	Guatenipa II	2 466	1 854.604	–0.2479	–0.1884
6	Jaina	1 347	1 846.185	0.3706	–0.1434
7	Palo Dulce	1 274	1 633.342	0.2821	–0.0908
8	Ixpalino	1 557	1 597.505	0.0260	–0.0841
9	La Huerta	1 431	1 595.249	0.1148	–0.0555
10	Toahayana	1 557	1 475.654	–0.0522	–0.0522
11	Chinipas	1 231	1 449.242	0.1773	0.0034
12	Tamazula	770	951.355	0.2355	0.0260
13	Naranjo	909	912.104	0.0034	0.0367
14	Acatitán	1 227	870.463	–0.2906	0.0809
15	Guamúchil	948	812.045	–0.1434	0.1148
16	Choix	461	748.496	0.6236	0.1773
17	Badiraguato	1 374	635.110	–0.5378	0.1902
18	El Quelite	707	573.822	–0.1884	0.2355
19	Zopilote	558	511.073	–0.0841	0.2821
20	El Bledal	401	378.755	–0.0555	0.3458
21	Pericos	354	321.872	–0.0908	0.3706
22	La Tina	144	311.959	1.1664	0.6236
23	Bamícori	270	291.842	0.0809	1.1664

Recursos Hidráulicos, Dirección de Hidrología, 1970 y 1975.

TASKER, G.D., HODGE, S.A., and BARKS, C.S. Region of influence regression for estimating the 50-year flood at ungaged sites. *Water Resources Bulletin*. Vol. 32, No. 1, 1996, pp. 163-170.

Author's address institutional

Dr. Daniel Francisco Campos-Aranda

Profesor jubilado
Universidad Autónoma de San Luis Potosí
Genaro Codina 240
colonia Jardines del Estadio
78280 San Luis Potosí, San Luis Potosí, México
campos_aranda@hotmail.com

Click here to write the autor

Table 10. Relative errors return period of 500 years estimated at 23 hydrometric stations in the Region Hydrological no. 10. The empirical equation given by MCR adjusted and corrected for bias.

No.	Name	Observed Predictions	$Q_{500} = 0.7329\ A^{0.3181}\ Lmc^{0.5130}\ MDR_{100}^{0.8364}$	Relative Error (*RE*)	*RE* ordinate
1	Huites	44 215	20 397.250	–0.5387	–0.7357
2	San Francisco	16 355	15 682.120	–0.0411	–0.5387
3	San Ignacio	7 305	14 451.770	0.9783	–0.3607
4	Santa Cruz	11 118	16 828.740	0.5136	–0.3449
5	Guatenipa II	8 001	14 114.110	0.7640	–0.2559
6	Jaina	14 199	14 295.490	0.0068	–0.1112
7	Palo Dulce	18 597	11 888.630	–0.3607	–0.0411
8	Ixpalino	11 455	19 475.170	0.7001	0.0068
9	La Huerta	2 709	10 701.950	2.9505	0.1488
10	Toahayana	5 123	8 924.988	0.7421	0.2451
11	Chinipas	4 919	9 272.124	0.8850	0.2833
12	Tamazula	3 543	6 585.969	0.8589	0.4134
13	Naranjo	7 009	5 215.279	–0.2559	0.4927
14	Acatitán	7 458	11 132.360	0.4927	0.5136
15	Guamúchil	6 599	4 322.990	–0.3449	0.7001
16	Choix	3 294	4 655.785	0.4134	0.7421
17	Badiraguato	28 652	7 573.219	–0.7357	0.7640
18	El Quelite	3 568	4 578.810	0.2833	0.8589
19	Zopilote	1 817	3 668.745	1.0191	0.8850
20	El Bledal	2 446	2 809.847	0.1488	0.9783
21	Pericos	1 184	2 744.513	1.3180	1.0191
22	La Tina	1 860	2 315.850	0.2451	1.3180
23	Bamícori	1 815	1 613.112	–0.1112	2.9505

Table 11. adjustment factors and objective functions (FO) of the empirical equations indicated adjusted with optimization numerical (Rosenbrock algorithm) for growing design (QTr) in Hydrological Region No. 10.

Adjustment factors and performance indices	Return periods (*Tr*) in spending years (Q_{Tr})					
	5	10	25	50	100	500
$Q_{Tr} = b_0 \cdot A^{b1}$						
b_0	9.6794	16.6157	31.8794	53.0888	66.9377	110.4147
b_1	0.5712	0.5488	0.5137	0.4779	0.4714	0.4542
FO initial	0.1215	0.1048	0.1070	0.1328	0.1883	0.5112
Number of stages	8	13	7	3	2	4
Assessments FO	48	70	41	22	18	30
FO final	0.0913	0.0818	0.0848	0.1029	0.1327	0.2536
$Q_{Tr} = b_0 \cdot A^{b1} \cdot Lcp^{b2}$						
b_0	15.1401	23.7836	35.4876	34.6689	57.1394	88.0143
b_1	0.7466	0.4465	0.3899	0.2958	0.3091	0.2327
b_2	–0.3970	0.0978	0.1914	0.4117	0.3245	0.4376
FO initial	0.1397	0.1107	0.1101	0.1322	0.1820	0.4730
Number of stages	11	4	3	13	3	3
Assessments FO	96	43	45	117	37	33
FO final	0.0983	0.0924	0.0901	0.1015	0.1310	0.2481

Table 12. adjustment factors and objective functions (FO) of the empirical equations indicated adjusted with optimization numerical (Rosenbrock algorithm) for growing design (QTr) in Hydrological Region No. 10.

Adjustment factors and performance indices	Return periods (*Tr*) in spending years (Q_{Tr})					
	5	10	25	50	100	500
$Q_{Tr} = b_0 \cdot A^{b1} \cdot PMD_{Tr}^{b3}$	PMD_{10}			PMD_{100}		
b_0	0.1821	0.2303	0.1971	1.1448	1.1822	0.9922
b_1	0.6011	0.5728	0.5747	0.5335	0.5436	0.4948
b_3	0.7873	0.8560	0.9641	0.6428	0.6649	0.8342
FO initial	0.1137	0.1129	0.1076	0.1405	0.2889	1.0430
Number of stages	7	2	12	2	4	7
Assessments FO	69	25	118	21	58	73
FO final	0.0914	0.0826	0.0879	0.1101	0.1442	0.2751
$Q_{Tr} = b_0 \cdot A^{b1} \cdot Lcp^{b2} \cdot PMD_{Tr}^{b3}$	PMD_{10}			PMD_{100}		
b_0	0.1953	0.5055	0.1966	0.9856	0.9080	0.4005
b_1	0.5755	0.5367	0.4034	0.3911	0.3636	0.1872
b_2	0.0502	0.0889	0.3017	0.3511	0.3844	0.7050
b_3	0.7667	0.6674	0.9616	0.5876	0.6559	0.8674
FO initial	0.1200	0.1176	0.1294	0.1730	0.2671	0.4899
Number of stages	8	21	10	8	5	16
Assessments FO	118	251	150	97	79	180
FO final	0.0962	0.0841	0.0853	0.1034	0.1350	0.2540

Table 13. 36 empirical equations obtained with the approach indicated for the six return periods indicated.

Adjustment for MCR domain logarithmic	Adjustment for MCR-corrected slantorrección por sesgo	Numerical optimization adjustment one FO
$Q_5 = 17.8007\ A^{0.5121}$	$Q_5 = 18.3055\ A^{0.5121}$	$Q_5 = 9.6794\ A^{0.5712}$
$Q_{10} = 26.7186\ A^{0.5036}$	$Q_{10} = 27.7196\ A^{0.5036}$	$Q_{10} = 16.6157\ A^{0.5488}$
$Q_{25} = 41.1347\ A^{0.4981}$	$Q_{25} = 43.5402\ A^{0.4981}$	$Q_{25} = 31.8794\ A^{0.5137}$
$Q_{50} = 47.9470\ A^{0.3586}\ Lcp^{0.2660}$	$Q_{50} = 59.0646\ A^{0.4965}$	$Q_{50} = 34.6689\ A^{0.2958}\ Lcp^{0.4117}$
$Q_{100} = 60.2210\ A^{0.3259}\ Lcp^{0.3285}$	$Q_{100} = 67.5652\ A^{0.3259}\ Lcp^{0.3285}$	$Q_{100} = 57.1394\ A^{0.3091}\ Lcp^{0.3245}$
$Q_{500} = 97.7937\ A^{0.2552}\ Lcp^{0.4670}$	$Q_{500} = 122.8478\ A^{0.2552}\ Lcp^{0.4670}$	$Q_{500} = 88.0143\ A^{0.2327}\ Lcp^{0.4376}$
$Q_5 = 0.2490\ A^{0.5618}\ PMD_{10}^{0.8116}$	$Q_5 = 0.2567\ A^{0.5618}\ PMD_{10}^{0.8116}$	$Q_5 = 0.1821\ A^{0.6011}\ PMD_{10}^{0.7873}$
$Q_{10} = 0.2335\ A^{0.5588}\ PMD_{10}^{0.9011}$	$Q_{10} = 0.2424\ A^{0.5588}\ PMD_{10}^{0.9011}$	$Q_{10} = 0.2303\ A^{0.5728}\ PMD_{10}^{0.8560}$
$Q_{25} = 0.1859\ A^{0.4671}\ Lcp^{0.1793}\ PMD_{10}^{1.0102}$	$Q_{25} = 0.1966\ A^{0.4671}\ Lcp^{0.1793}\ PMD_{10}^{1.0102}$	$Q_{25} = 0.1966\ A^{0.4034}\ Lcp^{0.3017}\ PMD_{10}^{0.9616}$
$Q_{50} = 0.9893\ A^{0.4065}\ Lcp^{0.3010}\ PMD_{100}^{0.6359}$	$Q_{50} = 1.0651\ A^{0.4065}\ Lcp^{0.3010}\ PMD_{100}^{0.6359}$	$Q_{50} = 0.9856\ A^{0.3911}\ Lcp^{0.3511}\ PMD_{100}^{0.5876}$
$Q_{100} = 0.8717\ A^{0.3781}\ Lcp^{0.3666}\ PMD_{100}^{0.6940}$	$Q_{100} = 0.9680\ A^{0.3781}\ Lcp^{0.3666}\ PMD_{100}^{0.6940}$	$Q_{100} = 0.9080\ A^{0.3636}\ Lcp^{0.3844}\ PMD_{100}^{0.6559}$
$Q_{500} = 0.5936\ A^{0.3181}\ Lcp^{0.5130}\ PMD_{100}^{0.8364}$	$Q_{500} = 0.7329\ A^{0.3181}\ Lcp^{0.5130}\ PMD_{100}^{0.8364}$	$Q_{500} = 0.4005\ A^{0.1872}\ Lcp^{0.7050}\ PMD_{100}^{0.8674}$

Table 14. Estimated Predictions (m^3/s) with empirical equations in six selected gauging stations unreliable registration Hydrological Region No. 10.

Equations the empirical	Piaxtla						Urique II					
	Return periods in years						Return periods in years					
	5	10	25	50	100	500	5	10	25	50	100	500
Table 3	1 439	2 008	2 948	3 882	5 020	8 831	1 245	1 741	2 561	3 405	4 413	7 799
Table 4	1 730	2 466	3 736	5 379	7 159	13 550	874	1 177	1 672	2 614	3 304	5 503
Table 7	1 479	2 083	3 121	4 176	5 632	11 094	1 280	1 806	2 711	3 629	4 952	9 797
Table 8	1 784	2 560	3 951	5 791	7 950	16 729	901	1 222	1 768	2 814	3 669	6 794
Table 11	1 299	1 840	2 612	3 372	4 043	5 665	1 105	1 575	2 259	2 962	3 573	5 051
Table 12	1 571	2 192	3 297	4 571	5 789	9 192	798	1 073	1 529	2 317	2 771	3 687
Q_{Tr} medium	1 525	2 138	3 209	4 374	5 711	10 143	1 003	1 399	2 014	2 888	3 621	5 923
Q_{Tr} observed	1 672	2 585	4 442	6 613	9 796	24 180	456	549	660	740	817	983
Equations the empirical	**Tecusiapa**						**Cazanate**					
	Return periods in years						Return periods in years					
	5	10	25	50	100	500	5	10	25	50	100	500
Table 3	1 208	1 691	2 488	3 042	3 867	6 542	830	1 169	1 727	2 360	3 078	5 510
Table 4	1 042	1 436	1 983	2 513	3 136	5 084	737	1 024	1 535	1 761	2 235	3 747
Table 7	1 242	1 754	2 633	3 525	4 338	8 218	854	1 213	1 828	2 450	3 454	6 921
Table 8	1 075	1 491	2 097	2 706	3 483	6 277	759	1 063	1 623	1 896	2 482	4 626
Table 11	1 069	1 526	2 192	2 526	3 138	4 286	703	1 020	1 504	2 062	2 529	3 666
Table 12	943	1 293	1 724	2 177	2 602	3 227	646	910	1 398	1 554	1 883	2 626
Q_{Tr} medium	1 072	1 509	2 145	2 616	3 311	5 681	748	1 044	1 579	1 979	2 506	4 187
Q_{Tr} observed	1 542	2 083	2 861	3 516	4 240	6 241	1 542	2 083	2 861	3 516	4 240	6 241
Equations the empirical	**Los Molinos**						**Chico Ruiz**					
	Return periods in years						Return periods in years					
	5	10	25	50	100	500	5	10	25	50	100	500
Table 3	430	612	910	1 147	1 468	2 514	378	540	804	960	1 213	2 017
Table 4	358	499	706	896	1 120	1 815	384	549	769	1 040	1 323	2 240
Table 7	442	635	963	1 294	1 648	3 158	389	560	851	1 144	1 361	2 534
Table 8	369	518	747	964	1 244	2 240	396	570	814	1 120	1 469	2 765
Table 11	337	504	777	942	1 237	1 772	293	440	684	763	1 028	1 444
Table 12	298	435	620	759	937	1 256	315	471	350	847	1 081	1 527
Q_{Tr} medium	364	511	762	953	1 241	2 028	387	545	792	1 000	1 268	2 129
Q_{Tr} observed	226	260	293	312	328	355	329	413	510	576	637	761

Table 15. Estimated Contrast predictions (m^3/s) with empirical equations in six selected stations hydrometric reliable record of Hydrological Region No. 10.

Equations the empirical	Santa Cruz						Jaina					
	Return periods in years						Return periods in years					
	5	10	25	50	100	500	5	10	25	50	100	500
Table 3	1 877	2 607	3 818	4 980	6 427	11 263	1 795	2 496	3 657	4 806	6 214	10 930
Table 4	2 184	3 087	4 617	5 762	7 528	13 630	1 875	2 620	3 884	5 025	6 516	11 578
Table 7	1 930	2 705	4 042	5 403	7 211	14 148	1 846	2 590	3 871	5 176	6 972	13 731
Table 8	2 251	3 205	4 883	6 204	8 359	16 829	1 933	2 720	4 107	5 411	7 236	14 296
Table 11	1 747	2 446	3 410	4 335	5 126	7 091	1 663	2 332	3 262	4 196	4 964	6 899
Table 12	2 028	2 774	4 072	4 996	6 145	8 948	1 740	2 365	3 459	4 392	5 356	7 627
Q_{Tr} medium	1 979	2 740	4 057	5 200	6 819	12 447	1 821	2 543	3 764	4 916	6 365	11 254
Q_{Tr} observed	1 434	2 104	3 258	4 410	5 883	11 118	1 347	2 029	3 309	4 692	6 589	14 199
Relative error (%)	38.0	30.2	24.5	17.9	15.9	12.0	35.2	25.3	13.8	4.8	–3.4	–20.7
Equations the empirical	**Ixpalino**						**Naranjo**					
	Return periods in years						Return periods in years					
	5	10	25	50	100	500	5	10	25	50	100	500
Table 3	1 554	2 165	3 177	4 324	5 636	10 089	887	1 248	1 842	2 566	3 363	6 081
Table 4	1 882	2 681	4 156	6 078	8 163	15 774	804	1 120	1 704	1 946	2 485	4 224
Table 7	1 598	2 246	3 363	4 499	6 323	12 674	912	1 294	1 950	2 613	3 773	7 638
Table 8	1 941	2 783	4 395	6 543	9 065	19 475	829	1 163	1 802	2 096	2 759	5 215
Table 11	1 415	1 997	2 821	3 832	4 524	6 411	757	1 096	1 608	2 270	2 755	4 017
Table 12	1 719	2 389	3 724	5 206	6 611	10 910	709	996	1 565	1 725	2 094	2 990
Q_{Tr} medium	1 659	2 318	3 544	4 853	6 467	11 792	817	1 142	1 753	2 183	2 757	4 720
Q_{Tr} observed	1 557	2 201	3 333	4 485	5 982	11 455	909	1 353	2 105	2 842	3 775	7 009
Relative error (%)	6.6	5.3	6.3	8.3	8.1	2.9	–10.1	–15.6	–16.7	–23.2	–27.0	–32.7
Equations the empirical	**Zopilote**						**El Bledal**					
	Return periods in years						Return periods in years					
	5	10	25	50	100	500	5	10	25	50	100	500
Table 3	497	706	1 049	1 516	2 004	3 687	368	526	784	997	1 279	2 200
Table 4	471	665	1 049	1 287	1 675	2 971	377	540	792	1 024	1 316	2 276
Table 7	511	732	1 110	1 490	2 248	4 631	379	545	829	1 114	1 436	2 764
Table 8	485	690	1 109	1 386	1 860	3 669	389	561	837	1 102	1 461	2 810
Table 11	397	589	813	1 348	1 676	2 532	284	427	666	820	1 084	1 567
Table 12	396	579	973	1 119	1 408	2 256	309	463	688	848	1 084	1 623
Q_{Tr} medium	478	678	1 049	1 367	1 768	3 320	373	533	788	1 011	1 298	2 238
Q_{Tr} observed	558	738	977	1 161	1 351	1 817	401	565	834	1 090	1 404	2 446
Relative error (%)	–14.3	–8.1	7.4	17.7	30.9	82.7	–7.0	–5.7	–5.5	–7.2	–7.5	–8.5

Iguazu Falls, Argentina.

Photo: Edith Salcedo.

Characterization of Biomass Burning Aerosols over Southeast Mexico

• Virginia Edith Cortés-Hernández* •
Posgrado en Ciencias del Agua del Instituto Mexicano de Tecnología del Agua
*Corresponding Author

• Javier Aparicio •
Consultor/Profesor de Postgrado en Ingeniería, UNAM

Abstract

CORTÉS-HERNÁNDEZ, V.E. & APARICIO, J. Characterization of Biomass Burning Aerosols over Southeast Mexico. *Water Technology and Sciences* (in Spanish). Vol. V, No. 1, January-February, 2014, pp. 141-151.

Characterization of aerosols is important for the atmospheric radiative process and the radiation budget of the climate system. This study presents some physical properties forming part of the optical and radiative characterization of atmospheric aerosols measured in two monitoring sites from the *AERONET* network located in Southeastern Mexico during 2005-2007. The location of both sites corresponded to the region of high biomass burning activity during 2005. Characterization of aerosols considered four study cases: 1) April 23, 2005 in Tenosique, Tabasco, 2) April 27, 2005, 3) May 8, 2006 and 4) May 24, 2007 in Tuxtla Gutierrez, Chiapas. Results show values of high atmospheric optical depth ($\tau > 1.4$), high values of the Ångström coefficient ($\alpha > 0.8$), fine accumulation mode particles ($r < 0.34$), single scattering albedo ($\omega_0 \sim 1$), as well as low values of refractive index complex ($k \sim 0$), as a result of an interaction between solar radiation and smoke aerosols mainly due to scattering over the southeastern Mexico.

Keywords: smoke aerosols, biomass burning, aerosol optical depth, Ångström coefficient, complex refractive index, single scattering albedo.

Resumen

CORTÉS-HERNÁNDEZ, V.E. & APARICIO, J. Caracterización de aerosoles por quema de biomasa en el sureste de México. *Tecnología y Ciencias del Agua.* Vol. V, núm. 1, enero-febrero de 2014, pp. 141-151.

La caracterización de los aerosoles atmosféricos es de gran importancia en los procesos de transferencia radiativa en la atmósfera y el balance de radiación del sistema climático. En este trabajo se presentan algunas propiedades físicas que forman parte de la caracterización óptica y radiativa de los aerosoles atmosféricos registrados en dos sitios de monitoreo pertenecientes a la red AERONET, *ubicados al sureste de México, durante el periodo 2005-2007. La ubicación de los dos sitios de monitoreo correspondió a la región de mayor quema de biomasa por incendios forestales durante el año 2005. La caracterización de los aerosoles atmosféricos consideró cuatro casos de estudio: 1) 23 de abril de 2005, en Tenosique, Tabasco; 2) 27 de abril de 2005; 3) 8 de mayo de 2006, y 4) 24 de mayo de 2007, en Tuxtla Gutiérrez, Chiapas. Los resultados muestran altos valores del espesor óptico del aerosol ($\tau > 1.4$), altos valores del coeficiente de Ångström ($\alpha > 0.8$), modos finos de acumulación del aerosol ($r < 0.34$ μm), valores del albedo de dispersión simple cercanos a 1 ($\omega_0 \sim 1$) y valores pequeños de la parte compleja del índice de refracción ($k \sim 0$), todo lo anterior como resultado de una interacción mayormente dispersiva de la radiación solar y los aerosoles atmosféricos registrados cerca de las fuentes emisoras de quema de biomasa en el sureste de México.*

Palabras clave: *aerosoles por quema de biomasa, espesor óptico del aerosol, coeficiente de Ångström, albedo por dispersión simple, índice de refracción complejo.*

Introduction

Biomass burning includes natural and anthropogenic forest, brush and pasture fires. It is estimated that approximately 90% of biomass burning is caused by humans (NASA, 2001) and results from a variety of activities, such as agricultural expansion, deforestation, land use changes and control of pesticides and weeds.

In Mexico, forest fires are one of the largest causes of loss of natural vegetation due to agricultural activities and removal of forests for other land uses.

Earlier studies to detect and monitor hot points (sources of heat with emissions in the near infrared range) using GOES-8 satellite images (Polanco-Martínez 2003) have identified southeastern Mexico as one of the most active regions in terms of biomass burning. This region presents a significant number of biomass burning episodes in the spring, which is the driest season in this region.

Just two decades ago, biomass burning was identified as a global source of chemical and radiatively active gas emissions and particles that contribute to the radiative balance of the climate system (Sevine, 1995).

tmospheric aerosols generated by natural as well as anthropogenic sources can be solid or liquid suspended particles in the earth's atmosphere with radii between 0.001 to 100 μm (1 μm = 1 x 10^{-6} m). They directly alter the radiative balance of the earth by interacting with solar and land radiation, and indirectly by changing the microphysical properties of clouds and precipitation processes.

A wide range of gaseous compounds and particles (Table 1) are emitted during a biomass burn, significantly contributing to tropospheric balances on the local, regional and global levels. An important characteristic of atmospheric aerosols is the size distribution, which makes it possible to identify the number of aerosols within a certain size interval. It is also the basis for obtaining the optical properties of aerosol using scattering theory (Toledano-Olmeda, 2005).

The distribution of particle sizes vary during transport, from nucleation mode (size ranging from nanometers to tenths of nanometers) to accumulation mode (generally smaller than a micrometer). The coarser particles are eliminated from the air through the precipitation process (Toledano-Olmeda, 2005).

A Biomass burning particles are defined according to their diameter (d) as: ultra fine ($d < 0.1$ μm) , fine ($d < 2.5$ mm) and coarse ($d > 2.5$ mm). Most biomass burning particles are ultra fine and only a small portion are larger (Morawska *et al*., 1999). Ultra fine particles quickly agglomerate to form fine particles. The mass of biomass burning particles can be divided into two categories: fine particles with an average diameter of 0.3 μm and coarse particles with a mean diameter over 10 μm.

In terms of size distribution, the accumulation mode of particles generated by biomass burning is represented by three main compounds: particulate organic matter (carbon with associated organic material), black carbon (for example, soot) and inorganic trace species (such as potassium, chlorine and calcium) (Reid *et al*., 2005).

Studies conducted by Reid *et al*. (2005) indicate that, on average, 80% of the composition of recently emitted particles from biomass burning correspond to particulate organic matter, 5 to 9% to black carbon and 12 to 19% inorganic trace species.

During biomass burning, the aerosols generated are transported and scattered by atmospheric dynamics, determining their

Table 1. Gas and Particle Emissions Generated during Biomass Burning (Gao *et al*., 2003; Reid *et al*., 2005).

Biomass Burning Emissions	**Greenhouse Effect**	Carbon dioxide (CO_2), methane (CH_4), nitrous oxide (N_2O)
	Chemically active gases	Nitrogen oxide (NO), carbon monoxide (CO), methane (CH_4), non-methane hydrocarbons (NMHCs), methyl chloride (CH_3Cl), methyl bromide (CH_3BR).
	Particles/aerosols	Volatile organic compounds (VOCs) and semi-volatile organic compounds, polynuclear aromatic hydrocarbons (PAH) composed of sulfur and nitrogen, organic carbon, black carbon, sulfates (H_2S_2, SO_2), nitrate (NO_x), ammonia (NH_3).

lifetime in the atmosphere (Cooter *et al*., 2002). While the aerosols are in the atmosphere, they interact with the earth's radiation through radiation and absorption processes. In the case of biomass burning aerosols, their lifetime is relatively short (5 to 10 days) and their chemical composition varies depending on the residence time in the atmosphere. Therefore, for example, the mass of young smoke particles is 80% organic carbon, 5 to 9% black carbon and 12 to 15% inorganic compounds such as potassium, sulfates, chlorides and nitrates (Reid *et al*., 2005). On the other hand, biomass burning particles with a longer lifetime contain a large amount of sulfates, nitrates, organic acids and semi-volatile organic compounds (Gao *et al*., 2003; Reid *et al*., 2005).

Scattering is a physical process through which a particle, during its trajectory as an electromagnetic wave, continually extracts energy from the incident wave and irradiates it in all directions (Liou, 2002). During scattering, a particle absorbs a certain amount of incident energy and later emits it in a solid angle centered in the particle, which is considered a point source of scattered energy. The particles in the atmosphere responsible for scattering vary in size from gas (~ 10^{-4} mm) to aerosol (~ 1 mm) molecules, small drops of water (~ 10 mm), ice crystals (~ 100 mm), water drops and hail particles (~ 1 cm).

La intensidad de la dispersión se determina mediante el parámetro de tamaño (χ), el cual es el resultado del cociente del tamaño de las partículas ($2\ \pi r$) y la longitud de onda de la radiación incidente (λ):

$$\chi = 2\pi\, r / \lambda$$

where r is the radius of the particles (presumably spherical).

If $\chi << 1$, the scattering is a Rayleigh type (Strutt, 1899), which describes scattering by molecules whose size is much smaller than the incident radiation wavelength (Figure 1). A good example of this is the scattering of visible light (from 0.4 to 0.7 μm) by air molecules, which explains the blueness of the sky (Rayleigh, 1871).

For particles whose sizes are comparable to or larger than the wavelength ($\chi \geq 1$), energy primarily scatters in the direction of the propagation of incident radiation, that is, Mie scattering (Mie, 1908). Based on the Mie theory, this solves the problem of the interaction between a flat electromagnetic wave and a dielectric sphere, presuming it to be homogeneous and isotope.

In addition, it relates Rayleigh molecular scattering theory with geometric optical scattering for spheres with sizes equal or larger than the incident wavelength ($\chi \geq 1$). According to this type of scattering, more is produced in the forward direction than in any other direction and as the size of the particle increases, forward scattering also increases.

Mie's theory is based on Maxwell's equations to obtain the vector wave equation with spherical coordinates. By separating the wave equation variables, the solution of the electric and magnetic fields of the incident wave can be expressed in the form of Legendre polynomials and Bessel spherical functions (Stratton, 1941).

The optical properties that describe the interaction between aerosols and solar radiation are the extinction coefficients (absorption and scattering), single scattering phase function and vertical optical depth which depends on the wavelength and is derived from microphysical quantities such as the complex refraction index and the aerosol size distribution based on Mie's theory, which presumes that the particles are spherical and homogeneous (Levoni *et al*., 1997).

Aerosol Optical Depth

The aerosol optical depth (AOD) is a quantitative measurement of the extinction of solar radiation, normalized in the atmospheric column due to spectral scattering or particle (aerosol) absorption processes.

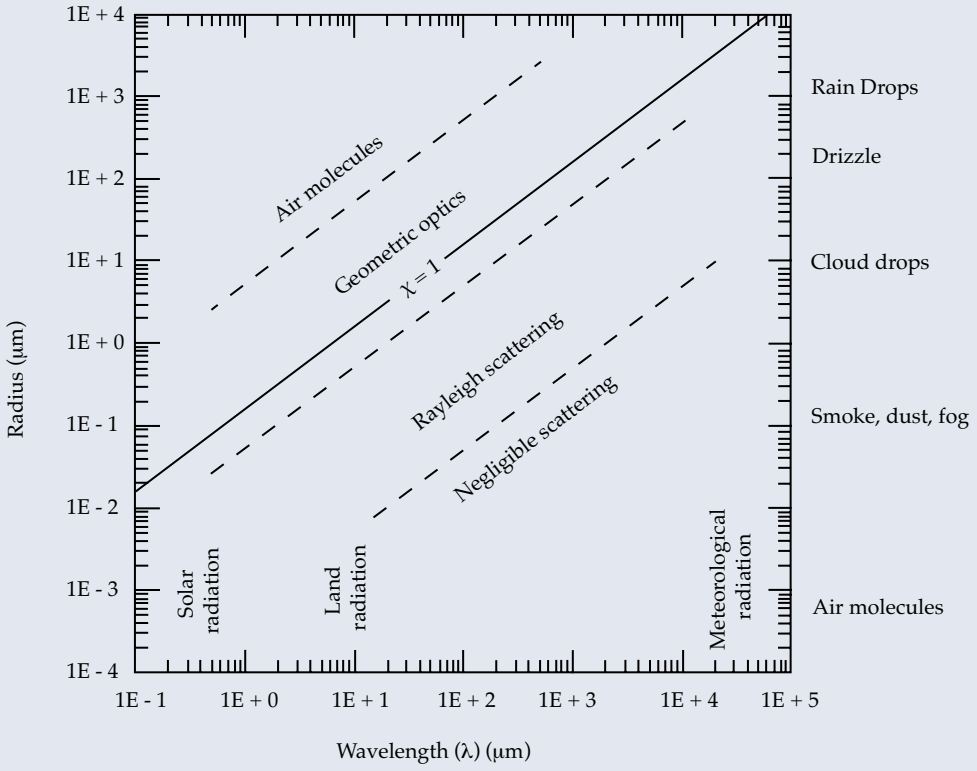

Figure 1. Types of Scattering in the Atmosphere according to the Size Parameter (Kidder and Vonder Haar, 1995).

For the case of atmospheric aerosols and according to Mie's theory ($\chi \geq 1$), the optical depth is defined as:

$$\tau = \int_{S_1}^{S_2} \beta_{e\lambda}(s)\, ds \qquad (1)$$

Where the extinction coefficient $\beta_{e\lambda} = \rho k_{e\lambda}$, ρ is the density, $k_{e\lambda}$ is the opacity and the aerosol optical depth τ is a dimensionless unit.

The spectral shape of the aerosol optical depth can be characterized based on the Mie equation (1908) and the size parameter (ratio between the particle size and incident radiation wavelength).

Since the optical depth depends on the wavelength, it is parametrized using the Law of Ångström (1929), which describes the aerosol size distribution in the integrated column and can be derived from simultaneous optical depth measurements for various wavelengths. This law is expressed as:

$$\tau(\lambda) = \beta\lambda^{-\alpha} \qquad (2)$$

where λ is the wavelength in micrometers (μm) and α and β are two fit parameters. The parameter α is the Ångström exponent, which is directly related to the aerosol size distribution. The values of this parameter are 0 to 4, in theory, where the lowest values correspond to large particles (Wagner and Silva, 2008). The parameter β is the turbidity coefficient and coincides with the aerosol optical depth of $\lambda = 1$ mm.

Nevertheless, the aerosol optical depth is not directly measured but rather calculated based on observations of atmospheric spectral transmission.

Size Distribution

Since aerosol particles range in size, it is appropriate to use a logarithmic scale to

describe their distribution. The parameter that is used most for the particle size distribution function is the volume size distribution $n_V(d_p)$. According to Seinfeld and Pandis (1998), $n_V(d_p)$ dd_p is the volume of the particles by m^3 of air in the diameter range d_p to $d_p + dd_p$.

Different authors indicate that the aerosol size distribution is fitted to a log-normal distribution (Hess *et al*., 1998; Remer and Kaufman, 1998):

$$\frac{dV_i}{dlnr} = \frac{V_0}{\sqrt{2\pi\pi}} e^{-\frac{\left(ln(r/rm.i)^2\right)}{2\sigma^2}} \qquad (3)$$

where $r_{m,i}$ is the radius mode (mean) related to the accumulation or depth mode (Remer and Kaufman, 1998); V_0 is the volume of the particle column per cross-section unit of the atmospheric column, and σ is the standard deviation of the natural logarithm of the radius; $dV/d\ ln\ r$ is measured in [$\mu m^3/\mu m^2$].

To recover the particle size distribution based on measurements with solar photometers in the almucantar and main plane, the *AERONET* network uses an inversion algorithm (Dubovik *et al*., 2000) to calculate the optical aerosol properties.

Single Scattering Albedo

The aerosol optical depth takes into account the extinction of incident radiation without concerning whether it is produced by absorption or scattering. The single scattering albedo determines the relationship between extinction due to scattering alone and due to scattering plus absorption. It is defined as (Seinfeld and Pandis, 1998):

$$w_0(\lambda) = \frac{\tau_s(\lambda)}{\tau_e(\lambda)} = 1 \quad \frac{\tau_a(\lambda)}{\tau_e(\lambda)} \qquad (4)$$

Single scattering albedo is an indicator of the absorbent capacity of the aerosol, which depends on it chemical composition, shape and size, and takes values between 0 (very absorbent particles) and 1 (little absorbent particles).

Complex Refraction Index

The refraction index is an optical parameter associated with the change in velocity of electromagnetic waves in a medium with respect to a vacuum, as described by Mie's theory (1908). It is also an optical characteristic of the medium, that is, when the electromagnetic radiation crosses a flat plane-parallel layer, the optical properties of the medium can be characterized using the complex refraction index (m), expressed as:

$$m = n - ik \qquad (5)$$

where the real part n represents a lag in the wave propagating through the medium and the imaginary part k determines the absorption of energy by the medium, which is associated with a decrease in energy in the wave during propagation (Sobrino *et al*., 2004).

The refraction index is especially important to evaluate the absorptivity of the aerosol component. If the imaginary part (k) is other than 0, the aerosol particles absorb solar radiation, and if there is no absorption then the radiation will be extinguished by scattering.

Methodology

Aerosols generated by biomass burning primarily in the area of the Lacandona jungle in Chaipas and northwestern Guatemala (Polanco-Martínez, 2003) are driven westward by advection and cross the states of Tabasco and Chiapas due to the effect of trade winds that are predominant in southeastern Mexico. Therefore, two aerosol monitoring stations were installed in those states (*AERONET*, Holben *et al*., 1998)— Tenosique in Tabasco and Tuxtla Gutiérrez in Chiapas.

Tenosique was the first station to be installed, in January 2005. It is located in

southeastern Mexico in the municipality of Tenosique, Tabasco (17.488º N, 91.426º W) at an altitude of 20 masl. Roughly at the same time the Tuxtla Gutiérrez station was installed in the municipality of Tuxtla Gutiérrez, Chiapas (16.755º N, 93.152º W) at an altitude of 150 masl (Figure 2).

Tenosique station only operated during 2005, while that of Tuxtla Gutiérrez worked during the period 2005-2010 (Table 2).

The *AERONET* station has a CIMEL Electronique spectral radiometer, a Stevens data logger, a SATLINK satellite transmitter-logger and two solar panels (SPS and ASP) (Figure 1).

The measurements at each AERONET site provide data about the spectral aerosol optical depth, aerosol size distribution and precipitable water in diverse aerosol regimes. The aerosol optical depth uses the deconvolution algorithm (SDA) described by O'Neill *et al*. (2003), which includes the optical depths for fine (sub-micron) and coarse (super-micron) modes with a standard wavelength of 500 nm.

The size distribution, phase function and aerosol optical depth are obtained using inversion algorithms proposed by Dubovik and King (2000) and Nakajima *et al*. (1996). Then, calibration coefficients are used to transform the radiance signals into physical quantities such as aerosol optical depth and the Ångström exponent (1929),among others.

Optical depth, for example, is calculated based on the spectral extinction of direct radiation for each wavelength, based on the Beer-Bouguer-Lambert Law (equation for atmospheric radiative transfer). Then, attenuation from Rayleigh scattering and ozone absorption (from the interpolated ozone climatology atlas) and contaminant gases are calculated and removed to isolate the aerosol optical depth. The data registered at each AERONET station include aerosol optical depth and the Ångström parameter, among others (Table 3).

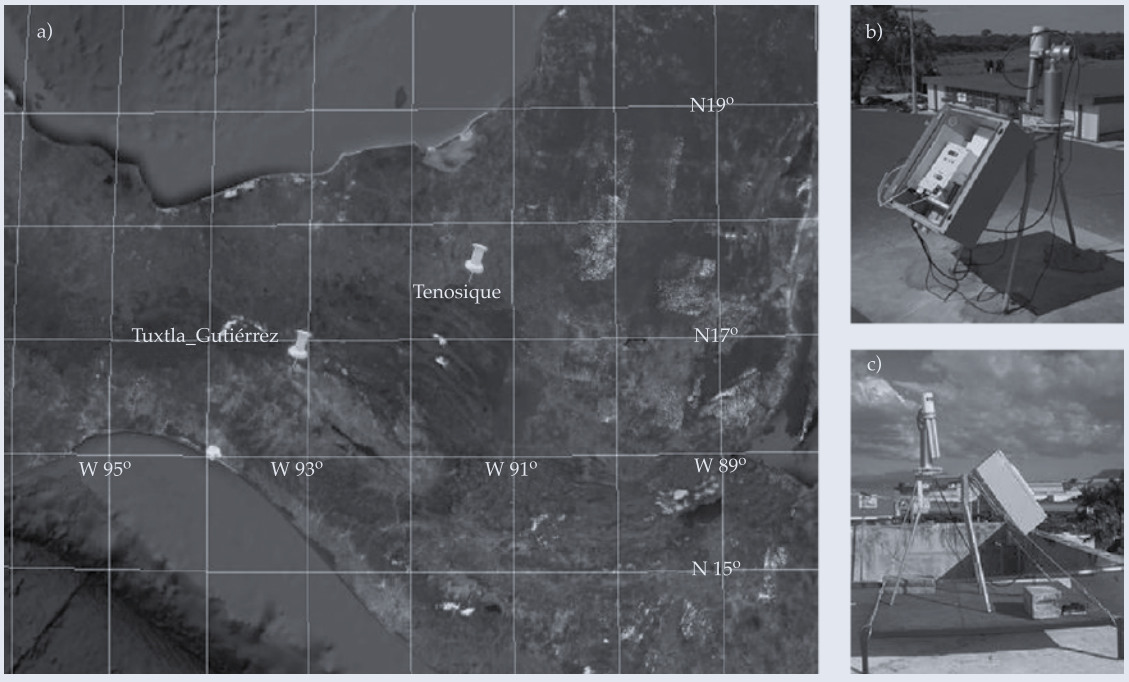

Figure 2. a) Location of Tenosique and Tuxtla Gutiérrez sites (Google Earth, http://aeronet.gsfc.nasa.gov), b) Tenosique stations and c) Tuxtla Gutiérrez.

Table 2. Operating Times for the Tenosique and Tuxtla Gutiérrez.

Stations	Operating time	Beginning date	End date
Tenosique	253 Days (0.693 Years)	January 24, 2005	January 9, 2006
Tuxtla Gutiérrez	1 302 Days (3.567 Years)	January 26, 2005	February 7, 2010

Table 3. Format in which the Aeronet Data is Available.

Format	Description
All points	Available data from each measurement or recovery time.
Daily average	Calculated as long as three or more data are available during a day.
Monthly averaged based on daily average	Calculated based on daily averages for a month. $\bar{X} = \frac{\sum X_i}{n}$

Having selected the variables of interest, the data is presented in three formats, as shown in Table 3.

The downloaded data are extracted in compressed zip files, in text format, which can later be imported into Excel spreadsheets, for example.

Results

Four case studies were conducted corresponding to days on which the maximum aerosol optical depth was measured at a wavelength of 500 nm (widely used wavelength to characterize atmospheric aerosols resulting from biomass burning) (Eck *et al*., 2003).

Table 4 presents the physical-radiative properties associated with the four case studies, such as background optical depth obtained based on the lowest AOD daily records.

Case 1 (Tenosique) registered the highest AOD of all the case studies and the largest water contents, while Tuxtla Gutiérrez (case 2) registered the largest aerosol optical depth; both occurred in 2005.

Table 4. Aerosal Parameters based on Version 2.

Aerosol parameter	Meaning
AOD	Aerosol optical depth.
440-870 Angström	Angström coefficient 440-870 nm.
SDA fine/coarse AOD	Spectral deconvolution algorithm for AOD fine/course.
SDA fine mode fraction	Spectral deconvolution algorithm for fine-mode fraction.

Table 5. Case Studies and Primary Optical Characteristics of Associated Aerosols.

Site	Cases		$\tau_{Background}$	$\tau_{aerosol}$	$\alpha_{440\text{-}870}$	Water (cm)
Tenosique	1	April 23, 2005	0.122	3.851	1.316	4.467
Tuxtla Gutiérrez	2	April 27, 2005	0.112	2.906	1.450	3.460
Tuxtla Gutiérrez	3	May 8, 2006	0.053	1.448	0.836	3.713
Tuxtla Gutiérrez	4	May 24, 2007	0.214	2.220	1.871	3.680

A dependence exists between the wavelength and the AOD primarily due to the aerosol distribution and, to a lesser extent, the absorption characteristics of aerosol. This dependence can be observed by comparing the Ångström coefficient for each case, which is calculated using the linear regression of the optical depth logarithm in function of the wavelength. The water vapor content is related to the regional characterization of aerosol. High water vapor contents indicate sand aerosols from the desert and low contents indicate bioactive (organic) aerosols.

Figure 3 shows the spectral optical depth distribution of the study cases in the range of 380 to 1 020 nm. Aerosol optical depths over 1.4 units with Ångström coefficients of 0.8 to 1.8 were identified for all cases.

In addition to the size and spectral variation of AOD, other very important physical-radiative properties are required to characterize aerosol, such as aerosol size distribution, single scattering albedo and the refraction index (imaginary part).

The distribution of the radius of the particles is shown in Figure 4, with significant differences among the sizes of fine mode particles associated with the lifetime of the particles and the conversion of gas to a particle. The lognormal distribution is frequently used to parametrize the accumulation mode of the volume size distribution of biomass burning aerosols (Remer and Kaufman, 1998).

The smallest radii were observed in the Tuxtla Gutiérrez stations in the year 2005 (Case 2), with a minimum radius of 0.16 μm at the peak modal volume of the radius. The largest radius (r = 0.34 μm) was registered in Tenosique (Case 1).

This radius distribution makes it possible to associate the aerosols found with aerosols from biomass burning, since the size range coincides with values identified by previous studies that characterized biomass burning aerosols(Eck *et al*., 2003).

To determine whether the extinction of biomass burning aerosol is due to absorbent or dispersive particles, the single scattering

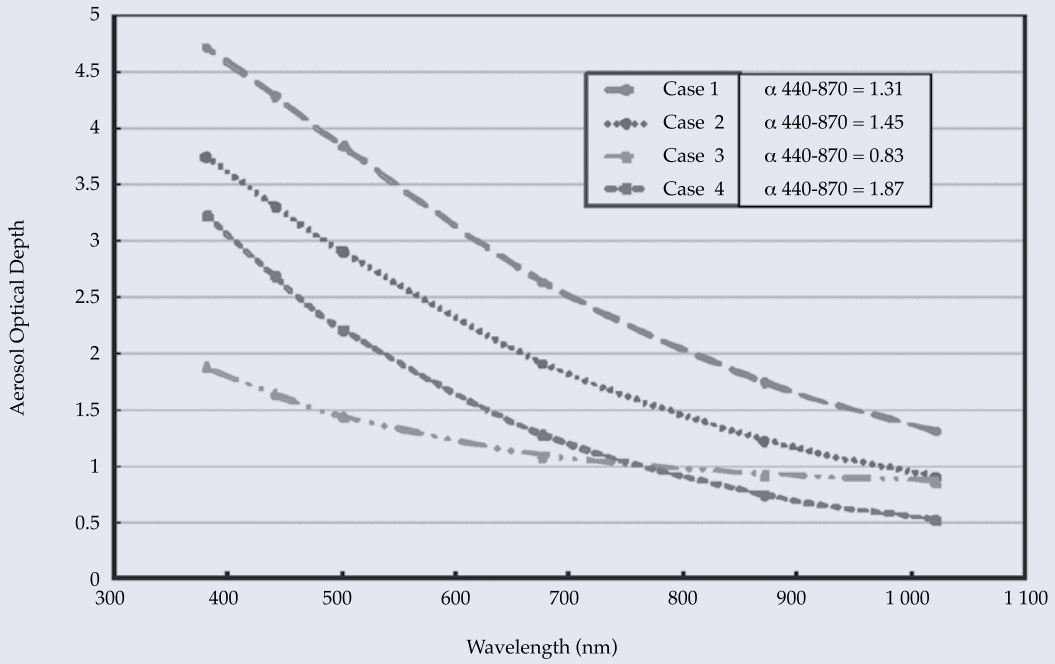

Figure 3. Spectral AOD Distribution and Angström Coefficient for each Case Study.

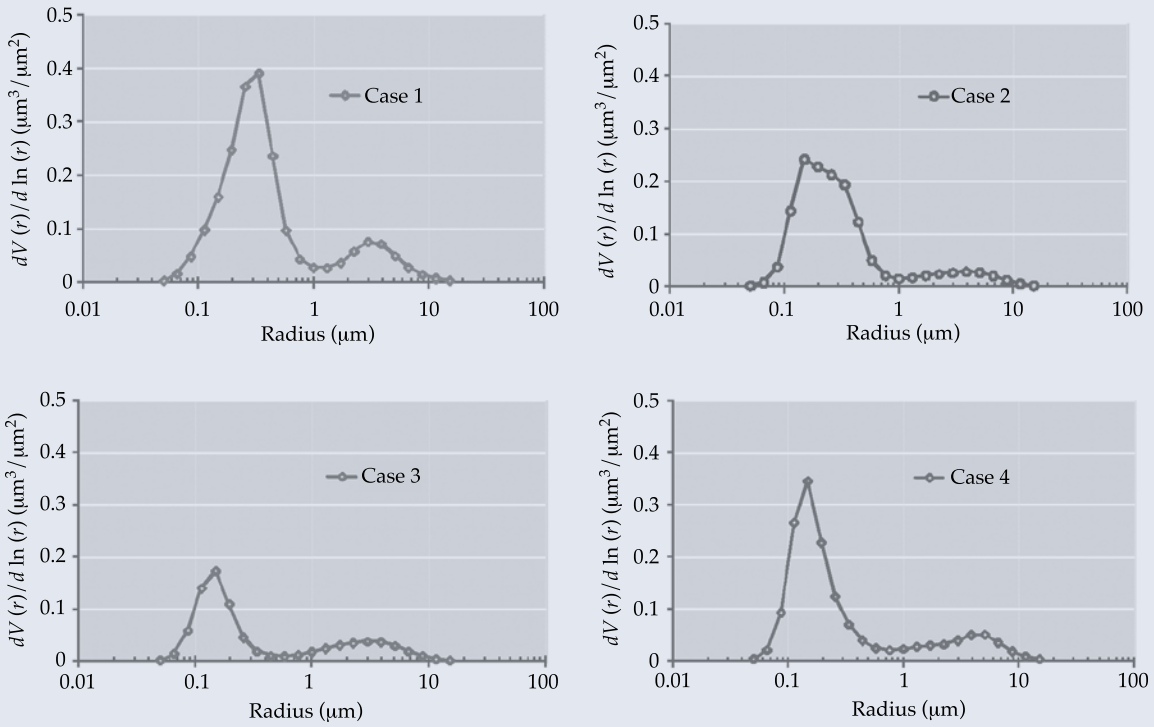

Figure 4. Aerosol Volume Size Distribution Distribución del tamaño del volumen for the Four Case Studies.

albedo (ω_0) is used. The single scattering albedo associated with biomass burning aerosols has a large influence on the attenuation of solar radiation and, therefore, decreases the incident irradiance of the earth's surface as a result of absorption within the atmospheric aerosol layer (Sundar *et al.*, 2000).

Figure 5 shows the spectral distribution of the single scattering albedo for each case study.

The largest ω_0 values were found for Case 1 (near 1, indicating little absorption), which associate the largest sized particles (Figure 5, Case 1) with the smallest values of the imaginary part of the refraction index (Table 6).

The analysis of these parameters is very important to adequately calculate the radiative contribution of aerosols, since they determine how much of the radiation is scattered back into space and how much is absorbed into the aerosol layer.

Conclusions

The comparison of different spectral aerosol optical depths for the two case studies in which the aerosol load was high (τ of 500 nm) showed high Ångström exponent values (α 440-870), from 1.4 to 2.1, due to differences in the sizes of the fine-mode particles and in refraction indices.

The characterization of aerosol is the first approximation of the aerosol distribution in the atmosphere, with fine-mode aerosols generated by biomass burning near the measurement sites.

The characterization of the aerosol enabled identifying the aerosol distribution in the atmosphere, with fine-mode aerosols associated with high water vapor contents and low absorption, characteristics pertaining to aerosols generated by biomass burning

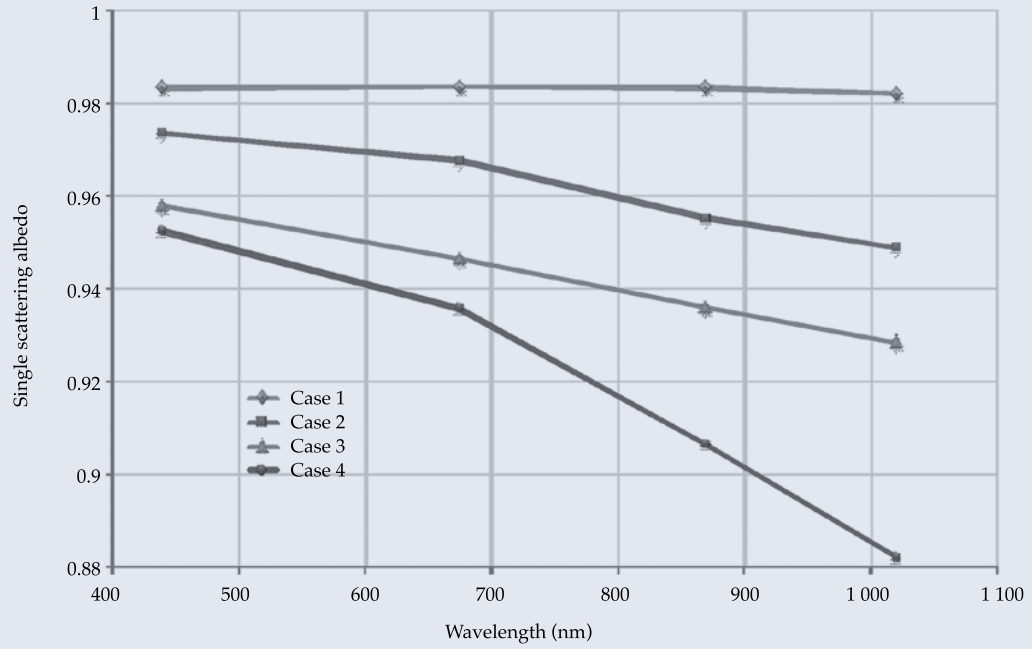

Figure 5. Spectral distribution of the single scattering albedo for the case studies.

Table 6. Imaginary Part of the Refraction Index for the Case Studies.

Site	Case	440 nm	675 nm	870 nm	1 020 nm
Tenosique	April 23, 2005	0.0022	0.0021	0.0018	0.0017
Tuxtla Gutiérrez	April 27, 2005	0.0036	0.0042	0.0051	0.0052
Tuxtla Gutiérrez	May 7, 2006	0.0058	0.0059	0.0061	0.0062
Tuxtla Gutiérrez	May 24, 2007	0.0064	0.0069	0.0083	0.0092

identified by studies in regions such as the Amazons (Eck *et al.*, 2003).

Published by invitation

References

ÅNGSTRÖM, A.K. On the atmospheric transmission of sun radiation and on the dust in the air. *Geogr. ANN*. Vol. 12, 1929, pp. 130-159.

DUBOVIK, A. SMIRNOV, B.N. HOLBEN, M.D., KING, Y.J., KAUFMAN, T.F., ECK, T.F., and SLUTSKER, I. Accuracy assessment of aerosol optical properties retrieval from AERONET sun and sky radiance measurements, *J. Geophys. Res*. Vol. 105, 2000, pp. 9791-9806.

DUBOVIK, O. and KING, M.D. A flexible inversion algorithm for retrieval of aerosol optical properties from Sun and sky radiance measurements, *J. Geophys. Res*. Vol. 105, No. 20, 2000, pp. 673-696.

ECK, T.F., HOLBEN, B.N., REID, J.S., O'NEILL, N.T., SCHAFER, J.S., DUBOVIK, O., SMIRNOV, A., YAMASOE, M.A., and ARTAXO, P. High aerosol optical depth biomass burning events: A comparison of optical properties for different source regions, *Geophys. Res. Lett*. Vol. 30, No. 20, 2003, p. 2035, doi:10.1029/2003GL017861.

GAO, S., HEGG, D.A., HOBBS, P.V., KIRCHSTETTER, T.W., MAGI, B.I., and SADILEK, M. Water-soluble organic components in aerosols associated with savanna fires in southern Africa: Identification, evolution, and distribution. *J. Geophys. Res*. Vol. 108, 2003, p. 8491.

HESS, M., KOEPKE, P., and SCHULT, I. Optical properties of aerosols and clouds: the software package opac. *Bull. Amer. Meteor. Soc*. Vol. 80, 1998, pp. 831-844.

HOLBEN, B.N., ECK, T.F., SLUTSKER, I., TANRÉ, D., BUIS, J.P., SETZER, A., VERMOTE, E., REAGAN, J.A., KAUFMAN, Y.J., NAKAJIMA, T., LAVENU, F., JANKOWIAK, I., and SMIRNOV, A. AERONET- A federated instrument network and data archive for aerosol characterization. *Remote Sens. Environ.* Vol. 66, 1998, pp. 1-16.

MIE, G. Beiträge zur Optik trüber Medien, speziell kolloidaler Metallösungen, Leipzig. *Ann. Phys*. Vol. 330, 1908, pp. 377-445.

MORAWSKA, L., THOMAS, S., JAMRISKA, M., and JOHNSON, G. The modality of particle size distributions of environmental aerosols. *Atmos. Environm.* Vol. 33, 1999, pp. 4401-4411.

NAKAJIMA, T., TONNA, G., RAO, R., BOI, P., KAUFMAN, Y., and HOLBEN, B. Use of sky brightness measurements from ground for remote sensing of particulate polydispersions. *Appl. Opt.* Vol. 35, 1996, pp. 2672-2686.

NASA. *Biomass Burning: A Hot Issue in Global Change. Biomass burning is the burning of living and dead vegetation*. FS-2001-02-56-LaRC. Hampton, USA: National Aeronautics and Space Administration Langley Research Center, 2001.

O'NEILL, N.T., ECK, T.F., SMIRNOV, A., HOLBEN, B.N., and THULASIRAMAN, S. Spectral discrimination of coarse and fine mode optical depth. *J. Geophys. Res.* Vol. 108, 2003, pp. 4559-4573.

POLANCO-MARTÍNEZ, J.M. *Monitoreo de quema de biomasa utilizando imágenes GOES-8 en el sureste de la República Mexicana*. Tesis de licenciatura. Xalapa, México: Facultad de Instrumentación Electrónica y Ciencias Atmosféricas, Universidad Veracruzana, 2003, 98 pp.

REID, J.S., ECK, T.F., CHRISTOPHER, S.A., KOPPMANN, R., DUBOVIK, O., ELEUTERIO, D.P., HOLBEN, B.N., REID, E.A., and ZHANG, J. A review of biomass burning emissions part III: intensive optical properties of biomass burning particles. *Atmos. Chem. Phys.* Vol. 5, 2005, pp. 827-849.

REMER, L.A. and KAUFMAN, Y.J. Dynamic aerosol model: Urban/industrial aerosol. *J. Geophys. Res*. Vol. 103, 1998, pp. 13859-13871.

SEINFELD, J.H. and PANDIS, S.N. Atmospheric chemistry and physics – from air pollution to climate change. New York: John Wiley & Sons, 1998.

SEVINE, J.S. The Global Impact of Biomass Burning: An Interview with EPA's Robert Huggett. *Environmental Science and Technology*. Hampton, USA: NASA Langley Research Center, 1995, 12 pp.

SOBRINO, J.A, JIMÉNEZ-MUÑOZ, J.C, and PAOLINI, L. Land surface temperature retrieval from Landsat TM 5. *Remote Sens. Environ.* Vol. 90, 2004, pp.434-440.

SUNDAR, C., LI, X., WELCH, R.M., REID, J.S., HOBBS, P.V., ECK, T.F., HOLBEN, B. Estimation of surface and top-of-atmosphere shortwave irradiance in biomass-burning regions during SCAR-B. *J. Appl. Meteor*. Vol. 39, 2000, pp. 1742-1753.

TOLEDANO-OLMEDA, C. *Climatología de los aerosoles mediante la caracterización de propiedades ópticas y masas de aire en la estación El Arenosillo de la red AERONET*. Tesis doctoral. Valladolid: Universidad de Valladolid, Departamento de Física Teórica, Atómica y Óptica, 2005.

WAGNER, F. and SILVA, A.M. Some considerations about Ångström exponent distributions. *Atmospheric Chemistry Physics*. Vol. 8, 2008, pp. 481-489.

Institutional Address of the Authors

M. en C. Virginia Edith Cortés-Hernández

Posgrado en Ciencias del Agua
del Instituto Mexicano de Tecnología del Agua
Paseo Cuauhnáhuac 8532, Colonia Progreso
62550 Jiutepec, Morelos, México
virginia.cortes.h@gmail.com

Dr. Javier Aparicio

Edificio de Posgrado
Instituto Mexicano de Tecnología del Agua
Paseo Cuauhnáhuac 8532, Colonia Progreso
62550 Jiutepec, Morelos, México
Teléfono: +52 (777) 1358 227
javieraparicio@prodigy.net.mx

Click here to write the autor

Main Canal Dam Josefa Ortiz de Domínguez, Sinaloa, Mexico.

Photo: Serge Tamari.

Technical Note

Behavior of the Damage Effect of Wells Using Data of their Production Measurements

• Alfonso Aragón-Aguilar* • Georgina Izquierdo-Montalvo •
• Víctor Arellano-Gómez •
Instituto de investigaciones Eléctricas, México
*Corresponding Author

Abstract

ARAGÓN-AGUILAR, A., IZQUIERDO-MONTALVO, G. & ARELLANO-GÓMEZ, V. Behavior of the Damage Effect of Wells Using Data of their Production Measurements. *Water Technology and Sciences* (in Spanish). Vol. V, No. 1, January-February, 2014, pp. 153-159.

The damage effect in a well is an influence factor in the productive characteristics decrease, along its exploitation stage. Ordinarily the damage effect has been determined from the equations to analyze transient pressure tests. However it is emphasized that the execution of such transient tests, requires of long periods time in order to reach the stabilization in the well. Due to difficulties to carry out transient pressure tests, were developed techniques for determining the damage effect using measurement production data, in order to avoid the extraction of the wells from production system. The geothermal inflow type-curve affected with damage and different examples for the damage determination are shown. The data used were obtained from production measurements in wells of Mexican geothermal fields, taken at different stages of its operative life. From the analysis carried out it was found that the damage value obtained in analyzed wells increases as function of exploitation time. The last thing is related with deterioration in productive characteristics of the wells. The knowledge of the damage effect helps to consolidate technical criteria for taking decisions about the appropriate operations to apply in the well (Such as cleanings, repairs, stimulations, fracturing, etc.).

Keywords: inflow curves, damage effect, production test, output curves, characteristic production curves, reservoir characterization, production decline.

Resumen

ARAGÓN-AGUILAR, A., IZQUIERDO-MONTALVO, G. & ARELLANO-GÓMEZ, V. Identificación del comportamiento del daño en pozos usando datos de sus mediciones de producción. Tecnología y Ciencias del Agua. *Vol. V, núm. 1, enero-febrero de 2014, pp. 153-159.*

El efecto de daño en un pozo es un factor de influencia en la disminución de sus características productivas durante su etapa de explotación. De manera tradicional, el efecto de daño se determina a partir de las ecuaciones para análisis de las pruebas transitorias de presión. Sin embargo, la ejecución de este tipo de pruebas requiere de periodos de tiempo relativamente largos para lograr la estabilización del pozo. Debido a las dificultades para realizar pruebas transitorias de presión, se desarrollaron técnicas para determinar el efecto de daño, usando mediciones de producción, con el fin de evitar el retiro de los pozos de los sistemas de producción. Se presenta la metodología para determinar el efecto de daño usando la curva-tipo geotérmica de influjo y se demuestra su aplicabilidad con diferentes ejemplos. Los datos utilizados fueron obtenidos de mediciones de producción de pozos de campos geotérmicos mexicanos en diferentes etapas de su vida operativa. A partir de los análisis se encuentra que el valor numérico del daño determinado en los pozos seleccionados aumenta en función del tiempo de explotación, lo cual indica un deterioro en sus características productivas. El conocimiento del efecto de daño ayuda a establecer criterios técnicos durante la toma de decisiones sobre las acciones pertinentes que se pueden ejecutar en el pozo (desde simples escariaciones y limpiezas hasta intervenciones mayores, como fracturamientos).

Palabras clave: *curvas de influjo, efecto de daño, pruebas de producción, curvas de salida, curvas características de producción, caracterización del yacimiento, declinación de la producción.*

Introduction

The different operations performed during drilling affect the initial stability of a reservoir, altering the walls of the hole and thereby causing the pressure to fall in abnormal increments. During this stage, the mud from drilling causes a decrease in the permeability

of the formation due to suspended solids and the concrete coating on the walls of the hole. The piping cementations and cement slurry invade the pours of the formation, changing the original conditions. Even when cleaning the wells after drilling in order to restore the original conditions of the formation, a complete cleaning is sometimes not possible. Changes to the formation result in reduced permeability which decreases productivity. Evinger and Muskat (1942) and Horner (1951) analyzed the behavior of abnormal decreases in pressure in wells with respect to their production, finding a relationship with production characteristics. This led to the introduction of the concept of damage to explain the reduction in permeability caused by the blockage of the formation as a result of the mud coating. The effect of the coating on the wall of a well is similar to that of a thin film such as skin, and therefore Evinger and Muskat named this the "skin effect."

Knowledge about the damage of a well has practical applications to planning interventions in wells such as cleanings, repairs, stimulations and chemical treatments, among others. The objective of undertaking any of these actions is to improve production. During continuous exploitation, damage occurs from incrustations, precipitation of salts, migration of solids from the formation to the well. Problems also exist such as partial penetration in the production stratum, mechanical failures, non-Darcian flow near the well, etc. (Liu and Masliyah, 1996; Hartmann and Beaumont, 1999; Valdez-Pérez *et al*., 2013).

Theoretical Concepts About the Damage Effect

The traditional expression used to calculate the damage factor value based on the analysis of pressure transients was initially proposed by Horner (1951). Accordingly, the damage effect is based on the presión de fondo fluyendo (p_{wf}), initial pressure (p_i), the slope of the semi-logarithmic graph of time versus p_{wf}, the duration time of the test (t), the permeability of the formation (k), porosity (ϕ), fluid viscosity (μ) and the well's radius(r_w). The curve characteristic of the well is constructed based on discharge or production tests, and is used to describe it and design its efficient exploitation. The curve characteristic of production is particular to each well and is associated with a particular time during its operating life. Based on the behavior of each characteristic curve, a possible decrease in its parameters is identified, according to which the existence of damage can be inferred. Gilbert (1954) describes the development of the technique to characterize the well using data from discharge tests. Weller (1966) demonstrates the incorporation of results from simulating well profiles and Vogel (1968) incorporates the inflow relationship using dimensionless variables (P_D and Q_D). With $p_D = (p_{wf})/p_e$ and $Q_D = Q_o/(Q_o)_{\max}$, where P_D is the dimensionless pressure, p_{wf} is the presión de fondo fluyendo, p_e is the reservoir pressure, Q_D is the dimensionless mass flow, Q_o is the mass flow and $(Q_o)_{\max}$ is the maximum mass flow during the time of the discharge test. Using dimensionless variables, Vogel (1968) proposed the inflow relationship whose expression as a function of Q_D is:

$$p_D = 0.9646 - 0.1939(Q_D) - 0.7021(Q_D)^2 \quad (1)$$

Different authors have proposed their respective inflow relationship assuming particular considerations (Standing, 1970; Fetkovich, 1973; Klins and Majcher, 1992; Klins and Clark, 1993; Wiggins, 1994, among others). Klins and Majcher (1992) analyzed petroleum systems and proposed the introduction of damage variables that influence the behavior of the inflow relationship.

For geothermal systems, different authors (Goyal *et al*., 1980; Garg and Kassoy, 1981; James, 1989; O´Sullivan *et al*., 2005; Grant and Bixley, 2011, among others) used the outflow curves as tools to characterize wells.

The characteristic production curves show the flow behavior with respect to pressure. Iglesias and Moya (1990) proposed the

dimensionless inflow curve for geothermal systems, considering fluid to be pure water. The development of this technique led to considering new geothermal fluid conditions, first as a binary system H_2O-CO_2 (Moya *et al*., 1997) and later as a mixed ternary H_2O-CO_2-NaCl (Meza, 2005), whose representative expression is:

$$p_D = 0.993 - 0.16(W_D) - 2.08(W_D)^2 + 3.95(W_D)^3 - 2.70(W_D)^4 \quad (2)$$

In order to incorporate the effect of damage in the inflow relationships of geothermal systems, Aragón *et al*. (2008) proposed a relationship considering the characteristics of geothermal systems. These characteristics are viscosity, enthalpy and the fluid density, in addition to the geometry of the well and the reservoir. The expression is:

$$M = \left(\frac{ln\frac{r_e}{r_w} - 0.6603}{ln\frac{r_e}{r_w} - 0.6603 + s} \right) \quad (3)$$

Geothermal Inflow Relationships Affected by Damage

Combining equations (2) and (3), the geothermal inflow relationship affected by damage is obtained:

$$p_D = M\left\{0.993 - 0.16(W_D) - 2.08(W_D)^2 + 3.95(W_D)^3 - 2.70(W_D)\right\}^4 \quad (4)$$

Using different damage values, equation (4) results in the damage-affected type-curve (Figure 1) used to determine this effect with production data from geothermal wells. The measurements (pressure, flow, temperature) are obtained from surface conditions. To use inflow relationships , these parameters need to be calculated for bottom conditions.

Application of the Type-Curve for Geothermal Inflow to Field Cases

To demonstrate the applicability of the methodology proposed, discharge test data were used from wells in the geothermal fields Los Azufres (Michoacán) and Cerro Prieto (northern Baja California). Los Azufres field is located in a volcanic system and the Cerro Prieto in a system of sandy formations (Figure 2). The data from the measurements in Los Azufres (Michoacán) correspond to wells Az-13 and Az-38 (Hiriart and Gutiérrez-Negrín, 1998). The production measurements from surface to bottom conditions were transformed using the simulation program *WELLSIM* (PBPower, 2005) for flows in wells.

The production of the wells was measured at the beginning of exploitation and during different stages of their operating life. Figure 3 shows the curves characteristic of production for Az-13. The values of the dimensionless variables (W_D, P_D) were calculated for each one of the points measured during discharge

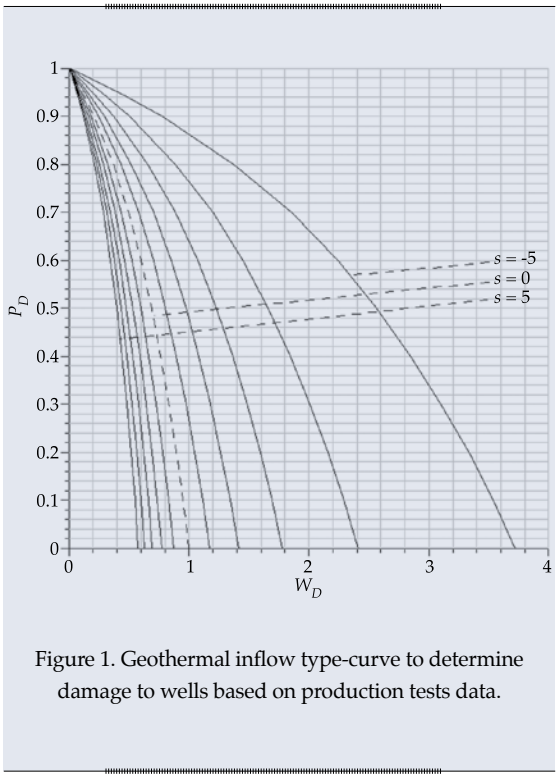

Figure 1. Geothermal inflow type-curve to determine damage to wells based on production tests data.

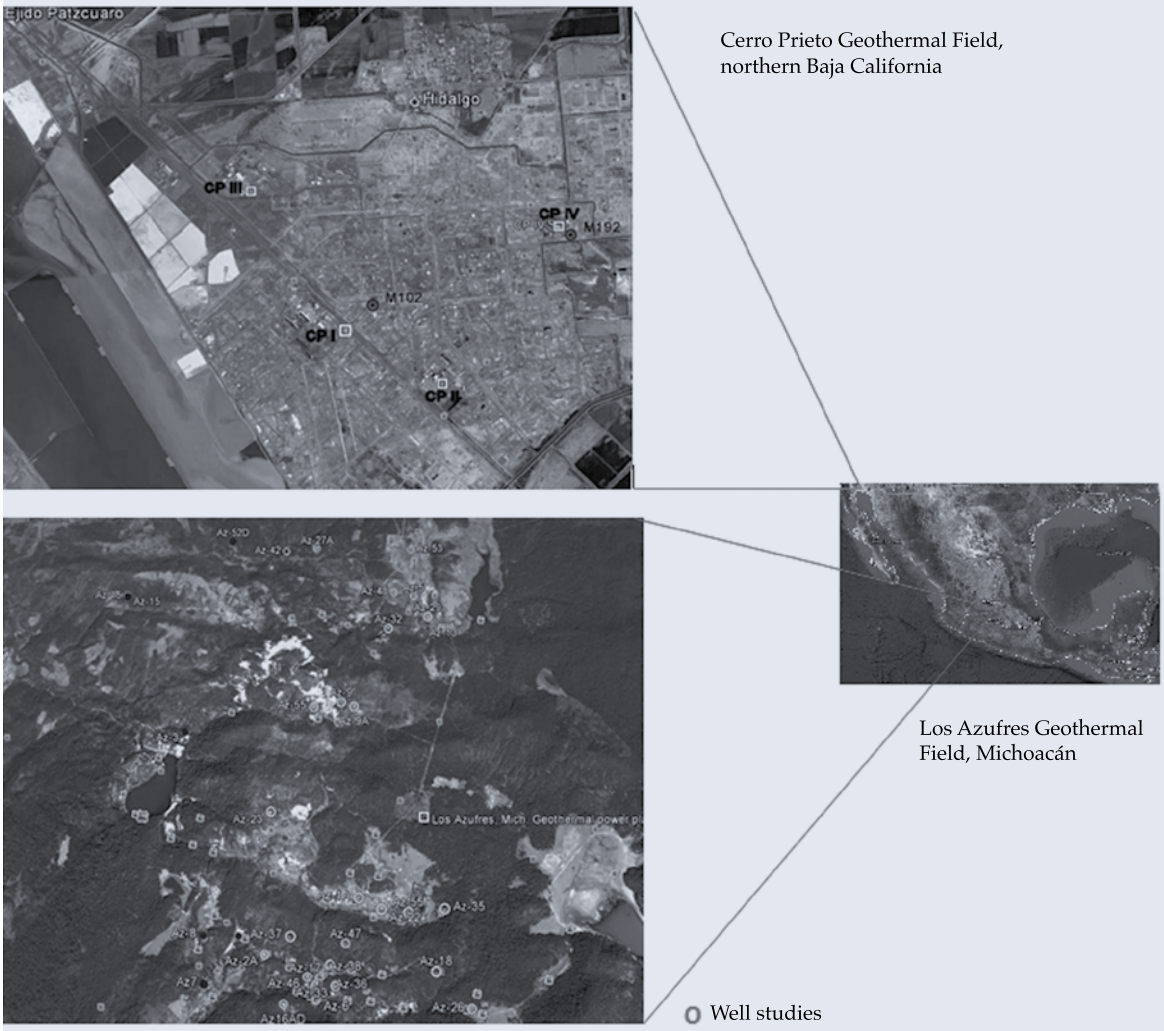

Figure 2. Location of Geothermal Fields Cerro Prieto, northern Baja California and Los Azufres, Michoacán, and the respective wells analyzed.

tests and were graphed in the geothermal type-curve for inflow affected by damage.

The damage is determined by identifying the curve on which the dimensionless values of the well (W_D, P_D) are located, obtained from the discharge test (Figure 4). Once damage is determined, its value is generally observed to increase during the operating life, which is also related to the exploitation time. The same procedure was applied to measuring wells Az-38 and M-102 and M-192 in the Cerro Preito field (Mexico) (Ribó, 1989) during different exploitation stages.

Discussion of Results

Table 1 shows a summary of the results obtained, in which a percentage decrease can be observed in the flow and pressure of the well at each stage of its operating life, as well as an increase in the damage value.

The negative damage value determined in the wells, mainly during initial conditions, indicates the existence of beneficial conditions due to cleaning the well after drilling is completed. The damage values that were determined indicate an increase throughout

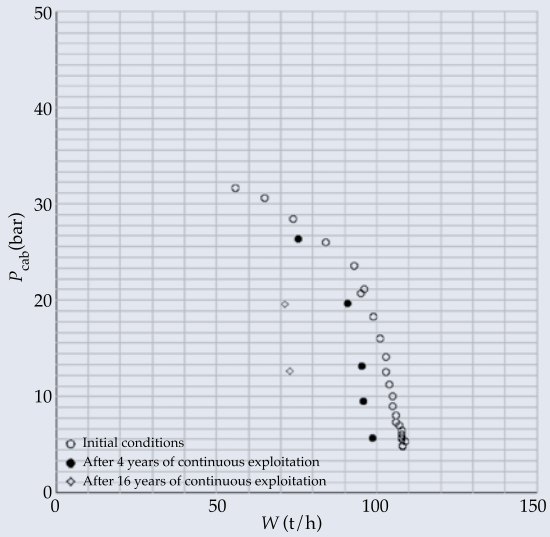

Figure 3. Production curves for well Az-13 in the Los Azufres Geothermal Field, Michoacán, Mexico, during initial conditions and with 4 and 16 years of continuous exploitation.

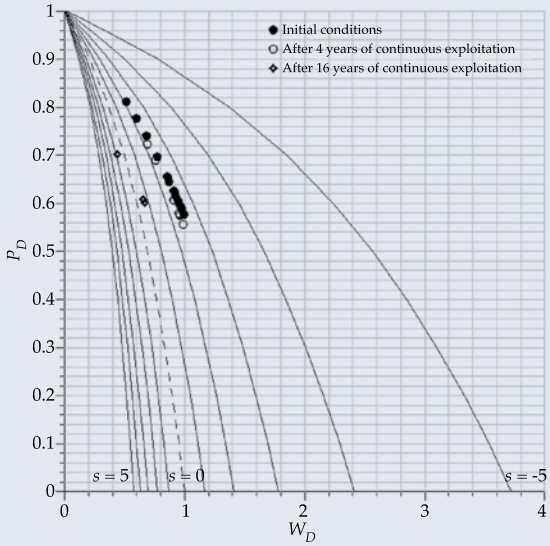

Figure 4. Demonstration of the use of the geothermal inflow type-curve to determine damage effects using production measurements data for well Az-13 (Hiriart and Gutiérrez-Negrín, 1998) in the Los Azufres geothermal field, Michoacán Mexico.

the operating life, which is directly related to exploitation time. Both parameters (damage effect and exploitation time) are inverse functions of the productivity of the well and directly related to its decline.

Conclusions

The innovativeness of the methodology proposed is the use of data from production measurements to calculate damage, which provides an advantage to monitoring reservoirs and wells in commercial power systems by preventing the need to retire them from continuous exploitation systems.

The geothermal inflow type-curve affected by damage makes it possible to determine the well's damage value according to the time in which discharge tests are conducted.

The increase in the numerical damage value determined for the selected wells is directly related to exploitation time, which is related to the decline in the productivity of the well.

The methodology enables determining the damage at different times during the productive life of a well. These results provide a technical basis for make decisions about possible interventions in the well in order to stop or decrease its decline in productivity and/or improve its productive characteristics.

Acknowledgements

The authors would like to express their thanks to the authorities at Investigaciones Eléctricas and the Federal Electric Commission for their support to conduct the present work.

Received: 27/08/10
Accepted: 30/05/13

References

ARAGÓN, A., MOYA, A.S., and GARCÍA-GUTIÉRREZ, A. Inflow performance relationships in geothermal and petroleum reservoir engineering: A review of the state of the art. *Geothermics*. Vol. 37, 2008, pp. 635-650.

Table 1. Results from Parameters Obtained with the Method Used, which characterizes the behavior of each well analyzed.

Well	Exploitation time (years)	$W_{máx}$ (t/h)	P_{yac} (bar)	Decrease (%)		*s* (Damage value)
				$W_{máx}$	P_{yac}	
Az-13	0	108	36.7			-2.1
	4	96	34.3	11.11	6.54	-1.9
	16	85	32.1	21.30	12.53	0.5
Az-38	0	167	49.4			-2.9
	11	126	38.1	24.55	22.87	-2
M-102	0	270	221			-0.7
	2	235	200	12.96	9.50	0
M-192	0	335	395			-3.5
	3	305	200	8.96	49.37	-1.4

EVINGER, H.H. and MUSKAT, M. Calculation of theoretical productivity factor. *Trans., AIME*. No. 146, 1942, pp. 126-139.

FETKOVICH, J.J. *The isochronal testing of oil wells. SPE 4529.* SPE 48th Annual Fall Meeting, Las Vegas, Nevada, USA, 1973, pp. 78-84.

GARG, S.K. and KASSOY, D.R. *Convective heat and mass transfer in hydrothermal and geothermal systems: Principles and case histories*. Rybach, L. and Muffler, L.J.P. (editors). New York: John Wiley and Sons Ltd., 1981, 565 pp.

GILBERT, W.E. *Flowing and gas-lift well performance. Drilling and Production Pract.* Los Angeles, USA: API, 1954, 126 pp.

GOYAL, K.P., MILLER, C.W., and LIPPMANN, M.J. Effect of measured wellhead parameters and well scaling on the computed downhole conditions in Cerro Prieto wells. *Procedure, 6th Workshop on Geothermal Reservoir Engineering*. Stanford University, California, USA, 1980, pp. 130-138.

GRANT, M.A. and BIXLEY, P.F. Geothermal reservoir engineering. Second edition. New York: Academic Press Imprint Elsevier, 2011, 378 pp.

HARTMANN, D.J. and BEAUMONT, E.A. *Predicting reservoir system quality and performance*. Chapter 9, Treatise of Petroleum Geology: Exploring for oil and gas traps. Special volumes. Tulsa, USA: American Association of Petroleum Geologist, 1999, pp. 9.1-9.154.

HIRIART, L.G. y GUTIÉRREZ-NEGRÍN, L.C. Resultados de la explotación geotérmica en México, en 1997. *Geotermia, Revista Mexicana de Geoenergía*. Vol. 14, núm. 2, 1998, pp. 71-77.

HORNER, D.R. Pressure build-up in Wells. *Procedures, Third World Petroleum Congress*. The Hague, Netherlands: Section II, E.J. Brill Leiden, 1951, pp. 503.

IGLESIAS, E.R. and MOYA, S.L. Geothermal inflow performance relationships. *Geothermal Resources Council Transactions*. Vol. 14, part II, 1990, pp. 1201-1205.

JAMES, R. One curve fits all. *Procedures, 14th Workshop on Geothermal Reservoir Engineering*. Stanford University, California, USA, 1989, pp. 329-334.

KLINS, M.A. and MAJCHER, M.W. Inflow performance relationships for damaged or improved wells producing under solution-gas drive. *Journal Pet. Tech.* SPE-AIME, Paper SPE 19852, Vol. 44, No. 12, 1992, pp. 1357-1363.

KLINS, M.A. and CLARK, L. An improved method to predict future IPR curves. *SPE Reservoir Engineering*. Vol. 8, No. 4, 1993, pp. 243-248.

LIU, S. and MASLIYAH, J.H. *Principles of single phase flow through porous media*. Chapter 5, Advances in Chemistry Series 251. Schramm, L.L. (editor). American Chemical Society, Washington, D.C., 1996, pp. 227-286.

MEZA, C.O. Efecto de la precipitación de sales en el diagnóstico de permeabilidades rocosas. Tesis de maestría. Cuernavaca, México: Centro Nacional de Investigación y Desarrollo Tecnológico, Secretaría de Educación Pública, 2005, 107 pp.

MOYA, S.L., ARAGÓN, A.A., and GONZÁLEZ, L. Estimation of production characteristics curves of geothermal wells, using two performance inflow dimensionless reference curves. *Hydraulic Engineering in México*, Vol. XII, No. 3, 1997, pp. 35-40.

O´SULLIVAN, M.J., CROUCHER, A.E., ANDERSON, E.B., KIKUCHI, T., and NAKAGOME, O. An automated well-test analysis system (AWTAS). *Geothermics*. Vol. 34, 2005, pp. 3-25.

PBPOWER. *WELLSIM, Software package*. Auckland, New Zealand: Geothermal Resources, 2005, http://software.pbpower.net/.

RIBÓ, M.O. Análisis de pruebas de presión en pozos de Cerro Prieto. *Proceedings, Symposium in the Field of Geothermal Energy*. San Diego, Estados Unidos: Convenio entre la Comisión Federal de Electricidad y el Departamento de

Energía de los Estados Unidos de Norteamérica, 1989, pp. 123-129.

STANDING, M.B. Inflow performance relationships for damaged wells producing by solution-gas drive. *Journal Pet. Tech.* Vol. 22, No. 11, 1970, pp. 1399-1400.

VALDEZ-PÉREZ, A.R., PULIDO, H., CINCO-LEY, H., and LARSEN, L. A new double porosity fractal model for well test analysis with transient interporosity transference for petroleum and geothermal systems. *Procedures, 38th Workshop on Geothermal Reservoir Engineering*. Stanford, California, USA, 2013, 12 pp.

VOGEL, J.V. Inflow performance relationships for solution gas drive Wells. *Journal Pet. Tech.* SPE 1476. Annual Fall Meeting of Society of Petroleum Engineers, Dallas Texas, USA, 1968, pp. 66-79.

WELLER, W.T. Reservoir performance during two-phase flow. *Journal Pet. Tech*. Paper SPE 1334, Vol. 18, No. 2, 1966, pp. 240-246.

WIGGINS, M.L. *Generalized inflow performance relationships for three-phase flow*. Oklahoma City, USA: SPE Production Operation Symposium, (SPE 25458), 1994, pp. 275-286.

Institutional Address of the Authors

Dr. Alfonso Aragón Aguilar
Dra. Georgina Izquierdo Montalvo
M.I. Víctor Arellano Gómez

Instituto de investigaciones Eléctricas
Calle Reforma 113, Colonia Palmira
62490 Cuernavaca, Morelos, México
Teléfono: +52 (777) 3623 811, extensión 7329
aaragon@iie.org.mx
gim@iie.org.mx
vag@iie.org.mx

Click here to write the autor

Measurement of infiltration, La Laja, Diguillín, Chile.

Photo provided by José Luis Arumí Ribera.

Technical Note

A Methodology for Concerted Water Allocation (CONWA)

• Julio César Jesús-Salazar* • Jesús Abel Mejía-Marcacuzco
Universidad Nacional Agraria "La Molina", Perú
*Corresponding Author

Abstract

JESÚS-SALAZAR, J.C. & MEJÍA-MARCACUZCO, J.A. A Methodology for Concerted Water Allocation (CONWA). *Water Technology and Sciences* (in Spanish). Vol. V, No. 1, January-February, 2013, pp. 161-170.

In recent decades, many models have been developed for simulation and mathematical optimization to solve the complexity of cross of natural and social variables domain for an integrated water resources management (IWRM); unfortunately, most of these applications do not incorporate the concept of equity in their quantitative estimates. This situation represents a limiting factor in the balance of resolution of conflicts over water use. This paper presents the methodology applied in a tutorial project of a pilot watershed, to develop a tool for integrated water resources management incorporating into a single architecture three fundamental components: *Equity*, Sustainability and *Efficiency*. The methodology for concerted water allocation (CONWA) has two stages: 1) assigns initial water use rights using a river basin node-link network and three allocation methods: the priority-based multiperiodo maximal network flow programming, modified riparian water rights allocation and lexicographic minimax water shortage ratios. 2) The second stage reassigns the rights to achieve efficient use of water through transfers of value; the reallocation of the net profit associated is carried out by applying the theory of Cooperative Games. This method was applied in a CHVS tutorial watershed, comprising four sub basins of a Pilot Regional Government, yielding high net benefits under simulated participation of a large alliance of actors.

Keywords: concerted allocation, reallocation, water use rights, water management.

Resumen

JESÚS-SALAZAR, J.C. & MEJÍA-MARCACUZCO, J.A. A Metodología para la asignación concertada de agua (MACA). *Tecnología y Ciencias del Agua*. Vol. V, núm. 1, enero-febrero de 2014, pp. 161-170.

En las últimas décadas se han desarrollado muchos métodos de simulación y optimización matemática para resolver la complejidad del cruce de variables de los dominios natural y social que permita gestionar de manera integral el agua; desafortunadamente, la mayoría de estas aplicaciones no incorporaron en sus cálculos el concepto de equidad. Tal situación representa un factor limitante en el balance de resolución de conflictos. Este artículo presenta la metodología aplicada a un proyecto piloto en una cuenca hidrográfica tutorial como herramienta de gestión integrada de recursos hídricos, e incorpora en una sola arquitectura tres componentes fundamentales: equidad, sostenibilidad *y* eficiencia. *La Metodología para la Asignación Concertada de Agua (MACA) se desarrolla en dos etapas: 1) asigna los derechos iniciales sobre el uso de agua, utilizando una red de trabajo nodo-enlace de la cuenca hidrográfica y tres procedimientos de asignación: Programación Multiperiodo Priorizado del Caudal Máximo de la Red, Ribereño Modificado de Asignación de Agua y Lexicográfico MiniMáx de Ratios de Sequía. 2) En la segunda etapa se reasignan los derechos hasta lograr el uso eficiente del agua a través de transferencias de valor; mediante la Teoría de Juegos Cooperativos se logra el beneficio neto asociado con el valor del agua. Este método, aplicado en una cuenca hidrográfica tutorial CHVS, comprendió cuatro subcuencas de un Gobierno Regional Piloto, obteniéndose altos beneficios netos en el marco de la participación, en alianza simulada de actores y escenarios.*

Palabras clave: *asignación concertada, reasignación, dere-chos de agua, valor del agua.*

Introduction

Water rights in developing countries may be allocated (Bruns *et al*., 2005; Koehler, 1995) according to three fundamental overall doctrines: riprarian rights, prior appropriation rights and public allocation rights. Over recent decades, many simulation and mathematical optimization models have been developed to improve the variables in the natural and social domains

(NSD) (Figure 1) (Grigg, 2005). Three natural variables related to water must be recognized¾ amount (A), quality (Q) and ecosystem flows (F)¾ whose interdependence and feedback can lead to restrictions and conflicts (Coplin and O'leary, 1974). The inherent and multi-faceted restrictions in a natural water system cannot be easily separated from social variables such as social values and norms (V), economy (E) and governability (G), which interact in a variety of ways, creating contextual differences that are often unsolvable (Islam and Susskind, 2013).

Unfortunately, most of these applications do not incorporate concepts of equity in their quantitative calculations (Dinar, 2001). The majority are allocated using non-zero sum criteria, creating conflicts in many cases (Becker and Ester, 1999). In addition, both minimum-cost network flow and linear programming lack formal systemic methods to set appropriate coefficients for unit costs (Aadland and Koplin, 2004) and assurances that water is allocated according to priorities, which can be observed when including return flows, ecological flows (Dinar and Howitt, 1997) and storage reservoir rights, since they can be used again by secondary users downstream.

Most of the studies were produced between 2000 and the present, with the focus of increasing efficiency and effectiveness in water resources management and centered on economic and market mechanisms (Dinar *et al.*, 2003; Islam and Susskind, 2013) to promote effectiveness. Fisher *et al*. (2002) argue that water markets are not really free and competitive markets but rather are usually regulated by the government and lack specific and independent sellers and buyers. In addition, in a free market with efficient allocation, social costs should coincide with private costs, and social benefits should be aligned with private benefits. Nevertheless, the use of water produces "externalities" which impact the amount and quality of water for other users, which is still not managed in a comprehensive manner.

In addition, typical individual costs and benefits do not apply to these externalities (Crossmit and Green, 1982; Dickinson and Heaney, 1982). On the contrary, social costs increases. Water policies (Coplin and O'leary, 1983) in many countries demonstrate that they consider the public value of water more important than the private value for certain uses (often agriculture), but at much lower costs. While water markets do not automatically function according to optimal social allocations, economical optimization methods can be constructed to guide policies and water allocation in order to obtain optimal social benefits (Dinar *et al*., 1986). To achieve sustainable development and a secure society, institutions using water allocation methodologies must be modernized by water

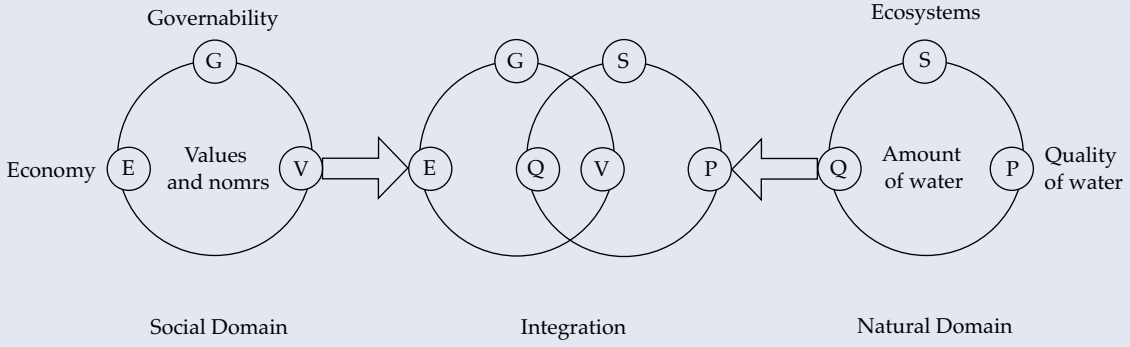

Figure 1. Natural and Social Domains in the Process to Allocate Water.

scarcity regions and consider water not as only public good or a private good but rather a combination of both.

The purpose of this work is to design a basic methodology for concerted water allocation (CONWA) similar to a non-zero sum game for water values (Caswell and Frisvold, 2000).

Methodology

CONWA is a general application for equitable, sustainable and efficient allocation of water resources in a hydrographic watershed, which is based on a node-link network representing the watershed, whose configuration is presented in Figure 2. The methodology is composed of two general stages (see figure 3).

Stage 1. Allocation of Initial Rights

This includes priority-based maximal multiperiod network flow programming, modified riparian water rights allocation and lexicographic minimax water shortage ratios to determine the allocation rights for initial water use based on competition (Dinar *et al.*, 1997). Priority-based maximal multiperiod network flow programming is very flexible and applicable to prior appropriation, riprarian and public water rights systems. Modified riparian water rights allocation is essentially a special type of the former, adapted to allocate water downstream in a river regime. Lexicographic minimax water shortage ratios is applicable to a public water rights system and adopts the concept of minimal lexicographic equity.

Stage 2: Reallocation of Water Use and Net Benefits

This includes the use of information from hydrological data, demand data and initial water rights, as well as water resources usage plans from which the corresponding net benefits are extracted. During this stage, alliances are produced between actors and users of the initial rights to equitably, sustainably and efficiently achieve concerted water allocation. Information from plans for a watershed

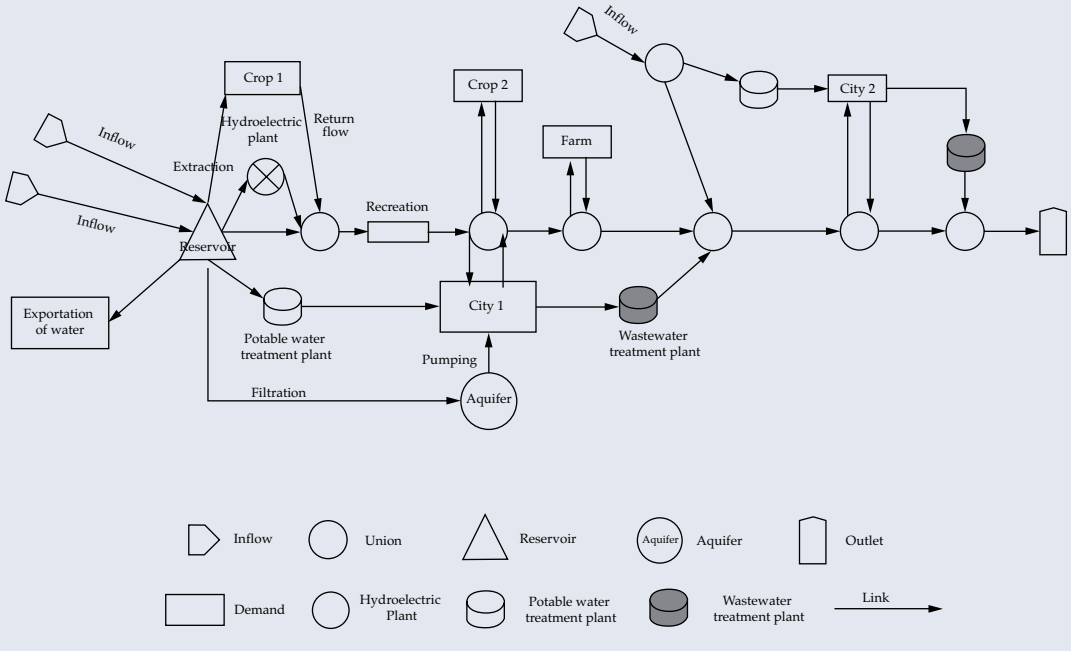

Figure 2. Example of a Hydrographic Watershed Network.

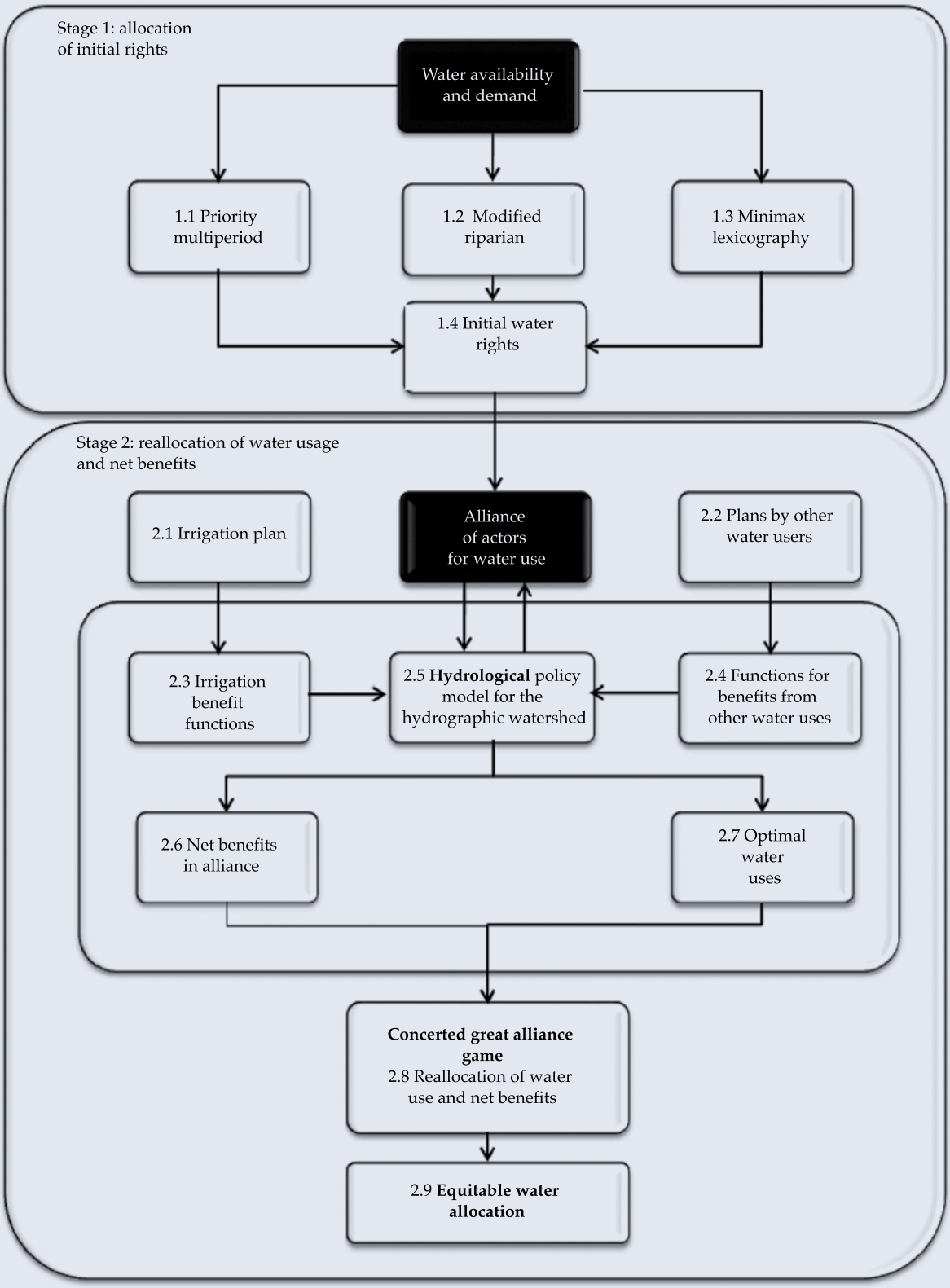

Figure 3. Flow Diagram for the Concerted Water Allocation (CONWA)Methodology.

network are inputted into the Hydrological Policy Model of the Hydrographic Watershed (HPMHW), with which uses and benefits are analyzed to determine optimal water allocation schemes and their net benefits jointly among allies.

In order to eliminate conflicts among actors over water usage, water reallocation and net benefits are adopted that result in a large alliance through the application of Cooperative Game Theory (Barret, 1994; Becker and Easter, 1991; Aumann and Dréze, 1974). The economically efficient use of water downstream from the large alliance is achieved by reallocating water according to initial water rights and the applied methods (Dinar *et al*., 2002).

Restricciones y balances

Existen tres tipos de restricciones en el método de asignación concertada del agua: (1) *restricciones del dominio natural,* (2) *restricciones políticas* y (3) *restricciones de control*. En su formulación se realizan algunos supuestos básicos.

Restricciones del dominio natural

Restrictions and Balances

Three types of restrictions exist in the method for concerted water allocation: (1) natural restrictions, (2) policy restrictions, and (3) control restrictions. Certain basic hypothesis were developed for their formulation.

Natural Restrictions

Natural restrictions occur due to mass balances and capacity limits. Figure 4 shows the balance for a general node.

Balance and pollution equations for a general node k during each period t are represented as:

$$S(k,t)-S(k,t-1)=\sum_{(k_1,k)\in L}Q(k_1,k,t)-\sum_{(k_1,k)\in L}Q_1(k_1,k,t)+Q_g(k,t)-Q_c(k,t)-\sum_{(k,k_2)\in L}Q(k,k_2,t)\;\forall k\in V \quad (1)$$

$$C_p(k,t)S(k,t)-C_p(k,t-1)S(k,t-1)=\sum_{(k_1,k)\in L}C_p(k_1,k,t)Q(k_1,k,t)-\sum_{(k_1,k)\in L}Z_{pl}(k_1,k,t)+Z_{pg}(k,t)-Z_{pc}(k,t)-\sum_{(k,k_2)\in L}C_p(k,k_2,t)Q(k,k_2,t),\forall k\in V \quad (2)$$

where t is the time period index (amplitude of the period is Δt), $t \in T = \{1, 2, ..., t\}$ (τ is the longest index for the periods); $S(k,t)$ is the storage volume of the storage node (reservoir or aquifer) $k \in STO$ at the end of period t; $Q(k_1, k, t)$ represents the flow from node k_1 to k *during period* t; $Q_1(k_1, k, t)$ represents the transport loss due to evaporation, leaks and flow filtrations

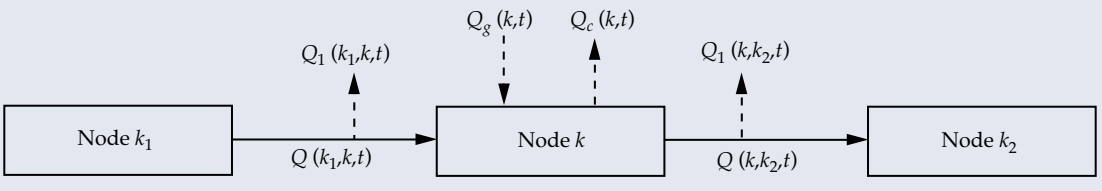

Figure 4. Balance of natural variables at general node k.

from node k_1 to k; $Q_g(k, t)$ is the gain from adjusting the inflow at node k during period t for discharges from small tributaries, local catchment drainage, filtrations in the section of the river or other flow sources; $Q_c(k, t)$ is the water consumed at node k by economic activities and evaporation; p is the index of pollutant types, $p \in P = \{1, 2, \ldots, x\}$ (ξ the largest pollutant index); $C_p(k, t)$ is the concentration of the pollutant p at storage node k at the end of period t; $C_p(k_1, k, t)$ represents the concentration of the pollutant p in the flow from node k_1 to k during period t; $Z_{pl}(k_1, k, t)$ represents the transport loss of pollutant p in the flow from node k_1 to k; $Z_{pg}(k, t)$ is the total amount of the pollutant p added at node k during period t due to the adjustment in the inflow $Q_g(k, t)$ and water use activities; $Z_{pc}(k, t)$ represents the elimination of the pollutants p at node k; and $S(k, t) = 0$, $\forall\, k \in V \setminus STO$.

For the source node $k \in IN$, the total inflow received from outside the fluvial network is represented as $Q_{IN}(k, t)$, while $Q(k_1, k, t)$ represents the flows from other nodes to k. For outflow node $k \in OUT$, the total outflow from node k outside the fluvial network is represented as $Q_{OUT}(k, t)$ and $Q(k, k_2, t)$ no longer exists. Though the storage units are not indicated throughout this work, they are Hm^3 (hectare-meter cubed), MMC (million meters cubed equivalents), g/l (concentration and discharge) and kton (thousands of tons).

Policy Restrictions

Policy restrictions represent a combination of hydrological, economic and social variables produced when allocating water rights. Typical policy restrictions are related to limits on demand at the nodes, storage or links, as well as capacity limits, consisting of upper and lower storage and flow limits, such as:

Minimal flow from k_1 to k:

$$Q(k_1,k,t) \geq Q_{\min}(k_1,k,t)\,\forall(k_1,k) \in L \qquad (3)$$

Maximum total inflow at a demand node j:

$$\sum_{(k_1,j)\in L\setminus L_{Seep}} \left(1-e_L(k_1,j,t)\right)Q(k_1,j,t) \leq \max\left(Q_D(j,t)-Q_a(j,t),0\right) \quad \forall j \in AGR \cup MI \cup HPP \qquad (4)$$

Minimum volume of a storage node k:

$$S(k,t) \geq S_{\min}(k,t)\,\forall k \in RES \cup AQU \qquad (5)$$

Minimum outflow at an outlet:

$$Q_{out}(k,t) \geq Q_{out\min}(k,t), \forall k \in OUT \qquad (6)$$

Maximum concentration of pollutant p at a link (k_1, k):

$$C_p(k_1,k,t) \leq C_{p\max}(k_1,k,t), \forall (k_1,k) \in L \qquad (7)$$

Maximum concentration of a pollutant p mixture in the inflow at a non-storage node k:

$$0 \leq C_{pN}(k,t) \leq C_{pN\max}(k,t), \quad \forall k \in V \setminus (RES \cup AQU) \qquad (8)$$

Maximum concentration of pollutant p at a storage node k:

$$C_p(k,t) \leq C_{p\max}(k,t), \forall k \in RES \cup AQU \qquad (9)$$

Maximum concentration of a pollutant p in the outflow at an outlet:

$$C_{pout}(k,t) \leq C_{pout\max}(k,t), \forall k \in OUT \qquad (10)$$

where $Q_D(j, t)$ is the total demand for water by a demand node j, and $C_{pN}(k, t)$ is the pollutant p mixture in the inflows at a non-storage node k, satisfying:

$$C_{pN}(k,t)\left[Q_a(k,t)+\sum_{(k_1,k)\in L}\left(1-e(k_1,k,t)\right)Q(k_1,kt)\right]$$
$$=C_{pa}(k,t)Q_a(k,t)$$
$$+\sum_{(k_1,k)\in L}\left(1-e_{pL}(k_1,k,t)\right)C_p(k_1,k,t)Q(k_1,k,t),$$
$$\forall k\in V\setminus(RES\cup AQU) \qquad (11)$$

Note: water quality restrictions will be used very cautiously and only when necessary, since imposing strict restrictions may be inappropriate or result in unfeasible solutions.

Control Restrictions

Sometimes using only restrictions on variables in the natural and policy domains does not completely restrict the solutions as they exist in the real world because of the simplified abstraction of the river network and the hydrological and socioeconomic processes. To compensate for this, restrictions on the control of the system are used. For example, if $SRC\in V\setminus STO$ is the set of non-storage nodes that are simplified to provide water supply to some of the demand sites and receive return flows from them, then the total inflow at any node $k\in SRC$, *excluding return flows, must exceed the total corresponding bypasses of k since in the real world those return flows are not available for the bypass of that node. Where j is a water demand node, then:*

$$\sum_{\substack{(k,j)\in L\\ \text{and}\\ (j,k)\in L}}Q(k,j,t)\le Q_a(k,t)+Q_{IN}(k,t)$$
$$+\sum_{(k_1,k)\in L}\left(1-e_L(k_1,k,t)\right)Q(k_1,k,t) \qquad (12)$$
$$-\sum_{\substack{(j,k)\in L\\ \text{and}\\ (k,j)\in L}}\left(1-e_L(j,k,t)\right)Q(j,k,t),\forall k\in(IN\cap SRC)$$

$$\sum_{\substack{(k,j)\in L\\ \text{and}\\ (j,k)\in L}}Q(k,j,t)\le Q_a(k,t)$$
$$+\sum_{(k_1,k)\in L}\left(1-e_L(k_1,k,t)\right)Q(k_1,k,t) \qquad (13)$$
$$-\sum_{\substack{(j,k)\in L\\ \text{and}\\ (k,j)\in L}}\left(1-e_L(j,k,t)\right)Q(j,k,t)\forall k\in SRC\setminus IN$$

Application and Results with the Pilot Watershed

Application

This section presents the application of the methodology to a pilot watershed named Verde Sur Hydrographic Watershed (VSHW), characterized by natural (amount, quality and ecological flow), social (economy or capital, values and governance) and policy variables. This methodology considers the combination of these six variables. The water network is shown in Figure 5. The natural historical flows of the VSHW were calculated based on recorded and adjusted daily flows. The annual average from 1912 to 2011 is 9 000 Hm³, with 17.9, 43.6, 38 and 0.5% in the Naranja, Rojo, Azul and Verde Sur sub-basins, respectively. The uses analyzed included irrigation, domestic, industrial, energy, ecological, and reserves or storage. The net benefit functions for each use was estimated with 50 runs of the application for each case. Six scenarios were designed (A, B, C, D, E and F) according to demands, hydrological conditions and the respective applications.

Results

Stage 1

The results from scenarios A, B and C were obtained with the first run, using the *natural restrictions* with 10 linear programs, each one having 2 615 control variables and 1 620 equations. Then, non-linear balance restrictions on salts were included, for which there were 4

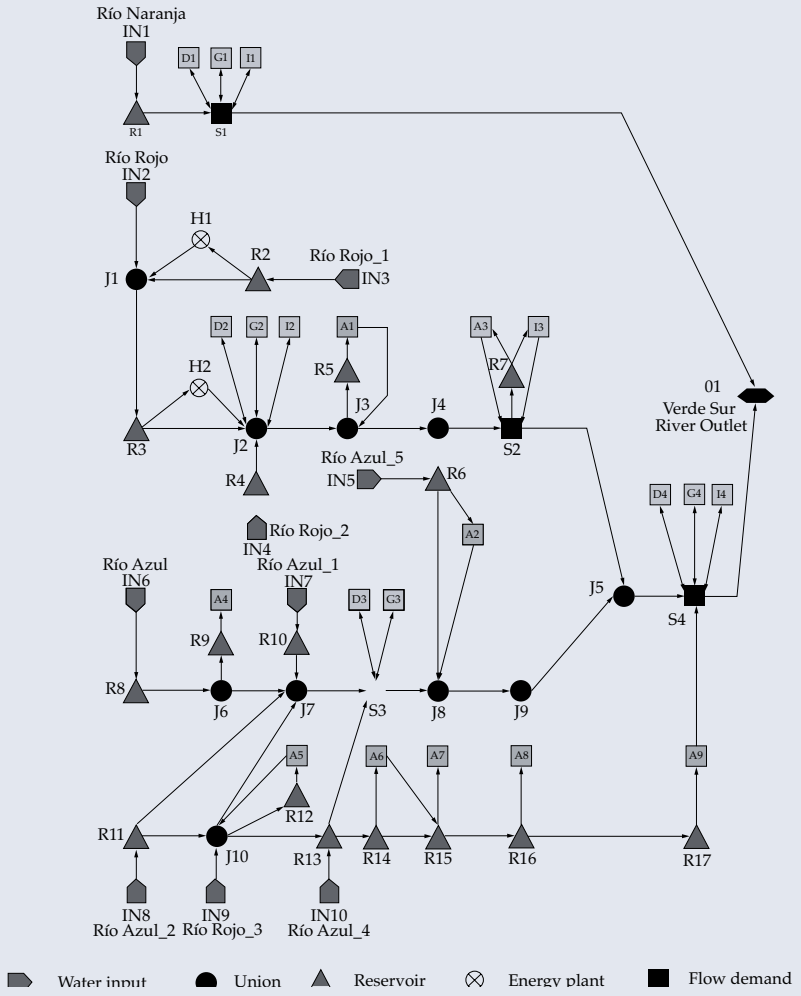

Figure 5. Network, Verde Sur Hydrographic Watershed in GORE Pilot.

523 and 4 212 equations. The final solutions were consistent with the initial values of the concentration of pollutants in the rivers and reservoirs. The scenarios satisfied annual supply/demand rates.

The results for scenarios D, E and F took into account only *natural restrictions* based on the input data. Using Solver parameters and the GAMS algorithm, 180 loops were iterated with 2 098 equations for the first and 1 634 for the second. The final solutions were consistent with the initial values of the concentration of pollutants in the rivers and reservoirs, with 150 iterations and 4 690 equations in the first loop and 4 226 in the last. These scenarios satisfied 80.2% of the annual supply and 93% of the demand rates.

Stage 2

Water usage was grouped into eight actors: (1) City N, (2) Río Rojo Hydrostations, (3) Pilot City, (4) East Industrial Region, (5) Río Rojo Irrigation Region, (6) City SO, (7) Río Azul Irrigation Region and (8) City SE. Because of the scarcity of data, ecological flows and reservoirs were not included. The eight actors included in the hydrological policy model used to apply the methodology to the watershed resulted in 255 alliances. Nevertheless, the

analysis of initial rights and the optimization of scenarios only included four actors¾ (2), (3), (5) and (7)¾ with significant changes in inflows and net benefits. These effects were null or very small for the other four actors. This reduction in actors decreased the alliances to only 15. According to the Solver reports, there were 4 801 control variables, 4 997 restrictions and 5 927 non-linear elements for each alliance. The participation value for each actor in the large alliance was represented as an additional gain over the independent net optimal benefit that could be produced by the initial rights granted.

Conclusion

This article presented a methodology developed to determine the equitable allocation of water for different uses in a pilot watershed. This methodology was implemented in close collaboration with eight actors. It consisted of developing a study of the history of initial allocation with three possible procedures defined by algorithms that balanced water availability and the respective demands, and identifying and modeling the solutions to reduce conflicts.

Data was prepared for a general case in order to characterize water use scenarios pertaining to comprehensive water management and to efficiently, sustainably and equitably allocate the water resource for different uses. It is concluded that each watershed has its own characteristics and, therefore, a single application to manage the allocation of resources does not exist. Rather, allocation requires decision-making that takes into account the flexibility of the resource, adapts to water demand problems and sets aside the view that water is a scarce resource.

Received: 28/05/2012
Accepted: 25/04/2013

References

AADLAND, D. and KOPLIN, V. Environmental Determinants of Cost Sharing. *Journal of Economic Behavior and Organization*. Vol. 53, No. 4, 2004, pp. 495-511.

AUMANN, J. and DRÉZE, J. Cooperative games with coalition structures. *International journal of game theory*. Vol. 3, No. 4, 1974, pp. 217-237.

BARRETT, S. *Conflict and Cooperation in Managing International Water Resources*. Washington, D.C.: Policy Research Working Paper, The World Bank, Policy Research Department, 1994, 1303 pp.

BECKER, N. and ESTER, K. Conflict and Cooperation in Managing International Water Resources such as the Great Lakes. *Land Economics*. Vol. 75, No. 2, 1999, p. 233.

BECKER, N. and EASTER, W. Cooperative and Noncooperative Water Diversion in the Great Lakes Basin. Dinar, A., Loehman, E. (editors). *Water quantity/quality management and conflict resolution: Institutions, processes, and economic analyses*. Westport: Praeger Publisher, 1991, pp. 321-336.

BRUNS, B.R., RINGLER, C., and MEINZEN-DICK, R. *Water Rights Reform: Lessons for Institutional Design*. Washington, D.C.: International Food Policy Research Institute, 2005.

CASWELL, M. and FRISVOLD, G. Transboundary Water Management. Game Theoretic Lessons for Projects on the US-Mexico Border. *Agricultural Economics*. Vol. 24, 2000, pp. 101-111.

COPLIN, W. and O'LEARY, M. Activities of the PRINCE Project. *Policy Studies Journal*. Summer, 1974.

COPLIN, W. and O'LEARY, M. Political Analysis through the PRINCE System. *Learning Packages in the Political Sciences (PS23)*. Public Affairs Program. Syracuse, USA: Syracuse University, 1983.

CROSSMIT, C. and GREEN, D. Water utility costs and rate design for fire protection services. *J. AWRA*. Vol. 74, No. 6, 1982, pp. 270-277.

DICKINSON, R. and HEANEY, J. Methods for Apportioning the Cost of a Water Resource Project. *Water Resources Research*. Vol. 18, No. 3, 1982, pp. 476-482.

DINAR, A. Scale and Equity in water Resource Development: a Nash Bargaining Model. *Natural Resource Modeling*. Vol. 14, No. 4, 2001, pp. 477-494.

DINAR, A. and HOWITT, R. Mechanism for Allocation on Environmental Control Cost: Empirical Tests of Acceptability and Stability. *Journal of Environmental Management*. Vol. 49, 1997, pp. 183-203.

DINAR, A., KANNAI, Y., and YARON, D. Sharing Regional Cooperative Gains from Reusing Effluent for Irrigation. *Water Resources Research*. Vol. 22, No. 3, 1986, pp. 339-344.

DINAR, A., MORETTI, S., PATRONE, F., and ZARA, S. *Applications of Stochastic Cooperative Games in Water Resources*. XV Italian Meeting on Game Theory and Application (IMGTA), Urbino, Italy, 2003.

DINAR, A., RATNER, A., and YARON, D. Evaluating Cooperative Game Theory in Water Resources. In: *Economics of Water Resources: the Contribution of Dan Yaron*. Dinar, A., Zilberman, D. (editors). Kluwer Academic Publisher, 2002, pp. 165-181.

DINAR, A., ROSEGRANT, M.W., and MEINZEN-DICK, R. *Water Allocation. Mechanisms Principles and Examples 1*. World Bank, Agriculture and Natural Resources Department, IFPRI, 1997.

FISHER, F.M., ARLOSOROFF, Z., ECKSTEIN, M., HADDADIN, S., HAMATI, A., HUBER-LEE, A., JARRAR, A., JAYYOUSI, U., SHAMIR, U., and WESSELING, H. Optimal water management and conflict resolution: The Middle East water project. *Water Resources Research*. Vol. 38, No. 11, 2002, pp. 12-43.

GRIGG, N.S. *Water Manager's Handbook. A guide to the water industry*. Aquamedia Publishing, 2005.

ISLAM, S. and SUSSKIND, L.E. *Water Diplomacy*. *RFF Press*. New York: Edwards Brothers, Inc., 2013.

KOEHLER, C. Water rights and the Public Trust Doctrine: Resolution of the Mono lake controversy. *Ecological Law Quarterly*. Vol. 22, No. 3, 1995, pp. 541-590.

Author's address institutional

Dr. Julio César Jesús Salazar
Dr. Jesús Abel Mejía Marcacuzco

Doctorado Recursos Hídricos
Escuela de Post Grado
Universidad Nacional Agraria "La Molina"
Haras De La Molina, Lima, Perú
Teléfono: +51 (1) 3401 180
julio.jesus@iclaro.com.pe

Click here to write the autor

Technical Note

Evaluation of Erosion Process in Varadero Beach, Cuba

• Luis Fermín Córdova-López •
Instituto Superior Politécnico José Antonio Echeverría, Cuba
*Corresponding Author

Abstract

CÓRDOVA-LÓPEZ, L.F. Evaluation of Erosion Process in Varadero Beach, Cuba. *Water Technology and Sciences* (in Spanish). Vol. V, No. 1, January-February, 2014, pp. 171-178.

The effect of extreme events, in particular hurricanes, cause changes in the morphology of the sand beaches and adverse effects from the economic point of view in beaches with high tourist value. The application of a train of mathematical models properly coupled for the generation, propagation of the wave and morphological changes in beaches are applied with the objective of evaluating the morphological changes during the occurrence of the hurricane Michelle (November, 2001) of well-known destructive effect in the Varadero beach, Matanzas, Cuba.

Keywords: beach, erosion, mathematical models, coast.

Resumen

CÓRDOVA-LÓPEZ, L.F. Evaluación del proceso de erosión en la playa de Varadero, Cuba. Tecnología y Ciencias del Agua. *Vol. V, núm. 1, enero-febrero de 2014, pp. 171-178.*

El efecto de eventos extremos, huracanes en particular, trae consigo cambios en la morfología de las playas de arena que provocan efectos adversos desde el punto de vista económico en playas con alto valor turístico. La aplicación de un tren de modelos matemáticos debidamente acoplados para la generación, propagación del oleaje y cambios morfológicos en playas de arena son aplicados con el objetivo de evaluar los cambios morfológicos durante la ocurrencia del huracán Michelle (2001) de conocido efecto destructivo en la playa de Varadero, Matanzas, Cuba.

Palabras clave: *playa, erosión, modelos matemáticos, costa.*

Introduction

The Island of Cuba, situated on the Hicacos penninsula, is the largest of the Greater Antillas, located in the northern Atlantic tropical zone. It is affected annually by hurricanes that cause major disasters. It is vitally important to forecast physical changes to coastlines and determine critical beach areas with high tourism.

The objectives of this investigation were to evaluate the erosion process on Varadero Beach during the passing of Hurricane Michelle from November 4th at 0:00 hours to November 6th at 12:00 UTC, and to define the most critical sectors for analysis by specialists and authorities and for developing future rehabilitation actions.

Materials and Methods

A Coastal and Marine Engineering System (CMES) was applied. The CMES consisted of a coupled and nested mathematical model train which included a field wind generation model associated with hurricanes based on wind parameters proposed by Holland (1980), with its B parameter calibrated by Córdova *et al*. (2012). The WWIII model was used for wave generation on the oceanic scale (Tolman, 2009) and propagation was generated using the SWAN model (Booij *et al*., 2009). Maritime weather information and sea levels represented boundary conditions for the modeling of morphological changes using XBeach (Roelvink, 2010). Figure 1 presents the CMES.

General Characteristics of the Study Area

Varadero Beach is at the northern most end of the island on the northern part of the Hicacos peninsula, located on the northwestern coast of Cuba, 130 km from Havana and 32 km from the city of Matanzas. The peninsula is 22 km long,

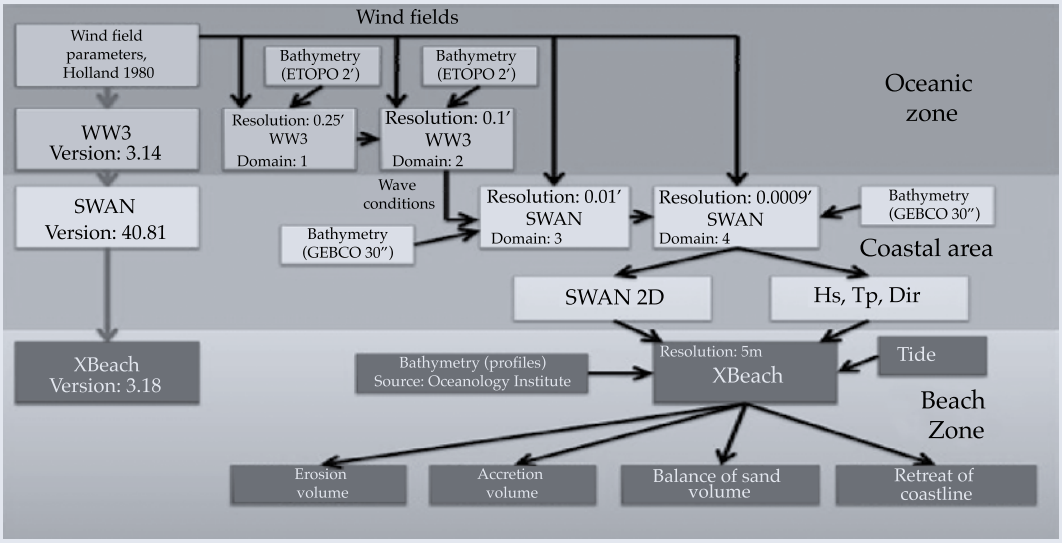

Figure 1. Coastal and Marine Engineering Systems (CMES).

has a maximum width of 500 meters and an azimuth projection (SW-NE) of 70% (Córdova and Torres, 2008; Izquierdo, 2004).

The current income of Varadero is approximately $400 million dollars per year, representing 37% of the total tourism income of Cuba and, therefore, plays an important role in the national economy (Torres, 2007; Van Bentum *et al*., 2010).

Beach Profiles and Bathymetry of the Study Zone

Profile data measured in March 2001 by the Cuba Oceanology Institute were used to conduct this investigation (Figure 2).

Bathymetry

As seen in Figure 2, the bathymetry of Varadero is virtually straight and parallel to the coastline.

It has a shallow submarine slope which progressively decreases towards the northeast due to the widening of the island platform, which begins at the 2/3 of the beach.

Sedimentology

Most of the sand in Varadero Beach consists of 0.25-0-55 mm grains with a mean diameter of 0.26 mm (native sand). Its main source is halimedaalgae.

Sea Levels

The tides at the peninsula have a range of approximately 0.5 m.

FMeteorological Phenomenon Selected for the Study

Hurricane Michelle occurred from October 29 to November 6, 2001. It was the fifteenth tropical depression of the year 2001. It arrived on the Island of Cuba at approximatDefinition of the Study Zone

The zones for the study of the Hicacos peninsula were compared and selected based on profiles presenting similar bathymetric behavior. Figure 3 presents the profiles selected.

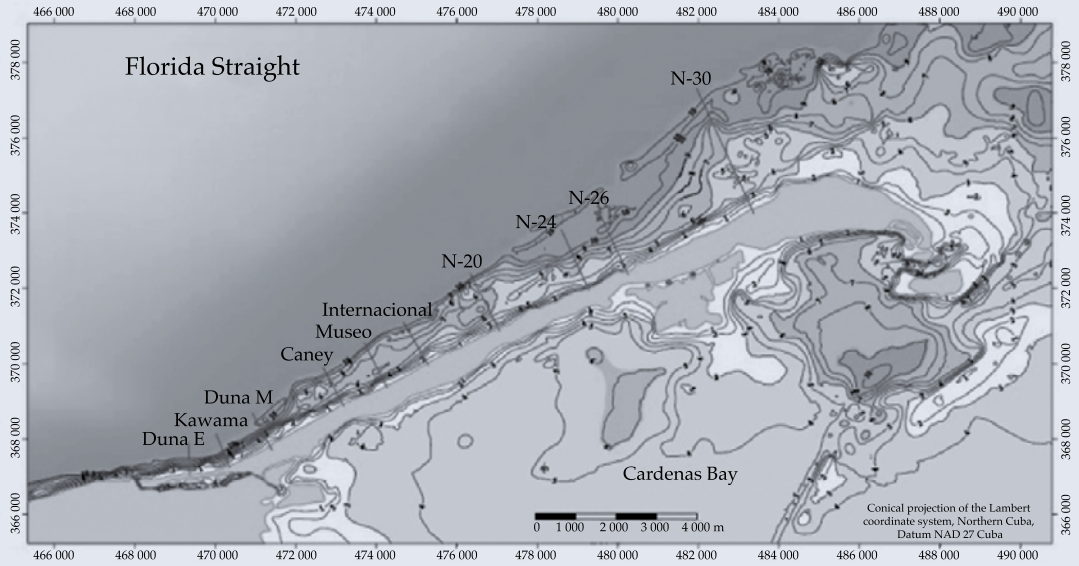

Figure 2. Location of the Profiles Selected (Izquierdo, 2004).

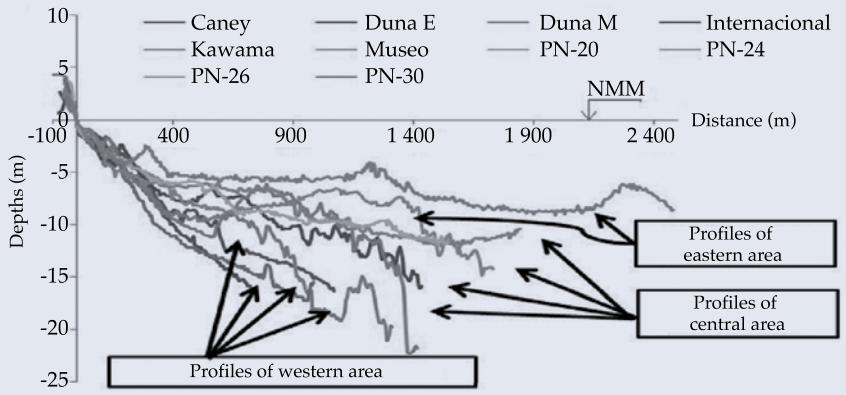

Figure 3. Comparison of Profiles.

The slopes of the bathymetry of the profiles for the western zone of the Hicacos peninsula were larger than those corresponding to the profiles in the central and eastern zones, declining towards the northwest. The area was divided into three zones based on the bathymetric behavior presented above: west, central and east (Figure 4).

Developing the XBeach model. Definition of boundary conditions

The one-dimensional model with spacings of 5 m was developed. A simulation was performed for each profile selected, according to calibration and validation results obtained by Córdova *et al*. (2010). The sea boundary

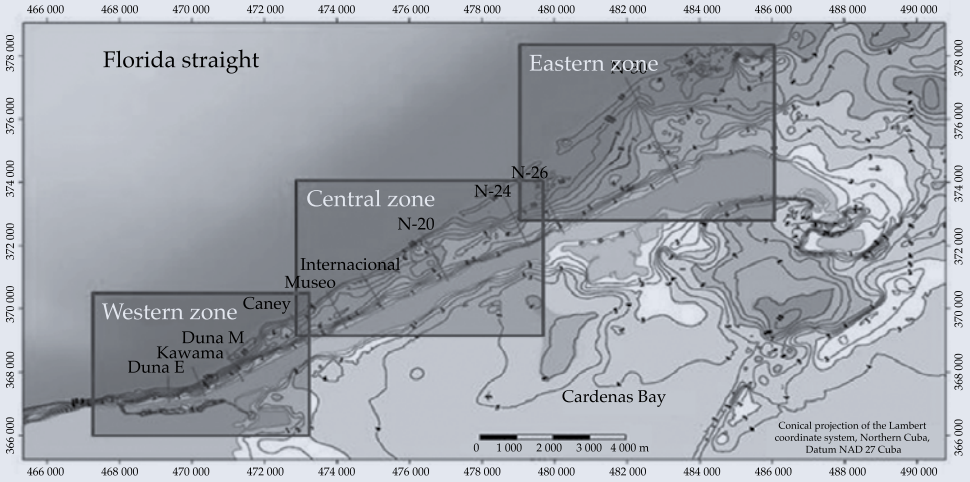

Figure 4. Hicacos peninsula, divided into zones (Izquierdo, 2004).

conditions were defined using the results from the propagation with the SWAN model.

Boundary Conditions

Waves

This procedure consisted of placing a virtual buoy in the last domain of the CMES system in the SWAN model, in front of each study zone selected. As can be seen in Figures 5, 6 and 7, the values of the wave characteristics were similar for the three buoys for the case of hurricane Michelle. The behavior was equal for all the others selected. The largest values for each virtual buoy were selected. Buoy V1 represents the western zone, buoy V2 the central and V3 the east. Figures 5, 6 and 7 compare the virtual buoys for the case of hurricane Michelle.

Definition of Morphological Variables and Statistical Calculations

In order to quantify the morphological changes that occurred during the simulations performed with the XBeach model for the three hurricane paths and profiles selected for the study, the following morphological variables

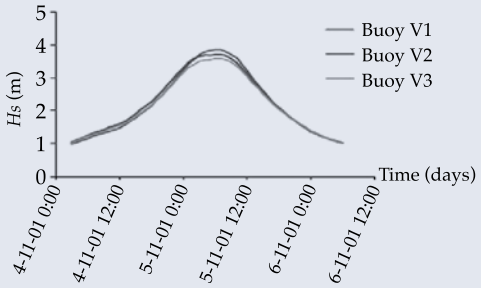

Figure 5. Height of the significant wave.

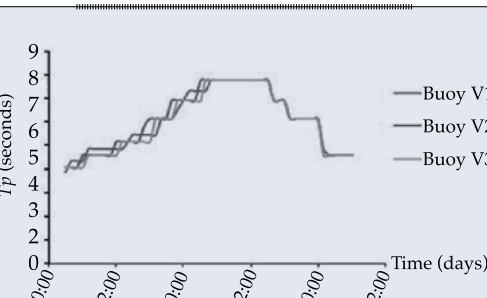

Figure 6. Peak period.

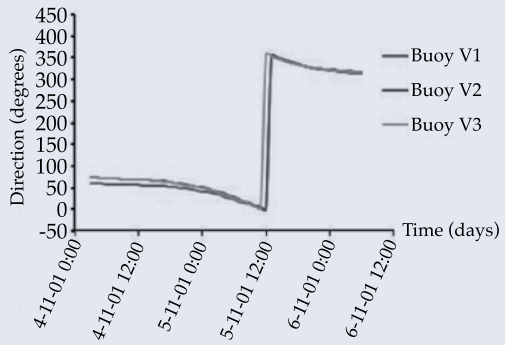

Figure 7. Wave direction.

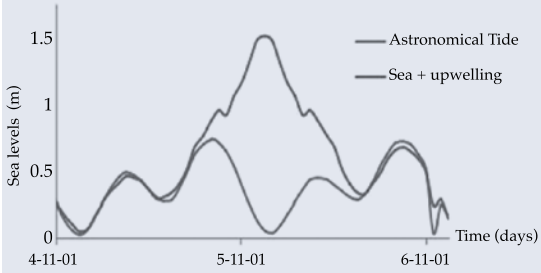

Figure 8. Over-elevation for simulation time for hurricane *Michelle*.

were defined as indicators of the different processes: erosion volume, accretion volume, sedimentary balance and length of retreat of the coastline.

Sea Levels

The XBeach model can include as a boundary condition the changes in sea levels resulting from meteorological tides. The behavior of this variable for each hurricane is defined below (hurricane Michelle, Figure 8).

Results and Discussion

The analysis was based on the morphological variables defined previously and the statistical results (quantitative comparison among study zones).

From Figures 9 and 10, it is concluded that the most actives area as hurricane Michelle passed was the central zone, with erosion values of 122.57 m^3/m and a coastline retreat of 17.44 meters.

The analysis of profiles showed that within the central zone, the area represented by the Museo profile was most critical, with a rate of erosion of 105.75 m^3/m, and profile PN-30 had the least volume of erosion, with a value of 50.07 m^3/m (Figure 11).

With respect to the sand balance, as seen in Figure 12, there was a supply of sand to the system in all profiles, especially in the case of PN-24, which demonstrated the greatest volume of accretion as compared to the other profiles.

The Duna M profile had the least volume and, therefore, this zone had the greatest balance between erosion and accumulation, or accretion. With respect to the retreat of the coastline, the largest retreat occurred in the central zone, in profile PN-24, as observed in Figure 13. Interestingly, the zone represented by profile PN-24 had the most overall accretion due to sand supplied from the sea, as well as greater sediment movement into the sea from the dry beach zone due to the effects of the hurricane, generating accumulation in the middle part of the profile.

The conclusion from the analysis of the path of hurricane Michelle is that the central zone was the most active portion of the Hicacos peninsula. The profiles with the largest morphological variables calculated¾ Museo and PN-24¾ are found in this zone. The critical profiles were determined according to zone in function of the length of the retreat of the coastline. These sectors, defined as critical points for this type of path, were: Kawama profile in the west with a coastline retreat of 25.38 meters; profile PN-24 in the central zone with a coastline retreat of 30.26 meters and ; PN-26 in the east with a coastline retreat of 24.52 meters.

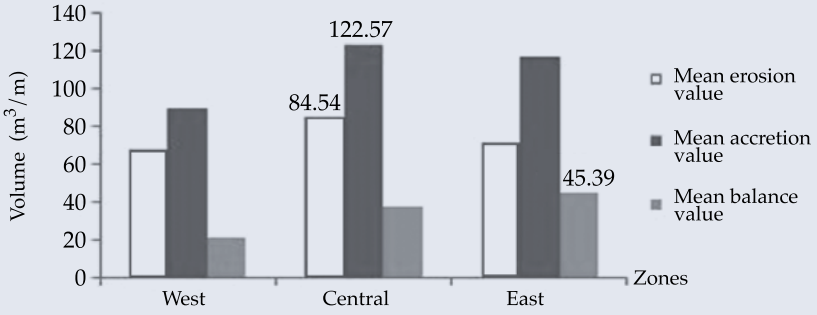

Figure 9. Mean volume of erosion, accretion and sand balance.

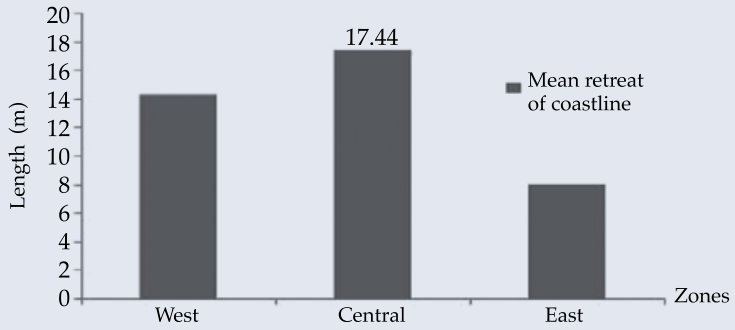

Figure 10. Mean length of retreat of coastline.

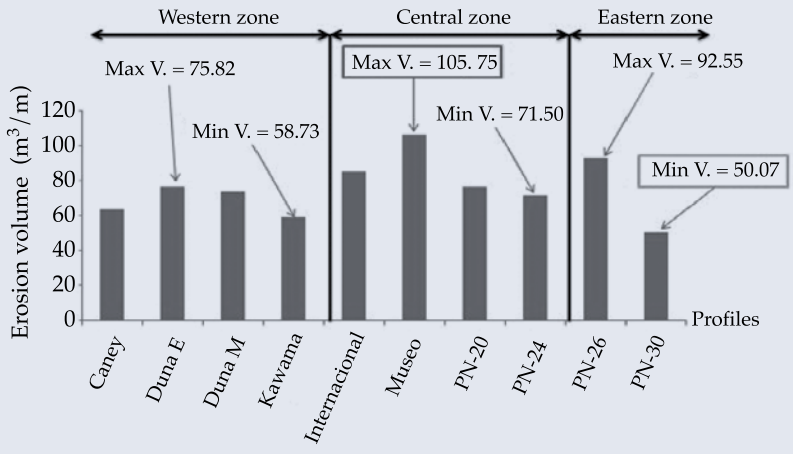

Figure 11. Maximum and minimum erosion volumes per zone.

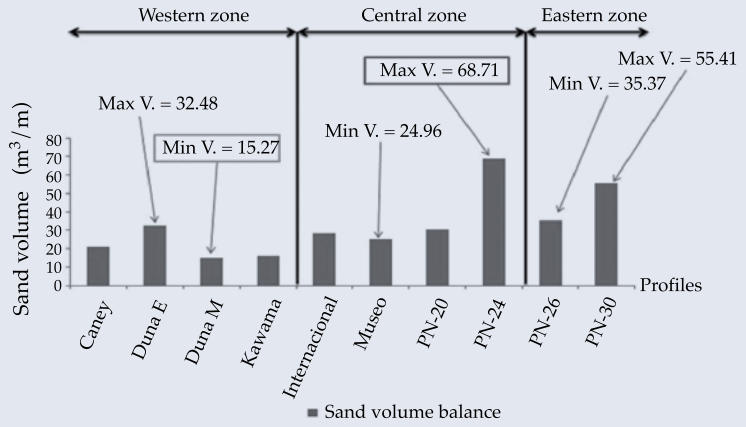

Figure 12. Maximum and minimum sand balance.

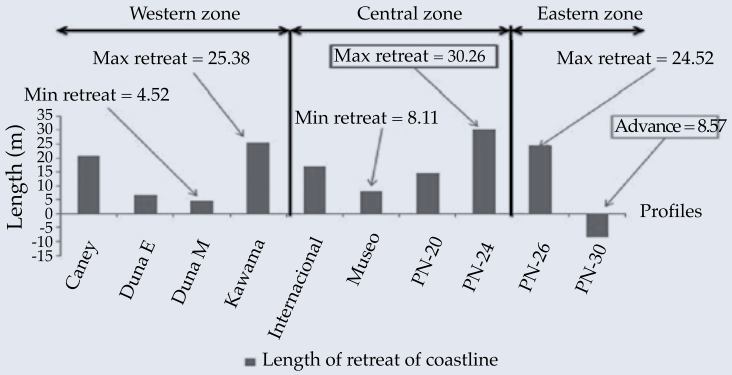

Figure 13. Maximum and minimum length of coastline retreat per zone.

Table 1 summarizes the critical profiles, showing in which profiles zones erosion and accretion occurred and, generally, which process was dominant based on the sedimentary balance. This latter factor was used a reference to define the overall occurrence of accretion. Nevertheless, there was a retreat of the coastline for all cases and erosion occurred in the dunes, the ledge and the first 70 meters of the submerged sloped, which represented the greatest effects on the area most used for recreation and, therefore, having the most significant impact on tourism. The variables in Table 1 are: PPS: Predominant Phenomena in the System; LRCL: Length of retreat of the coastline (m); V_{TE}: volume of total erosion and V_{TA}: volume of total accretion (m^3/m); GEZ and GAZ: greatest erosion zone and greatest accretion zone, respectively (from-to); SGEZ and SGAZ size of the greatest erosion and accretion zones (m^3/m).

Conclusions

The simulation of hurricane Michelle (November 2001) resulting in defining the central zone as being most dynamic, with average erosion volumes of 122.57 m^3/m.

Table 1. Summary of Morphological Changes of the Critical Profiles as a result of the passing of hurricane *Michelle*.

Profiles	PPS	LRCL (m)	V_{TE} (m^3/m)	V_{TA} (m^3/m)	GEZ (m)	SGEZ (m^3/m)	GAZ (m)	SGAZ (m^3/m)
Kawama	Acretion	25.38	58.73	74.99	0-65	56	105-160	57.84
PN-24	Acretion	30.26	71.5	140.21	0-60	60.33	65-175	131.14
PN-26	Acretion	24.52	92.55	127.92	5-70	84.19	75-195	118.33

This zone also had the longest mean coastline retreat, from 15 to 22 m. The sectors represented by profiles Kawama, PN-24 and PN-26 were defined as the most critical according to the length of the retreat of the coastline.

Received: 02/08/12
Accepted: 25/04/13

References

BEVEN, J. *Tropical Cyclone Report Hurricane Michelle*. Washington, D.C.: National Hurricane Center, January, 2002.

BOOIJ, N.C. *SWAN Cylce III version 40.81 user manual*. Delft: Delft Institute of Technology, 2009.

CÓRDOVA, L.L. y TORRES, R.H. *Estudio y Cuantificación de la erosión en el tramo Meliá; Varadero. Propuesta de Solución*. Informe técnico. La Habana: Instituto Politécnico José Antonio Echeverría, noviembre, 2008.

CÓRDOVA, L., LAMAZARES, R. y FERNÁNDEZ, S. *Simulación de los cambios morfológicos en playas de arena debido a la acción de campos de oleaje espectral debido a eventos extremos*. X Congreso Internacional de Ingeniería Hidráulica, Holguín, Cuba, octubre de 2010.

CÓRDOVA, L. y LAMAZARES, R. Simulación de los campos de vientos y oleaje asociados a huracanes. *Ingeniería Hidráulica y Ambiental*. Vol. XXXIII, núm. 2, 2012, pp. 50-65.

HOLLAND, G.J. An analytic model of the wind and pressure profiles in hurricanes. *Monthly Weather Review*. Vol. 108, No. 8, 1980, pp. 1212-1218.

IZQUIERDO, M.A. *Estudio de la dinámica litoral en la playa de Varadero, Cuba*. Tesina de máster. Santander, España: Universidad de Cantabria, 2004.

ROELVINK, D. *XBeach Model Description and Manual*. Report. UNESCO-IHE Institute for Water Education. Delft: Deltares and Delft University of Technology, June, 2010.

TOLMAN, H.L. *User manual and system documentation of WAVEWATCH III version 3.14*. Washington, D.C.: Environmental Modeling Center Marine Modeling and Analysis Branch, 2009.

TORRES, R.H. *HIDRICOS. Una herramienta para la Ingeniería de Costas*. Tesis presentada en opción al grado de Master en Ciencias Técnicas. La Habana: CUJAE, febrero de 2007.

VAN BENTUM, K., DUIJNDAM, L., GROENDIJK, L., and KNIPPING, D. *Varadero Beach, creating a better coastal situation near the Meliá Hotels*. Delft: Delft University of Technology, June, 2010.

Author's address institutional

Dr. Luis Fermín Córdova López

Instituto Superior Politécnico José Antonio Echeverría
Calle 114 número 11901, esquina 119 y 127
Marianao, Cuba
Teléfonos: +53 (7) 2601 416 y 2672 013
Fax: +53 (7) 2672 013
cordova@tesla.cujae.edu.cu

Click here to write the autor

Discussion

Technical notes and technical articles are open to discussion according to the following guidelines:

- The discussion will be written in the third person.
- The writer of the discussion shall use the term "commentator" when referring to oneself and the term "author" when referring to the one responsible for the technical note or article.
- The discussion shall be sent within 12 months of the last day of the quarter in which the a technical article or note was published.
- The length of the discussion may be extended by written request from the commentator.
- The discussion is to be presented according to the Guide for Collaborators published in this journal (omitting data referring to the length and abstract). In addition, the bibliographical citation of the technical notes or articles to which the discussion refers shall be included.
- The maximum length of the discussion is 4 journal pages (approximately 10 cuartillas, including figures and tables).
- The figures and tables presented by the commentator shall be progressively marked with Roman numbers and when citing those generated by the author the original numeration should be respected.
- The editors will suppress data that does not pertain to the subject of the discussion.
- The discussion will be rejected if it contains topics addressed by other sources, promotes personal interests, is carelessly prepared, raises controversy involving already established facts, is purely speculative or falls outside the purpose of the journal.
- The discussion will be published along with commentaries from the author or authors to which it refers.
- The discussion will be directed by the editor in chief.

The mermaid on a Dolphin, Malecon, La Paz Baja California Sur, Mexico.

Photo: Carlos Meneses del Arco.

Contributor's guide

The journal ***Tecnología y Ciencias del Agua*** invites specialists to collaborate with original technical articles or notes **related to water, that result from investigations and provide original contributions,** based on the disciplines of hydrology, hydraulics, water management, water and energy, water quality, and physical, biological and chemical sciences as well as political and social sciences, among others, according to the guidelines stated below.

PREPARATION OF THE ARTICLE

FORMAT

Font: Palatino throughout the entire document (body of text, tables and figures).

Font Size: Use 8, 9, 10 and 20 points, according to the following table:

8 points (Palatino)	9 points (Palatino)
• Tables. • Figures. • Acknowledgements.	• Name of authors. • Institution of authors. • Abstract. • *Abstract* and *keywords*. • Institutional address of the authors.
10 points (Palatino)	**20 points capital letters (Palatino)**
• Body of the text. • Title of the work in English.	• Title of the work in Spanish

Line Spacing: double-spaced.

Page Numbers: all pages shall be numbered.

Length

***Technical article*:** **30 pages** (numbered), including figures and tables.
***Technical note*:** **10 pages** (numbered), including figures and tables.

CONTENS

Contens

The article shall present significant contributions to scientific and technological knowledge pertaining to the specialty. It shall be based on finished works or those that have completed a development cycle. It shall show results from a series of experiences over 1 year or more of investigations and be supported by an adequate bibliographical review. **The basic structure of the text shall contain an introduction, the development and the conclusions.** The classic layout is preferable: abstract, introduction, methodology, results, discussion, conclusion and references.

Title

The title, written in Spanish and English, shall be informative and not exceed 12 words.

Abstract

The abstract, **written in Spanish and English**, shall be concise and provide a broad overview of the investigation (objective, method, results and conclusions) without exceeding 250 words.

Key Words

Eight words or key phrases (maximum) shall be provided **in Spanish and English** that facilitate the identification of the information.

Footnotes

Not admitted. The information is to be incorporated into the text.

Acknowledgements

To be included after the text and before the references.

Tables

- One page for each table.
- A list of all the tables cited shall be presented after the references.

Figures

- One page for each figure.
- All the names of the figures shall be included after the tables.
- They should be high-resolution (300 dpi).

Note: When the article is approved by the publication, the author shall send each figure in high-resolution (300 dpi) in JPG format.

References

- The entire bibliography must be referenced in the main body of the text.
- In the case of addressing scientific and technological topics that are common domain, works that denote the knowledge of the authors about the *state-of-art* shall be cited.
- Avoid self-citations to the extent possible
- International ISO-690 and ISO-690-2 standards are to be used as a basis. References to the literature used to develop the document are to be cited with last name of the author and date in parenthesis, for example, (Black, 1989), and ordered alphabetically by last name, ensuring that they are complete.

Examples of references:

Books

Last name of the author and initials in capital letters. Title of the book in capital/small letters and italics. Responsibilities related with the editorial work such as translating and editing. Edition (beginning with the second edition). Publication (city, publisher and year).

Example:

LEVI, E. *Tratado elemental de hidráulica*. Second edition. Jiutepec, Mexico: Instituto Mexicano de Tecnología del Agua, 1996, 303 pp.

When there are two or more authors:

GARCÍA R., E., GONZÁLEZ, R., MARTÍNEZ, P., ATHALA, J. and PAZ-SOLDÁN, G.A. *Guía de aplicación de los métodos de cálculo de caudales de reserva ecológicos en México*. Colección Manuales. Mexico: Convenio SGP-IMTA, 1999, 190 pp.

Titles of works or articles should not be translated. In the event a version exists in Spanish, it shall be indicated at the end of the original reference after the period.

Journals

Last name of the author and initials in capital letters. Title of the article in regular font, capital and small letters. Responsibilities related with the editorial work, such as translating and editing. Publication in capital/small letters and italics. Edition (volume, number, year, pages).

Example:

DÖLING, O.R. y VARAS, E. Operación de sistemas de recursos de agua multipropósito usando un modelo de simulación de procesos. *Ingeniería hidráulica en México*. Vol. XV, no. 2, May-August 2000, pp. 5-18.

Electronic Documents

Last name of the author and initials in capital letters. Title in capital/small letters and italics. Type of media in brackets. Responsibilities related with the editorial work, such as translating and editing (optional). Edition. City of publication. Publisher. Date of publication. Date of last review or update. Date in which the search was conducted in brackets. Series (optional). Notes (optional). Availability and access. Email.

Example:

CARROLL, L. *Alice's adventures in Wonderland* [online]. Textinfo ed. 2.1. Dortmund, Germany. WindSpiel, November 1994 [cited February 10, 1995]. Available in *World Wide Web*: http://www.germany.eu.net/books/carroll/alice.html.

Language

Spanish or English

Separation of numbers and use of decimal points

In *Tecnología y Ciencias del Agua*, the separation between thousands is denoted with a blank space. A decimal point is used to separate whole numbers from fractions. In this regard, refer to *Diccionario panhispánico de dudas*, edited by the Real Academia Española and the Asociación de Academias de la Lengua Española, in 2005, with respect to numeric expressions: "**the Anglo-Saxon use of the period is accepted, normal in some Hispano-American countries…: $\pi = 3.1416$.".**

Delivery of Article

Send the article in *Word* with the name of the authors and institutional address to revista.tyca@gmail.com, with copy to Elizabeth Peña Montiel, elipena@tlaloc.imta.mx.

General Information

The review process will begin once the material is received, during which it is possible that the manuscript could be rejected. If the text is suitable for review, having fulfilled the Editorial Policy and the Editorial Committee having determined so, it will proceed to the review stage.

Depending on the review process, the text may be accepted without changes, with minor changes, with extensive changes or rejected.

Once a work is published, the main author has the right to two journals and ten offprints free of charge.
In there are any questions, please write to Helena Rivas López, hrivas@tlaloc.imta.mx or Elizabeth Peña Montiel, elipena@tlaloc.imta.mx

Editorial Policy

Contents

Interdisciplinary, composed of previously unpublished articles and technical notes related to water, that result from research and provide original scientific and technological contributions or innovations, developed based on the fields of knowledge of diverse disciplines.

Topics Covered

Interdisciplinary, related to water, with priority topics in the following knowledge areas:

- Water and energy
- Water quality
- Hydro-agricultural sciences
- Physical, biological and chemical sciences
- Political and social sciences
- Scientific and technological development and innovation
- Water management
- Hydraulics
- Hydrology

Type of Contributions

- **Technical article**: scientific document that addresses and communicates, for the first time, results from a successful investigation or innovation, whose contributions provide and increase current knowledge about the topic of water.
- **Technical note**: text that addresses advances in the field of hydraulic engineering and professional practices in the field of water, while not necessarily making an original contribution in every case it must be a previously unpublished work.

Some of the articles submitted to the review process can result in being published as notes and vice versa. This will occur through a proposal and process of mutual agreement between the authors and the editor responsible for the topic. The article and the note have nearly the same structure (abstract, introduction, methodology, results, discussion, conclusion, references).

Review Process

The journal is governed by a rigorous review process which establishes that each article be analyzed separately by at least three reviewers who recommend its acceptance, acceptance with minor changes, acceptance with extensive changes, rejection or acceptance as a technical note with the required changes.

At least one of three reviewers will be sought from a foreign institution.

The reviewers may not belong to the same institution as the authors proposing the article for publication.

When the decisions are opposing or inconsistent, the involvement of other reviewers or the members of the Editorial Committee may be requested.

In exceptional cases, the approval of an article will be decided by two reviewers in addition to the opinion of the editor of the corresponding topic or, in extraordinary cases, the editor in chief.

A rejected article will not be received for a new review process.

The review process will be performed in such a way that neither the authors nor the reviewers know the names of the other party.

The review process is performed by high-level specialists and experts who are national and internationally renowned in their professional fields and have the ability to dependably evaluate, in a timely manner, the quality as well as the originality of contributions, in addition to the degree of scientific and technological innovation in the topic under which it is submitted for possible publication.

This participation is provided as a professional courtesy.

Final Ruling

The ruling resulting from the review process is not subject to appeal.

Authors

Works are published from authors of any nationality who present their contributions in Spanish or English.

Responsibility of the Authors

Submitting a proposal for the publication of an article commits the author not to simultaneously submit it for consideration by other publications. In the event an article has been submitted to another media for eventual publication, the author agrees to do so with the knowledge of the Editorial Department, which will suspend the review process and inform the Editorial Committee of the decision by the authors.

The collaborators whose authors have been accepted will formally cede the copyright to Tecnología y Ciencias del Agua.

The authors are responsible for the contents of the articles.

The author is responsible for the quality of the Spanish used. If the writing is deficient the work will be rejected. Tecnología y Ciencias del Agua will only be responsible for the editorial management.

The author commits to making the changes indicated by the Editorial Committee in the time frame they establish. In the event these indications are not met, the article will be removed from the review process and be marked as rejected.

The author shall address resolving the questions and proposals presented by the editors and the editorial coordinator.

Each author shall approve the final printed proofs of their texts. It is suggested that authors consult the "Guide for Collaborators."

Readers

Academics, investigators, specialists and professionals interested in the analysis, investigation and search for knowledge and solutions to problems related to water.

Reception of Articles

The reception of articles and notes is ongoing.

Time period

Bimonthly edition.

Suscription and Distribution

The journal is distributed through paid and courtesy subscriptions.

Water Technology and Sciences *is registered in the following national and international indices and abstracts:* • *Actualidad Iberoamericana, CIT-III, Instituto Iberoamericano de Información en Ciencia y Tecnología;* • *Applied Mechanics Reviews, The American Society of Mechanical Engineers;* • *CAB Abstracts, CAB International;* • *Cambridge Scientific Abstracts, CSA;* • *Fluid Abstracts: Civil Engineering, Fluid Abstracts;* • *Fluid Abstracts: Process Engineering, Fluid Abstracts;* • *GeoArchive, Geosystems;* • *Geotitles, Geosystems;* • *GeoSEARCH, Geosystems;* • *Hydrotitles, Geosystems;* • *Hydro ROM, Geosystems;* • *Índice de revistas mexicanas de investigación científica y tecnológica, Consejo Nacional de Ciencia y Tecnología;* • *International Civil Engineering Abstracts, CITIS;* • *Latindex, Universidad Nacional Autónoma de México* • *Marine, Oceanographic and Freshwater Resources, Geosystems;* • *NISC Export Services, National Inquiry Services Centre;* • *Periódica, Universidad Nacional Autónoma de México;* • *Thomson Reuters Science Citation Index® (ISI)* • *Expanded Thomson Reuters Research Alert® (ISI)* • *Water Resources Worldwide, Geosystems.*